

# Synthesis of nanosized BaSnO<sub>3</sub> powders

## **Dissertation**

zur Erlangung des Grades

**Doktor der Ingenieurwissenschaften**

an der Naturwissenschaftlich-Technischen Fakultät III

der Universität des Saarlandes

Vorgelegt von

Wensheng LÜ

Saarbrücken

2002

**Gedruckt mit Unterstützung des Deutschen Akademischen Austauschdienstes**

Tag des Kolloquiums: 25. 10. 2002

Dekan:	Prof. Dr. H. Vehoff
Gutachter:	Prof. Dr. H. Schmidt
	Prof. Dr. H. D. Breuer
Vorsitzender:	Prof. Dr. F. Mücklich
Beisitzer:	Dr. S. Schmitz-Stöwe

## **Acknowledgments**

I would like to thank Prof. Dr. H. Schmidt for his supervision during the course of this work. I am grateful for the guidance and the constructive ideas of K-P. Schmidt, Christian Göbbert, Dr. N. Bendzko and Dr. R. Nonninger.

As a recipient of the DAAD scholarship I want to thank DAAD for the financial support. My special thanks to Ms. H. Schädlich for her assistance.

I have had selfless support and help from many colleagues in INM. My hearty thanks to you all. I want to thank Rainer Wittmer, who gives me many constructive suggestions and all round support. I thank Annegret Hüntelmann, Heike Schmitt, Anja Mohr, Anne-Katrin Pannwitt and Dr. Mohammad Jilavi for their understanding, help and patiently enduring my distraction.

I want to thank my wife, my parents and my son for their love, understanding and support. My thanks also to my friends, my relatives and other people who make my life in Germany pleasant.

## Abstract

The metal alkoxide route for preparing nanocrystalline BaSnO<sub>3</sub> powders has been developed for the first time. Derived from the synthesized bimetal alkoxide precursor BaSn(OPr<sup>i</sup>)<sub>6</sub>, BaSnO<sub>3</sub> with a particle size of 20 to 60 nm has been obtained. Due to the high phase transformation temperature (above 550°C) the particles are strongly agglomerated and the specific surface area of the powder is only 17.0 m<sup>2</sup>/g. Therefore, a hydrothermal synthesis technique for preparing nanosize BaSnO<sub>3</sub> powders with a higher surface area and a lower aggregation degree has been developed. The reactivity of the SnO<sub>2</sub>·xH<sub>2</sub>O precursor in this technique is found to be dependent on the pH value. The influence of the concentration of Ba(OH)<sub>2</sub>, the Ba:Sn ratio, the temperature and duration of hydrothermal reaction and the solvent on the properties and the structure of the resulting powder has been studied. To minimize the agglomeration and aggregation, the precursor SnO<sub>2</sub>·xH<sub>2</sub>O is peptized with ammonia and modified with Genapol X-080, respectively. The SnO<sub>2</sub>·xH<sub>2</sub>O precursor becomes narrowly dispersed with a particle size of ca. 8 nm via peptization. Through modification the specific surface area of the obtained BaSnO<sub>3</sub> has been increased to over 50 m<sup>2</sup>/g by optimizing the concentration of the surfactant. The BaSnO<sub>3</sub> powder with a maximal specific surface of 57.0 m<sup>2</sup>/g has been obtained by combination of modification and peptization thanks to the limitation of agglomeration and the decreased particle size (10 to 30 nm). A densified ceramic tape has been fabricated at 1500°C through redispersing BaSnO<sub>3</sub> with TEA and thereafter tape casting. The solid solution region of BaSb<sub>x</sub>Sn<sub>1-x</sub>O<sub>3</sub> exists for 0 ≤ x < 0.12. The conductivity of BaSnO<sub>3</sub> is improved by doping 10 at.% Sb<sup>5+</sup>.

*Es wurde zum ersten Mal eine Alkoxid-Route zur Synthese von nanokristallinem Bariumstannatpulver entwickelt. Ausgehend vom synthetisierten Bimetallalkoxidprecursor BaSn(OPr<sup>i</sup>)<sub>6</sub>, wurde das BaSnO<sub>3</sub> mit einer Partikelgröße von 20 bis 60 nm hergestellt. Aufgrund der hohen Phasentransformationstemperatur (über 550°C) sind die Partikeln stark aggregiert, und die spezifische Oberfläche des Pulvers beträgt nur 17,0 m<sup>2</sup>/g. Deshalb wurde eine Hydrothermalsynthesetechnik zur Herstellung der Nano-Bariumstannatpulver mit einer höheren Oberfläche und einem niedrigeren Aggregationsgrad entwickelt. Die Reaktivität des Precursors von SnO<sub>2</sub>·xH<sub>2</sub>O in dieser Technik wurde gefunden, von dem pH-Wert abhängig zu sein. Es wurden die Einflüssen der Konzentration von Ba(OH)<sub>2</sub>, des Verhältnis von Ba:Sn, der Temperatur und Dauer der Hydrothermalreaktion sowie des Lösungsmittels auf die Eigenschaften und die Struktur der erhaltenen Pulver untersucht. Zur Minimierung der Agglomeration und Aggregation wurde der Precursor von SnO<sub>2</sub>·xH<sub>2</sub>O entweder mit Ammoniak peptiziert, oder mit Genapol X-080 modifiziert. Über Peptization wurde das Precursor von SnO<sub>2</sub>·xH<sub>2</sub>O auf der Nano-Ebene (ca. 8 nm) dispergiert. Per Modifikation hat die spezifische Oberfläche des hergestellten Pulvers durch Optimierung der Konzentration des Modifikators auf über 50 m<sup>2</sup>/g zugenommen. Das Bariumstannatpulver mit einer maximalen spezifischen Oberfläche von 57.0 m<sup>2</sup>/g wurde durch Kombination von Peptization und Modifikation hergestellt. Dadurch wurde die Agglomeration und Aggregation im Pulver beschränkt, und die Partikelgröße auf 10 bis 30 nm verkleinert. Eine dichte Keramikschiicht wurde bei 1500°C durch Redispersierung von BaSnO<sub>3</sub> mit TEA und demnach Foliengießen hergestellt. Der Festflüssigbereich von BaSb<sub>x</sub>Sn<sub>1-x</sub>O<sub>3</sub> befindet sich in 0 ≤ x < 0.12. Die Leitfähigkeit des mit 10 at.% Sb<sup>5+</sup> dotierten Bariumstannats wurde verbessert.*



# Contents

<b>1. Introduction</b> .....	<b>1</b>
<b>2. Literature review</b> .....	<b>2</b>
2.1 BaSnO <sub>3</sub> - structure, properties and application.....	2
2.2 Synthesis of barium stannate .....	5
2.2.1 Solid state reaction .....	5
2.2.2 Coprecipitation .....	6
2.2.3 Sol - Gel synthesis .....	7
2.2.4 Self-heat-sustained (SHS) route .....	8
2.2.5 Hydrothermal synthesis.....	9
2.3 Synthesis of multicomponent oxide powders from metal alkoxides .....	11
2.3.1 Basic process.....	12
2.3.2 Synthesis of metal alkoxide precursors.....	13
2.3.3 Prepared multicomponent powders including barium or tin.....	14
2.4 Hydrothermal synthesis of ceramic powders .....	14
2.4.1 Definition and characteristics .....	14
2.4.2 Hydrothermal conditions .....	16
2.4.3 Influence parameters .....	19
2.4.4 Mechanism.....	20
2.5 Surface modification for synthesis of nanoscaled powder.....	22
2.6 Doped barium stannate .....	23
<b>3. Objective</b> .....	<b>27</b>
<b>4. Experimental procedure</b> .....	<b>28</b>
4.1 Synthesis of BaSnO <sub>3</sub> via the low-temperature aqueous synthesis route .....	28
4.2 Preparation of BaSnO <sub>3</sub> Powder via metal alkoxide route .....	28
4.2.1 Synthesis of precursor BaSn(OR) <sub>6</sub> .....	28
4.2.2 Hydrolysis .....	30
4.2.3 Calcination .....	30
4.3 Hydrothermal synthesis of BaSnO <sub>3</sub> .....	30
4.3.1 Synthesis of SnO <sub>2</sub> ·xH <sub>2</sub> O.....	30
4.3.2 SnO <sub>2</sub> ·xH <sub>2</sub> O suspended with barium hydroxide .....	31
4.3.3 Hydrothermal treatment .....	31
4.3.4 Calcination .....	32
4.3.5 Milling and redispersion of the end-powder.....	32
4.3.6 Sintering of the powders and tape casting.....	32
4.4 Parameters measurement and materials characterization.....	32
4.4.1 pH measurement .....	32
4.4.2 Surface tension measurement .....	33
4.4.3 Charge adsorption of particle surface .....	33

4.4.4 Density measurement .....	33
4.4.5 Element analysis .....	34
4.4.6 Molecular spectroscopy .....	34
4.4.7 X-ray powder diffraction .....	34
4.4.8 Thermal analysis .....	35
4.4.9 Microstructure analysis .....	35
4.4.10 Particle size analysis .....	35
4.4.11 Specific surface area .....	36
4.4.12 Electrical properties .....	36
<b>5. Results and discussions .....</b>	<b>37</b>
5.1 LTAS route .....	37
5.2 Synthesis of BaSnO <sub>3</sub> powder from metal alkoxide .....	39
5.2.1 Double metal alkoxide .....	39
5.2.1.1 Starting materials .....	39
5.2.1.2 Characterization of barium tin alkoxide .....	42
5.2.1.3 Stabilization of precursor in alcoholic solution .....	46
5.2.2 Hydrolyzing process .....	47
5.2.3 Crystallization behavior .....	50
5.2.3.1 Conventional calcination .....	50
5.2.3.2 Hydrothermal calcination .....	57
5.2.4 Properties and microstructure analysis of the prepared powder .....	62
5.3 Hydrothermal synthesis of barium stannate powder .....	69
5.3.1 Synthesis of stannic hydroxide .....	69
5.3.1.1 Reactions between SnCl <sub>4</sub> and ammonia .....	69
5.3.1.2 Processing of tin oxide hydrate .....	73
5.3.1.3 Effect of pH value .....	75
5.3.1.4 Properties of tin oxide hydrate gel .....	78
5.3.2 Hydrothermal reaction between SnO <sub>2</sub> ·xH <sub>2</sub> O gel and Ba(OH) <sub>2</sub> .....	80
5.3.2.1 Barium source and concentration .....	80
5.3.2.2 Influence of the ratio of Ba to Sn .....	84
5.3.2.3 Hydrothermal temperature and time .....	86
5.3.2.4 Effects of the solvent .....	91
5.3.3 Improving the properties of the powder by peptization .....	92
5.3.3.1 Peptization of the tin oxide hydrate gel .....	92
5.3.3.2 Influence of the peptization .....	95
5.3.4 Improving the properties of the powder by surface modification .....	100
5.3.4.1 Preliminary choice of surfactants .....	100
5.3.4.2 Determination of surfactants .....	105
5.3.4.3 Influence of surfactant concentration and calcining temperature .....	107
5.3.5 Characterization of the powder .....	110
5.3.5.1 Thermoanalysis .....	111
5.3.5.2 Structure evolution .....	114
5.3.5.3 Crystallization behavior .....	116

5.3.5.4 Microstructure of the powders.....	120
5.3.5.5 Solid state $^{119}\text{Sn}$ NMR.....	125
5.3.5.6 Surface area and density.....	127
5.3.5.6 Sintering behavior.....	128
5.3.6 Fabrication of $\text{BaSnO}_3$ tape .....	131
5.3.6.1 Redispersion of the powder .....	131
5.3.6.2 Tape casting .....	134
5.3.7 Antimony doped barium stannate .....	135
5.3.7.1 $\text{Sb}^{3+}$ doped $\text{BaSnO}_3$ .....	135
5.3.7.2 $\text{Sb}^{5+}$ doped $\text{BaSnO}_3$ .....	137
<b>6 Summary and conclusions .....</b>	<b>142</b>
<b>7. Appendix .....</b>	<b>147</b>
7.1 Chemicals used .....	147
7.2 List of instruments and equipment used.....	149
<b>8. References .....</b>	<b>150</b>

## 1. Introduction

BaSnO<sub>3</sub> with cubic perovskite structure exhibits good dielectric properties. Because of these characteristic properties BaSnO<sub>3</sub> ceramic is becoming more and more important in material technology. It can be used to prepare thermally stable capacitors and to fabricate ceramic boundary layer capacitors. In recent years BaSnO<sub>3</sub> has been found to be a very promising sensor material and has therefore received most attention. In pure as well as doped forms stannates have been investigated as potential solid state sensor materials for many gases, including CO, NO<sub>x</sub>, H<sub>2</sub> and CO<sub>2</sub>. BaSnO<sub>3</sub> has also been used in the preparation of multifunctional temperature-humidity-gas sensors in combining with BaTiO<sub>3</sub>.

The detection of gas in the sensors containing BaSnO<sub>3</sub> is performed by measurement of the electrical properties changes in such as resistance and conductivity. The changes are induced in the semiconducting oxide of BaSnO<sub>3</sub> following the adsorption of some gases on the solid surface. The gas sensitivity of this semiconducting oxide is relevant to the surface reaction process. Thus a large surface area of the semiconducting oxide is of importance to its gas sensor devices.

Gas sensors are generally required to be inexpensive, reliable and durable. This means, the devices should be highly sensitive, should be atmospherically stable and should respond rapidly to the measured gas. It has been shown that the sensitivity, stability and response time of the devices contemplated here are intimately connected with material composition and microstructure, which depends on the control of powder preparation and handling. Hence, BaSnO<sub>3</sub> powder as a sensing material should be of a high quality, having small primary crystallite size, large surface area, low agglomeration and high purity.

In view of these facts non-agglomerated nanocrystalline BaSnO<sub>3</sub> powder is more suitable compared to traditional ceramic powder. Nanocrystalline ceramic powders have attracted increasing interest during the last few decades, especially in view of the large potential these powders have in many end applications. This includes significantly reduced the sintering temperature, which for example gives rise for material combinations in multilayer techniques, as well as the ability to produce ceramics with tailored properties by a post sintering heat treatment starting from prefabricated nanoscaled dense or porous microstructure. To achieve this a very important prerequisite is to prevent the agglomeration and aggregation of the particles during synthesis and redisperse the powders to their primary particle size to produce homogeneous green microstructures.

It is the aim of this dissertation to develop a suitable synthesis route for preparing nanocrystalline BaSnO<sub>3</sub> powder with high specific surface area. Furthermore doping BaSnO<sub>3</sub> with antimony ions for improvement of the electric properties will be attempted so that the fabricated gas sensor can exhibit high sensitivity and selectivity.

## 2. Literature review

### 2.1 BaSnO<sub>3</sub> - structure, properties and application

There exist three oxostannate (IV) compounds in the BaO - SnO<sub>2</sub> binary system, BaSnO<sub>3</sub>, Ba<sub>3</sub>Sn<sub>2</sub>O<sub>7</sub> and Ba<sub>2</sub>SnO<sub>4</sub>, but barium stannate is normally referred to as BaSnO<sub>3</sub> because among these BaSnO<sub>3</sub> is the best known, the most thoroughly investigated and the most useful compound. It shows a cubic perovskite structure. The perovskite structure<sup>1</sup> is related to the mineral perovskite CaTiO<sub>3</sub>. Perovskite type compounds have the general formula A<sup>2+</sup>B<sup>4+</sup>O<sub>3</sub>, where A can be a group IIA element or transition metal in the +2 oxidation state, and B is a transition metal, Sn or Se in the +4 oxidation state. The structure of BaSnO<sub>3</sub> is described in Fig. 1. In the cubic structure the Ba<sup>2+</sup> ions (1.34 Å) occupy the corners of the elementary cell, the Sn<sup>4+</sup> ions (0.71 Å) the volume center and the O<sup>2-</sup> ions (1.40 Å) the surface center. In this structure the larger Ba<sup>2+</sup> ions and the O<sup>2-</sup> ions build a cubic densest ball packing together and a quarter of the octahedral holes is filled with small Sn<sup>4+</sup> ions. Each Ba<sup>2+</sup> ion is coordinated with 12 O<sup>2-</sup> ions, each O<sup>2-</sup> ion is surrounded by four Ba<sup>2+</sup> ions and two Sn<sup>4+</sup> ions, so the crystallochemical formula is Ba<sup>[12]</sup>Sn<sup>[6]</sup>O<sub>3</sub><sup>[4+2]</sup>. The octahedrons of [SnO<sub>6</sub>] are linked by sharing corners to form a three-dimensional framework. It should be realized that this high-symmetry cubic structure can distort and deform under definite conditions so that the structure symmetry degree is lowered. The lattice constant of BaSnO<sub>3</sub> is a = 4.1163Å. The x-ray density measured at 25°C by Swanson et al<sup>2</sup> is 7.238 g/cm<sup>3</sup>.

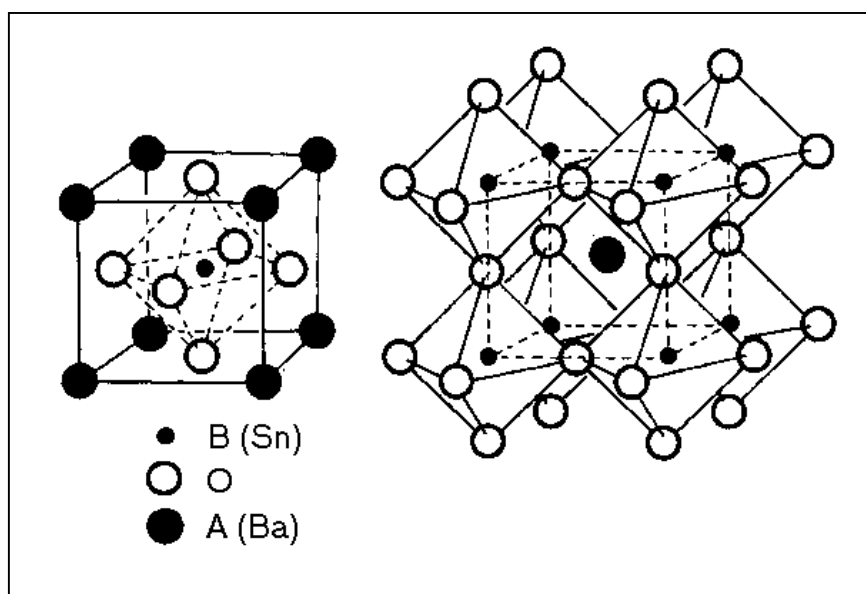


**Fig. 1** Perovskite structure of BaSnO<sub>3</sub>.

Barium stannate is a nearly colorless compound with a weak tinge of yellow. This compound can be dissolved in a hot diluted salt acid. It is used as the standard of the  $^{119m}\text{Sn}$  - Moessbauer - spectroscopy. No complete densification of  $\text{BaSnO}_3$  ceramic is reported. The sintering temperature is reported to be above  $1600^\circ\text{C}$  (a sample calcined by  $1600^\circ\text{C}$  is still porous<sup>3</sup>). The melting point of  $\text{BaSnO}_3$  measured by Wagner and Binder<sup>3</sup> is  $2060^\circ\text{C}$ , which is questionable, because this compound is reported to decompose into  $\text{BaO}$  and  $\text{SnO}_2$  at  $1950^\circ\text{C}$ <sup>4</sup>.

$\text{BaSnO}_3$  is paraelectrical and nonferroelectric. Its dielectric properties have been investigated by many researchers. Studies have shown that the dielectric properties of  $\text{BaSnO}_3$  are dependent on temperature and frequency. The dielectric coefficient  $\epsilon'$  and dielectric loss factor  $\delta$  varied in the range of 14 to 15 and 0.0001 to 0.001 respectively under the frequencies of  $10^2$  to  $10^5$  Hz and the temperatures of  $-200$  to  $400^\circ\text{C}$ <sup>5,6</sup>. At room temperature  $\tan \delta$  indicated a small decrease with the frequency increase from  $10^2$  to  $10^5$  Hz and is constant above  $10^5$  Hz. The capacity is barely dependent on frequency at normal temperature in the region from  $10^2$  to  $10^6$  Hz, it is 15.651 pF at 1 kHz and 15.626 pF at 10 kHz respectively. The values of the capacity and  $\tan \delta$  become very large at high temperature. The temperature and frequency nevertheless play a important role at a temperature below  $40^\circ\text{C}$ . This dependence of the capacity and  $\tan \delta$  on the temperature and frequency can be clearly seen from Fig. 2. The AC conductivity of  $\text{BaSnO}_3$  has been studied<sup>7</sup> in the temperature range of  $40$  to  $250^\circ\text{C}$  and the frequency range of 100 Hz to 1 MHz. Below  $150^\circ\text{C}$  the conductivity is almost independent of temperature while between  $150$  and  $250^\circ\text{C}$  it is temperature dependent. At 100 kHz the activation energy of these two regions is 0.08 and 0.35 eV, respectively.

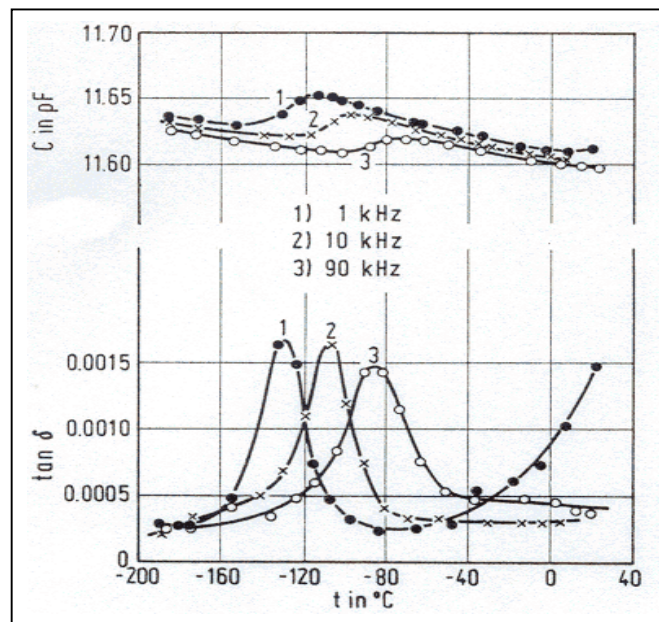


**Fig. 2** Capacity  $C$  and dielectric loss factor  $\tan \delta$  of  $\text{BaSnO}_3$  as a function of temperature<sup>7</sup>.

With its characteristic dielectric properties  $\text{BaSnO}_3$  has been used as a component of ceramic dielectric bodies to prepare thermally stable capacitors<sup>8,9</sup>, and to fabricate ceramic boundary layer capacitors when combined with  $\text{BaTiO}_3$ <sup>10,11</sup>. In recent years more and more attention has been shifted to study of the application of barium stannate as a sensor material. It has been found<sup>12,13</sup> that the electrical properties of barium stannate such as conductivity, resistance, capacitance or impedance are dependent on temperature, oxygen partial pressure, the nature of the measured gases and their concentrations. Based on the results many gas sensor devices made from  $\text{BaSnO}_3$  powder have been developed.

Williams et al<sup>12</sup> first found that a sensor containing or comprising a compound of Sn of the general formula  $\text{A}_{1-y}\text{B}_y\text{Sn}_{1-x}\text{C}_x\text{O}_{3-z}$ , where A = Ca, Sr or Ba, B = another alkali earth element, another divalent element (e.g. Pb) or a trivalent lanthanide (e.g. La, Y, Gd), C = a tri- or tetravalent element for example a transition element (e.g. Fe, Co, Ti, Zr or Ce) and  $0 \leq y < 1$ ,  $0 \leq x < 1$  and  $z =$  the oxygen deficiency, has an electric variable in response to the presence of  $\text{CO}_2$  or its mixture with other gases. This implies that  $\text{BaSnO}_3$  can be used as a sensing material for  $\text{CO}_2$ . According to this discovery Capteur Sensors and Analysers Ltd.<sup>14</sup> fabricated a carbon dioxide sensor from antimony based  $\text{BaSnO}_3$  material. The sensor is suitable for sensing  $\text{CO}_2$  in low concentrations. When combined with CuO,  $\text{BaSnO}_3$  can be used for sensing  $\text{CO}_2$  over a wide range of  $\text{CO}_2$  concentrations<sup>15,16,17</sup>. The capacitance of CuO -  $\text{BaSnO}_3$  is dependent on the  $\text{CO}_2$  concentration and this mixed oxide exhibits high  $\text{CO}_2$  sensitivity. A monotonic and approximate logarithmic relationship exists between the sensitivity and the concentration of  $\text{CO}_2$  below 50%. Furthermore, the response of this sensor to  $\text{CO}_2$  is very rapid. The grain interface between CuO and  $\text{BaSnO}_3$  is thought to play an important role for  $\text{CO}_2$  detection.

$\text{BaSnO}_3$  and  $\text{BaSn}_{1-x}\text{Zr}_x\text{O}_3$  ( $x = 0.05, 0.10$  and  $0.20$ ) are also sensor materials for  $\text{H}_2\text{S}$  gas in ambient conditions<sup>12,18</sup>. Solid solution formation in the  $\text{BaSnO}_3$  -  $\text{BaZrO}_3$  system and their electric conduction contribute to improved sensing characteristics of these materials.

$\text{BaSnO}_3$  can also be used for fabricating CO sensor<sup>12,19</sup>. It is thought<sup>19</sup> that the mechanism of CO sensitivity of this metal oxide is a surface reaction process. Thus, to achieve high gas sensitivity,  $\text{BaSnO}_3$  is fabricated as a thin film. The CO sensitivity shows a maximum in the temperature range of 600 to 700°C under dry conditions. Humidity has a different influence on the CO sensitivity, which depends on the oxygen concentration. A gas sensor for detecting the presence of CO in polluted air, comprising a perovskite compound such as  $\text{Ba}_{0.9}\text{Gd}_{0.1}\text{SnO}_3$ , is reported by Moseley and his colleagues<sup>20</sup>.

$\text{BaSnO}_3$  as a semiconducting oxide is also a very promising sensor material for detecting nitric oxide<sup>21</sup>. The sensitivity of the  $\text{BaSnO}_3$  thin films to NO depends on the temperature and the oxygen concentration. The NO sensitivity, under dry conditions, shows a maximum in the range of 450 to 550°C. A sensor comprising  $\text{BaSnO}_3$  is found to be selectively sensitive to  $\text{NO}_2$ <sup>22</sup>. Kurosawa et al<sup>23</sup> designed a sensor comprising an ion-conductive solid electrolyte and a pair of electrodes to detect  $\text{NO}_x$  concentration in a gas sample by measuring EMF changes between the first electrode containing perovskite-type mixed oxide of formula  $\text{MSnO}_3$  (M = Mg, Ca, Sr, Ba, Mn, Co, Ni, Zn, Cd), and a second electrode. The sensor is sensitive and stable in high temperature waste gases due to the high heat resistance of the electrodes.

Oxygen sensors used as controlling air-fuel ratio in boilers or engines (sometimes called exhaust gas sensor or air-fuel ratio sensor) have been fabricated from sintered  $\text{BaSnO}_3$ <sup>24,25,26,27,28,29,30,31</sup>. The sensitive material comprising  $\text{BaSnO}_3$  can be pellet<sup>32</sup>, membrane<sup>24</sup> or film<sup>33</sup>. Sensors working at 350 to 500°C in a rich exhaust gas<sup>26</sup> and at 650 to 1000°C from a rich atmosphere to a lean atmosphere during heating and cooling periods are reported<sup>34,35</sup>. These sensors show a good response when the exhaust gas changes from rich side towards the lean side<sup>36</sup>. The exhaust gas sensor made of  $\text{Ba}_{1-x}\text{La}_x\text{SnO}_3$  ceramic ( $x = 0.00003 - 0.02$ ) was developed<sup>37</sup> for controlling air-fuel ratio in engines or boilers. Studies on the sensor for flue gases from boilers and stoves consisting of  $\text{BaSnO}_3$ <sup>38</sup> show that addition of alkali metal, Ag, or Cu coated on the calcined  $\text{BaSnO}_3$ , which is then pressed to prepare a sensor device, improves the sensitivity of the device to oxygen. It is also reported<sup>39</sup> that the dioxide additives give the exhaust gas sensor containing  $\text{BaSnO}_3$  improved sensitivity to oxygen with reduced temperature dependence. Addition of the noble metals increases the sensitivity to the combustion gas level.

The application of  $\text{BaSnO}_3$  to detect humidity is reported by Shimizu et al<sup>40</sup>. The humidity sensitivities of  $\text{BaSnO}_3$  are enhanced slightly by calcining barium tin hydroxides, which are prepared by a coprecipitation method. The partial substitution of the A-site element of the perovskite-type oxides with La was more useful for the enhancement of the sensitivity.

A new multifunctional sensitive ceramic,  $\text{BaTiO}_3\text{-BaSnO}_3$  (BTS), which is a metal-oxide porous ceramic semiconductor, is reported by Zhou and Zhao<sup>41,42</sup>. It is capable of detecting temperature, humidity, and gas type with a single sensing element.

## 2.2 Synthesis of barium stannate

Barium stannate applied in industry and in the laboratory is almost all prepared via solid state reaction. Because of the high preparation temperature (above 1000°C) it is impossible to obtain fine powders directly, let alone nanoscaled powders. In recent years some new synthesis routes to prepare fine barium stannate powders at low calcining temperature have been developed, but as far as a concrete synthesis route is concerned, there is often only one or two papers reporting it.

### 2.2.1 Solid state reaction

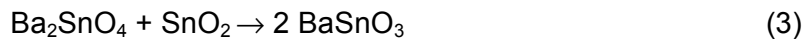
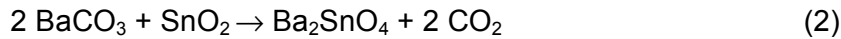
$\text{BaSnO}_3$  is conventionally prepared by ceramic solid reaction through sintering  $\text{BaCO}_3$  and  $\text{SnO}_2$  at a high temperature ranging from 1200 to 1400°C<sup>43,44,45,46</sup> according to equation 1:



The mixture of  $\text{BaCO}_3$  and  $\text{SnO}_2$  pressed in pellets at a pressure of  $10^4$  to  $2 \times 10^4$  kg/cm<sup>2</sup> is calcined at 1300 to 1400°C for 8 hours in the air and then ground, pressed again and calcined at the same temperature for another 8 hours<sup>43</sup>. Instead of 8 hours the pellets can also be calcined once 2 hours and once for 1 to 1.5 hours at 1250°C, or 2 hours between



1000 to 1200°C and 4 hours between 1250 to 1350°C<sup>44</sup>. After the calcination the pellets react completely and convert into BaSnO<sub>3</sub>. If the stoichiometric mixture of BaCO<sub>3</sub> and SnO<sub>2</sub> in the powder form is heated at a temperature between 900 and 1000°C, Ba<sub>2</sub>SnO<sub>4</sub> not BaSnO<sub>3</sub> is formed. It reacts continually at 1100°C to build BaSnO<sub>3</sub>. Single phase BaSnO<sub>3</sub> appears in the sample after being sintered at 1200°C for 2 hours<sup>45</sup>. The reactions were described as follows:



In almost all cases high purity of BaCO<sub>3</sub> and SnO<sub>2</sub> (above 99.5%) has to be used to prevent the introduction of impurity phases. The attempt<sup>46</sup> to improving the density of BaSnO<sub>3</sub> (80% of the theoretical density sintered at 1380°C) by increasing the sintering temperature is not successful. The grains with a cubic structure developed at such a high sintering temperature show a size of 2 to 4 μm. No dense ceramic has been obtained<sup>3</sup> even with a sintering temperature of 1600°C.

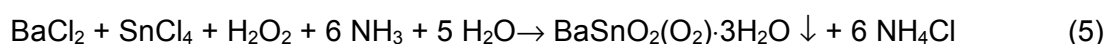
To lower calcining temperature, Azad and Hon<sup>47</sup> employed barium nitrate to substitute barium carbonate and successfully prepared BaSnO<sub>3</sub> at 1000°C. The formation of BaSnO<sub>3</sub> from metal nitrates via solid state reaction is assumed to take place as follows:



In this case the mixture of raw materials is ball milled for 4 hours, then calcined first at 800°C for 8 hours and fired again at 1000°C for 24 hours. The traditional several repetitions of "heat and beat" steps are avoided in this modified route. However, the barium stannate powders are still difficult to sinter. The relative density of the sintered bodies is only up to 70 - 80% of the theoretical value even in samples sintered at 1600°C for 12 hours. Up to date a high degree of densification in the solid - state derived BaSnO<sub>3</sub> samples has not been achieved.

### 2.2.2 Coprecipitation

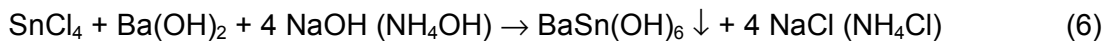
Coprecipitation from solution is one of the oldest techniques for the preparation of mixed oxide powders. It consists of preparing an aqueous solution containing the desired cations and then mixing with another solution which contains the precipitating agent. The precipitated product is separated from the liquid by filtration, dried and thermally decomposed to the desired compound. Paff<sup>48</sup> synthesized BaSnO<sub>3</sub> powders from a peroxo-precursor, which is precipitated by adding BaCl<sub>2</sub>·2H<sub>2</sub>O and SnCl<sub>4</sub> solution to a solution of H<sub>2</sub>O<sub>2</sub> and ammonia in water as follows:



The peroxo-precursor converts to BaSnO<sub>3</sub> via thermal degradation including the evaporation of water and the liberation of oxygen. The formation of BaSnO<sub>3</sub> begins at 550°C, and the pure form is obtained by calcination at 900°C for 1 hour with a grain size of 50 to 200 nm. The specific surface area of BaSnO<sub>3</sub> powder calcined at 1000°C for 1 hour is 14 m<sup>2</sup>/g. The powder becomes sinter active above 1200°C, and the highest density of 6.74 g/cm<sup>3</sup> after sintering at 1400°C for 4 hours is about 93% of the theoretical density.

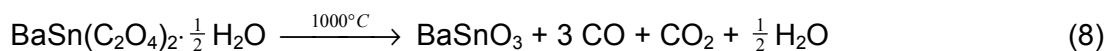
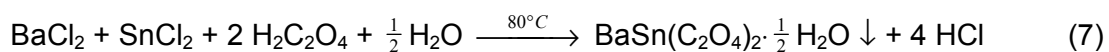
It has also been reported<sup>6,49</sup> that BaSnO<sub>3</sub> can be prepared by coprecipitation of tin and barium chloride solutions at room temperature. The precipitate has a composition of BaSnO<sub>3</sub>·3H<sub>2</sub>O. The evaporation of water during heating occurs up to 330°C, and the first BaSnO<sub>3</sub> reflections in the x-ray diffractograms can be seen at temperatures of ca. 400°C. The precipitate is heated to 1000°C and the often simultaneously formed solid barium tin hydroxide makes it difficult to obtain phase-pure BaSnO<sub>3</sub> even at higher temperatures.

Leoni et al<sup>50</sup> employed a so-called low-temperature aqueous synthesis route (LTAS) to prepare BaSnO<sub>3</sub> from SnCl<sub>4</sub> and Ba(OH)<sub>2</sub>. The route can be summarized as:



The mixture of Ba(OH)<sub>2</sub> and SnCl<sub>4</sub> at 80°C is precipitated by a basic solution and then the reactor is maintained at that temperature for times ranging from 5 to 100 hours. It was assumed that a solution should have a pH high enough to exceed the BaSnO<sub>3</sub> solubility and cause its precipitation, so that excess alkali was added. The obtained precipitate is barium tin hydroxide, which converts to perovskite structured BaSnO<sub>3</sub> at about 270°C. The specific surface area of BaSnO<sub>3</sub> is very low (6.12 m<sup>2</sup>/g). The cause is thought to be the transition to perovskite from the hydroxo form BaSn(OH)<sub>6</sub>.

Oxalate has also been used as a precipitating agent by Bao et al<sup>51</sup> for preparing BaSnO<sub>3</sub>. The chemical reactions during synthesis processing are described as follows:



The particle size of BaSnO<sub>3</sub> calcined at 1000°C is less than 0.2 μm. The ceramic of Ba(Ti,Sn)O<sub>3</sub> prepared from the mixture of BaSnO<sub>3</sub> and BaTiO<sub>3</sub> showed better dielectric properties<sup>51</sup>.

### 2.2.3 Sol - Gel synthesis

A widely applied technique in research for the preparation of the multicomponent oxide is sol - gel synthesis which consists of formation of an amorphous gel from solutions followed by dehydration at relatively low temperature<sup>52</sup>. The most advantageous characteristics of this method are the high purity and the excellent control of the composition of the resulting mixed oxide powders. Different routes may be used to produce highly dispersed mixed

oxide powders such as alkoxide route, citrate-type methods and hydrous oxide solutions route.

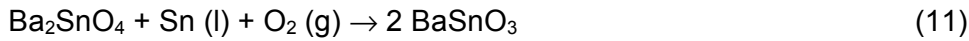
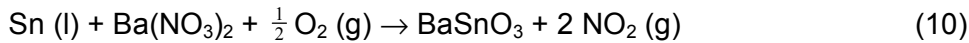
Among the above mentioned routes only the citrate route has been used to prepare BaSnO<sub>3</sub> powder. In this route amorphous gel mixtures are prepared from solutions containing the required cations and an organic polyfunctional acid, such as citric, malic, tartaric, glycolic or lactic acid. This technique, frequently called the citrate process, contains a step where the gel is rapidly dehydrated at low temperatures. The advantage of this route lies in the limitation of segregation of different metal ions, and is achieved by forming stable metal-chelate complexes, which then grow by polymerization. Immobilization of metal-chelate complexes in such a rigid organic polymer net is helpful for reducing segregation of individual metals during the pyrolysis process of the polymer at high temperatures.

Pechini<sup>53</sup> first prepared perovskite powders by dispersing metallic cations in a polyester resin resulting from polycondensation between ethylene glycol and citric acid. The process here for the preparation of BaSnO<sub>3</sub> consists of gelation of an aqueous solution containing the appropriate ratio of the required elements through an organic polymer network such as citric acid<sup>54,55</sup>. Tin tetrachloride and barium carbonate are used as starting materials. Licheronet al<sup>54</sup> dissolved tin chloride in distilled water and stabilized it with a chelating agent to prevent hydrolysis or condensation, and then mixed it with BaCO<sub>3</sub> and citric acid. The obtained transparent citrate complex sol was neutralized by addition of ammonia and thereafter heated at 80°C. The aqueous gel synthesized by introducing N-N'-methylene-bis-azobisisobutyronitrile in the sol had to be calcined at 600°C for 5 hours and then annealed at 1000°C for 17 hours to convert into BaSnO<sub>3</sub> powder with a size of 5 μm. Udawatte and his colleagues<sup>55</sup>, however, dissolved the SnCl<sub>4</sub> in ethylene glycol instead of water and then mixed with citric acid. A transparent citric acid complex was formed by addition of barium carbonate powders at 80°C. A brown transparent gel was synthesized by heating the sol at 135°C for one day. The gel changed to BaSnO<sub>3</sub> powder when treated at a temperature range of 600 to 900°C, but it was difficult to remove the trace amounts of BaCO<sub>3</sub> and SnO<sub>2</sub> even at 900°C. The particles of BaSnO<sub>3</sub> sample treated at 800°C for 2 hours show faceted morphology and are strongly aggregated. The onset crystallization temperature of BaSnO<sub>3</sub> from amorphous precursors is assumed to be 600°C. This process is also called polymerized complex method (PC).

#### 2.2.4 Self-heat-sustained (SHS) route

The self-propagation high-temperature of self-heat-sustained (SHS) synthesis is an attractive and viable alternative to the conventional methods of advanced materials production, which is gaining rapid popularity in the field of ceramic- and metal-matrix composites. The main feature of the SHS technique is the ability of highly exothermic reactions to be self-sustained and therefore, energetically efficient. In the self-heat-sustained process for preparing barium stannate<sup>47</sup>, metallic tin powder is intimately mixed with anhydrous Ba(NO<sub>3</sub>)<sub>2</sub>. Because the melting point of metal tin is relatively low (232°C), tin can disperse uniformly in Ba(NO<sub>3</sub>)<sub>2</sub> when heated at 250°C for 4 hours. The reaction between molten and free flowing tin and Ba(NO<sub>3</sub>)<sub>2</sub> takes place at 800°C and lasts 4 hours.

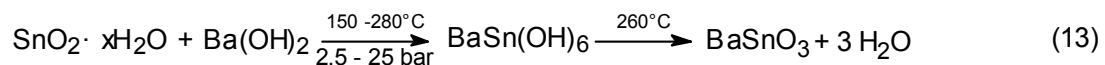
The mixture has to be subsequently calcined at a temperature above 1200°C to prepare phase-pure BaSnO<sub>3</sub>. An intermediate Ba<sub>2</sub>SnO<sub>4</sub> appears when the sample is treated below 1200°C. It is assumed that in the initial stages, molten metallic tin reacts as in equations 9 and 10. The Ba-rich phase subsequently reacts with more Sn or SnO<sub>2</sub> to form BaSnO<sub>3</sub> as shown in formulae 11 and 12.



The particles sintered at 1350°C for 12 hours show spherical morphology and have a size of 1 to 2 μm. Sintering at 1350°C for a duration in the range of 24 to 36 hours is found to yield microstructural features almost identical to those observed in the case of solid-state derived samples. The average size ranged from 1 to about 20 μm in some overly grown grains. The SHS derived BaSnO<sub>3</sub> samples could be well densified by sintering the powder at 1600°C for 2 hours, with good microstructural features, typically as ceramics.

### 2.2.5 Hydrothermal synthesis

Hydrothermal synthesis is a potentially superior method for low cost production of advanced mixed oxides because complex oxide powders can usually be formed directly. This synthesis route has been widely employed to prepare ceramic powders, and will be further described in section 2.4. Preparation of BaSnO<sub>3</sub> via the hydrothermal route was developed by Kutty and Vivekandan<sup>56</sup>. They used stannic hydroxide gel (SnO<sub>2</sub>·xH<sub>2</sub>O), which was freshly precipitated from tin chloride solution by addition of ammonia, and Ba(OH)<sub>2</sub> solution as starting materials for hydrothermal treatment. The mixture was handled in a teflon-lined autoclave at a temperature between 150 and 280°C. The as-prepared powder was a hydrated phase BaSn(OH)<sub>6</sub>. On heating in air or on releasing the pressure of the autoclave in situ at about 260°C, this hydrated phase converted into fine BaSnO<sub>3</sub> powders. The whole process is presented as formula 13:



The particles of the intermediate BaSn(OH)<sub>6</sub> are highly aggregated with no definite morphology. Their particle size varies from 0.5 to 3 μm. By adding 0.1 wt% polyvinyl alcohol (PVA) as a surface modifier, the particle size decreases and ranges from 0.2 to 1 μm. The lattice of the particle shows a low order of symmetry and none of the structure is identified. The particle size of BaSnO<sub>3</sub> varied from 0.2 to 0.6 μm with nearly cubic morphology. The electron diffraction patterns of the sample heated at 280°C has hexa-net symmetry and can be indexed on the basis of a perovskite lattice with the electron beam emerging parallel to

the [111] direction. The formation of the hydrated phase is thought to result from the amphoteric nature of  $\text{SnO}_2 \cdot x\text{H}_2\text{O}$  gel which stabilizes  $\text{Sn}(\text{OH})_6^{2-}$  anions under elevated water-pressure and higher temperatures.

The incomparable advantage of this method over others for preparation of  $\text{BaSnO}_3$  lies in the very low calcination temperature ( $260^\circ\text{C}$ ). Such a temperature makes it possible to keep the activity of the added surfactant for modifying the surface of the powder particles and thereafter to reduce the particle size. Thus this method is promising for preparing nanosize  $\text{BaSnO}_3$  powder. However, no other reports on the hydrothermal preparation of  $\text{BaSnO}_3$  are available in the literature.

### Stannic hydroxide

In the processing of hydrothermal preparation of  $\text{BaSnO}_3$  stannic hydroxide gel is used by Kutty and Vivekandan<sup>56</sup> as the precursor. This compound is commonly known as stannic acid. It has always been thought to exist in the form of  $\text{H}_2[\text{Sn}(\text{OH})_6]$ , but no free state of this has been proved apart from its corresponding hexahydroxo stannates like  $\text{Ca}[\text{Sn}(\text{OH})_6]$ . It is also reported<sup>57</sup> that the form of  $\text{Sn}(\text{OH})_4$  exists in weak alkali solutions as thin film on the anodic Sn-electrode. Stannic acid has traditionally been divided into two categories, namely  $\alpha$ -stannic acid and  $\beta$ -stannic acid. These are not different compounds but the same compound in different forms. Generally  $\alpha$ -stannic acid is chemically active and very soluble in alkalis and acids while  $\beta$ -stannic acid is inactive and only weakly soluble. Nowadays both of these are regarded as tin (IV) oxide hydrate with the formula  $\text{SnO}_2 \cdot x\text{H}_2\text{O}$ , where  $x$  is related with activity and decreases with aging. When the stannic hydroxide is rich of water, it corresponds to the  $\alpha$  form and is reactive. With aging the bound water is gradually lost and the stannic hydroxide appears in the  $\beta$  form<sup>58</sup>. Stannic hydroxide is a much stronger acid than it is a base, thus justifying the name of stannic acid commonly applied it.

Stannic hydroxide can be synthesized from metal tin. Metal tin can be oxidized in  $\alpha$  or  $\beta$  form by the addition of nitric or sulfurous acid<sup>59,60</sup>. Normally the  $\alpha$ -stannic hydroxide is obtained at room temperature. If the mixture is heated or the heated acid is added, then the synthesized product appears in the  $\beta$  form. Through acidification of sodium hydroxide stannate  $\text{Na}[\text{Sn}(\text{OH})_6]$  Williams and Pace<sup>61</sup> also successfully synthesized  $\alpha$ -stannic acid. The first "ion-free" sample of stannic hydroxide gel was prepared by the hydrolysis of stannic ethoxide<sup>62</sup>.

The widely used route to synthesize stannic hydroxide is nevertheless the hydrolysis of tin tetrachloride solution because of its low costs and simplicity. Mixing a  $\text{SnCl}_4$  solution with alkalis like sodium hydroxide or ammonia solution leads to a precipitate. After a purification of the precipitate through washing by distilled water a stannic hydroxide gel can be obtained, which is partly crystallized and consists of tin oxide according to x-ray analysis. However, there are different opinions about the pH at which the  $\text{SnCl}_4$  should be precipitated. Duan and Huang<sup>63</sup> suggested that the optimal pH range for preparing stannic hydroxide should lie in the range of 2 to 5. Similarly Ocana et al<sup>64</sup> synthesized stannic hydroxide by hydrolysis of  $\text{SnCl}_4$  solution with hydrochloric acid at a low acidity. They assume that the high acidity leads to the formation of a large number of nuclei which later

aggregate to minimize the high free energy of the system, while at low pH the hydrolysis is slower producing fewer nuclei which do not aggregate either due to their higher surface charge or due to the lower surface energy. On the other hand, Brito et al<sup>65</sup> prepared the stannic hydroxide at pH > 8 by gradual addition of ammonia to tin chloride solution and eliminated Cl<sup>-</sup> and NH<sub>4</sub><sup>+</sup> through dialysis. Ribeiro et al<sup>66</sup> and Harrison et al<sup>67</sup> obtained stannic hydroxide precipitates at pH = 11 and pH = 6.5 respectively.

The amount of NaOH for precipitating tin chloride solution quantitatively is reported to be less than the corresponding theoretic value and will decrease with the increase in reaction temperature<sup>68</sup>. If the amount of OH<sup>-</sup> exceeds 4 equivalent of SnCl<sub>4</sub>, the precipitate will partly dissolve again. In very diluted solution 25% of the theoretic OH<sup>-</sup> amount is enough for a complete precipitation. The absorption of stannic hydroxide to sodium and chloride ions depends on the pH value. Lower pH value leads to more absorption to sodium ions and less to chloride ions. In contrast to this, the amounts of impurity of NH<sub>4</sub><sup>+</sup> and Cl<sup>-</sup> can be lowered by fast mixing and a complete removal of the impurity through washing is proved by the negative reaction of NH<sub>4</sub><sup>+</sup> and Cl<sup>-</sup><sup>69</sup>.

The structure of stannic hydroxide and the combination form of water is still not clear. Although there is synthesis processing, by which the stannic hydroxide with a definite content of water is reproducible, it is still thought<sup>69</sup> that there is no independent, definite hydrate. The seemingly reasonable explanation<sup>69</sup> of the structure is that the water is not completely chemically bound, and those products are only clusters with different OH<sup>-</sup> groups. In stannic hydroxide, part of the water is considered as an intermicellary solution and part of the water serves as coordination saturation of Sn on the particle surface. The important proof for this is that the water of the stannic hydroxide is released continually up to complete dehydration according to the thermogravimetric and differential thermoanalytic results.

The freshly prepared stannic hydroxide gel can be converted to colloid solution through peptization with acids or alkalis. The peptizing effect increases according to the order of hydrochloric acid, tartaric acid, oxalic acid and potassium hydroxide. The mineral acid cannot be easily separated from the end-solution, for example a sample after peptization with tartaric acid and purification through dialysis showed a composition of SnO<sub>2</sub>: C<sub>4</sub>H<sub>6</sub>O<sub>6</sub> = 243 : 1<sup>70</sup>. Ammonia<sup>71</sup> is also used to peptize stannic hydroxide gel. An advantage of this peptizator is that the excess NH<sub>3</sub> can be easily removed by boiling the solution. The pH of a freshly peptized solution without impurity of chloride and ammonium measured by Aditya<sup>72</sup> is 6.80, it changes with aging and becomes 6.40 after a month.

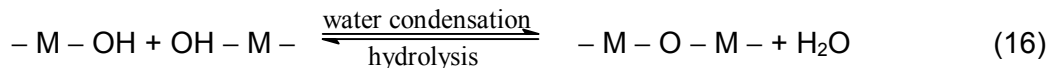
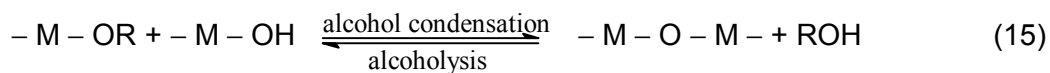
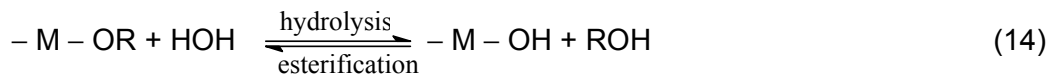
### 2.3 Synthesis of multicomponent oxide powders from metal alkoxides

The ceramic powders prepared by chemical reaction in the solution have been effectively used as sources for preparing high-purity, high-density, controlled-texture ceramic bodies<sup>73</sup>. The preparation of the powders is carried out using metal alkoxides as starting material via hydrolysis, polycondensation and thermal decomposition. One of the principal advantages of this metal alkoxide route is that of the chemical homogeneity on the molecular level

attained in very complex compositions, this homogeneity is to retain as much of that homogeneity as possible in the ceramic powder and ultimately in the fabricated and sintered ceramic pieces. More important is that the high homogeneity of the components leads to lower processing temperatures as well as a low crystallization temperature and therefore offers the possibility of preparing ceramic powders and tailoring their properties at low temperatures. In the light of this it is of interest to study the metal alkoxide route for preparing BaSnO<sub>3</sub> although no literature has reported it to date.

### 2.3.1 Basic process

Metal alkoxides have the general formula M(OR)<sub>n</sub>, where M is a metal element and R is an alkyl group. The OR group in a metal alkoxide is a strong Lewis base undergoing hydrolysis and polycondensation to form a sol. The overall reaction can be generally described as following<sup>73,74,75:</sup>



These reactions are reversible so that excess water and aliphatic alcohol are usually added in order to prevent esterification and alcoholysis. As the polycondensation reactions proceed the degree of polymerization increases, which is accompanied by an increase in the viscosity of the sol until the formation of a gel. This sol-gel conversion for alkoxides is irreversible. A gel is a three dimensional continuous network which consists of a solid skeleton and a continuous liquid like alcohol and water surrounding and supporting it. The ceramic powders are prepared by removing the solvents and the remaining organic groups by drying and calcining the gel. In order to prepare multicomponent oxide ceramic powders, alkoxides are blended together in a solvent at the sol stage and doped with metal salts if the corresponding alkoxide is unavailable. The synthesis of double metal alkoxide will be described in the following section 2.3.2.

In the sol-gel process the control of the hydrolysis and the condensation is especially important for obtaining powders with high quality. Because the hydrolysis and condensation during the sol formation proceed simultaneously, the relative rates of reaction for the hydrolysis and condensation decide the structure and properties of an alkoxide gel. The hydrolysis and condensation rates are dependent on many parameters. In addition to adjusting pH, the reaction rates may be varied by the temperature, the type of catalysis, water concentration, and the choice of alkoxide ligands. The steric interactions of the alcohol solvent chosen also influence the reaction rates. It is reported<sup>76</sup> that the morphology and the particle size of a hydrolysis product can be controlled by changing the hydrolysis and condensation rates, and spherical particles have been obtained at a relatively slow

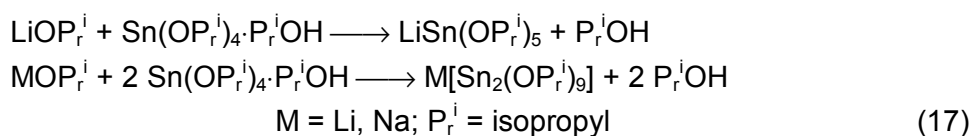
hydrolysis rate. In the case of multicomponent systems the susceptibility of different alkoxides to hydrolysis plays an important role.

It is generally believed that the powder prepared via the sol-gel route is formed through a nucleation - grain growth mechanism, as demonstrated by Lamehr and Dinger<sup>77</sup>. Nucleation occurs through dispersed phase concentration and a self-nucleation area is formed at an oversaturated concentration. In this area, nuclei incorporating the dispersed phase grow accompanied by the formation of new nuclei. In the lower concentration area, grains grow by diffusion, but not nucleation. A monodispersed powder can thus be obtained when the period of nucleation is relatively short. When using metal alkoxides, spherical particles are obtained, provided the hydrolysis rate is less than that of the condensation rate<sup>76</sup>. Computer simulation<sup>78</sup> has shown that structures ranging from weakly branched to highly branched clusters and from linear chain structures to smooth spherical particles can be synthesized by varying the hydrolysis conditions.

### 2.3.2 Synthesis of metal alkoxide precursors

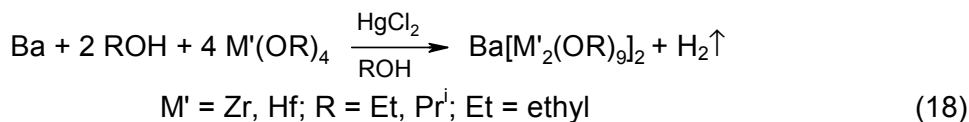
A survey of the literature indicates that the alkoxides of most of the metal elements in the periodic table have been synthesized and their chemistry has been investigated. For preparing multicomponent oxide powders, a double or multiple metal alkoxide precursor needs to be synthesized in order to get a homogenous hydrolysis product. The synthesis and properties of double metal alkoxides have been studied for more than half a century and the reviews of these were summarized by Brandley et al<sup>79,80</sup>. Among these synthesis methods, there are three methods which are suitable for synthesizing double metal alkoxides including barium or tin.

The first synthesis method, reactions of alkali alkoxides with another metal alkoxide, was investigated and reported by Meerwein and Bersin<sup>81</sup>. A number of tin double metal alkoxides (with alkali metals) were synthesized and isolated by Agrawal<sup>82</sup> according to the following formula:

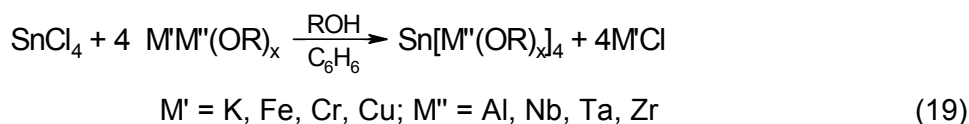


Alkoxides of alkaline earth metals like barium can also be prepared by the reactions of metal with alcohol in the presence of a catalyst like mercuric chloride and these are generally insoluble in common organic solvents (see formula 18). These alkaline earth metals dissolve at an extremely slow rate in alcohol, but their rate of dissolution increases in the presence of other metal alkoxides. It has also been reported<sup>83</sup> that a precursor of barium titanium alkoxide is synthesized without addition of the mercuric chloride as catalyst.





The third method to synthesize bimetallic alkoxide is the reaction of metal halides with other bimetallic alkoxides like  $\text{KAl}(\text{OPr}^i)_4$  which have been synthesized previously (see formula 19). Using this method Jain and his colleagues<sup>84</sup> synthesized tin bimetallic alkoxides successfully.



### 2.3.3 Prepared multicomponent powders including barium or tin

Most of the precursors for preparing barium compounds are synthesized by the second method described above. For example, barium titanate powders<sup>85</sup> have been prepared from metal Ba and titanium tetraisopropoxide,  $\beta\text{-BaB}_2\text{O}_4$ <sup>86</sup> from Ba and  $\text{B}(\text{OEt})_3$ ,  $\text{Ba}_2\text{NaNb}_5\text{O}_{15}$ <sup>87</sup> from Ba, NaOEt and  $\text{Nb}(\text{OEt})_3$ . The preparation of multicomponent powders such as  $\text{Sr}_{0.5}\text{Ba}_{0.5}\text{Nb}_2\text{O}_6$ <sup>88</sup> and  $\text{Ba}(\text{Mg}_{1/3}\text{Ta}_{2/3})\text{O}_3$ <sup>89</sup> via this route has also been reported. The first synthesis method has been used to prepare powders like barium titanate<sup>90</sup> and  $\text{YBa}_2\text{Cu}_3\text{O}_{7-x}$  superconductor<sup>91</sup>. The precursor is synthesized by reaction of  $\text{Ba}(\text{OC}_3\text{H}_7)_2$  with other metal alkoxides. Fukui and his colleagues<sup>92</sup> developed an alkoxide-hydroxide-method as an alternative to the alkoxide route. The reaction of alkoxides with barium hydroxide ( $\text{Ba}(\text{OH})_2 \cdot 8\text{H}_2\text{O}$ ) instead of barium alkoxide is used to prepare fine powders with perovskite structure such as  $\text{BaTiO}_3$  and  $\text{Ba}(\text{Mg}_{0.33}\text{Nb}_{0.67})\text{O}_3$ . In the reaction the hydrolysis rate is controlled by the crystal water of barium hydroxide.

There are some reports about preparation of tin multicomponent powders. Gulliver et al<sup>93</sup> synthesized  $\text{ZnSnO}_3$  according to the third method referred to in 2.3.2. A bimetallic alkoxide of  $\text{Ti}_2\text{Sn}(\text{OEt})_6$  is first synthesized from  $\text{TiOEt}$  and  $\text{Sn}(\text{OEt})_4$ . Zinc chloride reacts with the bimetallic alkoxide and generates  $\text{ZnSn}(\text{OEt})_6$ , which converts into  $\text{ZnSnO}_3$  at  $676^\circ\text{C}$ . The powder of  $(\text{Zr, Sn})\text{TiO}_4$  is prepared<sup>94</sup> by hydrolysis of the mixture of their alkoxides.

## 2.4 Hydrothermal synthesis of ceramic powders

### 2.4.1 Definition and characteristics

Hydrothermal reactions are usually defined as the reactions in water above its boiling point under a pressure more than 1 atm. Historically the first hydrothermal experiments were performed by Schafhaeupt<sup>95</sup> who synthesized quartz crystals from amorphous silica, although long before the formation of numerous minerals through naturally hydrothermal reactions had been discovered. Since then hydrothermal synthesis has been studied

extensively because of the industrial usefulness of grown crystals, the geological and mineralogical importance for mineral synthesis and phase equilibrium studies as well as confirming predictions concerning the genesis of minerals. Morey<sup>96</sup> characterized the underlying theories of hydrothermal synthesis, and studied numerous mineral systems. Many other investigators have used the study of hydrothermal synthesis for determination of the origins of important mineralogical systems, and later for investigations of single-crystal growth and ceramic powder synthesis. Laudise<sup>97</sup> has extensively investigated the use of hydrothermal synthesis for growth of quartz and other mineral crystals. Even though alumina has been produced via the Bayer process for decades, hydrothermal synthesis has only recently been recognized as a viable chemical process for production of a wide variety of commercially important advanced ceramic powders<sup>103</sup>.

Hydrothermal synthesis, as applied to ceramic powder preparation, is an aqueous chemical process for preparation of crystalline, anhydrous ceramic powders. The typically employed temperatures fall between the boiling point of water and the critical temperature of 374°C, and pressures range to 15 MPa. As the temperature is raised well above the boiling point and under high pressure condition, the solvation properties of water are altered so as to acquire a more nonpolar character<sup>98</sup>. Therefore reactants otherwise difficult to dissolve go into solution under hydrothermal conditions as complexes, in whose formation water itself or very soluble mineralizers can participate, hydrothermal reaction can thus be considered as a special case of chemical transport reactions. Under hydrothermal conditions there are several methods for producing powders<sup>99,100,101</sup> including hydrothermal oxidation, hydrothermal precipitation, hydrothermal crystallization, hydrothermal decomposition, hydrothermal dehydration, hydrothermal anodic oxidation, reactive electrode submerged arc and hydrothermal mechanochemical reaction.

For the synthesis of superfine ceramic oxides only hydrothermal precipitation and hydrothermal crystallization have to be considered. General details of both techniques are given in the literature<sup>101,102</sup>. While hydrothermal precipitation starts from metal salt solutions, hydrothermal crystallization uses hydroxide gels or sols. A generalized flow diagram is shown in Fig. 3. The nature of the precursor can be critical to the formation of a controlled particle size, chemically homogeneous ceramic powders. Raw materials can include those used in the production of sol-gel powders. A subsequent hydrothermal treatment of the sol can assist in control of the particle size. However, it is much more likely that inexpensive raw materials such as oxides, hydroxides, chlorides and nitrates will be employed.

The major difference between hydrothermal processing and other techniques is that there is no need for high-temperature calcination and that it eliminates the need for milling. In many cases this route can even be used for ceramic processes without a calcination step. Powders can be formed directly from solution by taking advantage of the complex reactions which take place in high-temperature water. Since there is no solid state calcination step, the formation of hard agglomerates and aggregates can be more easily avoided. Powders produced by this method have been demonstrated to be highly reactive toward sintering.

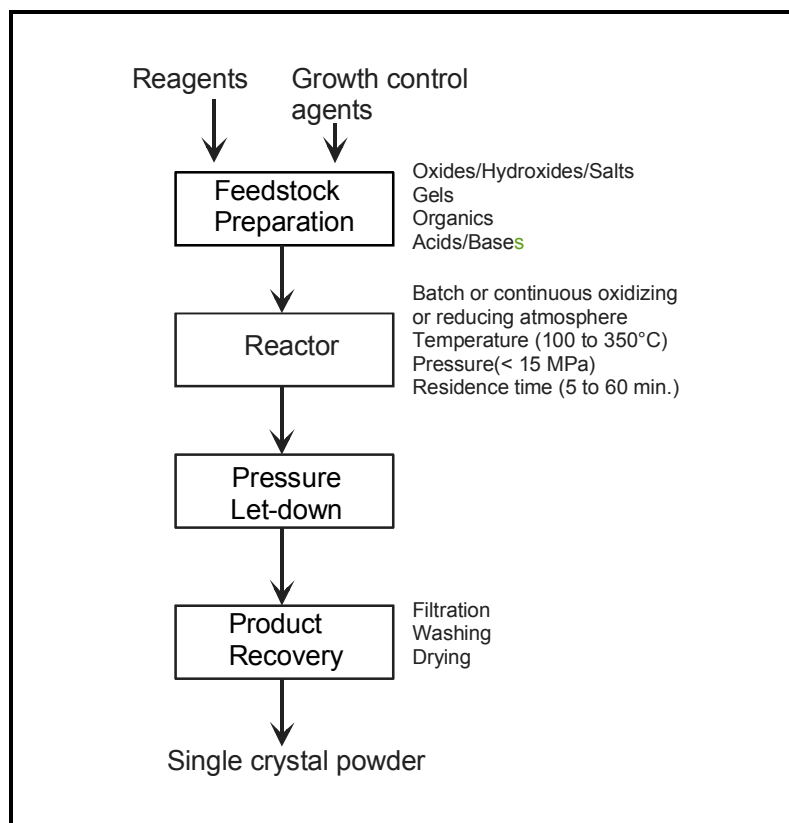


**Fig. 3** Hydrothermal process steps (taken from Dawson<sup>103</sup>).

### 2.4.2 Hydrothermal conditions

To withstand the temperatures and the pressures involved in hydrothermal synthesis, the use of autoclaves is usually required. They serve to protect the reaction vessel, in some situations the autoclave itself assumes the role of reaction vessel. The state of the types of autoclave is summarized in a number of reviews<sup>96,100,104,105</sup>.

The Morey bomb and the Tuttle type are the most commonly used autoclaves for hydrothermal synthesis in many laboratories. The early versions of the Morey bomb were sealed off with a fixed volume of water, the pressure therefore being fixed by the temperature and water volume. This is the most suitable arrangement for work up to 400°C and 400 bar because of its easy manipulation. The Tuttle type vessel is also called a test-tube or a cold-seal pressure vessel. Pressure is maintained by a cone-in-cone arrangement. It is safer and better with the thermocouple well outside the bomb and its ability to hold high pressure with a simple closing system. The newly developed TZM alloy type autoclave is one of the test-tube types. It can be used for high temperatures up to 1100°C. The materials chosen for the vessel play an important role in hydrothermal reaction. Thus, the corrosive properties of the solution under the desired conditions, as well as the danger of undesirable contamination of the reaction product must be considered. The teflon-lined autoclave is preferred in the synthesis of ceramic powders because of its stability to corrosion either in acid or alkaline media, nevertheless it is only usable within a limited

pressure-temperature range. The metal autoclave can resist high temperature and pressure, but when using it as a reaction vessel it is very important to consider its compatibility with the reactions being studied. In a neutral or acidic medium, glass or quartz glass is well-suited for hydrothermal syntheses, provided the pressure and temperature conditions permit it.

Hydrothermal conditions include the temperature and the pressure as well as the duration of the hydrothermal reaction. Nanoscaled simple oxide ceramic powders have been prepared by controlling the suitable hydrothermal conditions. They include  $\text{Al}_2\text{O}_3$ <sup>106,107</sup>,  $\text{TiO}_2$ <sup>108,109</sup>,  $\text{ZrO}_2$ <sup>110,111,112,113</sup>,  $\text{CeO}_2$ <sup>114,115,116</sup>,  $\alpha\text{-Fe}_2\text{O}_3$ <sup>117,118</sup> and  $\text{SnO}_2$ <sup>119</sup>. The size of the powders varies from several nanometers to 100 nm and is controllable. More attention is now being focused on preparing fine multicomponent oxide powders. A central research domain here is to prepare fine titanate powders or the mixture of titanate and zirconate powders such as  $\text{CaTiO}_3$ <sup>120,121</sup>,  $\text{SrTiO}_3$ <sup>120</sup>,  $\text{BaTiO}_3$ <sup>117,120,122,123,124,125,126</sup>,  $\text{PbTiO}_3$ <sup>127,128,129</sup>,  $\text{Pb}(\text{Zr,Ti})\text{O}_3$ <sup>130,131,132</sup>,  $\text{Ba}(\text{Ti,Zr})\text{O}_3$ <sup>117,122,133</sup> and so on. Other multicomponent compounds which have been reported to be hydrothermally prepared are  $\text{Mn}_{0.5}\text{Zn}_{0.5}\text{Fe}_2\text{O}_4$ <sup>134</sup>,  $\text{MnZnFe}_2\text{O}_4$ <sup>117,135</sup>, chromium ferrite<sup>136</sup>,  $\text{Y}_{0.39}\text{Al}_{0.56}\text{Tb}_{0.05}\text{O}_3$ <sup>137</sup>,  $\text{ZrO}_2\cdot\text{SiO}_2$ <sup>138</sup>,  $\text{HfO}_2\cdot\text{Eu}_2\text{O}_3$ <sup>135</sup>,  $(\text{Ce, Sm or Ca})\text{O}_x$ <sup>139</sup>, Talc<sup>140</sup>,  $\text{Ca}_2\text{P}_2\text{O}_7$ <sup>141</sup>,  $\text{Ca}_5(\text{PO}_4)_3\text{OH}$ <sup>142</sup>,  $\text{NaTi}_2(\text{PO}_4)_3$ <sup>143</sup>,  $\text{BaF}_{19}\text{O}_{12}$ <sup>144,145</sup>,  $\text{ZrO}_2$  mixed oxides<sup>146</sup>, etc.

In the institute for new materials (INM) a lot of research work<sup>147,148,149,150,151,152,153,154,155</sup> has been done on fabrication nanoscale oxide powders by hydrothermal processing. The obtained powders and their properties are listed in Table 1. Powders such as  $\text{SnO}_2$ ,  $\text{In}_2\text{O}_3$ , ATO, ITO and  $\text{TiO}_2$  can be redispersed to the primary particle size and can be produced on the pilot scale.

**Table 1** INM nanopowders fabricated by hydrothermal processing

Powder	Primary particle size (nm)	Dopants (mol%)	Redisperitivity to primary particle size
$\text{SnO}_2$	3 – 5		completely
$\text{In}_2\text{O}_3$	10 - 30		completely
$\text{Y}_2\text{O}_3$	10 -20	$\text{Eu}^{3+}$ , 0 - 3	no data available
$\alpha\text{-Al}_2\text{O}_3$	60		not yet completely
$\text{TiO}_2$	5 - 50	$\text{Al}^{3+}$ , 0.5	completely
$\text{In}_2\text{O}_3\text{:Sn}$ (ITO)	10 - 30	$\text{Sn}^{4+}$ , 1 - 10	completely
$\text{SnO}_2\text{:Sb}$ (ATO)	3 - 5	$\text{Sb}^{3+}$ , 0 - 10	completely
PZT	10 - 20		not yet completely
Hydroxy apatite (HAP)	5 - 30		not yet completely
$\text{BaTiO}_3$	50 - 100		no data available
Talcum	x, y: 500 z: 5 - 10		not yet completely

It can be discovered from the literature that most of the multicomponent powders are synthesized at a temperature ranging from 150 to 300°C, while the pressure varies from 1 to 170 bar and the reaction time from 0.5 hours to 7 days. It is worth noticing that some experiments are performed even at a temperature lower than 100°C. Chien and his colleagues<sup>125</sup> reported the successful production of barium titanate powder via the hydrothermal route at 90°C and ambient pressure. Vivekanadan et al<sup>133</sup> synthesized fine powders of Ba(Ti, Zr)O<sub>3</sub> at a hydrothermal temperature ranging from 85 to 130°C. The particle size of the prepared multicomponent powders varies from several nanometers to several micrometers with different morphology (sphere, cubic, needle, angular or other forms).

The physical and chemical properties of water and aqueous solutions in the pressure and temperature ranges required for hydrothermal syntheses are well investigated. These are described in several reviews<sup>156,157,158,159,160</sup>. The study<sup>156</sup> shows that the viscosity of water decreases with temperature, hence the mobility of molecules and ions in the hydrothermal conditions<sup>157</sup> is much higher than under normal conditions. The dielectric constant of water<sup>158</sup> decreases with rising temperature and increases with rising pressure, the temperature effect predominating. Electrolytes which are completely dissociated under normal condition will therefore tend to associate with rising temperature, and for a large number of substances this transition lies between 200°C and 500°C<sup>159</sup>. For experimental hydrothermal syntheses the pressure-temperature (PT) diagram of water<sup>160</sup> is important. The pressure prevailing under work conditions is determined by the degree of fill, i.e. by the volume of the reaction vessel that was originally filled with solvent. One factor to be considered in connection with syntheses is that the vapor pressure over aqueous solutions is in general less than that over pure water, and the critical point is shifted to higher temperatures.

The temperature of hydrothermal reaction is one of the most important parameters which control the composition of the products and their particle size. Morey<sup>96</sup> found that the rate of increase in solubility of quartz increased with the temperature, and only a sufficiently larger solubility could cause the formation of quartz veins. In the preparation of TiO<sub>2</sub> powder Kutty and Vivekanadan<sup>120</sup> found that an amorphous phase appeared at temperatures ranging from 110 to 150°C whereas a rutile phase at 160 to 230°C. Variation in the amount of anatase and rutile in products with temperature was also observed by Somiya<sup>100</sup>. In general, the particle size or the crystallite size becomes larger with the increase in temperature<sup>110,111,114,116</sup>. Sato and his colleagues<sup>128</sup>, however, found that the mean particle sizes obtained in the preparation of PbTiO<sub>3</sub> powder decreased with the increase in reaction temperature.

To form the desired crystal phases the reactants must be kept under the hydrothermal condition for a definite time<sup>120,121</sup>. The duration under hydrothermal conditions also affects the particle size of the resulting products. The longer the reactants are treated, the larger the synthesized particles are<sup>110,116,128,161</sup>. In almost all cases of hydrothermal synthesis autogenous pressure is employed. No extra pressure is added. The reason may be that<sup>96</sup> the solubility of reactants is not determined by pressure but by the amount of water present.

### 2.4.3 Influence parameters

Many parameters of hydrothermal synthesis have been studied in order to obtain powders with high quality. Starting materials are found to affect the resulting product to a varying extent. To prepare ceramic powders the precursors usually used are hydroxide gels which are precipitated from the reaction between metal chloride (e.g.  $\text{TiCl}_4$ ) or oxychloride (e.g.  $\text{ZrOCl}_2$ ) by ammonia<sup>155,112,117,120,122,126</sup>. Oxide<sup>125</sup>, metal alkoxide<sup>108,130</sup> and other chemicals have also been used<sup>113,128</sup>. Cheng et al<sup>113</sup> found that as a starting material  $\text{ZrO}(\text{NO}_3)_2$ ,  $\text{Zr}(\text{OH})_2$  or  $\text{ZrOCl}_2$  has no effect on the product, the results are almost the same and therefore anions have no obvious effect on the formation of the  $\text{ZrO}_2$  phase. However, Dutta and his colleagues<sup>124</sup> found that in the preparation of  $\text{BaTiO}_3$  powders presence of anions in the reactants composition influences the particle size and phase content of the product in the following order:  $\text{I}^- \sim \text{Br}^- \sim \text{Cl}^- > \text{acetate} > \text{NO}_3^- > \text{OH}^-$ . Many studies<sup>112,162,163,164,165,166</sup> indicate that the starting material ratio is an important parameter to control the composition, morphology and particle size of the multicomponent oxides. For example, a high Ba to Ti ratio can result in smaller particle size of  $\text{BaTiO}_3$ <sup>165</sup> but can increase the degree of aggregation<sup>165,166</sup>. Furthermore, different concentrations of the starting materials will also result in different particle size of the prepared powders<sup>116,128,167</sup>. No crystalline  $\text{BaTiO}_3$  powder is obtained when the  $\text{Ba}(\text{OH})_2$  concentration is less than 0.02 M<sup>165</sup>. Hirano and Kato<sup>114</sup> reported that the valence of the raw material also affects the crystallinity and crystallite size of the products.

For hydrothermal reactions a minimum solubility of 2 to 5% for the least soluble component is necessary, which is usually not obtained in pure water<sup>168</sup>. Therefore, components that are named in geology as mineralizers such as acids, bases, or other complex forming substances are added to improve the solubility of the precursor in the media and to promote the crystallization. Addition of  $\text{CaCl}_2$  favors the formation of the cubic  $\text{ZrO}_2$  phase and decreases the particle size<sup>113</sup>. Similarly, urea instead of ammonia can lead to the building of the pure phase of  $\text{ZrO}_2$ <sup>110</sup>. In contrast to this,  $\text{NH}_3$  addition in synthesis of hydroxyapatite does not promote the reacting rate as expected<sup>169</sup>. Alkalis have been found to catalyze thermal synthesis of some perovskite-type metal oxides<sup>170</sup>. Sato et al<sup>128</sup> studied the effectiveness of  $\text{LiOH}$ ,  $\text{NaOH}$ ,  $\text{KOH}$  and ammonia for the synthesis of  $\text{PbTiO}_3$ , and confirmed that  $\text{PbTiO}_3$  was synthesized catalytically by the strong alkalis as well. Beal<sup>131</sup> has systematically studied the effect of mineralizers on the synthesis of lead zirconate titanate and concluded that mineralizer selection determined purity and concentration determined morphology of the powders. Of the evaluated mineralizers, fluorides have the most significant effect on crystallite size, growth rate and retained mineralizer. Abe and Matsumoto<sup>118</sup> obtained variously shaped  $\alpha\text{-Fe}_2\text{O}_3$  by using different mineralizers.

Surfactant adsorbed on the surface of the particles can decrease the Gibbs free energy of the system, which leads to a monodispersed state of the particles when the Gibbs free energy reaches the minimum value. This is a very useful technique to prevent agglomeration<sup>171</sup>. Tween-80 (polyoxethylene(20) sorbitate) and  $\beta$ -alanine are proved to be so effective that they produce a narrow size distribution of aluminum oxide with small particle sizes in the order of nanometers<sup>155</sup>. Similarly, PVA (polyvinyl alcohol) contributes to

the obvious decrease of the particle size by the preparation of  $\text{CaTiO}_3$ <sup>121</sup>,  $\text{BaSn}(\text{OH})_6$ <sup>56</sup> and  $\text{Ba}(\text{Ti,Zr})\text{O}_3$ <sup>133</sup> and also influences the morphology of the particles. PVA has nevertheless a negative effect<sup>128</sup> on the synthesis of fine  $\text{PbTiO}_3$  powders, which leads to the formation of impurity phase. PAAm (polyacrylamide) as an alternative surfactant decreases the particle size and narrows the size contribution.

Normally the hydrothermal reaction takes place in the aqueous medium, there are a great number of nonaqueous solvents which also come into consideration for preparative purposes. Although nonaqueous solvents (with the exception of ammonia) have attained little significance for solvothermal transformations, they can be considered in cases in which the required solubility cannot be reached in an aqueous medium, in cases in which the solvent itself participates in the synthesis, and, most importantly, in cases where the reaction product reacts with water. Their critical temperatures and pressures are often lower than those of water<sup>104</sup>. The overall development relating to hydrothermal reactions in liquid ammonia (called ammonothermal synthesis) has been summarized by Jacobs and Schmidt<sup>172</sup>. It has been found<sup>165</sup> that the presence of hydrophilic solvent such as alcohol or acetone in preparing  $\text{BaTiO}_3$  can bring about a faster reaction because of their affinity to  $\text{H}_2\text{O}$ . Powders prepared in ethanol exhibited a more uniform particle size distribution. Isopropanol is thought<sup>173</sup> to be the optimal medium by way of completion of the reaction to prepare  $\text{SrTiO}_3$ . Since  $\text{Sr}(\text{OH})_2$  has limited solubility in pure isopropanol, various proportions of isopropanol and water used as solvent are investigated. Products of smaller particle size and low residual  $\text{H}_2\text{O}$  contents were obtained for higher propanol concentrations. Methanol or 2-methoxyethanol<sup>174</sup> also contributes to nanosized  $\text{PbTiO}_3$  particles exhibiting a lower agglomeration and a narrow size distribution. Replacing the solvent water by 1,5-pentandiol<sup>175</sup> has even reduced the particle size of the  $\alpha\text{-Al}_2\text{O}_3$  powder by more than a factor of 10.

For colloidal precursors, peptization can lead to a homogeneous dispersion of the particles and therefore improve the homogeneity of the product. Bacsá and Graetzel<sup>108</sup> studied the effect of peptization on the phase transformation of colloids precipitated from alkoxide. It has been found that the phase transformation of peptized samples depends on the size of the alkoxide ligand, the ethoxide yields a predominately rutile phase at 250°C and peptization promotes the formation of the nanocrystals.

Sharma et al<sup>155</sup> demonstrated that in the presence of  $\alpha\text{-Al}_2\text{O}_3$  seeds the physical properties of synthesized  $\alpha\text{-Al}_2\text{O}_3$  powders such as density, pore size and pore volume of powders were improved.

Microwave aided hydrothermal synthesis<sup>123</sup> can enhance the kinetics of crystallization of various ceramic oxides such as  $\text{TiO}_2$ ,  $\text{ZrO}_2$ ,  $\text{Fe}_2\text{O}_3$ ,  $\text{KNbO}_3$  and  $\text{BaTiO}_3$  by one or two orders of magnitude. The catalytic role of microwaves on the crystallization is assumed<sup>176</sup> to be the creation of localized high temperatures at the reaction sites which enhances reaction rates.

#### 2.4.4 Mechanism

It has been summarized<sup>103,177</sup> that the basic mechanism for the hydrothermal formation of ceramic oxide particles is the dissolution and precipitation mechanism. As precursors

(normally oxides or hydroxides, or component oxides) are heated, their solubility increases. Eventually, a sufficient concentration of the components exists in solution to begin formation of a more stable oxide phase. The driving force in these reactions is the difference in solubility of the oxide phase from the least soluble precursor or intermediate. However, very few data are available in the literature to predict the solubility and hence formation of oxides under hydrothermal conditions. The reported hydrothermal solubility and thermodynamic data<sup>178,179</sup> are limited to some ceramic systems only. On the basis of these data a thermodynamic model of hydrothermal synthesis of ceramic powders such as barium titanate and lead titanate<sup>178</sup> has been built.

As far as the nucleation and growth of the ceramic powder is concerned, different suggestions are given in the literature. Matigevic<sup>180</sup> assumes that hydrothermal precipitation of particles from solutions at elevated temperatures and pressures is a homogeneous nucleation and growth process. Nucleation occurs in one burst at a critical supersaturation concentration and particle growth takes place by diffusion of soluble species to the nuclei. An intermediate soluble species prior to precipitation is formed before precipitation and it is these soluble species that are precursors to nuclei and affect particle growth.

Chien and his colleagues<sup>125</sup> assume that BaTiO<sub>3</sub> heterogeneously nucleates on the TiO<sub>2</sub> particles, and that the crystal grows by a ledge mechanism. Because of the difference in solubility between TiO<sub>2</sub> and BaTiO<sub>3</sub>, inward diffusion of the Ti<sup>4+</sup>-bearing species and outward diffusion of the excess Ba<sup>2+</sup> to the ledges of the interface will cause the interfacial roughness. The diffusion transport of species then becomes easier at protruding points and more difficult at the reentrant nodes, magnifying the instability until the effect is counteracted by capillarity or changes in the solute field.

Kerncher et al<sup>126</sup> assume that BaTiO<sub>3</sub> nucleates heterogeneously on the anatase particles via a dissolution and recrystallization process and grows at the expense of the neighboring anatase. Due to relatively high solubility of Ba<sup>2+</sup> ions, the Ba<sup>2+</sup> species cover the entire surface of the TiO<sub>2</sub> throughout the reaction. The Ti-O-Ti bonds in the highly cross-linked network break and undergo rearrangement which permits chemical interaction between the TiO<sub>2</sub>(s) and Ba<sup>2+</sup>(aq). Local nucleation and initial growth result from Ba<sup>2+</sup> incorporation to the nuclei lattice. Later growth occurs via aggregation with unstable smaller BaTiO<sub>3</sub> primary crystallite clusters.

Kutty and his colleagues<sup>121,133</sup> also think that the crystallites have been produced through heterogeneous nucleation and growth in the case of using the hydrous gel as precursor. They point out that alkaline ions enter the gel in the formation of titanate, which produces chemical changes involving the cleaving of Ti-O-Ti bridging bonds accompanied by dehydration and dehydroxylation, leading to heterogeneous nucleation within the gel. This thought later develops into the gel-crystallite (G-C) conversion mechanism<sup>165,166,181</sup>. According to this theory the metal hydroxide gels are in general polymeric chains forming an entangled network, in which the solvent is entrapped, ionic pressure resulting from the faster migration of ions such as Ba<sup>2+</sup> through the solvent cavities within the gel framework leads to the instability of the metal hydroxide gel. Thus de-olation of the bridging groups such as Ti-OH-Ti and Ti-O-Ti takes place, followed by oxolation, leading to the formation of



corner-sharing octahedra  $[\text{TiO}_6]$  which are charge compensated by metal alkali ions such as  $\text{Ba}^{2+}$ .

## 2.5 Surface modification for synthesis of nanoscaled powder

Nanocrystalline materials, which have a very high surface or interfacial area, exhibit dramatic changes in properties<sup>182</sup>, such as enhanced sinter ability at low temperatures, very high hardness and wear resistance, enhanced gas sensitivity, superior magnetic and dielectric strength, and enhanced optoelectric properties. Nanoparticles are suited to the fabrication of new types of ceramic membranes<sup>183</sup>, as well as coatings and composites<sup>184</sup> in applications such as high performance cutting tools, high surface area supports for catalysts and chemical gas sensors<sup>185</sup>.

Wet chemical preparations of ceramic nanosized powders often involve the generation of supersaturated conditions in a liquid followed by precipitation of a solid particulate phase. In this case, a nucleation step is necessary to initiate precipitation. The nucleation rate<sup>171</sup> depends on the free energy of the nucleation step (for overcoming the critical radius for nucleation) and the free energy for the diffusion, which is a function of the temperature, medium and size of the dissolved components to be deposited. Similarly the growth rate of particles after the nucleation depends on the free energy of condensation or crystallization. In this case, the surface free energy of the growing particle becomes extremely important. One model suggests<sup>186</sup> that the surface free energy of the system should reach its minimum when the particles of the powder are in the monodispersed state. It is of interest to regulate the growth process through the control of the surface free energy and thereafter to avoid or minimize agglomeration.

The most useful method to adjust the surface free energy is the addition of surfactants that will be adsorbed on the surface of particles. It is well known that agglomeration of the particles arises from interparticle attractive forces. Attractive forces include short-range forces (hydrogen bonding, acid/base interaction, etc.) and long-range Van der Waals forces. The surfactant which aids in keeping particles from agglomerating is added to prevent the particles from interacting through short-range forces. After the surfactant is adsorbed on the surface of the particles, the interaction between particles is controlled by Van der Waals forces only. Van der Waals forces are much weaker compared to short-range forces, so the particles can be easily redispersed in suitable solvents even after drying.

The major characteristic of a surfactant in a liquid is that it is at higher concentration at the surface than in the bulk of the liquid. The presence of a surfactant at the surface increases the compatibility and reduces the surface energy of the particle in a liquid. A surfactant molecule normally consists of a hydrophilic head and a lipophilic tail. The water-soluble head is often a small ionic (or polar or hydrogen-bonding) group while the oil-soluble tail a hydrocarbon chain. To minimize the size of the contacting zone between hydrophilic head and hydrophobic tail, the hydrophobic part will be repelled from the water and the hydrophilic part orientates toward the polar solvent. The spherical assemblies formed in this way are known as micelles, where the interior of the micelle resembles a hydrocarbon

separate phase. The most basic surface active properties of a surfactant are the critical micelle concentration (CMC) and its surface tension. The concentration at which micelles first form is defined as CMC. The addition of the surfactant causes a decrease in surface tension, and when surfactant concentration is over CMC the surface tension becomes constant or nearly constant. Another characteristic parameter of the surfactant is the value of HLB (hydrophilic - lipophilic balance), which is a measure of the affinity of a surfactant to aqueous phase compared to an oil phase. The maximum HLB number is 20 and represents a completely water soluble surfactant. An HLB of 0 to 9 indicates the hydrophobic and an value of 11 to 20 the hydrophilic property of the surfactant<sup>187,188,189,190</sup>.

Based on the chemical structure of the hydrophilic head, surfactants can be generally classified in anionic, cationic and non-ionic types. The ionic surfactants show their surface modifying effect through the interactions of the layers of adsorbed surface ions. The repulsive forces resulting from the interaction of the same charge between the particles will counteract the attractive interaction forces which cause the agglomeration of particles. On the other hand, the non-ionic surfactants, especially polymer surfactants, give rise to a steric interaction by surface modification. Steric interaction forces result from interaction of the absorbed long-chain groups and can be either attractive or repulsive, depending to a large extent part on the compatibility among solvent, functional group, and particle in the system considered. A sufficiently high repulsive steric interaction with respect to Van der Waals forces can prevent the agglomeration of particles and lead to the formation of monodispersed powder<sup>191</sup>.

As noted in section 2.4.3, some nanoscaled powders have been prepared by combination of hydrothermal synthesis and surface modification. This is called "controlled growth process". There are also many nanosized powders which have been synthesized by using surface modification and other wet chemical synthesis methods. A typical example is microemulsion method which uses interfacial free energy as a tool. There are many reviews<sup>192,193,194</sup> concerning this subject and the yield rate of the microemulsion process is especially low, therefore no description will be given here.

## 2.6 Doped barium stannate

Barium stannate behaves as a pure, n-type semiconductor below 900°C<sup>40</sup>. The measured band gap of BaSnO<sub>3</sub> is 3.4 eV<sup>195</sup>. The behavior of semiconducting oxide material can be manipulated<sup>196,197</sup> by manipulation of the crystallite size and specific surface area of the material exposed to the gas, and of the concentration of electrically active donor species present in the lattice, so as to give changes characteristic either of n-type materials (resistance decreases in reducing gases and increases in oxidizing gases), or of p-type materials (resistance increases in reducing gases and decreases in oxidizing gases), or of mixed behavior. By a fortuitous combination of the concentration of electrically active donors and the specific surface area, some selectivity to certain gases might be obtained. In the light of these discoveries, it is possible to try substituting elements of different valence into some parent composition, and to try making variations in the preparation of materials so as to obtain different specific surface areas, in an attempt to achieve a degree of selectivity.

It will be appreciated, especially from the study of the art of catalysis, that substitutions of different elements in a lattice can serve to vary the surface density and nature of the gas adsorption sites present on the surface of the material. To obtain desired properties, some ions that are designed to substitute for either the Sn site or the Ba site have been doped in barium stannate.

Among these doping ions antimony is used to substitute for the Sn site because of the similarity of their ionic radii and electronic configuration. By studying the solid-state reaction in a BaO-SnO<sub>2</sub>-Sb<sub>2</sub>O<sub>3</sub> system Yan and Li<sup>198</sup> have found that below the synthesizing temperature of 1000°C, there exists a SnO<sub>2</sub>-Sb<sub>2</sub>O<sub>3</sub> solid solution in the form of Sn<sub>1-x</sub>Sb<sub>x</sub>O<sub>2</sub>. However, at the synthesizing temperature 1000°C, a large amount of BaSnO<sub>3</sub> phase rather than Ba<sub>2</sub>SnO<sub>4</sub> phase is observed. This result is different from those reported for the BaO-SnO<sub>2</sub> system. Above 1000°C, the speed of formation of the BaSnO<sub>3</sub> phase depends on the decomposition of BaCO<sub>3</sub> and diffusion of Ba<sup>2+</sup> ions. Following the decomposition of BaCO<sub>3</sub>, Ba<sup>2+</sup> ions immediately enter into reaction with Sn<sub>1-x</sub>Sb<sub>x</sub>O<sub>2</sub>, and form Ba(Sn<sub>1-x</sub>Sb<sub>x</sub>)O<sub>3</sub>. The content of BaSnO<sub>3</sub> phase increases with the synthesizing temperature. The studies on the surface electronic structure<sup>199</sup> and Moessbauer spectra<sup>200</sup> of antimony doped barium stannate show that doped Sb is present in BaSnO<sub>3</sub> only in the form of Sb<sup>5+</sup> ions. This result is also confirmed by Claessen et al<sup>201</sup> with the help of photoemission and bremsstrahlung isochromat spectroscopy. They suggested therefore that the electrons introduced by the Sb doping occupy the lowest-lying Sn-5s derived conduction band states. By studying the occurrence of superconductivity in BaSn<sub>1-x</sub>Sb<sub>x</sub>O<sub>3</sub> perovskite, Cava et al<sup>202</sup> found that the BaSn<sub>1-x</sub>Sb<sub>x</sub>O<sub>3</sub> perovskite solid solution only exists for 0 ≤ x ≤ 0.2. The best electrical conductivity occurs for x near 0.15, which is much larger than the value reported by Lu et al (0.02)<sup>203</sup>. The experimental results of Herrmann et al<sup>204</sup> reconcile with those of Cava et al. Sb dissolves in the stannic sites of the stannate perovskite structure up to a mole fraction of 0.17 in pentavalent state (Sb<sup>5+</sup>). The conduction activation energies decrease from 134 kJ/mol for pure BaSnO<sub>3</sub> to 39.8 kJ/mol for x = 0.15 and increase then with the further increase in doping amount. An insulation second solid phase Ba<sub>2</sub>Sb<sub>2</sub>O<sub>7</sub> appears when x is about 0.17 and causes a decrease in electrical conductivity. Oxygen has a slight influence on the conductivity S of the doped perovskites for x ranging from 0.05 to 0.40 with the relation: S = kP(O<sub>2</sub>)<sup>-1/n</sup>, n ≈ 8, while for pure barium stannate it is independent of oxygen partial pressure P(O<sub>2</sub>). Antimony doped barium stannate is sensitive to CO<sub>2</sub><sup>12,205</sup> and has been used by McGeehin et al<sup>14</sup> to prepare a carbon dioxide sensor which is suitable for detecting low concentrations of CO<sub>2</sub> (up to 5%). This kind of sensor with general formula BaSn<sub>1-x</sub>Sb<sub>x</sub>O<sub>3</sub> (0 < x < 0.1) is operated at a working temperature (300°C) at which its resistance is measured to detect the presence of CO<sub>2</sub>. Another possible application of antimony doped barium stannate as thermistor with linear negative temperature coefficient has been reported recently<sup>206</sup>. In all the above cases antimony is imported by adding the Sb<sub>2</sub>O<sub>3</sub> and the corresponding semiconducting oxide is prepared via solid state reaction at temperatures above 1000°C.

Another doping ion which can be used for substitution for Sn<sup>4+</sup> is Pr<sup>4+</sup>. The electronic configuration of the tetravalent praseodymium ion is [Xe]4f<sup>1</sup>, which can make the electronic structure analysis simple, so Pr<sup>4+</sup> ion doped BaSnO<sub>3</sub> has also been studied<sup>207,208,209,210</sup>. The

results show that the  $\text{Pr}^{4+}$  doping ions are incorporated into the  $\text{Sn}^{4+}$  site and have a large effect on the octahedral crystal field of  $[\text{SnO}_6]$ . However there is no report about how the dopant affects the properties of  $\text{BaSnO}_3$ .

The doping effect of iron ions on Sn site has been investigated by Roh et al<sup>211</sup>. The solid solutions of  $\text{BaSn}_{1-x}\text{FeO}_{3-y}$  are formed in the whole range of  $x = 0$  to 1. The Fe ions substituted for Sn ions could have the mixed valence states of  $\text{Fe}^{3+}$  and  $\text{Fe}^{4+}$ . The formation of  $\text{Fe}^{4+}$  ions begins at  $x = 0.50$ , which is identified by the potentiometric titration and the Moessbauer resonance spectra.

Lanthanum has been found<sup>212</sup> to be able to substitute for barium in  $\text{BaSnO}_3$  crystal. A solid solution  $\text{Ba}_{1-x}\text{La}_x\text{SnO}_3$  with a perovskite structure exists only for  $x \leq 0.02$ . The temperature dependence of the electric resistance reveals the semiconductor behavior of the solid solution when the dopant amount ( $x$ ) is above 0.0025. The  $\text{La}^{2+}$  doped  $\text{BaSnO}_3$  can be used as gas<sup>12,37</sup> and humidity<sup>40</sup> sensing materials. Bogatina<sup>213</sup> studied the effect of doped ions such as  $\text{La}^{3+}$ ,  $\text{Sm}^{3+}$ ,  $\text{Nb}^{5+}$ ,  $\text{Ta}^{5+}$  and  $\text{Bi}^{3+}$  on the electric resistance and the permittivity of  $\text{BaSnO}_3$  ceramics containing 1 wt%  $\text{SiO}_2$  with a dopant content from 0.05 to 5 at.%. With increasing content, electric resistance smoothly decreases and permittivity increases. The introduced trivalent and pentavalent ions occupy in general sites in the Ba and Sn sublattices respectively.

The synthesis and the fluorescence of europium-doped barium stannates are also reported<sup>214</sup>.  $\text{Eu}^{3+}$  doped  $\text{BaSnO}_3$  belongs to the cubic system. The excited and emission spectra of the phosphors show that the energy of the charge transfer transition for  $\text{Eu}^{3+}$  shifts to the blue, and the energy of the f-f transition for  $\text{Eu}^{3+}$  shifts to the red. Its phosphors show a major magnetic dipole transition.

Small amount of noble metals such as Pt, Pd, Rh, Ru and Ag were also directly doped to barium stannate to prepare a semiconductor gas sensor<sup>215</sup>. Study of the gas sensing behavior of these materials to various reducing gases such as CO and  $\text{CH}_4$  indicates that the addition of these noble metal promotes not only the gas sensitivity but also improves the rate of response.

To sum up it can be said that barium stannate is of technological importance, either as a dielectric material or as a gas sensing material. However it has not been as thoroughly and systematically studied as other typical perovskite structure ceramic powders such as barium titanate. For example, no sound and reliable data is available on thermodynamic stability of this compound. Moreover, any information on processing and evolution of microstructure in this material and their impact on the electrical characteristics is also lacking in the literature. The traditional solid state reaction route for preparing  $\text{BaSnO}_3$  powders needs high calcining temperatures which lead normally to powders of relatively large and varied grain sizes. There are also problems obtaining phase-pure material because of the intermediate formation of the phase  $\text{Ba}_2\text{SnO}_4$  during the  $\text{BaSnO}_3$  synthesis. Furthermore, the powders prepared via state solid reaction are very difficult to sinter.

To overcome these shortcomings some new synthesis methods are being developed. By using the sol-gel method in forming a citric complex the synthesis temperature can be obviously lowered, but it is still relatively high (600 - 1000°C). Only hydrothermal synthesis and LTAS route show low synthesis temperatures at 260°C and 270°C respectively, but the

resulting powders are constituted of aggregated particles which result in the low specific surface area of the powders. No attempts to prepare nanocrystalline or nanoscaled  $\text{BaSnO}_3$  powders have been reported in the literature to date.

However, experiments in synthesizing other multicomponent, nanoscaled ceramic powders have shown the advantages of the metal alkoxide route and hydrothermal synthesis, and could therefore be used for synthesis of nanocrystalline  $\text{BaSnO}_3$  powder. Different Ba or Sn bimetallic alkoxides have been successfully synthesized via three different methods. Double metal alkoxide precursors will guarantee the homogeneity of the end-product and offer the possibility to manipulate its properties on the molecular level. In the processing one important issue that needs to be solved is the control of the hydrolysis and condensation rate. As for hydrothermal synthesis, the low synthesis temperature makes the aggregation and agglomeration avoidable or minimizes it, especially when combined with the surface modification techniques which can tailor the particle size through controlling the surface free energy and particle growth. The optimizing of hydrothermal conditions is the key to a successful powder synthesis. Equally important is the choice of a useful surfactant in the surface modification.

Doping is a useful tool for improving the electrical conductivity of barium stannate oriented toward gas sensing. Antimony as dopant has been proved effective in  $\text{BaSnO}_3$  prepared via the solid state route through the building of a solid solution with  $\text{BaSnO}_3$ .

### 3. Objective

The aim of this investigation is to develop a synthesis route for preparing nanocrystalline  $\text{BaSnO}_3$  powders. The properties of the prepared powder such as high purity, large surface area and narrow size distribution are of importance, because the powders will be used as the starting material for fabricating a gas sensitive device which is intended to detect gas through a surface reaction process. The solid state route is the only one that has been reported to support this application up to now, but it has many drawbacks. The main drawback lies in the high calcining temperature that leads to the growth of particles and low specific surface area.

The optimal synthesis of nanocrystalline barium stannate powder should therefore be carried out at low synthesizing temperature. The only routes worthy of consideration which have been used to prepare barium stannate powders are low-temperature aqueous synthesis (LTAS) and hydrothermal synthesis, according to the literature review. The metal alkoxide route has shown its advantages in the synthesis of multicomponent oxides through controlling the reaction on the molecular level, though this route has not been attempted to prepare  $\text{BaSnO}_3$  in the literature to date. It is hoped that a suitable route among those will be found for synthesizing nanocrystalline powder.

In the following research the conditions for synthesizing the precursor should be optimized. The important parameters include the ratio and the concentrations of starting materials, medium, pH value and reaction temperature. A good precursor should be homogeneous and highly reactive.

Study of the crystallization behavior of the precursor is expected to modify the constitution and the particle size of the powder. Another measure to control the particle size, to decrease the agglomeration and aggregation, and to increase the specific surface area is to import surfactants into the system for an in situ surface modification. The surfactant must be stable under the reaction conditions (pH value, temperature, pressure) in order to guarantee the effect of surface modification and the subsequent redispersion of the particles. The powders obtained should be characterized by different means (e.g. XRD, TEM, BET, UPA) under the following aspects:

- Phase constitution
- Specific surface area
- Particle size / crystallite size
- Microstructure / agglomeration

After the successful synthesis of nanocrystalline  $\text{BaSnO}_3$  powder the next target is to dope the powders with antimony ions so as to improve the electrical properties, which is the key for fabrication of a gas sensor device. What remains to be investigated is the integration of doping element in the crystal phase, the effect of doping contents and the electrical properties of the doping barium stannate.

## 4. Experimental procedure

Three synthesis methods including the low-temperature aqueous synthesis route (LTAS), the metal alkoxide route and the hydrothermal synthesis route were employed to prepare barium stannate powders. The synthesis processes and the analytical techniques for characterizing the precursor and the prepared powders are described in this chapter. The chemicals and instruments used are listed in the appendices.

As the most suitable route, hydrothermal synthesis has been studied systematically and in detail. In the process tin oxide gel as precursor was first synthesized. Peptization of the tin oxide gel was carried out through addition of ammonia solution. Surfactants were imported for surface modification during the synthesis of  $\text{BaSnO}_3$  powder. These two measures were designed to control the particle size and limit the agglomeration and aggregation. Antimony was used as doped ion and the doped barium stannate powders were also prepared.

### 4.1 Synthesis of $\text{BaSnO}_3$ via the low-temperature aqueous synthesis route

0.2M  $\text{Ba}(\text{OH})_2$  solution was kept at  $85^\circ\text{C}$  in a water bath while excess 25% ammonia solution or 4M NaOH solution was added to maintain a sufficiently high pH ( $\text{pH}>14$ ). White precipitates were formed immediately after the dropwise addition of 1M  $\text{SnCl}_4$  solution. The mixture was either stirred continuously for 24 hours at reflux temperature or hydrothermally treated in a 250 ml teflon-lined autoclave at  $250^\circ\text{C}$  for 6 hours. Desiccated Argon as the protecting gas flowed through the system throughout the process to minimize the carbonation. The centrifuged precipitates or hydrothermal educts were washed 4 to 6 times with distilled water until the pH value was near 7 and then dried at  $120^\circ\text{C}$  for 24 hours. The dried precipitate was calcined at  $300^\circ\text{C}$  for 4 hours. The obtained powders were characterized with x-ray diffraction analysis. Fig. 4 shows the whole process.

### 4.2 Preparation of $\text{BaSnO}_3$ Powder via metal alkoxide route

#### 4.2.1 Synthesis of precursor $\text{BaSn}(\text{OR})_6$

Transparent barium alkoxide solutions were prepared either by adding metallic barium to distilled alcohol (ethanol or isopropanol) at  $90^\circ\text{C}$  under reflux conditions for 24 hours or by dissolving the commercial barium(II) isopropoxide in isopropanol. The corresponding tin and barium alkoxide solutions were then mixed. The molar ratio of Ba:Sn was kept at 1. The mixture could be transparent only when a stabilizer such as distilled diethylamine (DEA) alcoholic solution was added. It was heated at  $90^\circ\text{C}$  under reflux conditions for 24 hours. The resulting solution was used as a precursor which was assumed to have a stoichiometric constitution of  $\text{BaSn}(\text{OR})_6$  ( $\text{R} = \text{C}_2\text{H}_5$  or  $\text{C}_3\text{H}_7$ ). In the whole process desiccated argon was used as protecting gas. The synthesizing process is shown in Fig. 5. For characterization

the precursor no stabilizer was added. The precipitates were filtered, washed 2 times with alcohol and then dried in a vacuum furnace at 60°C.

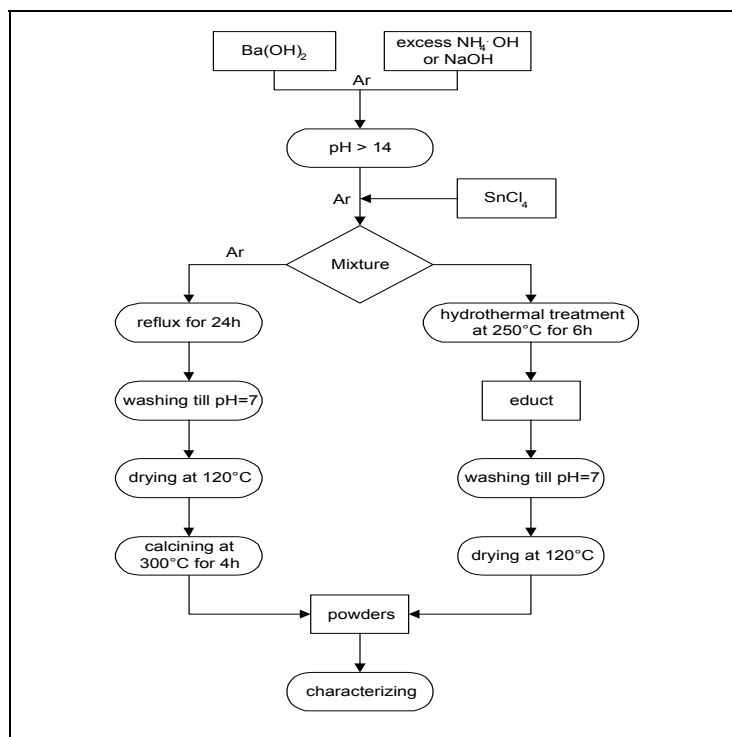


**Fig. 4** Flow chart of low-temperature aqueous synthesis.

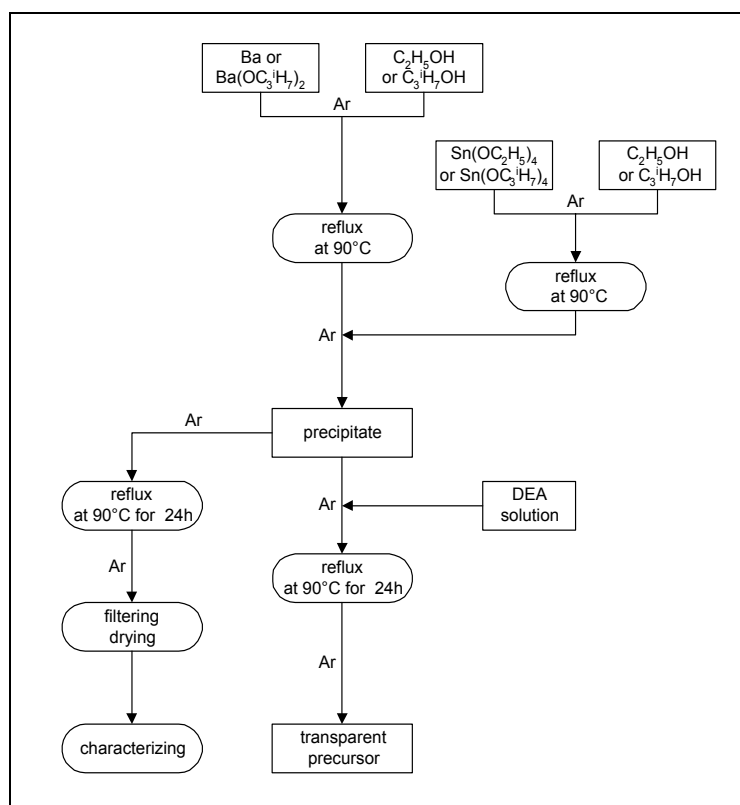


**Fig. 5** Flow chart of synthesis of the precursor BaSn(OR)<sub>6</sub>.



### 4.2.2 Hydrolysis

Water was added dropwise to the precursor under vigorous stirring to hydrolyze the precursor. The molar ratio of water to the precursor varied from 6 to 500. The pH value of the solution was kept at 8 to 9 by addition of 25% aqueous ammonia solution. Water in ammonia solution was included by calculation of the molar ratio of water to metal alkoxide. After being heated at 90°C for one day under stirring a milky product was formed. The whole process was carried out by using argon as the protecting gas to avoid the adsorption of CO<sub>2</sub> from the atmosphere which leads to the formation of barium carbonate.

### 4.2.3 Calcination

#### Conventional calcination

The hydrolyzed products were washed with ethanol 2 - 3 times and then evaporated under reduced pressure to remove the solvent. The obtained powder was dried in a vacuum furnace at 60°C for 2 to 3 days. The dried powders were calcined in an oven at a temperature between 300 and 800°C for 6 hours with a heating rate of 2°C/min.

#### Hydrothermal calcination

In hydrothermal calcination the mixture of hydrolyzed products was put into a 250 ml teflon beaker which was placed in an autoclave. To remove the CO<sub>2</sub> the beaker was washed with nitrogen gas several times. The reaction lasted for 6 hours at 250°C under autogenous pressure. The temperature referred to here is the temperature of the autoclave mantle not that of the beaker. The educts were washed with ethanol two times and then with water 3 - 4 times to remove ions and organic parts. The drying process was carried out in a vacuum furnace at 60°C for 2 to 3 days.

## 4.3 Hydrothermal synthesis of BaSnO<sub>3</sub>

### 4.3.1 Synthesis of SnO<sub>2</sub>·xH<sub>2</sub>O

#### SnO<sub>2</sub>·xH<sub>2</sub>O gel

Aqueous 25% ammonia solution was added to 1M SnCl<sub>4</sub> solution. When the amount of added ammonia reached a certain level, precipitation occurred. Further addition of ammonia led to the gelation of the mixture, which was subsequently crushed into a milky solution by stirring. After aging 0.5 to 2 hours the obtained mixture was centrifuged and washed with distilled water several times until its electric conductivity was less than 50 μS/cm.

### **Peptization of $\text{SnO}_2 \cdot x\text{H}_2\text{O}$ gel**

The washed gel was diluted by distilled water and then a small quantity of 25% ammonia solution was added. The mixture was stirred slowly for 2 to 24 hours at room temperature until a transparent solution was obtained.

### **Surfactant modified $\text{SnO}_2 \cdot x\text{H}_2\text{O}$**

During synthesis of the  $\text{SnO}_2 \cdot x\text{H}_2\text{O}$  gel a surfactant such as Tween 80 was added to ammonia and  $\text{SnCl}_4$  solution with the same concentration respectively. To modify the peptized  $\text{SnO}_2 \cdot x\text{H}_2\text{O}$ , the surfactant was added with the same concentration during both synthesis and peptization.

### **Antimony doped $\text{SnO}_2 \cdot x\text{H}_2\text{O}$**

$\text{SbCl}_3$  or  $\text{SbCl}_5$  was dissolved in ethanol and mixed with an ethanolic solution of tin tetrachloride and the modifier. Ammonia was then added to them. The obtained gel was peptized as above described.

### **4.3.2 $\text{SnO}_2 \cdot x\text{H}_2\text{O}$ suspended with barium hydroxide**

The  $\text{SnO}_2 \cdot x\text{H}_2\text{O}$  precursor or the antimony doped  $\text{SnO}_2 \cdot x\text{H}_2\text{O}$  was mixed with  $\text{Ba}(\text{OH})_2$  under vigorous stirring. In the case of modification, the same concentration of the surfactant was also added to  $\text{Ba}(\text{OH})_2$ . The percentage of the surfactant is the total weight of the added surfactant divided by that of theoretic prepared  $\text{BaSnO}_3$  powder. After mixing, a white suspension was formed which was treated ultrasonically for 10 minutes.

### **4.3.3 Hydrothermal treatment**

The suspension was charged in a teflon-lined autoclave (two types: 250 ml and 1l) if the reaction temperature is not more than  $250^\circ\text{C}$  or in a steel autoclave if the reaction temperature is above  $250^\circ\text{C}$ . It was then kept at the specified temperature for a given time. In using the 1l teflon-lined autoclave or the steel autoclave 5 to 10 bar pre-pressure of nitrogen gas was employed for protective purposes. After hydrothermal treatment the autoclave was cooled in the air to room temperature. The educts were taken out and washed with distilled water until their electric conductivity was less than  $50 \mu\text{S}/\text{cm}$ . A dry powder was obtained by placing the washed educt in a vacuum furnace at  $60^\circ\text{C}$  for 1 to 2 days. This powder was referred to as as-prepared powder.

#### 4.3.4 Calcination

The as-prepared powders were heated in an oven at a rate of 10°C/min to the calcining temperature for a certain time. The calcined powder was also called end-powder for purposes of distinction.

#### 4.3.5 Milling and redispersion of the end-powder

The milling experiments on the end-powder were carried out in a mortar mill. The pestle is made of corundum. 2.5 wt% TEA (triethyl amine) as a dispersant was added. The 25 wt% used solvent is the mixture of diethylen glycol - monobutyl ether and ethylen glycol (volume ratio = 1:1). The paste (72.5 wt% powder) was milled for 2 hours. For redispersion 5 wt% powder was suspended in the aqueous solution with a dispersion agent. The suspension was disintegrated ultrasonically for 30 minutes.

#### 4.3.6 Sintering of the powders and tape casting

Samples for the sintering were pellets with a dimension of about  $\Phi$  10 x 1 mm which were formed firstly by a uniaxial pressure of 400 MPa and then by a cold isostatic pressure of 800 MPa for 1 minute. The green body was heated to the sintering temperature at 10°C/min in air atmosphere and soaked for 4 hours.

For the tape casting to form the green compact, 60 wt% powder was dispersed with 3.5% TEA in water. The pH value of the suspension was adjusted with ammonia solution to 10. The suspension was then disintegrated ultrasonically for 10 minutes. Corresponding to the 80 solid wt% of BaSnO<sub>3</sub>, 5.5 wt% PVA M26-88 and 5.5% PVA M4-88 as binder and 4.6 wt% glycerin as plasticizer were added to the suspension. The resulting paste was cast on a plastic film to form a tape with a thickness of the wet film from 40 to 200  $\mu$ m. Thereafter the tape was dried in an oven at 80°C for about 10 minutes for the removal of the plastic film. The sintering experiment was carried out in a high temperature oven. The green tape placed on an Al<sub>2</sub>O<sub>3</sub> substrate was heated to 600°C at a rate of 1°C/min and then heated to 1500°C at a rate of 5°C/min. The soaking time at 1500°C was 10 hours.

### 4.4 Parameters measurement and materials characterization

#### 4.4.1 pH measurement

For the titration experiment a pH-meter with integrated temperature sensor was used because of the temperature variation resulting from the reaction heat. During measuring the solution was kept stirred. As for the colloidal solution the pH value was taken from the supernatant after the colloidal solution was centrifuged at 4000 rpm for 30 minutes. On the

one hand, the pH difference between colloidal solution and supernatant is very small, on the other hand, the colloidal particles can impair the accuracy of the pH meter.

#### **4.4.2 Surface tension measurement**

To compare the surface activity of the surfactants, the surface tension of their aqueous solutions was measured at 22°C by using the Wilhelmy-plate-method. The used plate is made of platinum. Each measure was repeated 10 times with a 10 second measure interval.

#### **4.4.3 Charge adsorption of particle surface**

##### **Zeta potentials**

Solid particles acquire a charge when placed in an electrolyte solution or polar medium because of selective adsorption of ions of the particle surface. The zeta potential is the potential due to the concentration of counter ions in the solution around the solid particle in order to achieve overall neutrality of the solution. The zeta potential of samples was measured with a Zetasizer (Malvern). The instrument works according to the principle of microelectrophoresis. Powders were dispersed ultrasonically in water to obtain a 5 wt% suspension. Zeta potentials of the suspension at different pH values from 3 to 10 were measured.

##### **Particle charge detector**

The charge amount of the adsorbed ions on the surface of particles was measured by the particle charge detector PCD02 (Mütek). The charge amount is characterized via current potential with a unit of millivolt. Because the potential depends on outside factors like electrical conduction of the sample dispersion as well as the viscosity of the sample, the measuring results are principally not reproducible and therefore express only the type of charge (cationic or anionic) and the relative amount of the charge during the titration. 10 ml 5 wt% suspension was placed in the measure cell and 1 wt% dispersant aqueous solution was titrated in it stepwise. The dependence of the potential on the amount of the dispersant was recorded.

#### **4.4.4 Density measurement**

The bulk density of the sintering ceramic was measured by the Archimedes method with water as the immersing media. For each sample three pellets were sintered under the same conditions and their density was averaged.

The density of powder samples was measured by a gas pycnometer. The sample was dried at 110°C for one day in a vacuum drying furnace before being measured. For each sample the measurement was repeated 5 times.

#### 4.4.5 Element analysis

For the chemical analysis, 50 mg powder samples were dissolved in 5 ml concentrated HCl at 140°C for 4 hours. The solution was diluted and analyzed using atomic emission spectroscopy with inductively coupled plasma (ICP-AES) for the determination of barium, tin and antimony. For chloride element analysis, 60 µl ISA-solution (ionic strength adjustment) was added to the supernatant of the SnO<sub>2</sub>·xH<sub>2</sub>O gel to keep a constant ionic strength.

#### 4.4.6 Molecular spectroscopy

##### Fourier transform infrared spectroscopy (FTIR)

FTIR spectra were recorded to obtain information regarding the structure of molecules and the structure change during heat treatment. 100 mg KBr pellets containing 1.5 mg sample were pressed under 600 MPa and measured via a Bruker FTIR spectrometer in the wavenumber range of 400 to 4000 cm<sup>-1</sup>.

##### Solid state <sup>119</sup>Sn nuclear magnetic resonance (<sup>119</sup>Sn NMR)

To compare the structure of barium stannate powders prepared via different routes, solid state <sup>119</sup>Sn NMR spectra of samples were recorded by using a Bruker AC 200 spectrometer (magnetic field strength: 4.7 T). The experiments were carried out by single pulse sequence with high power decoupling. Resonance frequency: 74.58 MHz, external reference: tetracyclohexyl tin (δ = -97.46 ppm), repetition time: 10s, number of scans: 1000 to 7000, magnetic angle spinning (MAS): 3 kHz.

#### 4.4.7 X-ray powder diffraction

X-ray powder diffraction (XRD) was used to identify the crystal phase of the prepared powder and determine the lattice constants. The samples were analyzed by a D500 model diffractometer (Siemens, radiation CuKα1) operating at 40 kV. The crystallite size was calculated from Scherrer equation<sup>216</sup>, which is only suitable for crystallite sizes less than 100 nm:

$$D = 0.89 \lambda / \beta \cos \theta, \quad \beta = (B^\alpha - b^\alpha)^{1/\alpha} \quad (20)$$

Where:

D: crystallite size; λ: wavelength of x-ray; θ: reflection angle; β: physical line width  
B: measured line width; b: apparatus line width; α: constant factor

For determining the lattice constant of the crystalline phase, the samples were analyzed by an X'Pert MRD diffractometer (Philips, C-monochromator). The operating conditions are: 40 kV, 50 mA; 2θ 0.01°/ step, 6 - 7 sec/step, continuous scan, divergence slit = 1°, mask 20 mm; anti-scatter slit 1°, receiving slit 0.6 mm.

#### 4.4.8 Thermal analysis

##### **Thermogravimetric analysis and differential thermal analysis (TG-DTA)**

40 to 70 mg dried samples were placed in Al<sub>2</sub>O<sub>3</sub> crucibles with pre-fired  $\alpha$ -Al<sub>2</sub>O<sub>3</sub> powders as reference and then heated from room temperature to 1400°C at a heating rate of 10°C/min in synthetic air atmosphere.

##### **TG-DTA coupling with mass spectrometry (TG-DTA-MS)**

A mass spectrometer (QMS420, Netzsch) was coupled with TG-DTA thermal analysis to detect the components of the sample released during thermal analysis. The sample was heated at a rate of 10°C/min to 1300°C in synthetic air atmosphere.

##### **Dilatometry**

The linear shrinkage of a pellet sample which was uniaxially pressed in a dimension of ca.  $\Phi$  5mm x 5 mm under 800 MPa was measured with a differential dilatometer (Linseis). The pellet was heated from room temperature to 1650°C at a rate of 10°C/min in air atmosphere. The temperature was held at 1650°C for 30 minutes.

#### 4.4.9 Microstructure analysis

##### **Scanning Electron Microscopy (SEM)**

The powder morphology was investigated with the help of a scanning electron microscope (JSM 6400F, JEOL). The secondary electron image was formed by exiting the sample with a primary electron beam under 10 kV accelerating voltage. To obtain a charge free surface imaging samples were sputtered with a gold film with the SCD 030 (Balzers) using a current of 25 mA for 40 seconds. For a quantitative element analysis, energy dispersive x-ray spectrometry was applied (EDX, Noran Instruments).

##### **Transmission Electron Microscopy (TEM)**

The structure and morphology of powders were studied with common TEM (JEM 200CX, JEOL) and high resolution TEM (HRTEM: CM 200 FEG, Philips) respectively. The powders were dispersed in water or ethanol with the help of an ultrasonic bath and then collected onto a carbon film mounted on electron microscope grids. Investigation was carried out at an accelerating voltage of 200 kV. Diffraction and scattering absorption contrasts, structure imaging and the selective area electron diffraction patterns were recorded.

#### 4.4.10 Particle size analysis

##### **Photon correlation spectroscopy (PCS)**

The average size of the peptized gel particles was measured with a photon correlation spectrometer (ALV5000D, ALV-Laser). The measurement principle was based on the

particle oscillation resulting from the Brownian motion of molecules. With an incident light in a solution where the molecules continuously move about, the light scattering intensity fluctuates about an average value. The rate of change of the scattered intensity becomes a measure of the rate of relative motion of particles in the solution. PCS characterizes these fluctuations with a correlation function that is calculated by a computer. The correlation function determines the diffusion coefficient of the particles which is used to calculate the average particle radius according to the Stokes-Einstein equation. The voltage used on the photon multiplier is 1.4 kV. The sample was diluted until the counts number lay in the range of 100 to 250 kHz. The measurement was carried out at an incident angle of  $60^\circ$  and repeated 3 times.

#### **Ultrafine particle analysis (UPA)**

The particle size distribution of powders was measured with a Grimm UPA 400 ultrafine particle analyzer. 5 wt% powder was ultrasonically dispersed for 10 minutes with an ultrasonic disintegrator (duty cycle 50%, output 20%). During the experiment the loading index indicated that the signal level was controlled in the range of 0.1 to 0.5. Each measurement lasted 60 seconds and was repeated 3 times. Because the reflective index of barium stannate is unknown, a default value of 1.81 was used according to the operator's manual. The source of the incident light is a laser diode with 780 nm wavelength and a power of 3 mV. The principle lies in the fact that the frequency shift between incident and reflective light is the sum of the frequency contribution resulting from the particle size distribution. The scattered intensity can therefore be modeled in terms of particle volume as well as molecular weight.

#### **4.4.11 Specific surface area**

The BET specific surface area was measured by a Micrometrics ASAP 2400 gas adsorption processor. Samples which were dried in a vacuum drying furnace at  $110^\circ\text{C}$  for one day were degassed at  $120^\circ\text{C}$  under vacuum before measurement. The average particle diameter of powders ( $d$ : nm) can be calculated from the specific surface area ( $S$ :  $\text{m}^2/\text{g}$ ) and the density ( $\rho$ :  $\text{g}/\text{cm}^3$ ) according to  $d = 6000/(\rho \cdot S)$ .

#### **4.4.12 Electrical properties**

For the electrical measurements, powder samples were uniaxially pressed at 100 MPa in pellets and then pressed at a cold isostatic pressure of 800 MPa for 1 minute. The obtained pellets have a dimension of about  $\Phi 10\text{mm} \times 1\text{mm}$ . A ca. 300 nm thick Pt film with a diameter of 8.5 mm was symmetrically sputtered on both sides of the pellets. The pellet was connected with a power and the applied voltage was 60 V. The electric current passing the pellet was measured at  $40^\circ\text{C}$  by a Keithley 485 auto-ranging picoammeter. The resistance of the pellet was calculated from the voltage and the current.

## 5. Results and discussions

### 5.1 LTAS route

To select a suitable synthesis method, LTAS route was chosen because of its low temperature for synthesis of  $\text{BaSnO}_3$  powder (section 2.2.2). The molar ratio of ammonia to barium hydroxide as high as 7 was used to keep the pH value of their mixture higher than 14. However, after the mixture reacted with  $\text{SnCl}_4$  solution, the pH value of the resulting suspension lay between 10 - 11 and it changed very little by further increasing the molar ratio.

Fig. 6 shows that the as-prepared powder, which was precipitated from alkaline solution with a molar ratio of ammonia to barium hydroxide of 7, consists of a not well-crystallized tin oxide phase. After further calcination at  $300^\circ\text{C}$  for 4 hours the powder consists of  $\text{SnO}_2$  phase. No trace of  $\text{BaSnO}_3$  phase was found.

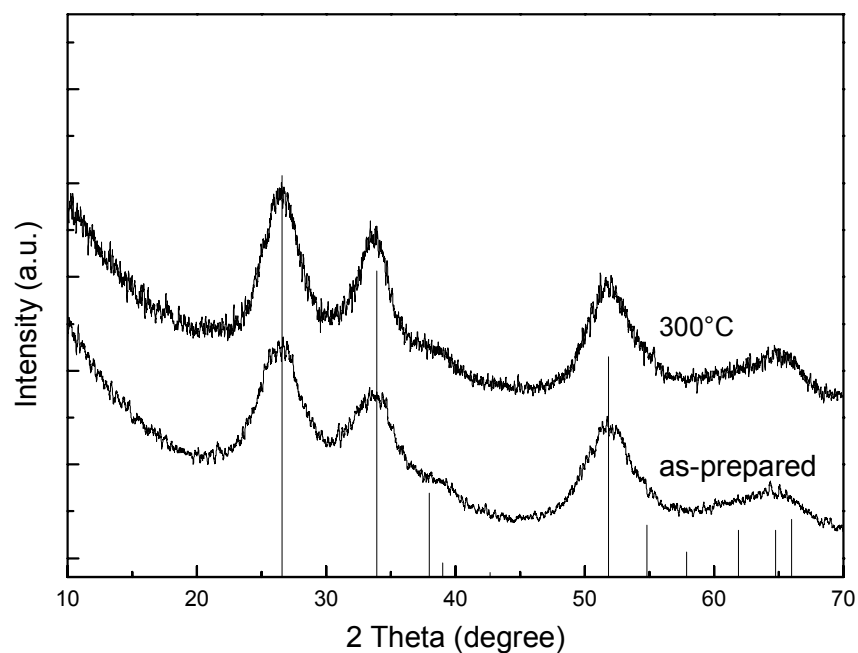


**Fig. 6** XRD patterns of the as-prepared powder and the calcined powder treated at  $300^\circ\text{C}$  for 4 hours, ammonia was used as alkaline medium, molar ratio of  $\text{NH}_4\cdot\text{OH}$  to  $\text{BaOH}$  = 7. The inserted lines correspond to the JCPDS data of tin dioxide (77-0477).

To increase the alkalinity of the medium, sodium hydroxide was used to substitute for ammonia. Excess  $\text{NaOH}$  solution could increase the pH value of the resultant over 14 at the molar rate of  $\text{NaOH}$  to  $\text{Ba}(\text{OH})_2$  = 7. The as-prepared powder was calcined in an oven at  $300^\circ\text{C}$  for 4 hours.



The XRD pattern in Fig. 7a does not indicate the formation of  $\text{BaSnO}_3$ . Increasing alkalinity only leads to better crystallization of  $\text{SnO}_2$  compared to Fig. 6. The crystallite size of  $\text{SnO}_2$ , which is calculated according to Scherrer equation, is 26 nm. The attempt to crystallize the suspension in hydrothermal conditions to obtain barium stannate was not successful. The educts after hydrothermal treatment at  $250^\circ\text{C}$  for 6 hours shows no trace of barium stannate or other barium tin compounds (Fig. 7b). The powder consists nevertheless of nanosized  $\text{SnO}_2$  (5 nm).

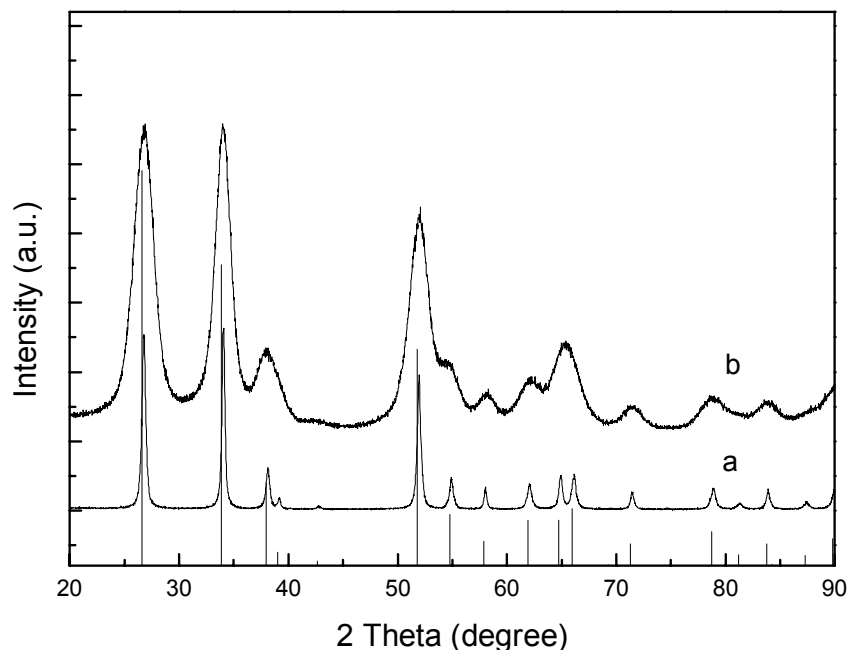


**Fig. 7** XRD patterns of powders prepared via LTAS route using sodium hydroxide as alkaline medium: (a) calcined in an oven at  $300^\circ\text{C}$  for 4 hours, (b) hydrothermally treated at  $250^\circ\text{C}$  for 6 hours, molar ratio of  $\text{NaOH}$  to  $\text{Ba}(\text{OH})_2 = 7$ . The inserted lines correspond to the JCPDS data of tin dioxide (77-0477).

The failure in preparing barium stannate via LTAS route means that the formation of barium tin coprecipitate in the alkaline solution maybe requires restricted conditions such as concentration, mixing speed and molar rate of reagents. That ammonia as a weak base can not generate a sufficient pH to exceed  $\text{BaSn}(\text{OH})_6$  solubility and cause its precipitation<sup>50</sup> may be a factor but at least not be the decisive factor, because no coprecipitation occurred by using  $\text{NaOH}$  instead of ammonia.

It is well known that  $\text{Ba}(\text{OH})_2$  is soluble in water and that  $\text{SnCl}_4$  hydrolyzes rapidly into tin oxide hydrate gel. When the coprecipitation conditions of barium and tin in alkaline solution cannot be met, barium ions in the solution will be removed by washing, and tin oxide hydrate converts into tin oxide by heat treatment. That is the reason for the appearance of the tin oxide phase in the XRD patterns of the powders. In view of the above results further study on this route was given up.

## 5.2 Synthesis of BaSnO<sub>3</sub> powder from metal alkoxide

### 5.2.1 Double metal alkoxide

#### 5.2.1.1 Starting materials

A barium tin bimetal alkoxide is the ideal precursor to obtain BaSnO<sub>3</sub> powder for the metal alkoxide route. To synthesize such a precursor metallic barium or the commercial barium isopropoxide was used as the source of barium. Tin ethoxide or tin tetraisopropoxide was used as the source of tin. Reactions of barium isopropoxide with tin tetraisopropoxide in isopropanol and reactions among metallic barium, alcohol and tin alkoxide were first investigated.

Experiments show that the commercial barium isopropoxide has low solubility in isopropanol even if the mixture is heated. The highest concentration of the barium isopropoxide solution obtained after heating at 90°C was 0.082M. The mixture of equimolar 0.08M Ba(OP<sub>r</sub><sup>i</sup>)<sub>2</sub> and 0.08M Sn(OP<sub>r</sub><sup>i</sup>)<sub>4</sub> isopropanolic solution was cloudy and changed into two phases after refluxing at 90°C for 24 hours. These indicate the immiscibility of Ba(OP<sub>r</sub><sup>i</sup>)<sub>2</sub> and Sn(OP<sub>r</sub><sup>i</sup>)<sub>4</sub> solution and the difficulty in formation of a single-phase precursor through the reaction of barium alkoxide with tin alkoxide.

Compared to barium alkoxide, metallic barium reacted with alcohol fast and could easily generate a transparent alcoholic solution with a concentration over 0.2M. As this solution was added to tin isopropoxide equivalently under a reflux condition at 90°C, the resulted solution appeared transparent first, and then became a precipitate. The precipitate changed into a homogeneous solution again with the addition of a stabilizer such as diethanol amine (DEA). Therefore a homogeneous precursor from metallic barium could be synthesized.

The precursor synthesized either from metallic barium (without addition of the stabilizer) or barium isopropoxide with tin isopropoxide in isopropanol was hydrolyzed under reflux conditions for one day with excess of water. The products after washing and drying were characterized with IR. The IR spectra are shown in Fig. 8. It can be seen that the wide bands of the two samples ranging from 2500 to 3300 cm<sup>-1</sup> are very different. Two sharp bands at 3590 and 3550 cm<sup>-1</sup> appear only in the spectrum of the sample using metallic barium as starting material while bands around 2960 cm<sup>-1</sup> exist only in the spectrum of the sample using barium isopropoxide as the source of barium. Another difference is that the strong peak localized at 1550 cm<sup>-1</sup> in the latter almost disappears in the former. Furthermore, the peak at 1410 cm<sup>-1</sup> in the case of barium is lower and the peak around 500 cm<sup>-1</sup> higher compared to the corresponding peak in the case of barium isopropoxide.

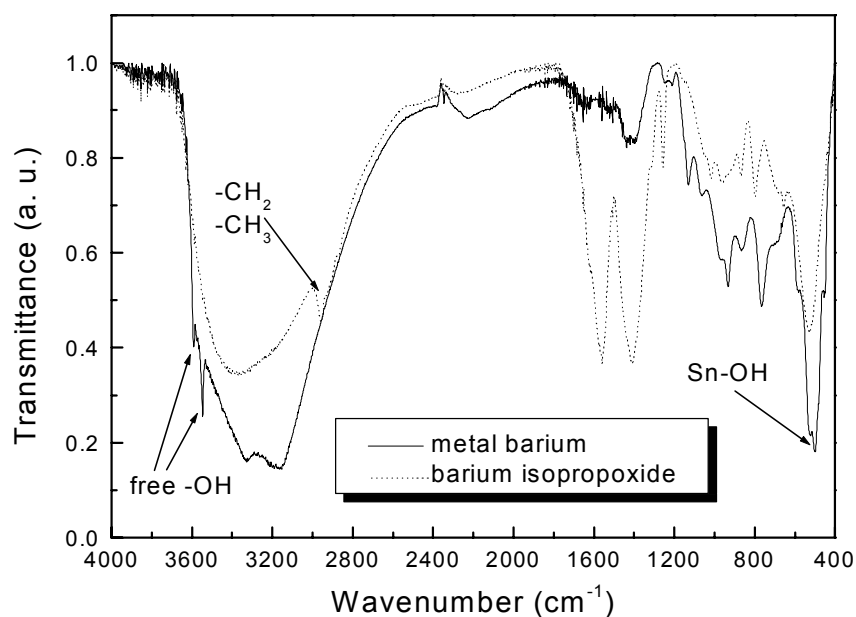


**Fig. 8** IR spectra of hydrolyzed products using metallic barium or barium isopropoxide as the source of barium.

It is well known<sup>217</sup> that the sharp bands at 3590 and 3550 cm<sup>-1</sup> arise from the stretching vibration of free hydroxyl groups, the bands around 2960 cm<sup>-1</sup> from C-H stretching vibration of -CH<sub>2</sub> and -CH<sub>3</sub> groups. Although the bands around 1550 cm<sup>-1</sup> has not yet been identified, it is thought to be related to an organic group, because this band, when its intensity is high, always coexists with the bands of C-H around 2960 cm<sup>-1</sup> and it never appears in the powder prepared via hydrothermal synthesis (section 5.3). The bands positioning around 500 cm<sup>-1</sup> represent for the Sn-OH bending vibration<sup>218,219</sup> and the wide bands around 3300 cm<sup>-1</sup> for the hydrogen bonded hydroxyl groups<sup>217</sup>. The origin of the peak centered at 1410 cm<sup>-1</sup> is not clear, which most probably correlates to barium groups, because a peak appearing in the same position can be found in most of the barium inorganic compounds<sup>220</sup>.

It can be deduced from IR spectra that the hydrolyzed product using barium isopropoxide as starting material contains a definite amount of remaining organic groups which cause the appearance of the bands around 2960 and 1550 cm<sup>-1</sup> and the lowering of the peak signifying Sn-OH. This means that the hydrolysis of the corresponding precursor is incomplete. In contrast to this, the hydrolysis of the precursor in the case of metallic barium is almost completely and therefore no obvious signal of organic groups but different types of hydroxyls are shown in the IR spectra.

The thermal behaviors of these samples have been investigated and the TG-DTA curves are illustrated in Fig. 9 and Fig. 10. In the case of metallic barium, the DTA curve in Fig. 9 shows two endothermic peaks at 150°C and 740°C which corresponds to the evaporation of the solvent and the decomposition of carbonate<sup>54</sup>. The exothermic peak at 335°C results from the decomposition and combustion of the remaining organic groups respectively. In accordance with these thermal behaviors three weight loss stages appear in the TG curve

in Fig. 9. The solvent evaporation up to 230°C attributes to 6.9 wt%, the decomposition and combustion of the organic species to 6.3 wt% and the decomposition of carbonate to 3.5 wt% weight loss. There is little weight change above 800°C.

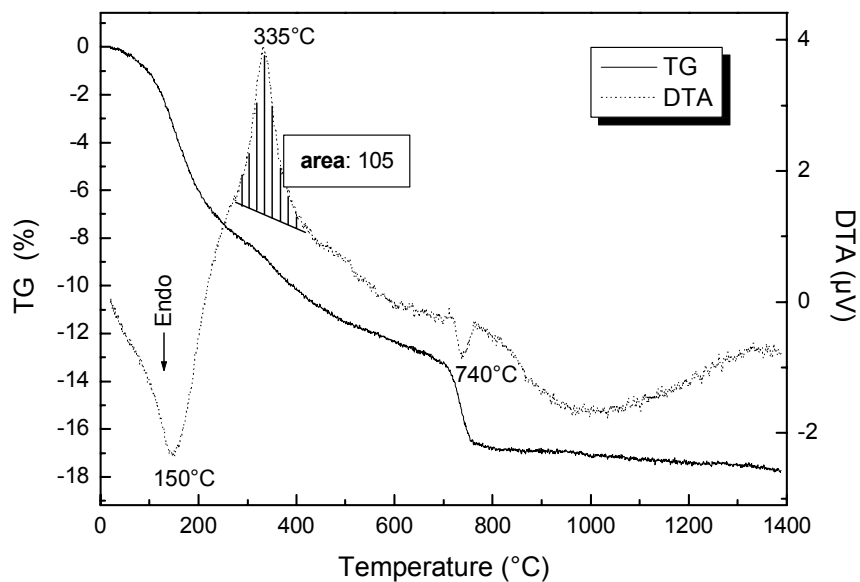


**Fig. 9** TG-DTA curve of the hydrolyzed product using metallic barium as starting materials, shadow section represents the exothermic peak area.

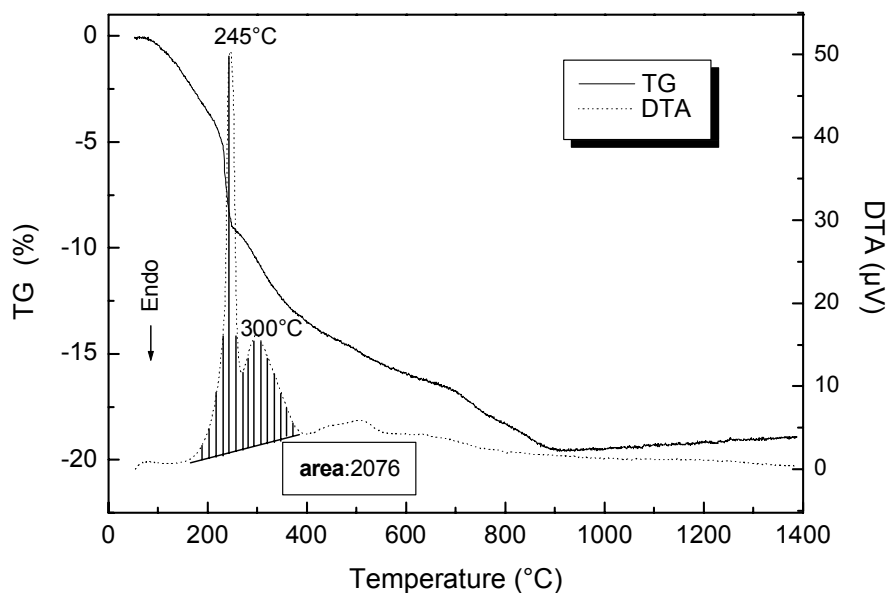


**Fig. 10** TG-DTA curve of the hydrolyzed product using barium isopropoxide as starting materials, shadow section represents the exothermic peak area.

The curves in Fig. 10 related to barium isopropoxide are different from those in Fig. 9.

There are two exothermic peaks at 245°C and 300°C which arise from the decomposition and combustion of different types of remaining organic groups. In their corresponding weight loss stages from 170°C to 260°C and from 260°C to 400°C the weight loss amounts to 6.8 wt% and 4.3 wt% respectively. A very small peak at 800°C resulting from decomposition of the carbonates<sup>54</sup> can be discerned which leads to a corresponding weight loss of 2.8 wt% from 700°C to 900°C.

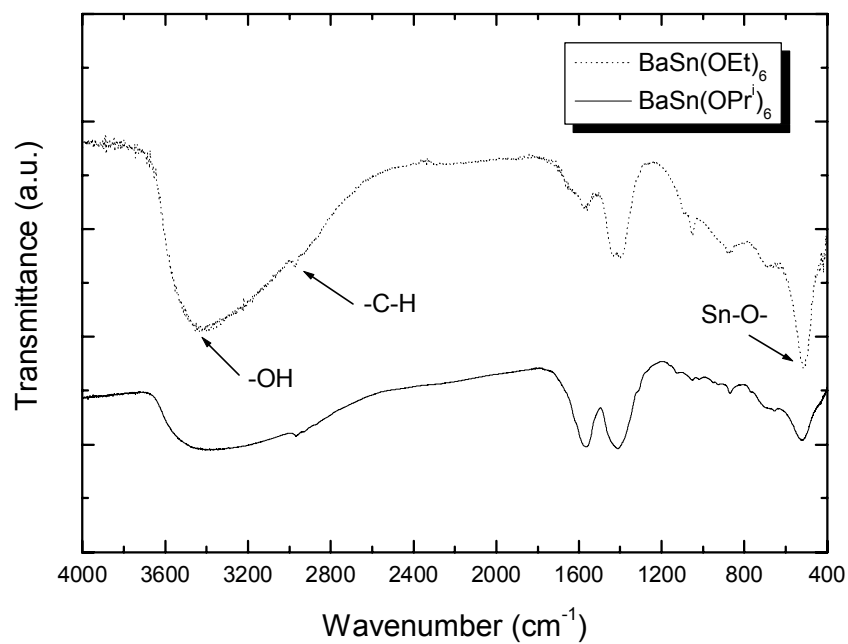
Comparing the shadow areas in the two diagrams we can find that the former is about one twentieth of the latter. This means the portion of the remaining organic groups in the case of metallic barium is far less than that in the case of barium alkoxide. Its amount is so small that it can not be characterized in IR spectrum. The weight loss ending temperature in Fig. 9 is about 100°C less than that in Fig. 10, which suggests the better potential of lowering the synthesis temperature by the case of metallic barium.

It can be concluded from above discussions that metallic barium as starting materials is superior to barium alkoxide because barium can form homogenous precursor that intends to hydrolyze completely. Its end-product has less remaining organic groups and shows better thermal behaviors. Based on these facts barium was chosen as starting materials in the later experiments.

### 5.2.1.2 Characterization of barium tin alkoxide

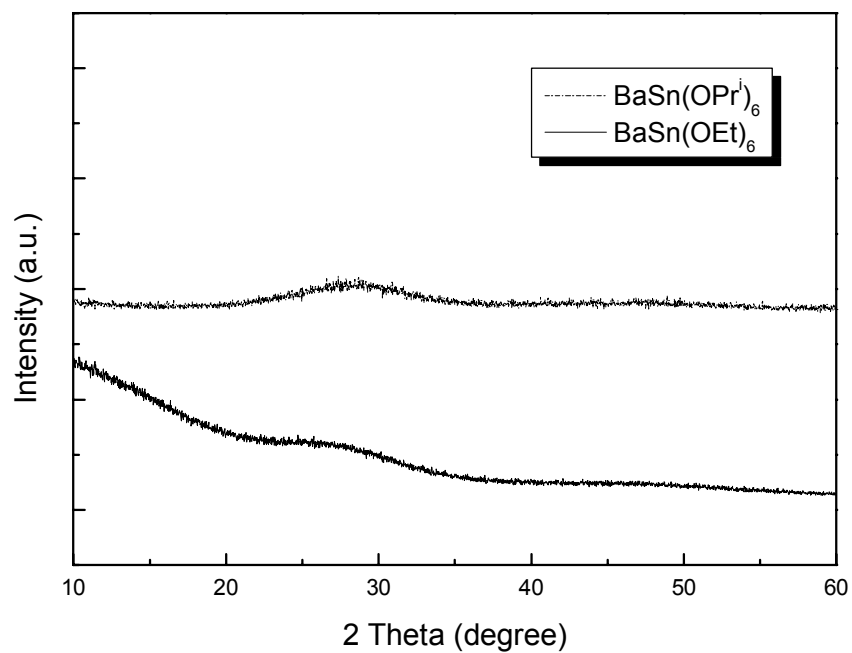
The alkoxide precursors to be characterized were obtained by reacting the freshly synthesized barium alkoxide from metallic barium with tin alkoxide and the following evaporation of the solvent from the resulted precipitate. The alkoxide precursors synthesized from barium and tin ethoxide in ethanol (referred later as **ethanol system**) or from barium and tin isopropoxide in isopropanol (referred later as **isopropanol system**) are yellow powders. They were simply noted as BaSn(OEt)<sub>6</sub> and BaSn(OPr<sup>i</sup>)<sub>6</sub> and characterized with IR, XRD, TG-DTA, SEM and chemical analysis. It should be pointed out that the characterized samples (also see Fig. 5) could hydrolyze during measurement because of the susceptibility of metal alkoxide to water, this means, it can absorb and react with the water in the atmosphere rapidly. In a strict sense, it is no more the precursor which was protected by argon and underwent no hydrolysis. However, their characterization is still of interest for comparing the both systems and for determining the proportion of Ba and Sn in the precursors.

Fig. 11 shows the IR spectra of the synthesized barium tin alkoxide precursors. The peaks around 2970 and 515 cm<sup>-1</sup> represent -C-H and Sn-O- group respectively. The peak localized at 1565 and 1405 cm<sup>-1</sup> is assumed to correlate to Ba-O- and an organic group respectively. The broad band around 3400 cm<sup>-1</sup> indicates the existence of a large amount of hydroxyl groups. This means the precursor hydrolyzed to a large extent during measurement, which can be contributed to water absorbed from the air. The IR spectra of the both precursors are very similar, nevertheless the larger OH group band of BaSn(OEt)<sub>6</sub> suggests its easier hydrolysis in comparison to BaSn(OPr<sup>i</sup>)<sub>6</sub>.



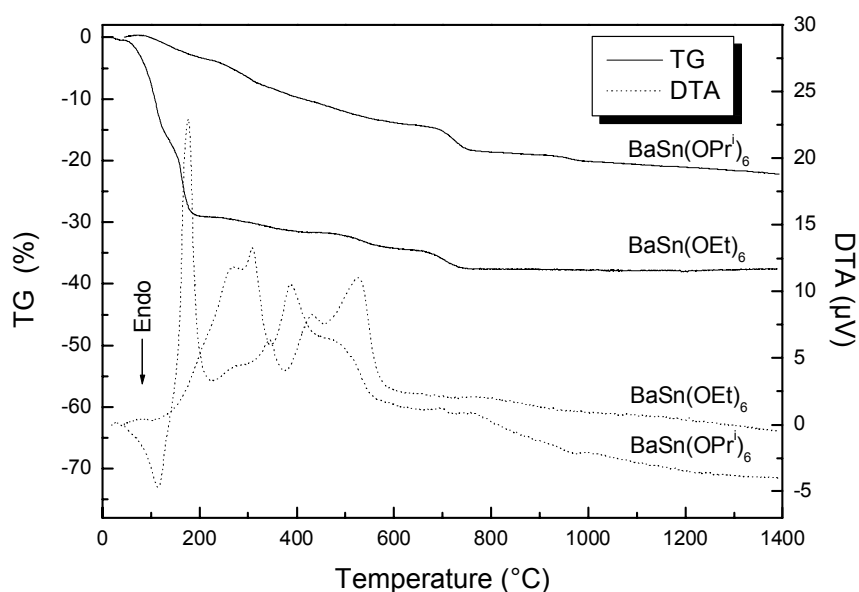
**Fig. 11** IR spectra of the synthesized barium tin alkoxides (KBr pellets).

The x-ray diffraction diagrams of barium tin ethoxide and isopropoxide are depicted in Fig. 12. Apparently the bimetal alkoxides are amorphous.



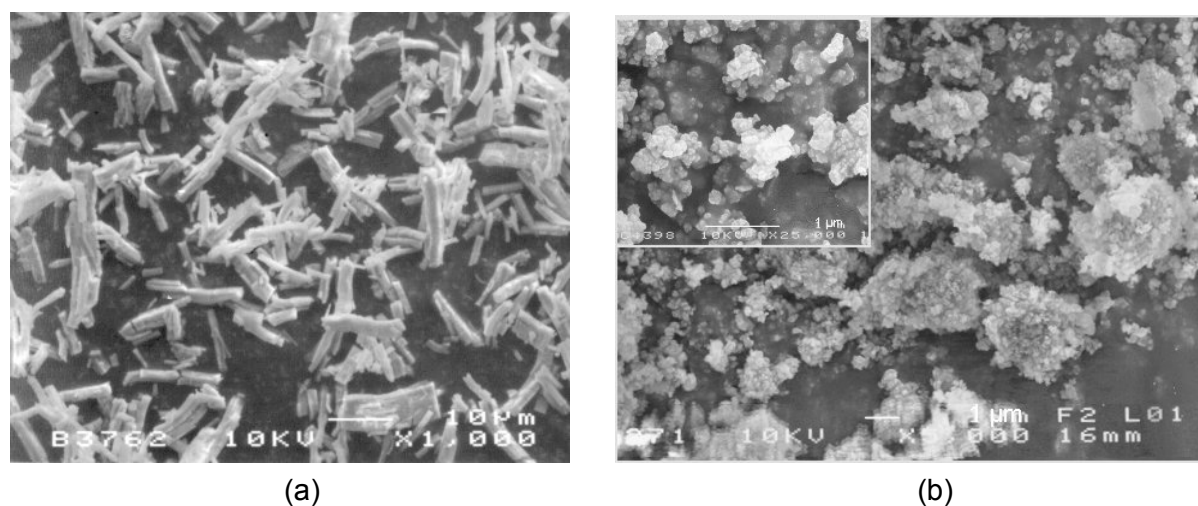
**Fig. 12** XRD patterns of the synthesized barium tin alkoxide precursors.

Fig. 13 shows the thermal behavior of the synthesized precursors. In the DTA curve of barium tin ethoxide appear an endothermic peak at 115°C corresponding to the evaporation of the solvent and four exothermic peaks at 175, 345, 430 and 525°C connecting with thermal degradation of the organic groups. In the DTA curve of barium tin isopropoxide four exothermic peaks of the decomposition of organic species appear at 270, 305, 390 and 500°C, and no endothermic peak appears. The appearance of the endothermic peak at 115°C in the case of barium tin ethoxide can be contributed to the susceptibility of the precursor to water. Barium tin isopropoxide is more thermally stable than barium tin ethoxide because of its lower onset decomposition temperature. The main reason for this is that the dissociation of an ethoxyl group is easier than an isopropoxyl group. It is well known that the chain branching of the alkyl group affects the electron releasing tendency (inductive effect) which makes the metal-oxygen-carbon bond stronger. For example, the average dissociation energy of Ti-OR in  $Ti(OR)_4$  is 101 Kcal/mole at R = ethyl and 103 Kcal/mole at R = isopropyl<sup>79</sup>. Therefore splitting of the Sn (or Ba)-OEt bond is easier than that of Sn (or Ba)-OPr<sup>i</sup> bond during the thermal decomposition. The different bonds such as Sn-O-C and Ba-O-C and the complexity of the dissociation are the reasons of the multipieaks in the DTA curve. In accordance with the DTA curves, the beginning stage (up to 150°C) of the TG curves of the both precursors is different. In the case of barium tin ethoxide the weight loss of this stage amounts to 20 wt% while it is less than 5 wt% in the case of barium tin isopropoxide. The two curves are almost parallel after 150°C and show the similar weight loss behaviors. The second stage of weigh loss from 150°C to ca. 660°C results from the decomposition and combustion of organic species. The third stage ranging from 660°C to 760°C contributes to 3 - 4 wt% weight loss which arises from the decomposition of the carbonate. There is no further weight loss above 760°C in the curve of ethoxide precursor, but a slow weight change in the curve of isopropoxide can still be observed.



**Fig. 13** TG-DTA curves of the synthesized barium tin alkoxide precursors.

The morphology of the precursors were observed under the scanning electron microscope and the SEM photographs are shown in Fig. 14. It can be seen that the barium tin ethoxide particles are rod-shaped and separated from each other. The particle size is in the micrometer range. In contrast to this, the particles of barium tin isopropoxide show a finer grain shape and aggregate strongly with each other. The inserted enlarged photo indicate their submicron size. The molar rate of Ba to Sn in the rod particle is 1.04 and 1.02 in the grain particle according to the energy dispersion spectrum (EDS).



**Fig. 14** SEM micrographs of synthesized barium tin alkoxides:  
(a)  $\text{BaSn}(\text{OEt})_6$ , (b)  $\text{BaSn}(\text{OPr}^i)_6$ .

The percentage of Ba and Sn in ethoxide and in isopropoxide were also chemically analyzed by means of ICP and listed in Table 2. Although the total percentage of barium and tin in precursors deviates from that theoretical value based on  $\text{BaSn}(\text{OR})_6$ , the molar rate of Ba:Sn in ethoxide (1.11) and in isopropoxide (0.99) is near 1. One important reason for this percentage deviation lies in the hydrolysis of the precursor during measurement. Therefore it is still reasonable to assume the precursor as  $\text{BaSn}(\text{OR})_6$  because it has much less chance to contact with water than the samples isolated for characterization.

**Table 2** Percentage of Ba and Sn and the Ba:Sn ratio in the prepared precursors.

Samples	Ba (wt%)	Sn (wt%)	(Ba + Sn) (wt%)		Ba:Sn mol %
			measured	theoretical	
$\text{BaSn}(\text{OEt})_6$	35.75	27.71	63.46	48.67	1.11
$\text{BaSn}(\text{OPr}^i)_6$	36.38	31.90	68.28	41.97	0.99

The above descriptions indicate that the synthesized precursors in ethanol and isopropanol system have similar structure and thermal behavior. However, the morphology of their



particles is very different, and the ethoxide shows higher susceptibility to water than the isopropoxide.

### 5.2.1.3 Stabilization of precursor in alcoholic solution

The barium tin alkoxide  $\text{BaSn}(\text{OR})_6$  showed a low solubility in alcohol. To obtain a homogeneous precursor, barium alkoxide and tin alkoxide were mixed in alcohol and then homogenized by addition of a stabilizer. Three chemicals, ethylen glycol-monoethyl ether (EGMEE:  $\text{C}_2\text{H}_5\text{OC}_2\text{H}_4\text{OH}$ ) and ethylen glycol-monobutyl ether (EGMBE:  $\text{CH}_3(\text{CH}_2)_3\text{OC}_2\text{H}_4\text{OH}$ ), diethanol amine (DEA:  $\text{NH}(\text{C}_2\text{H}_4\text{OH})_2$ ) were chosen as the stabilizer because of their stabilizing ability to strontium barium niobium ethoxide and barium boron ethoxide<sup>86,88</sup>.

Equimolar 0.3M DEA showed good stabilizing effect on 0.1M  $\text{BaSn}(\text{OEt})_6$  and a homogenous ethanolic solution was formed in a short time. A transparent solution could be obtained if EGMEE was added, but only after the mixture was refluxed for 12 hours. The addition of EGMBE showed no obvious stabilizing effect on the precursor. According to the results DEA was selected as the stabilizing agent.

The relation of the stabilizing effect of DEA on barium tin ethoxide and the concentration of the ethoxides was investigated. It is shown in Fig. 15 that the stabilizing effect of DEA depends on the concentration of  $\text{Ba}(\text{OEt})_2$  and  $\text{Sn}(\text{OPr}^i)_4$  (molar rate of DEA to  $\text{BaSn}(\text{OEt})_6$  is 1:1). The criteria for stabilization is that the precursor alcoholic solution should be transparent. The precursor can be easily stabilized in the low concentration region at room temperature. It becomes more difficult to get a homogenous solution with the increase in concentration. The half hollow points in the diagram represent that the corresponding precursors in ethanol are translucent at room temperature and become transparent solutions under refluxing condition for 12 hours. Therefore the shade section shows the region where a homogeneous precursor has been obtained. When the ethoxide concentrations are higher than 0.2 M, no homogenous ethanolic solution of the precursor has been obtained even with the help of heating. Because a high concentration means a higher yield rate, 0.15 M was determined as the concentration of both metal ethoxides in the subsequent experiments. For the isopropanol system, DEA showed the similar stabilizing effect and 0.15M was also determined as the concentration of the metal isopropoxides.

The stabilizing effect of DEA on barium tin alkoxide can be simply explained as shown in formula 21 (also see reference 79). The precursor is thought to include a four-membered ring structure. The two hydroxyl groups in DEA can couple with any two alkoxy groups of the precursor through Van der Waals force. Furthermore, nitrogen atom in DEA is rich of electrons and can associate either with barium or tin atoms to form a bridge structure. The formation of hydrogen bonds between the molecules of DEA and alcohol leads to the solubilization of the precursor in alcohol.

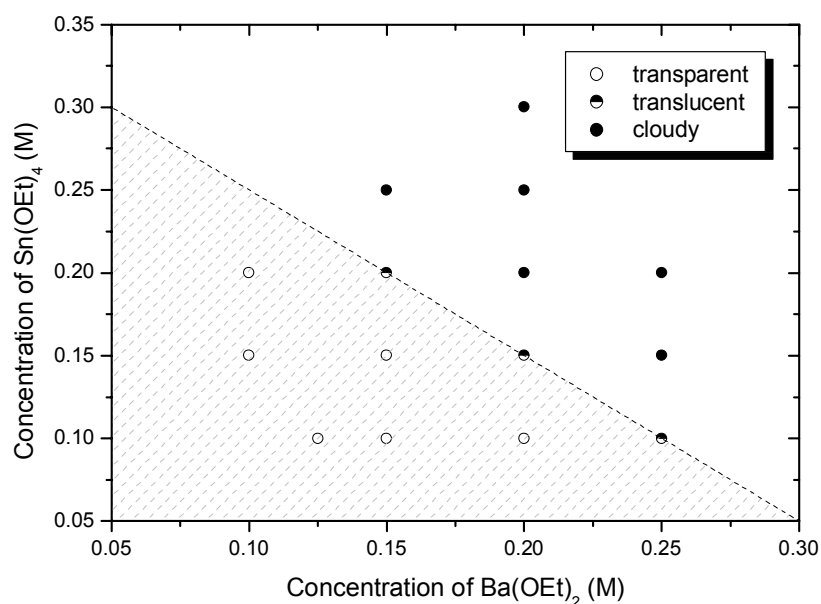
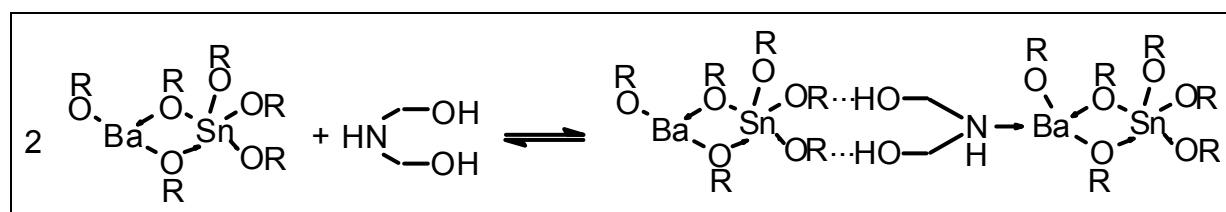


**Fig. 15** Region of the formation of a homogenous  $\text{BaSn}(\text{OEt})_6$  solution in ethanol with the addition of DEA, molar rate of DEA to  $\text{BaSn}(\text{OEt})_6 = 1:1$ .



$R = \text{Et}, \text{Pr}^i$

(21)

The percentage of the coupled alkoxy group in the solution will be lowered with an increase in concentration of the precursor, so that the steric effect of alkoxy group becomes important and limits the bonding interaction between DEA and alcohol molecules. As a result, the stabilizing effect of DEA gets weak and the solution turns into cloudy because of the low solubility of the precursor in alcohol.

### 5.2.2 Hydrolyzing process

Water was mixed with alcohol and then dropwise added to the precursors. Heat was released while  $\text{BaSn}(\text{OEt})_6$  hydrolyzed rapidly in water. The experimental results showed that the molar ratio of water to precursor ( $R_w = \text{H}_2\text{O} : \text{BaSn}(\text{OEt})_6$ ) and the addition of DEA as stabilizer affected the properties of the hydrolysis products. It can be seen from Table 3 that the form of the hydrolysis product can be controlled through changing the  $R_w$  value. A

low  $R_w$  leads to the formation of a sol while a high  $R_w$  results in a precipitate product. An intermediate product appears in the system without DEA when the  $R_w$  is 12. The addition of DEA extends the sol formation range from  $R_w = 6$  to 18.

**Table 3** Effects of the molar ratio  $R_w$  on the form of the hydrolysis product of  $\text{BaSn}(\text{OEt})_6$

$R_w$	6	12	18	60	$\geq 270$
System without DEA	sol	separate layers*	precipitate	precipitate	precipitate
System with DEA	sol	sol	sol	precipitate	precipitate

\*the upper transparent layer is still a sol and the underneath milk white layer is the suspension of the precipitate.

Fig. 16 shows the IR spectra of the hydrolysis products at different  $R_w$ . (The IR samples were prepared with KBr pellet method after evaporation of the solvent and removal of DEA by washing with ethanol). The band around 2750 to 3030  $\text{cm}^{-1}$  signaling the alkyl groups indicates the hydrolysis degree of the precursor. It is clearly shown that the system without DEA hydrolyzes nearly completely at  $R_w = 12$  because of the disappearance of the alkyl band. However, the alkyl band can be discerned till  $R_w = 60$  in the DEA-stabilized system and it disappears at  $R_w = 270$ . Because in the presence of OH the characteristic peak of N-H stretching vibration derived from DEA at 3350  $\text{cm}^{-1}$  is a very weak and broad vibration, which, as a rule, cannot be sure, if NH is present. Apparently, the addition of DEA delays the hydrolysis. However, by adding excess of water in the DEA-stabilized precursor a almost complete hydrolysis can still be reached.

The effect of temperature on hydrolysis was investigated in the DEA-stabilized system. The precursor  $\text{BaSn}(\text{OEt})_6$  hydrolyzed at room temperature or under refluxing condition at an oil bath temperature of 90°C for 24 hours. Fig. 17 presents the IR spectra. It can be found that the area of the OH stretching wide band around 3300  $\text{cm}^{-1}$  at 90°C is larger than that at 25°C. Furthermore, the enlarged diagram indicates that the alkyl band around 2900 to 3000  $\text{cm}^{-1}$  which exists in the sample hydrolyzing at 25°C disappears as the sample hydrolyzed at 90°C. These suggest that a higher hydrolyzing temperature is beneficial to a complete hydrolysis.

It has been found from experiments that the hydrolysis speed of  $\text{BaSn}(\text{OPr}^i)_6$  is slower than that of  $\text{BaSn}(\text{OC}_2\text{H}_5)_6$ . Temperature and  $R_w$  show the similar effects on hydrolysis in the isopropanol system like in the ethanol system. Therefore excess water ( $R_w \geq 60$ ) and refluxing condition (90°C for 24 hours) were employed in the hydrolysis of the DEA-stabilized precursor if no special specification is given. Although the added DEA limits the hydrolysis of the precursor, it can homogenize the precursor, thus the later experiments were done only in the DEA-stabilized system.

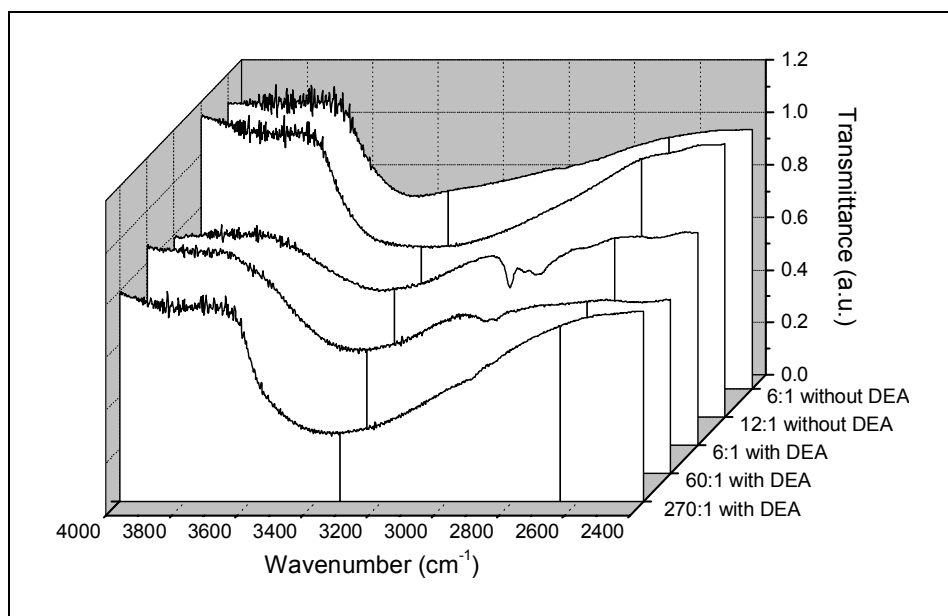


**Fig. 16** IR spectra (KBr pellets) of hydrolysis products of DEA-stabilized (the molar ratio of DEA:  $\text{BaSn}(\text{OEt})_6 = 1$ ) and non-stabilized  $\text{BaSn}(\text{OEt})_6$  hydrolyzed with different molar ratios of water to precursor ( $R_w$ ) at 25°C. The numbers in the direction of y axis indicate the  $R_w$  value.

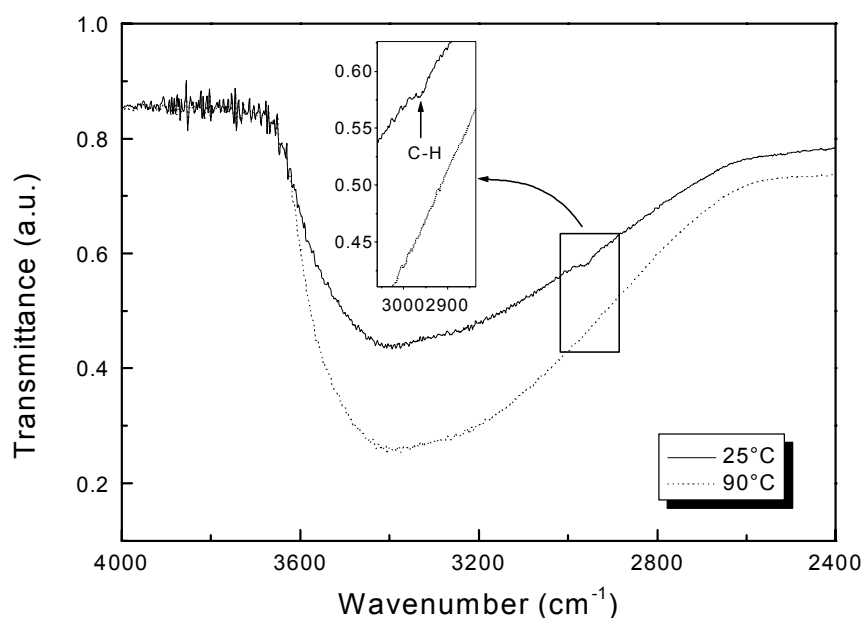


**Fig. 17** IR spectra of DEA-stabilized  $\text{BaSn}(\text{OEt})_6$  hydrolyzing at 25°C and 90°C for 24 hours ( $R_w=150$ ).

### 5.2.3 Crystallization behavior

The hydrolysis product derived from DEA-stabilized precursor is still a hydroxide compound which possibly contains a small amount of remaining organic species. To obtain ceramic oxide powders the product was either directly calcined in a furnace or intensively crystallized under hydrothermal conditions and then calcined (hydrothermal treatment of the hydrolyzed product was designed to obtain a  $\text{BaSnO}_3$  powder directly, but the obtained educt was still a hydroxylate, so it was further calcined). The former processing is called conventional calcination and the later is called hydrothermal calcination for distinction. The phase transformation and the crystallizing temperature from as-prepared powder to  $\text{BaSnO}_3$  in the ethanol or isopropanol system have been investigated by means of thermal analysis, FTIR and XRD. The results will be presented in this section. FTIR was used to analyze the change of the molecular structure during thermal treatment, which is helpful to determine the composition of the powders.

#### 5.2.3.1 Conventional calcination

To determine the calcining temperature the thermal behavior of the as-prepared powder after hydrolysis was analyzed. Fig. 18 shows the TG-DTA curves of the as-prepared powder in the ethanol system and Fig. 19 illustrates the TG-DTA-MS curves of the as-prepared powder in the isopropanol system.

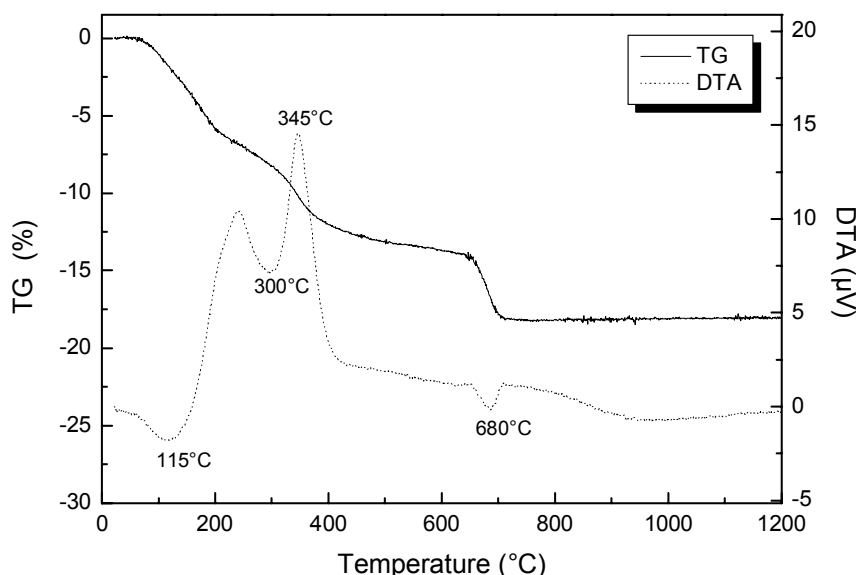


**Fig. 18** TG-DTA curves of the as-prepared powder hydrolyzed from precursor  $\text{BaSn}(\text{OEt})_6$  at  $90^\circ\text{C}$  for 24 hours.

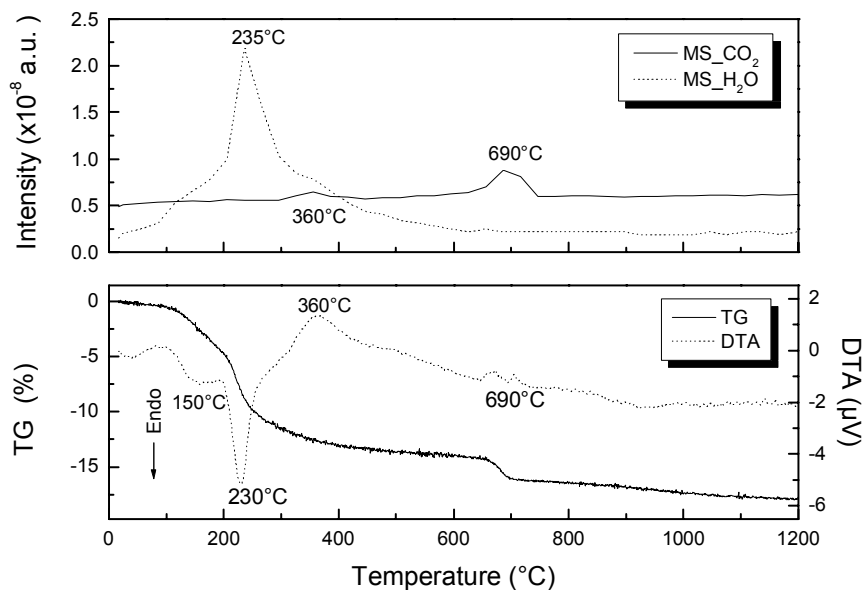


**Fig. 19** TG-DTA-MS curves of the as-prepared powder hydrolyzed from precursor  $\text{BaSn}(\text{OPr}^i)_6$  at  $90^\circ\text{C}$  for 24 hours, detected  $\text{H}_2\text{O}$  and  $\text{CO}_2$  is depicted in MS curve.

Comparing the TG-DTA curves of both figures, it can be found that the thermal behavior of both systems is similar. The weight loss can be divided in four phases: from room temperature to  $450^\circ\text{C}$ ,  $450^\circ\text{C}$  to  $650^\circ\text{C}$ ,  $650^\circ\text{C}$  to  $750^\circ\text{C}$  and above  $750^\circ\text{C}$ . In the second and fourth phase the weight loss is small. The weight loss in the first phase amounts to ca. 13 wt% in the both systems. The weight loss in the third phase is 4.0 wt% in the ethanol system and 2.1 wt% in the isopropanol system. The corresponding DTA curves show two endothermic peaks and one exothermic peak in the first weight loss phase. The exothermic peak localizes nearly in the same position (about  $350^\circ\text{C}$ ), although the two endothermic peaks center at different positions in the two systems. There is no peak in the second and fourth weight loss phases. A small endothermic at near  $700^\circ\text{C}$  is found in the third weight loss phase.

The MS curve of Fig. 19 shows that a water peak centered at  $235^\circ\text{C}$  appears in the temperature range of  $100^\circ\text{C}$  to  $450^\circ\text{C}$  and two  $\text{CO}_2$  peaks appear at  $360^\circ\text{C}$  and  $690^\circ\text{C}$ .

The above results indicate that the first two endothermic peaks result from the vaporization of absorbed water and the dehydroxylation of  $\text{BaSn}(\text{OH})_6$ . The organic remaining species decompose and combust at about  $350^\circ\text{C}$ , which causes the release of carbon dioxide. These contribute to the first phase weight loss. The release of carbon dioxide and the endothermic peak at about  $700^\circ\text{C}$  is consistent with the assumption that the third phase weight loss is caused by the decomposition of carbonates<sup>54</sup>. In the second and fourth weight loss phases there is no obvious thermal change and therefore the weight loss is small. The sum of the weight loss amounts to 18.1 wt% and 17.8 wt% in ethanol and in isopropanol system respectively, which deviates to some extent from the theoretical value of 13.6% because of the water absorbed from air and the existence of remaining organic species.

According to the TG-DTA curves, the as-prepared powder was treated at 120°C and 200°C for 4 hours to remove absorbed water, and then calcined at different temperatures from 350°C to 760°C for 6 hours to study the structure and the crystal phase changes (the heating rate is 2°C/min).

The structure change during the thermal treatment process is detected with the IR spectra. Fig. 20 shows the IR spectra of the powder in the ethanol system calcined at different temperatures. The broad band at 1420 cm<sup>-1</sup> in as-prepared sample is thought to be correlated with Ba-O- groups (also see Fig. 8), but its identification becomes complex with the later appearance of carbonate, because one of the two characteristic peaks of CO<sub>3</sub><sup>2-</sup> (1430 cm<sup>-1</sup>:ν<sub>s</sub>(CO<sub>2</sub><sup>-</sup>)) also lies in the same region. Thus, the CO<sub>3</sub><sup>2-</sup> group can be identified only when another characteristic peak of 870 cm<sup>-1</sup> (its vibration type is not described in the literature)<sup>54</sup> coexists. The band at 1570 cm<sup>-1</sup> resulting most possibly from an organic carboxylate (ν<sub>a</sub>(CO<sub>2</sub><sup>-</sup>) = 1580 cm<sup>-1</sup>, this band does not appear in the powder prepared via hydrothermal synthesis, see Fig. 66 and Fig. 74), disappears while the relative sharp band of Sn-OH at 520 cm<sup>-1</sup> becomes broader as the as-prepared powder is heated to 350°C. At the same time the band associated with CO<sub>3</sub><sup>2-</sup> appears at 860 cm<sup>-1</sup>. It can be explained that at 350°C the remaining organic species decompose, dehydroxylation occurs and BaCO<sub>3</sub> is formed. With the increase in temperature, the intensity of the Sn-OH band and the CO<sub>3</sub><sup>2-</sup> band at 860 cm<sup>-1</sup> decreases gradually. The two bands disappear between 550°C and 600°C. (In Fig. 20, the band of 1420 cm<sup>-1</sup> at 350°C, 400°C and 500°C can partly result from ν<sub>s</sub>(CO<sub>2</sub><sup>-</sup>), also refer to Fig. 22). A band with a peak centered at 630 cm<sup>-1</sup> that results from SnO<sub>3</sub><sup>2-</sup><sup>220</sup> appears at 550°C. The CO<sub>2</sub> band is detected at 500°C and intensifies at 550°C. It disappears at 600°C. No band corresponding to OH group above 600°C indicates the accomplishment of the dehydroxylation. There is no difference between the spectra at 670°C and 720°C.

A similar structure changes in the powder of the isopropanol system can be found by comparing Fig. 21 with Fig. 20: The band at 1560 cm<sup>-1</sup> disappears and the CO<sub>3</sub><sup>2-</sup> band appears simultaneously at 350°C. The CO<sub>2</sub> band appears at 500°C and disappears at 600°C. The Sn-OH band rounds off and broadens with the increase in temperature. It disappears at 600°C accompanied by the appearance of the SnO<sub>3</sub><sup>2-</sup> band. It is nevertheless apparent in Fig. 21 that the broad band around 1420 cm<sup>-1</sup> at 350°C and 500°C includes the ν<sub>s</sub>(CO<sub>2</sub><sup>-</sup>) peak.

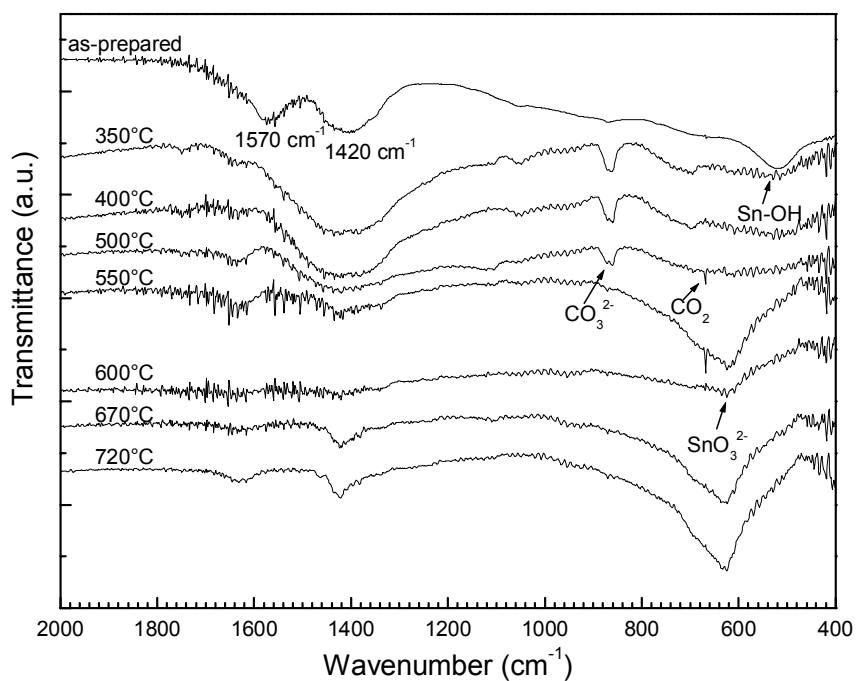


**Fig. 20** IR spectra of the as-prepared powder hydrolyzed from precursor BaSn(OEt)<sub>6</sub> at 90°C for 24 hours and the powders calcined at a temperature from 350°C to 720°C for 6 hours (KBr pellets).

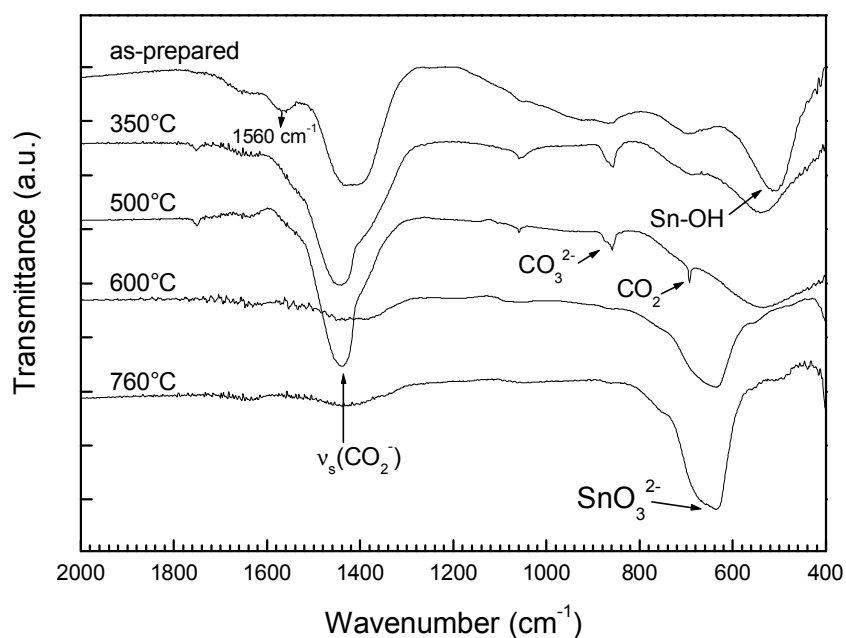


**Fig. 21** IR spectra of the as-prepared powder hydrolyzed from precursor BaSn(OPr)<sub>6</sub> at 90°C for 24 hours and the powders calcined at a temperature from 350 to 760°C for 6 hours.



It can be inferred from above results that the decomposition of the remaining organic species takes place at about 350°C, as a result, a carbonate is formed which reacts again and gives out CO<sub>2</sub> at the temperature range from 400-600°C while the dehydroxylation proceeds. The conversion of [SnO<sub>6</sub>] from Sn-OH finishes at 600°C and begins at 350°C because of the band Sn-OH rounding off and broadening at that temperature.

The x-ray diffractograms of some of the samples in Fig. 20 are presented in Fig. 22. The inserted lines correspond to the JCPDS data of BaSnO<sub>3</sub> (15-780). The powders calcined at a temperature under 500°C are amorphous. Corresponding that CO<sub>3</sub><sup>2-</sup> band appears in IR spectra as the sample is treated at a temperature between 350 and 500°C, the traces of a carbonate phase is found in the XRD pattern at 500°C. It indicates that the amount of the carbonate is very small. A pure, single-phase of perovskite BaSnO<sub>3</sub> is formed by heating at 550°C or a temperature above this. The crystallite size of the formed BaSnO<sub>3</sub> calculated with Siemens software according to Scherrer equation for the (110) peak is nevertheless larger than 100 nm. The amorphous phase crystallizes and transforms into BaSnO<sub>3</sub> between 500°C and 550°C.

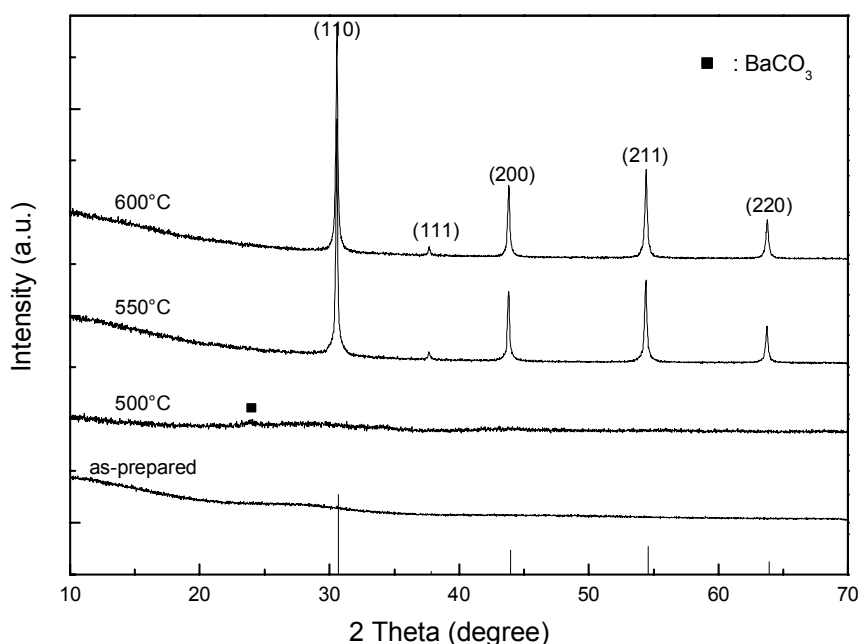


**Fig. 22** XRD patterns of the as-prepared powder hydrolyzed from BaSn(OEt)<sub>6</sub> at 90°C for 24 hours and the powders calcined at 500, 550 and 600°C for 6 hours. The inserted lines correspond to the JCPDS data of BaSnO<sub>3</sub> (15-780).

In the system using BaSn(OPr<sup>i</sup>)<sub>6</sub> as the precursor, the phase changes of the powder with calcining temperature (Fig. 23) are similar to that in the ethanol system. In addition, the crystalline peaks of BaCO<sub>3</sub> appearing at 500°C are more apparent, which is consistent with the structure changes showed in the corresponding IR spectra. The crystallite size of BaSnO<sub>3</sub> calcined at 600°C and 760°C is 48 nm and 60 nm respectively.

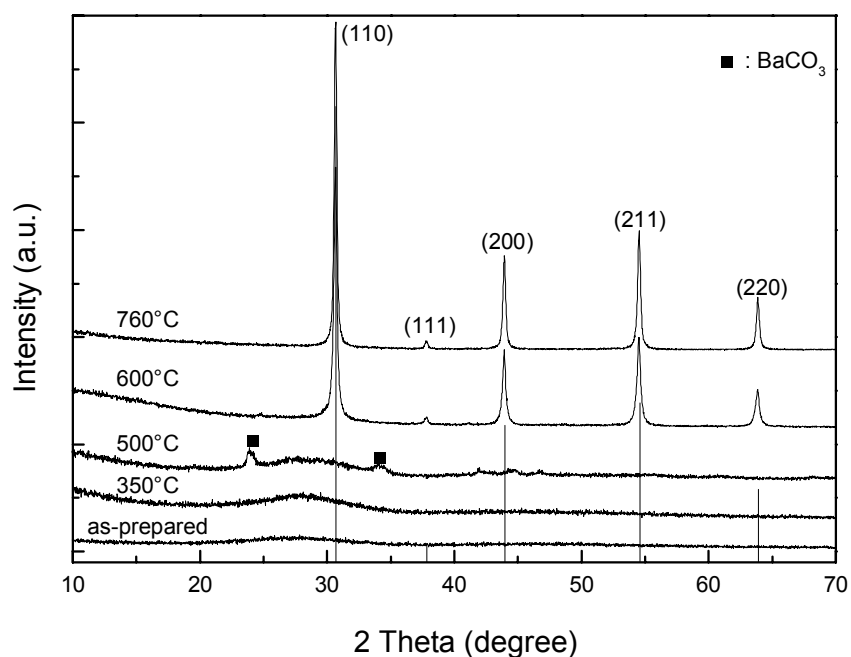
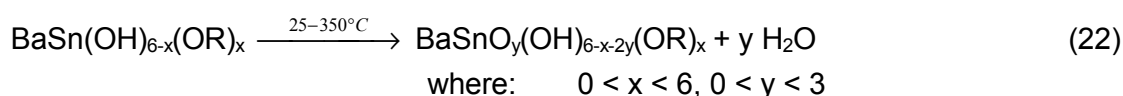


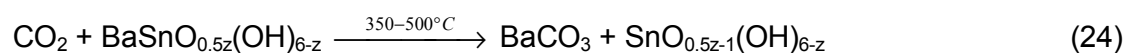
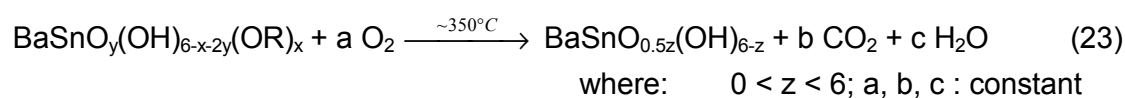
**Fig. 23** XRD patterns of the as-prepared powder hydrolyzed from  $\text{BaSn}(\text{OPr})_6$  at  $90^\circ\text{C}$  for 24 hours and the powders calcined at 350, 500, 600 and  $760^\circ\text{C}$  for 6 hours. The inserted lines correspond to the JCPDS data of  $\text{BaSnO}_3$  (15-780).

The above results (Fig. 18, Fig. 19, Fig. 20 and Fig. 21) show that the hydrolysis product of the bimetal alkoxide precursor still contains a small amount of remaining organic groups despite excess added water. Here the absorbed solvent as the only source of the remaining organic species can be excluded, because the absorbed alcoholic solvent in the hydrolysis products should be removed before  $360^\circ\text{C}$  and therefore cannot cause to the exothermal peaks at  $345^\circ\text{C}$  in Fig. 18 and at  $360^\circ\text{C}$  in Fig. 19. So it is more reasonable that the amorphous hydrolysis product is formulated as  $\text{BaSn}(\text{OH})_{6-x}(\text{OR})_x$  than as  $\text{BaSn}(\text{OH})_6$ , but  $x$  should be small because no C-H groups can be seen in the region about  $3000\text{ cm}^{-1}$  (see Fig. 17 at  $90^\circ\text{C}$ ), R is either ethyl or isopropyl which depends on the chosen solvent. The crystallization behaviors of powders during calcination can then be described as following. Dehydroxylation between OH groups takes place with an increase in temperature and leads to the release of water, which can be represented as formula 22. As a result, endothermic peaks appear in TG-DTA curve at temperatures below  $350^\circ\text{C}$  (Fig. 18 and Fig. 19), a water peak centered at  $235^\circ\text{C}$  appears in MS-curve (Fig. 19) and the intensity of Sn-OH decreases correspondingly (Fig. 20 and Fig. 21).

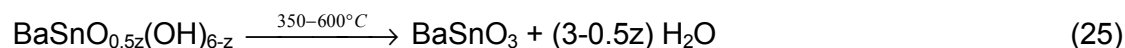


At about  $350^\circ\text{C}$  the organic remaining species decompose and combust, which contributes to the release of  $\text{CO}_2$ , at the same time the dehydroxylation proceeds. This explains why

the exothermic peak appears at about 350°C in DTA curves (Fig. 18 and Fig. 19) and the CO<sub>2</sub> peak appears in MS curve (Fig. 19). Because the IR spectra of powders calcined at 350°C (Fig. 20 and Fig. 21) show no signal of organic groups, the product can be formulated as a barium tin oxyhydroxide BaSnO<sub>0.5z</sub>(OH)<sub>6-z</sub> which is amorphous according to the XRD results. This process is simplified as formula 23, where a, b, c are constants used only as coefficients for balancing the equation. The released CO<sub>2</sub> combines with the element barium to form carbonate in the temperature range of 350°C to 500°C (formula 24). The CO<sub>3</sub><sup>2-</sup> band in IR spectra of (Fig. 20 and Fig. 21) and the appearance of barium carbonate in XRD (Fig. 22 and Fig. 23) are the reflection of this process. A tin oxide hydrate resultant of SnO<sub>0.5z-1</sub>(OH)<sub>6-z</sub> (or described as SnO<sub>2</sub>·(3-0.5z)H<sub>2</sub>O) is assumed, which should be amorphous because no corresponding crystal phase is found in the XRD patterns.

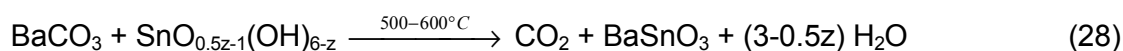
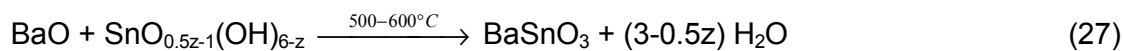


The pure phase barium stannate appears at 550°C in the ethanol system (Fig. 22) and at 600°C in the isopropanol system (Fig. 23) respectively. But the formation of BaSnO<sub>3</sub> begins at 350°C according to the above IR spectra and the micrographs of the powder which will be discussed in section 5.2.4. The release of water ending at about 600°C (MS curve in Fig. 19) indicates the finish of dehydroxylation. So the transformation of BaSnO<sub>3</sub> from amorphous phase can be represented with formula 25 and the crystallizing temperature can be determined in the range of 550 - 600°C.



In the temperature range of 500 to 600°C, the disappearance of CO<sub>3</sub><sup>2-</sup> and the appearance of CO<sub>2</sub> band in IR spectra as well as the disappearance of BaCO<sub>3</sub> phase in XRD should result from the decomposition of barium carbonate (formula 26) according to the literature 54. Because no BaO phase is found in the XRD patterns, it can be assumed that BaO reacts further with tin oxide hydrate to form barium stannate as shown in formula 27. The formulae 26 and 27 can be combined to obtain formula 28. However, the decomposition temperature of pure BaCO<sub>3</sub> is about 1300°C<sup>221</sup>, it is still not clear whether such a decomposition takes place at a low temperature as 500 – 600°C when there exists other compounds and the particle of BaCO<sub>3</sub> is very small. If the decomposition does not occur, the whole process can be explained by the one-step reaction of formula 28, such an explanation can also be found in reference 55. The weight loss and the exothermic peak at about 690°C in DTA-TG curve and the CO<sub>2</sub> peak at 690°C in MS curve (Fig. 18 and Fig. 19) should correspond to this process. The deviation of the temperature most possibly derives from a difference in the temperature policy employed during thermal analysis and calcination. It is more difficult to rearrange the inner structure by transformation at a rapid heating rate of 10°C/min in thermal analysis than at a slow heating rate of 2°C/min by

calcination, thus appears the temperature hysteresis in the TG-DTA and the TG-DTA-MS curves.



The further increase of temperature after 600°C leads to the growth of crystallite of BaSnO<sub>3</sub> phase, and the nanosized barium stannate powder can only be obtained from the isopropanol system. Characterization of the obtained BaSnO<sub>3</sub> powder in these system will be described in section 5.2.4.

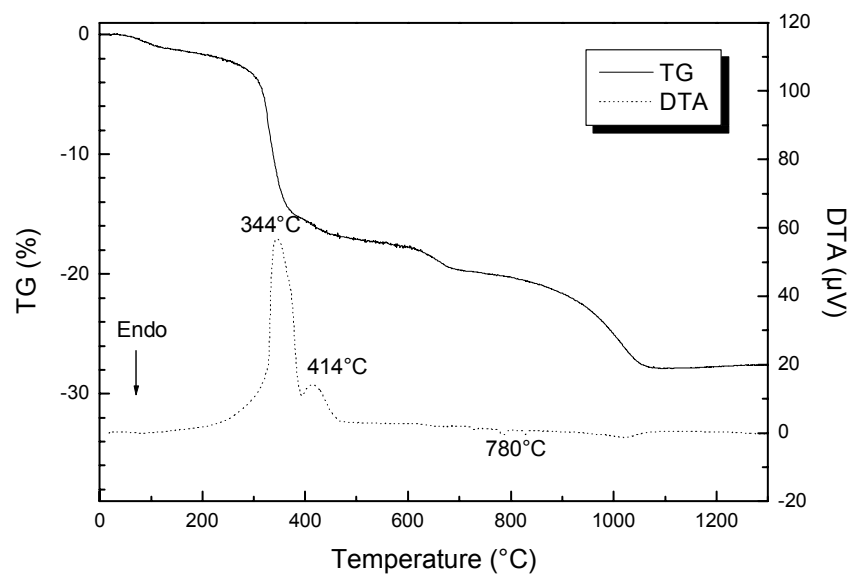
### 5.2.3.2 Hydrothermal calcination

The hydrothermal calcination was first tried in the ethanol system. The precursor was synthesized in the presence of DEA by reacting metallic barium with ethanol first and then with tin ethoxide. After the hydrolysis of the transparent precursor the resulted suspension was immediately transferred to an autoclave and treated at 250°C for 6 hours. In the whole process argon was used as the protection gas to avoid absorbing CO<sub>2</sub> and water from atmosphere. The educt separated by centrifuge was washed first with ethanol and then with water. To dry the powder it was placed in a vacuum furnace at 60°C for two days. The dried powder was called as-prepared powder and characterized with TG-DTA, IR and XRD. The as-prepared powder after hydrothermal treatment is gray as the  $R_w$  value is low ( $R_w = 6$ ) and is white as the  $R_w$  is high ( $R_w = 500$ ). The gray color seems to result from the carbonization of the remaining organic species in the hydrolyzed product under hydrothermal conditions. Because the as-prepared powder did not consist of BaSnO<sub>3</sub> but of BaSn(OH)<sub>6</sub> (refer to Fig. 26), it had to be calcined in a furnace for the crystal phase transformation.

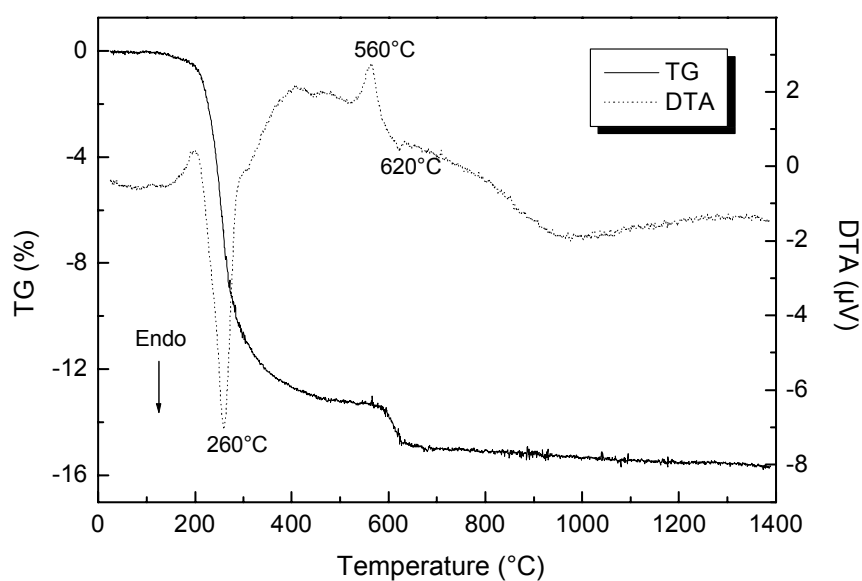
The results of the thermal analysis for the as-prepared powders are shown in Fig. 24. In the case of  $R_w = 6$  (Fig. 24a), the exothermic peaks at 344°C and 414°C resulting from the decomposition and combustion of the remaining organic species causes about 17 wt% weight loss. The endothermic peak at 780°C is assumed in the literature<sup>54</sup> as the decomposition of the carbonate, however, the weight loss between 800°C and 1000°C suggests the decomposition of the carbonate occur in this temperature range, thus, the endothermic peak at 780°C assumed<sup>55</sup> as the result of the reaction between BaCO<sub>3</sub> and SnO<sub>2</sub> to form BaSnO<sub>3</sub> is more reasonable. The weight of the sample loses gradually between 450°C and 1100°C.

In contrast to above, a sharp endothermic peak appears in the DTA curve of  $R_w = 500$  (Fig. 24b), which arises from the dehydroxylation of the sample and contributes to 13.3 wt% weight loss. No exothermic peak is observed between 300°C and 400°C. The crystallization exothermic peak of BaSnO<sub>3</sub><sup>55</sup> locates at 560°C. Corresponding to the endothermic peak at 620°C, a weight loss of 1.5% is observed in the temperature range of 570 to 630°C. The

cause of this peak should be the same as that at 780°C in Fig. 24a. No apparent weight loss is observed above 630°C.



(a)



(b)

**Fig. 24** TG-DTA curves of the as-prepared powder derived from precursor BaSn(OEt)<sub>6</sub> after hydrothermal treatment at 250°C for 6 hours: (a) R<sub>w</sub> = 6, (b) R<sub>w</sub> = 500.

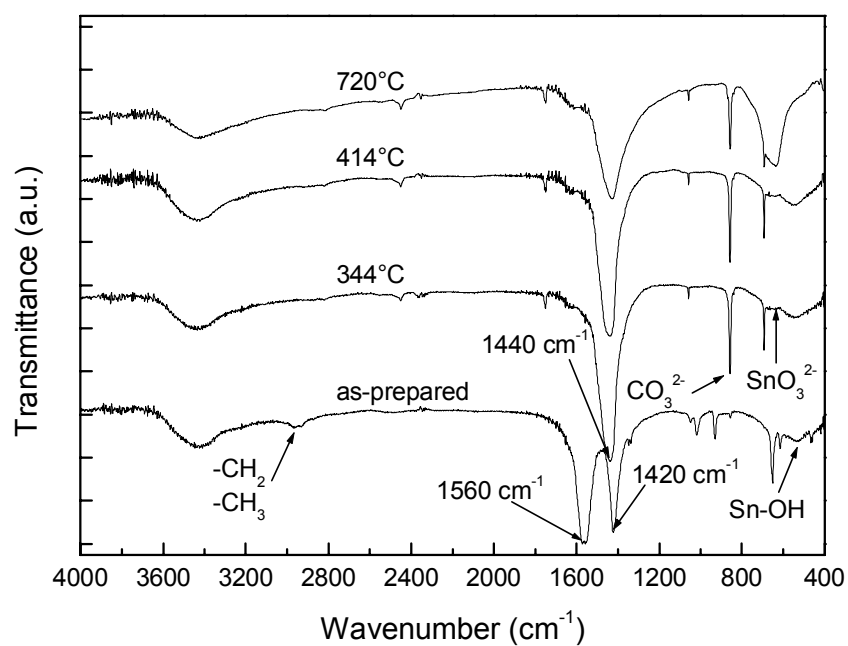
The hydrolysis of the precursor at a low R<sub>w</sub> is found to be incomplete because the alkyl bands around 2900 cm<sup>-1</sup> in Fig. 25(a) show the percentage of the organic species in the

sample is not low (the band around  $1560\text{ cm}^{-1}$  can also be an indicator, and the band at  $1420\text{ cm}^{-1}$  is assumed to be related with Ba-O group). These organic groups disappear as the temperature increases to  $344^\circ\text{C}$ . Simultaneously  $\text{CO}_3^{2-}$  groups form ( $\nu_s(\text{CO}_2^-)$  at  $1440\text{ cm}^{-1}$  and the peak at  $860\text{ cm}^{-1}$  appear) and Sn-OH groups begin to transit into stannate (phase changes can be seen later in Fig. 26). No obvious change in the IR spectra can be found by increasing the temperature from  $344^\circ\text{C}$  to  $414^\circ\text{C}$ . The further increase of temperature to  $720^\circ\text{C}$  leads to the accomplishment of the transition of Sn-OH in stannate (Sn-OH band disappears). Although the carbonate band is still obvious, its intensity decreases, which indicates that  $\text{BaCO}_3$  is consumed either for yielding  $\text{BaSnO}_3$  or by decomposition. The broadening of the band around  $1400\text{ cm}^{-1}$  at  $720^\circ\text{C}$  can be contributed to the formation  $\text{BaSnO}_3$ , because in its standard spectrum a peak also localizes in this position<sup>220</sup>.

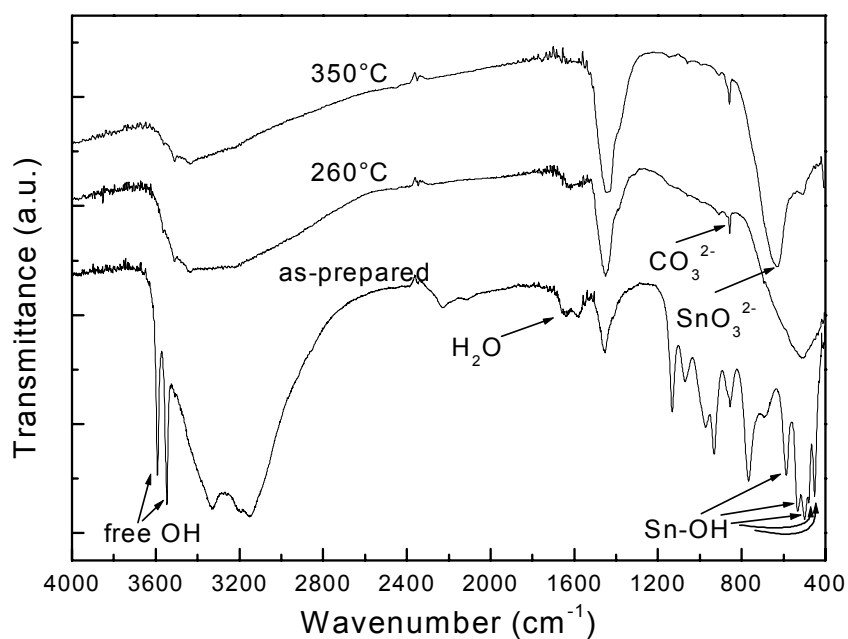
In the case of the high  $R_w$ , the free OH bands and the five sets of bands of Sn-OH<sup>79</sup> in the region  $500\text{-}700\text{ cm}^{-1}$  as well as the very small peak at  $1560\text{ cm}^{-1}$  in Fig. 25(b) indicate the nearly complete hydrolysis of the precursor. The calcination of the as-prepared sample at  $260^\circ\text{C}$  causes the weakening of OH bands, the appearance of a small carbonate band and the rounding-off of the Sn-OH bands, which correspond to the dehydroxylation, the formation of barium carbonate as well as the building of barium stannate. Increasing the calcining temperature to  $350^\circ\text{C}$ , the band of stannate becomes obvious but a small band of Sn-OH is still discernible. It can be deduced that the transformation of  $[\text{SnO}_6]$  from Sn-OH is incomplete.

The XRD patterns in Fig. 26 (a:  $R_w = 6$ , b:  $R_w = 500$ ) show that the as-prepared powders after hydrothermal treatment are crystalline. The as-prepared powder at  $R_w = 6$  consists of unknown phases and these phases transform into barium carbonate and barium stannate at  $414^\circ\text{C}$ . Increasing the calcining temperature to  $720^\circ\text{C}$  causes the further formation of barium stannate and the growth of crystallite, and the crystallite size of  $\text{BaSnO}_3$  is 49 nm.

In comparison to this, the as-prepared powder at the high  $R_w$  shows better crystallization and is made from  $\text{BaSn}(\text{OH})_6$ . After being treated at  $260^\circ\text{C}$ , the  $\text{BaSn}(\text{OH})_6$  phase converts in amorphous and the building of barium stannate takes place. The impurity of  $\text{BaCO}_3$  can also be detected. Increasing calcining temperature to  $350^\circ\text{C}$  leads to the further crystallization of  $\text{BaSnO}_3$ , its calculated crystallite size is 52 nm. A trace of an unknown phase in this powder can still be found from the diagram.

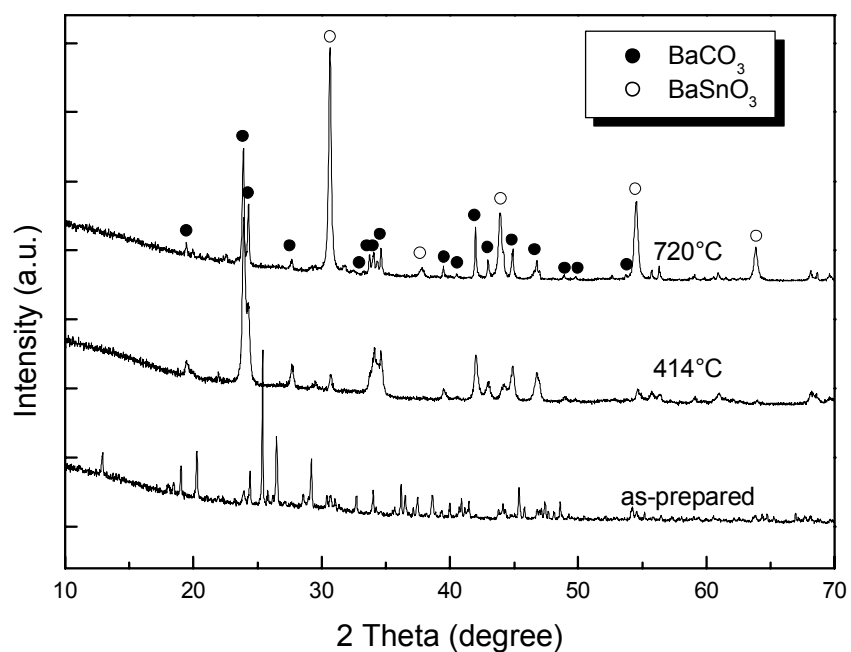


(a)

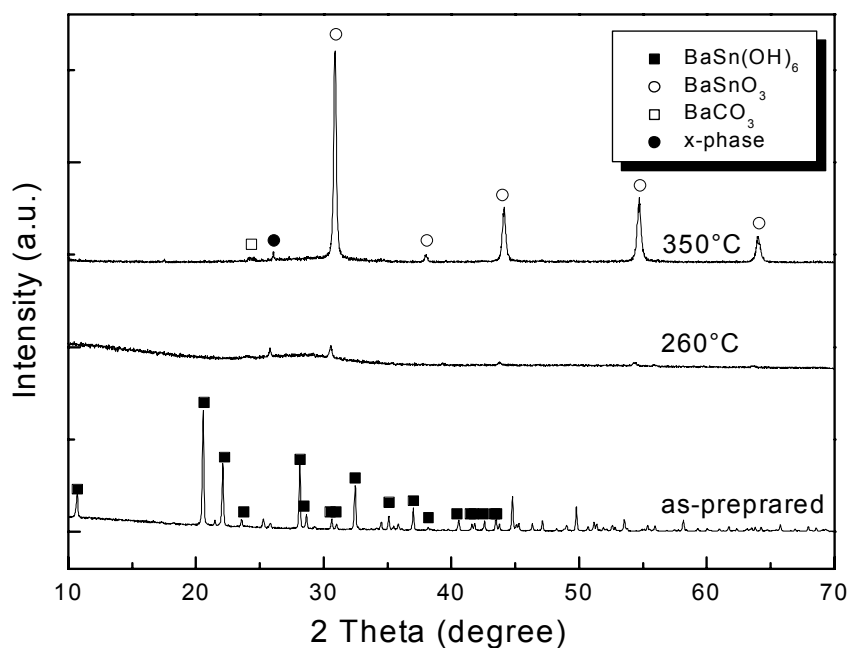


(b)

**Fig. 25** FTIR spectra of the as-prepared powder derived from  $\text{BaSn(OPr)}_6$  after hydrothermal treatment at 250°C for 6 hours and the powders calcined at different temperatures for 6 hours: (a)  $R_w = 6$ , (b)  $R_w = 500$ .



(a)



(b)

**Fig. 26** XRD patterns of the as-prepared powder derived from  $\text{BaSn(OPr)}_6$  after hydrothermal treatment at 250°C for 6 hours and the powders calcined at different temperatures for 6 hours: (a)  $R_w = 6$ , (b)  $R_w = 500$ .



In summary, the hydrothermal treatment to the hydrolysis products can intensify their crystallization. However, barium stannate cannot be directly obtained through this treatment. The constituents of the as-prepared powder depend on the value of  $R_w$ . As far as a low value of  $R_w$  is concerned, the hydrolysis proceeds incompletely and thus there are still large amounts of organic species in the powder. The decomposition and combustion of these organic species at 344°C and 414°C leads to the building of carbonate which impedes the formation of  $BaSnO_3$ . Even as the temperature is elevated to 720°C a single-phase  $BaSnO_3$  cannot be obtained, as also shown by  $CO_3^{2-}$  in the IR (Fig. 25a).

In the case of  $R_w = 500$ , the hydrothermal treatment promotes both the hydrolysis and the crystallization. Unlike the amorphous hydrolysis product which underwent no hydrothermal treatment, the as-prepared powder with a high  $R_w$  treated under hydrothermal conditions consists mainly of  $BaSn(OH)_6$ , although small amounts of remaining organic groups and a trace of an unknown phase have also been discovered in the powder. The dehydroxylation of the as-prepared powder at 260°C leads to the transformation of  $BaSn(OH)_6$  in an amorphous phase.  $BaSn(OH)_6$  does not directly convert into  $BaSnO_3$  because no coexistence of  $BaSn(OH)_6$  and  $BaSnO_3$  but coexistence of an amorphous phase and  $BaSnO_3$  has been observed.  $BaCO_3$  can be detected at the stage but its amount is very small.  $BaSnO_3$  nucleates from the amorphous phase at 260°C and grows with the increase in calcining temperature. Although a nanosized  $BaSnO_3$  is formed by calcination the powder at 350°C for 6 hours, the IR spectra and XRD diagram as well as TG-DTA curves show the existence of impurities. This means that a higher calcining temperature is necessary to obtain powders of the phase-pure  $BaSnO_3$  under hydrothermal conditions. However, the further increase in calcining temperature will make hydrothermal treatment insignificant compared to the conventional calcination. In view of above facts, the microstructure analysis of the resulted powder was not carried out and the hydrothermal calcination in the isopropanol system was not investigated.

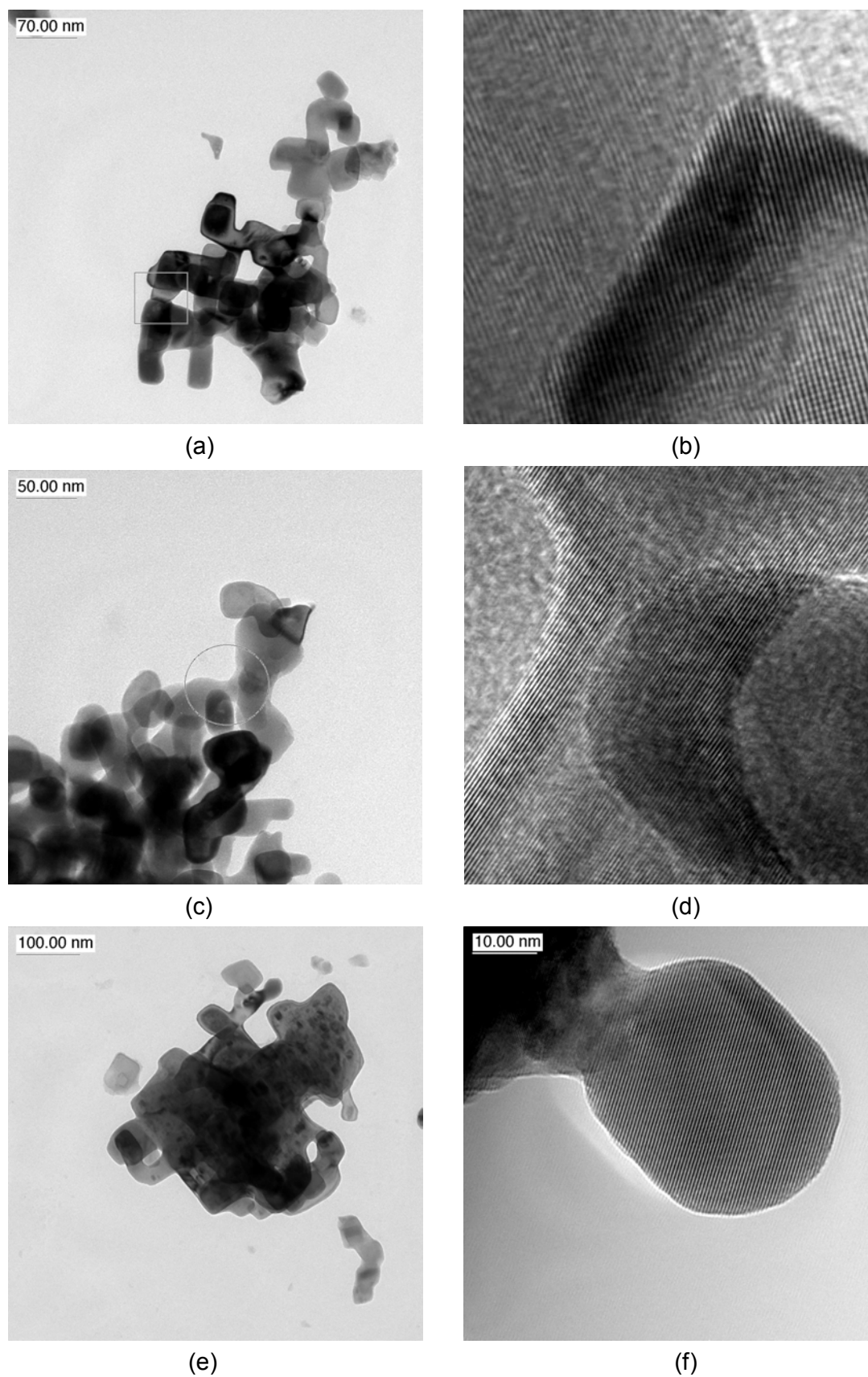
#### 5.2.4 Properties and microstructure analysis of the prepared powder

The characterized powders included only these powders calcined conventionally in the furnace (see section 5.2.3.1) because no pure  $BaSnO_3$  has been obtained through hydrothermal calcinations (section 5.2.3.2). Sample BSOE is here notes as the as-prepared powder derived from  $BaSn(OEt)_6$  and sample BSOP is that derived from  $BaSn(OP_r^i)_6$ .  $BaSnO_3$  powders are obtained by calcining BSOE and BSOP at 760°C for 6 hours. The synthesis conditions and their properties are listed in Table 4 (also see section 5.2.3.1 about their thermal behaviors, structural changes and crystallization behaviors during heat treatment). From the table we can find that the specific surface area of the calcined BSOE is about one fourth of that of the calcined BSOP. The crystallite size of the former is over 100 nm. As for the calcined BSOP powder, its crystallite size is only 60 nm. These results indicate that isopropanol system is more suitable for preparing nanosized  $BaSnO_3$  powders. For this reason the microstructure analysis in the ethanol system is only carried out for the sample calcined at 760°C while in the isopropanol system the as-prepared sample and the samples calcined at 350°C and 760 have been analyzed.

**Table 4** Properties of the prepared BaSnO<sub>3</sub> powder

Samples	BSOE calcined at 760°C	BSOP calcined at 760°C
<b>Preparation conditions</b>		
Precursors	BaSn(OEt) <sub>6</sub>	BaSn(OPr) <sub>6</sub>
Hydrolysis	90°C, 24 hours, R <sub>w</sub> =150	90°C, 24 hours, R <sub>w</sub> =150
Calcination	760°C, 6 hours	760°C, 6 hours
<b>Properties</b>		
Color	light yellow	white
Phase	BaSnO <sub>3</sub>	BaSnO <sub>3</sub>
Impurities, e.g. BaCO <sub>3</sub>	no	no
Crystallite size from XRD (nm)	>100	60
Density (g/cm <sup>3</sup> )	7.32	6.60
BET specific surface area (m <sup>2</sup> /g)	4.2	17.0
Particle size from BET (nm)	195	53

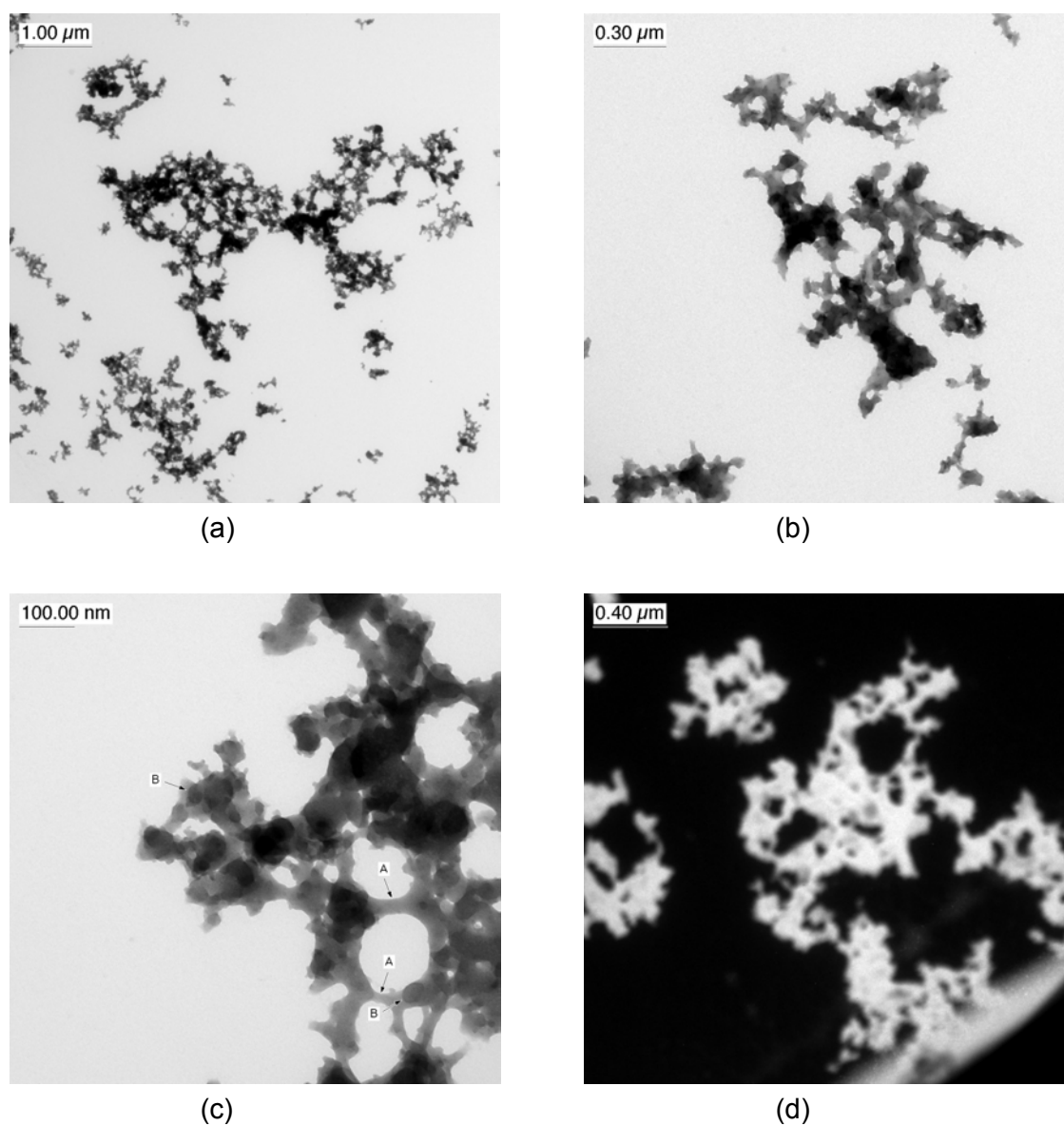
The crystallite morphology and the lattice structure of the sample BSOE calcined at 760°C was observed under the high resolution transmission electron microscope (HRTEM). Fig. 27 shows its HRTEM images. Image a, c and e indicate the typical particle cluster structure. The length of the observed clusters varies from 200 nm to 900 nm. The primary particle shows a dimension from 10 to 100 nm as well as a cubic habitus. The marked region in image a is two contacting particles, and the Fourier-filtered structure image b shows clearly that the particles adapt their cristallographic orientation to each other although there still exists a orientation discrepancy of some degrees. The distinguishable surface boundary of the two particles signalizes still no inner fusion between them. The structure image d of the fused connecting neck region marked in image c illustrates that both particles grow together after adapting their cristallographic orientation to the same angle. They combine physically with each other so that it is difficult to separate them with chemical methods. Image e shows that the structure of the cluster becomes compact with the growth and coalescence of crystallite. Image f shows clearly a single nanoparticle with a size of ca. 30 nm as well as its near cubic form. All the results show that the primary particles of BaSnO<sub>3</sub> are strongly aggregated and even coalesced. This explains why the surface area of the sample is small (4.2 m<sup>2</sup>/g).



**Fig. 27** HRTEM micrographs of BSOE hydrolyzed from  $\text{BaSn}(\text{OEt})_6$  at  $90^\circ\text{C}$  for 24 h followed by calcination at  $760^\circ\text{C}$  for 4 hours: (a)(c)(e) Diffraction and contrast images, (b)(d)(f) Structure images processed by Fourier filtering.

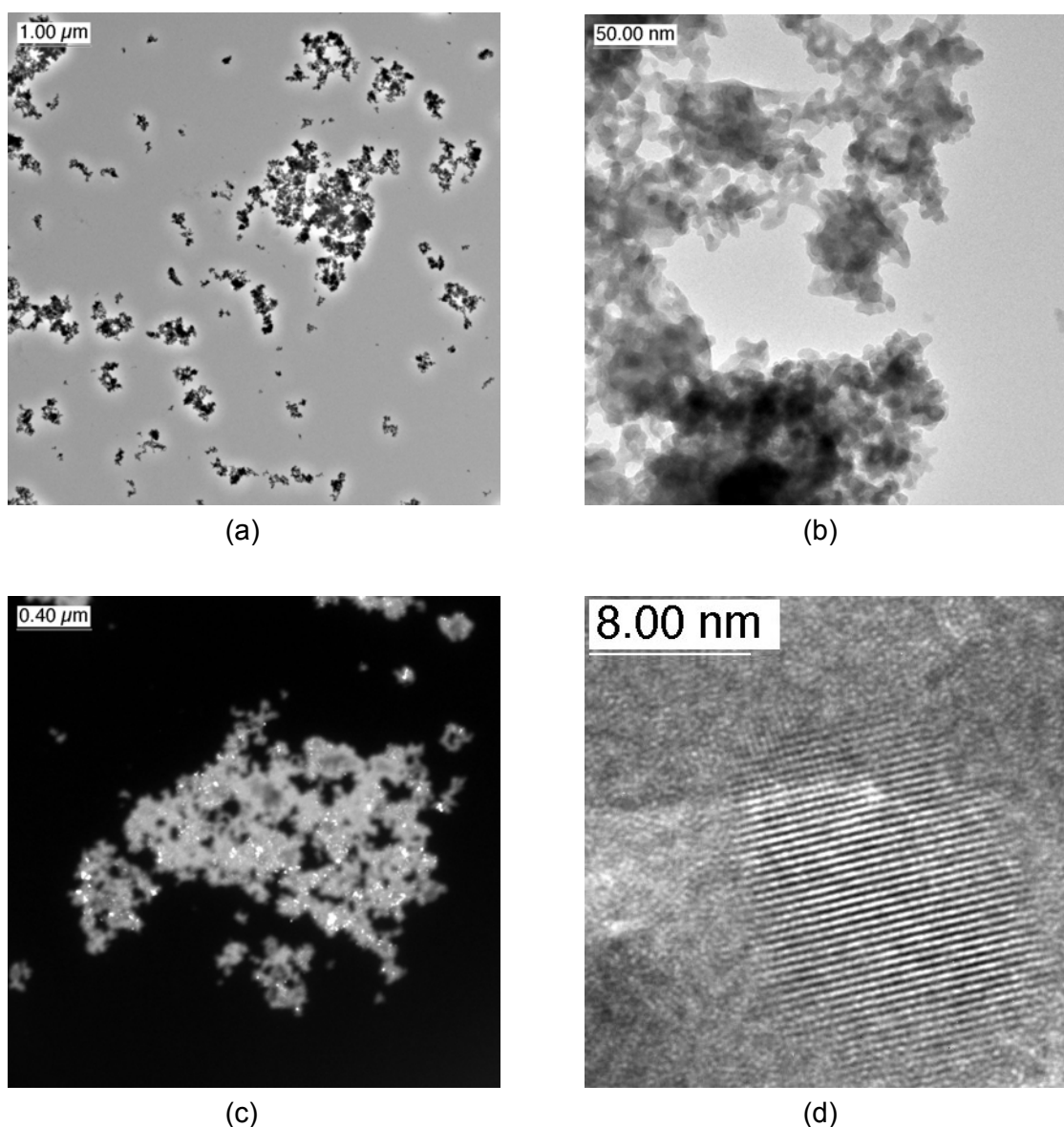
The as-prepared sample BSOP in isopropanol system and its powders calcined at 350°C and 760°C were observed under HRTEM to investigate the particle morphology and the structure transition from the as-prepared powder to BaSnO<sub>3</sub>.

Fig. 28 presents the HRTEM micrographs of the sample BSOP, the hydrolyzing product of BaSn(OPr)<sup>i</sup><sub>6</sub>. Image a and b show the branch skeleton-structured cluster of the particles. The cluster in image a is 5.0 μm long and 2.9 μm wide. Image b shows that breaking occurs in a cluster. It can be found from image c that the skeleton structure is built through the connecting bridges (arrow A), and in the compact region a single particle can also be discerned according to its contour (arrow B), its size is about 10 to 50 nm. The dark field image d shows clearly that the sample is amorphous, this is consistent with the results of XRD.



**Fig. 28** HRTEM micrographs of BSOP hydrolyzed from BaSn(OPr)<sup>i</sup><sub>6</sub> at 90°C for 24 h: (a)(b)(c) Diffraction and contrast images, (d) dark field image.

After being calcined at 350°C for 6 hours, the sample exhibits finer dendritical structure as show in Fig. 29(a). Image b shows that the skeleton structure of clusters (Fig. 28(c)) changes into a structure of agglomerated particles. The particle size is about 10 to 50 nm. The dark field image c indicates the part crystallization of the sample, and the measured lattice constant of 2.92 Å from the structure image d is well consistent with the spacing distance between 110 (2.91 Å) of BaSnO<sub>3</sub>. This confirms that the formation of BaSnO<sub>3</sub> begins at 350°C.



**Fig. 29** HRTEM micrographs of BSOP hydrolyzed from BaSn(OPr)<sub>6</sub> at 90°C for 24 h followed by calcination at 350°C for 6 hours: (a)(b) Diffraction contrast images, (c) dark field image, (d) structure image.

Fig. 30 presents the micrographs of BaSnO<sub>3</sub> powder obtained by calcining at 760°C for 6 hours. Image a show the well-crystallized particles. It can be seen from image b that the particle size varies from 20 to 60 nm. The remains of the thin bridge as indicated by the

arrows strongly suggest the breaking of the binding. The structure image c shows the formation of the twin crystal. In image d a particle has fused with another one and there is no structure defect in the contacting region. The above results indicate that on the one hand, the breaking of the connecting bridges takes place, on the other hand, the particles aggregate and even coalesce with each other with the increase in temperature.

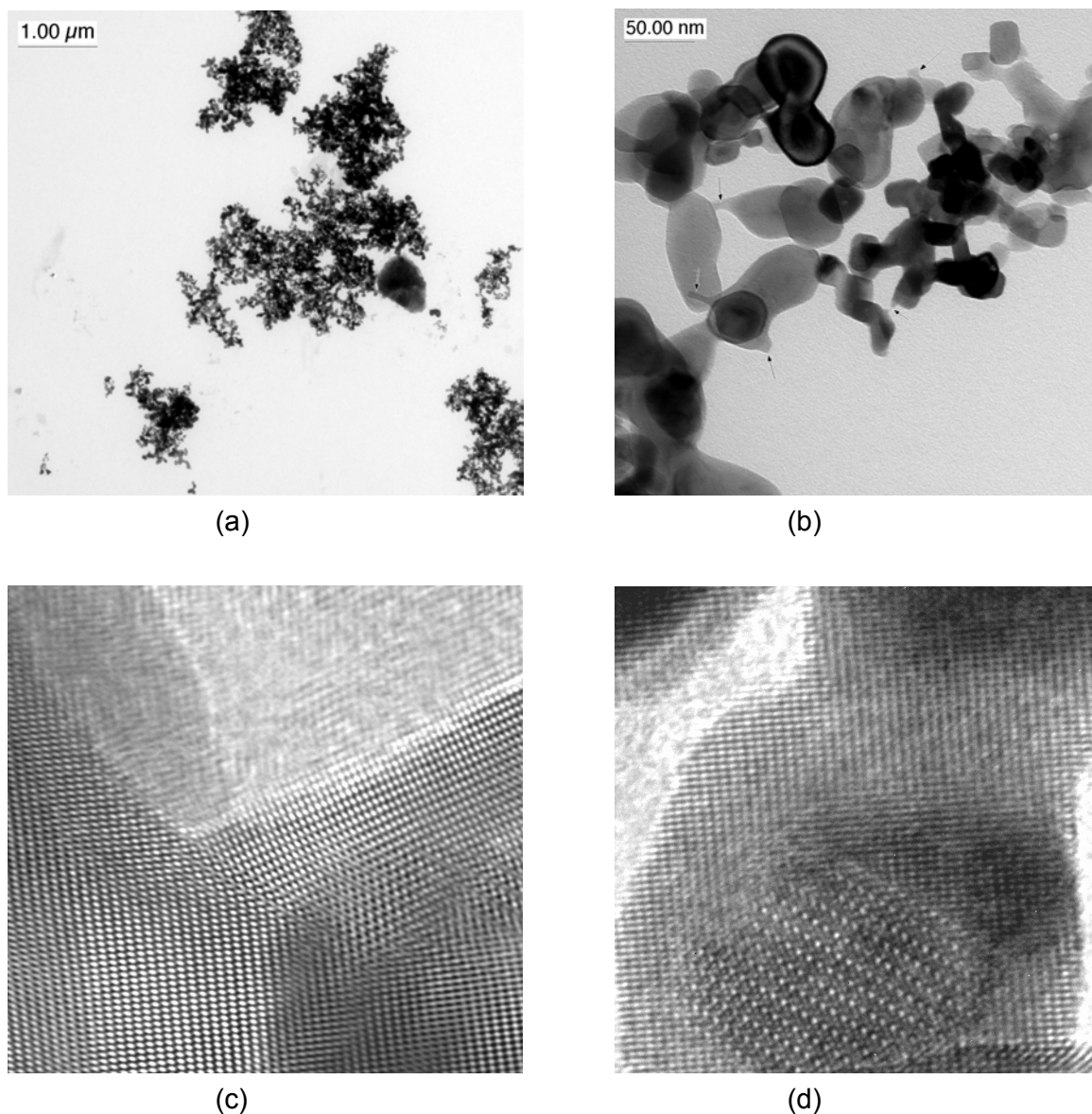
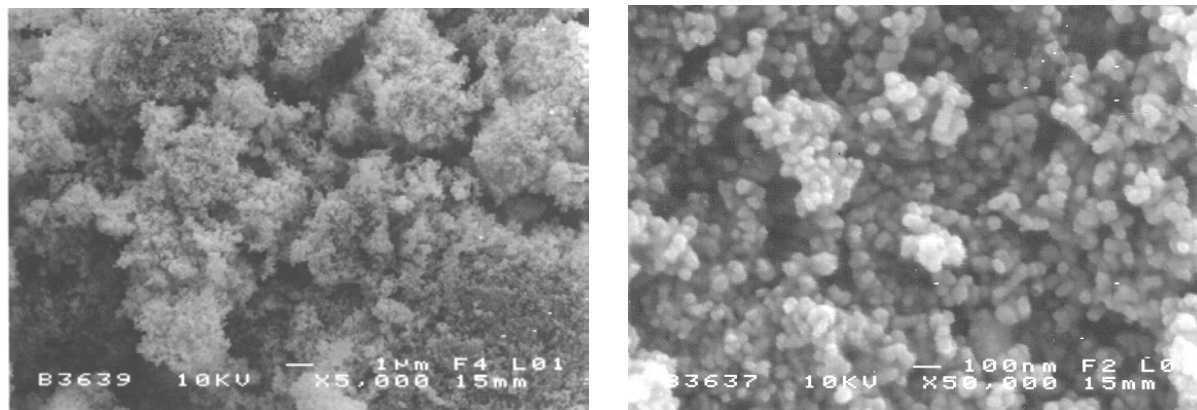


Fig. 30 HRTEM micrographs of BSOP hydrolyzed from  $\text{BaSn}(\text{OPr})_6$  at  $90^\circ\text{C}$  for 24 h followed by calcination at  $760^\circ\text{C}$  for 6 hours: (a)(b) Diffraction and contrast images, (c)(d) structure images.

The SEM photos of the same  $\text{BaSnO}_3$  sample (Fig. 31) show the cluster structure of the aggregated spherical particles with a size of 40 - 60 nm, which matches well with the result of XRD (53 nm).



**Fig. 31** SEM micrographs of BSOP hydrolyzed from  $\text{BaSn}(\text{OPr})_6$  at  $90^\circ\text{C}$  for 24 h followed by calcination at  $760^\circ\text{C}$  for 6 hours.

The above results illustrate the network skeleton structure of the hydrolyzing product in the isopropanol system. It is well known that the skeleton structure forms through the connection of hydrogen and oxygen bridges with metal atoms. It can be concluded from the micrographs that the splitting of these binding bridges occurs during the thermal treatment. This splitting corresponding to the dehydroxylation processes leads to the rearrangement of the structure and the formation of nanoparticles. It has shown that the nucleation of  $\text{BaSnO}_3$  begins at  $350^\circ\text{C}$ . The agglomeration of the particles and the further increase in temperature contribute to the fusion of particles. The  $\text{BaSnO}_3$  particles calcined at  $760^\circ\text{C}$  are strongly aggregated.

A nanosized barium stannate powder has been prepared via the metal alkoxide route for the first time. However, the aggregation of the  $\text{BaSnO}_3$  particles are severe. The main reason lies in the high calcining temperature (the minimal temperature is  $550^\circ\text{C}$ ). It has been found that  $\text{BaSnO}_3$  can form at  $350^\circ\text{C}$ , but the decomposition of the remaining organic species, which can not be removed even by addition of excess of water and by intensifying the hydrolyzing condition such as hydrothermal treatment, results in an impure carbonate phase and makes it impossible to obtain the single-phase  $\text{BaSnO}_3$  at a low temperature. This is a fatal drawback by using the metal alkoxide route to obtain  $\text{BaSnO}_3$  powder. Furthermore, the high cost of the tin alkoxide and the low yield rate of this route are also obstacles to its application in industry. In view of these factors, another synthesis route - hydrothermal synthesis based on tin oxide gel ( $\text{SnO}_2 \cdot x\text{H}_2\text{O}$ ) for preparing the nano- $\text{BaSnO}_3$  powder has been studied and the results will be presented and discussed in the following sections.

## 5.3 Hydrothermal synthesis of barium stannate powder

### 5.3.1 Synthesis of stannic hydroxide

Stannic hydroxide (also called tin oxide hydrate or stannic acid) is the precursor used in the hydrothermal synthesis route for preparing barium stannate powder. As mentioned in the literature, there are different methods for synthesizing stannic hydroxide. The widely used route is nevertheless hydrolysis of tin chloride in an alkaline solution because of its low costs and simplicity. However, there are still some problems to solve in this route. First of all, it is not clear under which conditions a reactive stannic hydroxide can be obtained. As far as barium stannate is concerned, an active stannic hydroxide should react with barium hydroxide to form barium tin compounds which can convert into  $\text{BaSnO}_3$ . In this section synthesis of a reactive stannic hydroxide and characterization of this precursor will be described.

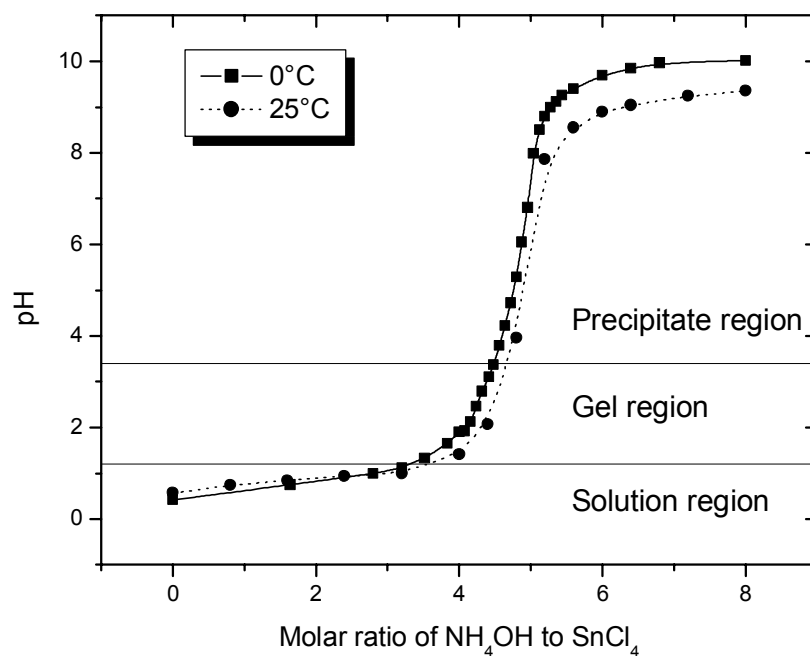
#### 5.3.1.1 Reactions between $\text{SnCl}_4$ and ammonia

It is well known that tin oxide hydrate is an amphoteric compound whose properties depend on the pH value of the solution. It is indicated from experiments that the reaction between  $\text{SnCl}_4$  and ammonia solution is an exothermal reaction. To study the pH change of this reaction with the reactant ratios, 1 M tin chloride was titrated with 2.5 M ammonia solution at  $0^\circ\text{C}$  and  $25^\circ\text{C}$  respectively. It can be found from Fig. 32 that at  $25^\circ\text{C}$  the pH value increases rapidly in the ratio range of 4 to 5.5 and that an equivalency point appears at 5. As the temperature was lowered from  $25^\circ\text{C}$  to  $0^\circ\text{C}$ , a shift of the titration curve to the lower molar ratio has been observed. This indicates that decreasing temperature promotes the accomplishment of the reaction, which is consistent with the reaction balance theory that decreasing temperature is beneficial to the accomplishment of an exothermic reaction. It is also shown that the appearance of the resultant is dependent on pH, but has little relation with temperature. The resultant appears as a gel in the pH range of 1.2 to 3.4. When pH is higher than 3.4, it precipitates.

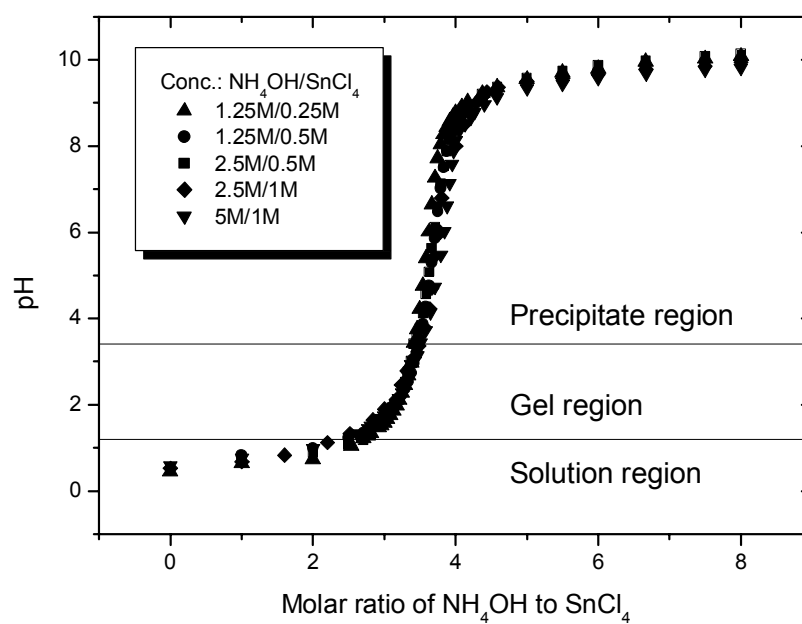
The existence of the colloidal solution regime (or sol regime), gel regime and precipitate regime can be explained by colloidal theories<sup>75</sup> as following. The initial nuclei of  $\text{SnO}_2 \cdot x\text{H}_2\text{O}$  grow because of Ostwald ripening. With the particle growth its surface is charged with ions, which leads to the formation of an electric double-layer on the particle surface according to DLVO theory. The repulsive barrier of this layer stabilizes the whole system which appears as a colloidal solution. With increasing in pH, the ion concentration increases, as a result, the double layer is compressed and becomes thinner. As the double-layer repulsion is reduced to that point that the net interparticle potential is attractive, the colloidal solution will coagulate. The aggregates of particles (clusters) collide with each other so that links form between them to produce a single giant cluster, at that point, a gel is formed. When the pH



reach to a definite value, the higher aggregation rate let the formation of a giant cluster spanning the whole vessel impossible because of the stiffness of the clusters, then small clusters can exist simultaneously, and the product appears as a precipitate.



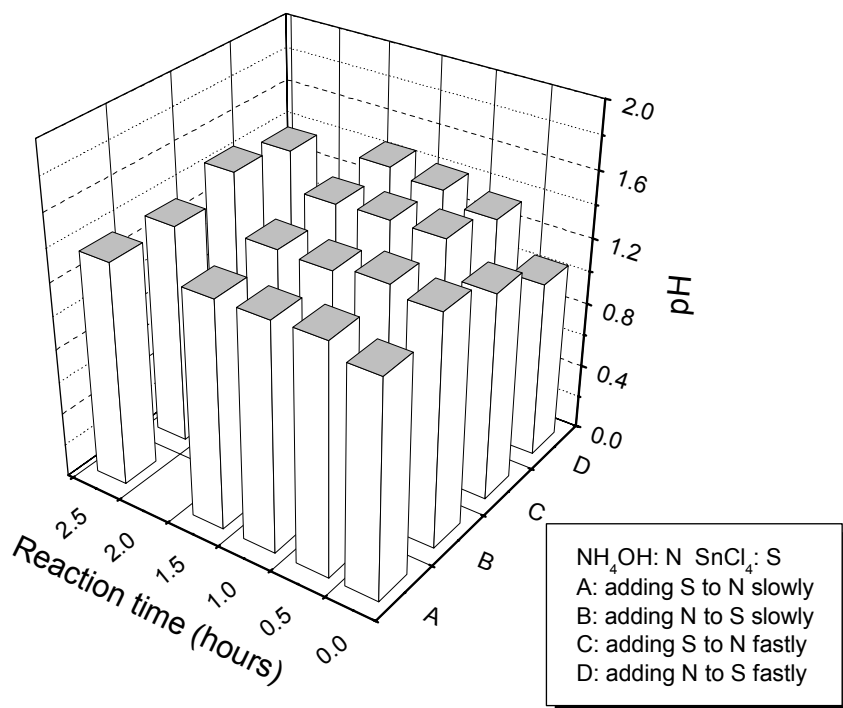
**Fig. 32** Titration curves of 1 M tin chloride by adding 2.5 M ammonia at 0°C and 25°C, the resultant shows different forms in different pH regions.



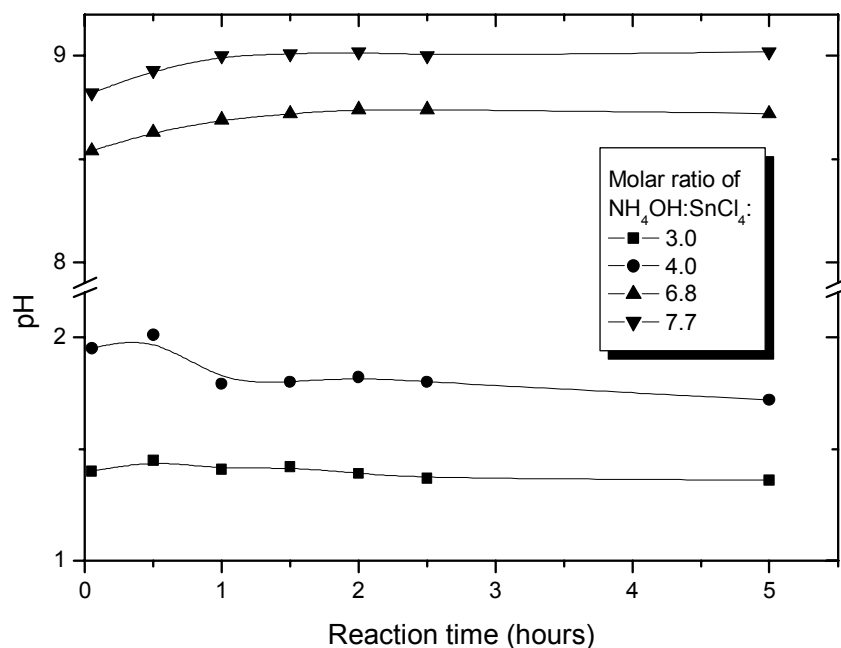
**Fig. 33** pH dependence on concentrations by titration of  $\text{SnCl}_4$  with ammonia at 0°C, the resultant shows different forms in different pH regions.

Fig. 33 presents the titration curves measured at 0°C at different concentrations of tin chloride and ammonia solution. The nearly overlap of the curves clearly shows that the concentration of tin chloride and ammonia solution has little effect on the pH value and therefore does not affect the results of the reaction. If no special specification, the concentration of tin chloride and ammonia solution used are 1 M and 2.5 M respectively.

By comparison of Fig. 32 with Fig. 33, it can be concluded that it is the pH value not the reactant molar rate that determines the forms of the resultant. Although the pH value depends mainly on the molar ratio of ammonia to tin chloride, pH at the same molar ratio of the titration curve (1M SnCl<sub>4</sub>/2.5M NH<sub>4</sub>OH at 0°C) in the two figures is different. The molar ratio difference at the equivalency point in the both figures even reaches 1. One reason for this is that the ammonia is volatile and its concentration in solution decreases with the using times. Another reason is that the pH value of the resultant is dependent on other parameters. This can be seen from Fig. 34. It is shown that the pH value changes with the mixing wise, namely adding ammonia to tin chloride solution or on the contrary, the mixing speed and the duration of the reaction. In the later synthesis of tin oxide hydrate the ammonia solution was slowly added to the tin chloride solution, and the reaction was controlled by adjusting pH with the addition of the ammonia solution. A further study of the change of pH with the reaction time is shown in Fig. 35. The pH value of the resultant becomes constant after the reaction at different molar ratios lasts for one hour. Thus, it is assumed that the reaction ends in one hour. During the synthesis of the precursor the reaction was maintained for 1 hour with stirring.

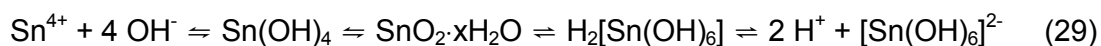


**Fig. 34** pH dependence on the mixing wise , the mixing speed and the reaction time (at 0°C, molar rate = 3).



**Fig. 35** pH changes with the reaction time at different molar ratios of ammonia to tin chloride at 0°C.

The reaction between tin chloride and the ammonia solution is a reversible reaction. It reaches the acid-base balance at the equivalency point. Theoretically the yield rate of the tin oxide hydrate at that point is the highest. However, pH changes dramatically near that point, which makes it very difficult to control the reaction precisely at the point. Therefore, it is necessary to study the completeness degree of the reaction related to pH. To characterize it the concentration of the remaining  $\text{Sn}^{4+}$  ions in the supernatant of the resultant separated with centrifugation was measured by ICP. It can be seen from Fig. 36 that the concentration of  $\text{Sn}^{4+}$  in the pH range of 1.7 - 8.8 is lower than the lowest detectable limit of ICP ( $8.1 \times 10^{-7}$  M). Even at the beginning of the gel formation region (pH = 1.2) the remaining tin concentration is low enough ( $5.1 \times 10^{-4}$  M) to be considered as negligible. Thus, it is reasonable to assume that in a wide pH range (from 1.2 to 9.5) all  $\text{Sn}^{4+}$  ions are incorporated in the tin oxide hydrate after reacting. The increase in concentration of tin ions at lower and higher pH also indicates the amphoteric properties of the tin oxide hydrate which can be expressed as formula 29:



As pH is decreased, tin oxide hydrate shows its alkalinity. The neutralization reaction shifts the balance to the left. As pH is increased, the acidity of the tin oxide hydrate leads to the shifting of the balance to the right side. As a result in both cases, the concentration of tin ions in solution increase.

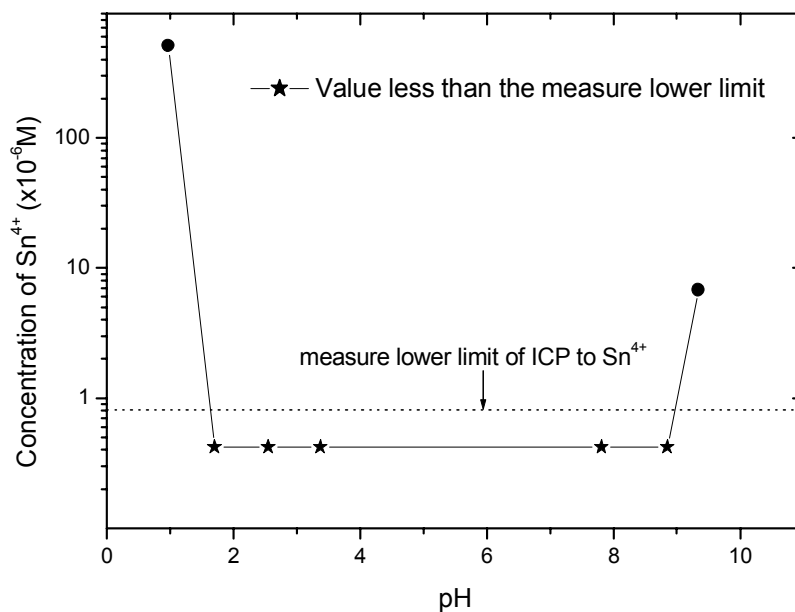


**Fig. 36** Concentrations of Sn<sup>4+</sup> in the supernatant of tin oxide hydrate separated by centrifugation as a function of the pH value.

### 5.3.1.2 Processing of tin oxide hydrate

Chloride ions are found<sup>124,165</sup> to impede the formation of multicomponent oxide powders and can lead to the particle growth because they perturb the dissolution-recrystallization process<sup>124</sup>, therefore these ions must be washed out. In experiments the synthesized SnO<sub>2</sub>·xH<sub>2</sub>O separated through centrifugation was washed several times with distilled water to remove chloride ions.

It was found that as the pH of the resultant was more than 4, the precipitate SnO<sub>2</sub>·xH<sub>2</sub>O reprecipitates in water during washing. The higher the pH value of the resultant was, the more obvious this peptization phenomenon was. Fig. 37 shows the dependence of the weight loss of the samples synthesized at pH = 2 and pH = 6 on the washing times (The basic weight is the weight of the tin oxide hydrate which was washed once. 200 ml water per 0.01 mol tin oxide hydrate was used each time). At pH = 6, the educt reprecipitates almost completely after being washed 3 times, while at pH = 2 the weight loss (including the removed impurity) after 5 times washing is only 5 wt%. Thus, the removal of Cl<sup>-</sup> ions is only possible for the tin oxide hydrate gel.

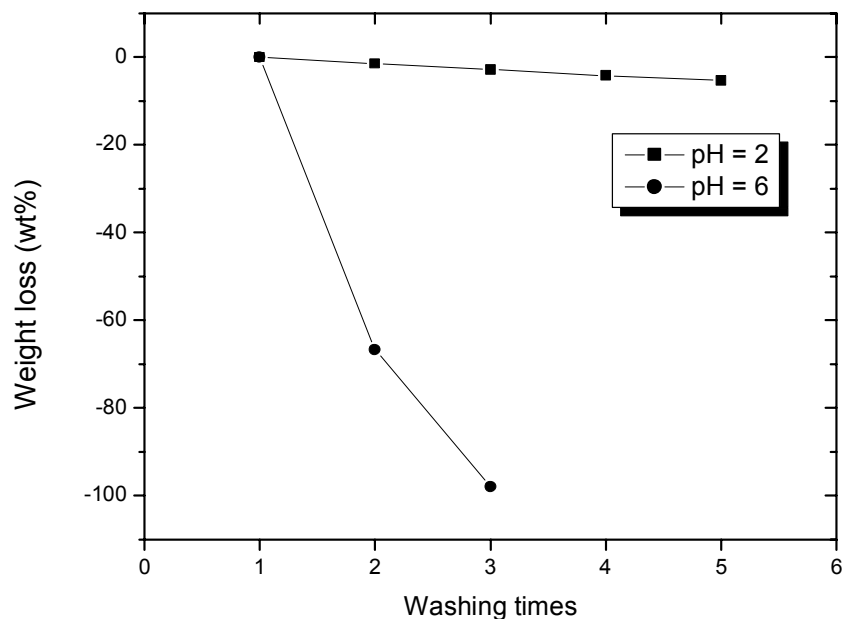


**Fig. 37** Weight loss of the tin oxide hydrate synthesized at pH 2 and pH 6 versus washing times.

The pH and the conductivity changes of the tin oxide hydrate gel synthesized at pH = 2 with washing times are shown in Fig. 38. The pH value of the gel increases with an increase in washing times because of the dilution of  $H^+$  concentration. The tin oxide hydrate is still acidic after being washed 6 times because of the acidity of the tin oxide hydrate. On the other hand, the conductivity of the gel decreases logarithmically for the first 5 washing times to  $41 \mu\text{S}/\text{cm}$  and then changes slowly. The  $\text{Cl}^-$  concentration (measured by ICP) in the tin oxide hydrate gel which was washed 5 times is  $4.0 \times 10^{-5} \text{ wt}\%$ . It is so small that the obtained  $\text{SnO}_2 \cdot x\text{H}_2\text{O}$  gel can be considered to be free of chloride ions (the  $\text{AgNO}_3$  test to the supernatant of this  $\text{SnO}_2 \cdot x\text{H}_2\text{O}$  suspension separated by centrifugation is negative). As conductivity is directly proportional to the ionic concentration of a solution, it is used here for controlling the content of ions in the gel. In experiments a tin oxide hydrate gel was normally washed 4 to 6 times until its conductivity was less than  $50 \mu\text{S}/\text{cm}$ . As to the tin oxide hydrate precipitate, it was washed only 1 to 2 times, depending on the reprecipitating degree.

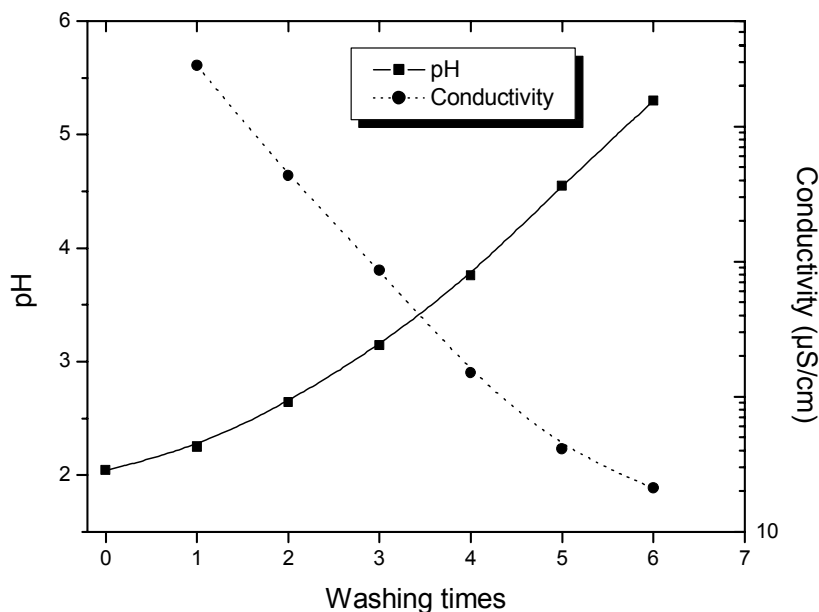


**Fig. 38** pH and conductivity of the tin oxide hydrate versus washing times.

### 5.3.1.3 Effect of pH value

As described above, pH determines the appearance of the tin oxide hydrate, and the remaining tin concentration in the pH range of 1 to 10 is very low. However, the rapid pH change in the range of 4 to 8 (see Fig. 32 and Fig. 33) makes the control of pH in this region during synthesis almost impossible. In other words, the tin oxide hydrate can only be synthesized either at a pH value of 1 to 4 or at a pH value of 8 to 10. Therefore it is important to find out how differently the pH in the acidic and alkaline regions affects the properties of the obtained tin oxide hydrate, especially its reactivity with barium compounds for preparing  $\text{BaSnO}_3$ . Only on this basis an optimal pH can be determined.

It is shown in Fig. 39 that pH affects the BET specific surface area, the density and the average particle size of  $\text{SnO}_2 \cdot x\text{H}_2\text{O}$ . As pH is controlled at near 2, the specific surface area of  $\text{SnO}_2 \cdot x\text{H}_2\text{O}$  reaches the maximum ( $197 \text{ m}^2/\text{g}$ ). The surface area of tin oxide hydrate synthesized at a pH in the acidic region is higher than that in the alkaline region. Despite the density of the precursor changes less with pH compared to the specific surface area, a similar change tendency can be observed. The largest density also locates at near  $\text{pH} = 2$ . In addition, the calculated average particle size of the tin oxide hydrate obtained in the acidic region is obviously smaller than that obtained in the alkaline region, and its minimum appears at near  $\text{pH} = 2$ . It can be concluded that the properties of a tin oxide hydrate synthesized in the acidic region is superior to that synthesized in the alkaline region, and that the optimal pH value for preparing  $\text{SnO}_2 \cdot x\text{H}_2\text{O}$  lies in near 2.

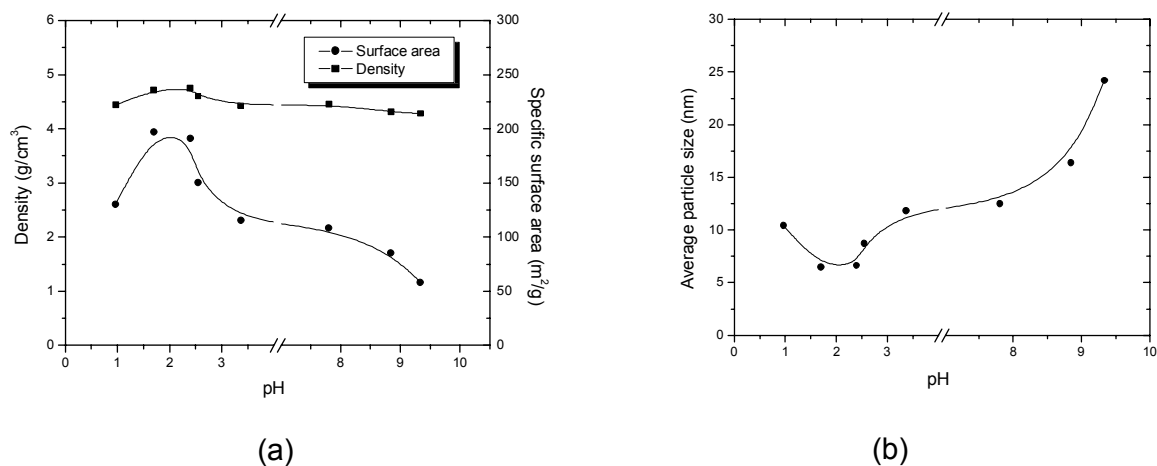


**Fig. 39** Effects of pH on the properties of the dried tin oxide hydrate: (a) Density and BET specific surface area, (b) calculated average particle size. Tin oxide hydrate samples were dried in a vacuum furnace at 80°C for 2 days and dried at 120°C for 1 day before measurement.

The reactivity of the tin hydroxide hydrate synthesized at different pH with barium hydroxide under hydrothermal conditions was investigated. Fig. 40 shows the IR spectra of the as-prepared powders. It can be seen that the molecular structure of the powders changes with an increase in pH. Compared to those derived from the alkaline tin oxide hydrate, the powders derived from the acidic tin oxide hydrate are rich of free OH groups (2800 - 3800 cm<sup>-1</sup>) and contain finer structured Sn-OH band (five peaks at 400 - 650 cm<sup>-1</sup>).

Fig. 41 illustrates the XRD patterns of the powders calcined at 260°C for 4 hours. The powders prepared from alkaline tin oxide hydrate show no signal at the position corresponding to the (110) face of BaSnO<sub>3</sub>. In contrast, at pH = 2.1 and 2.4 a BaSnO<sub>3</sub> phase with the crystalline size of 39 nm and 47 nm respectively can be identified.

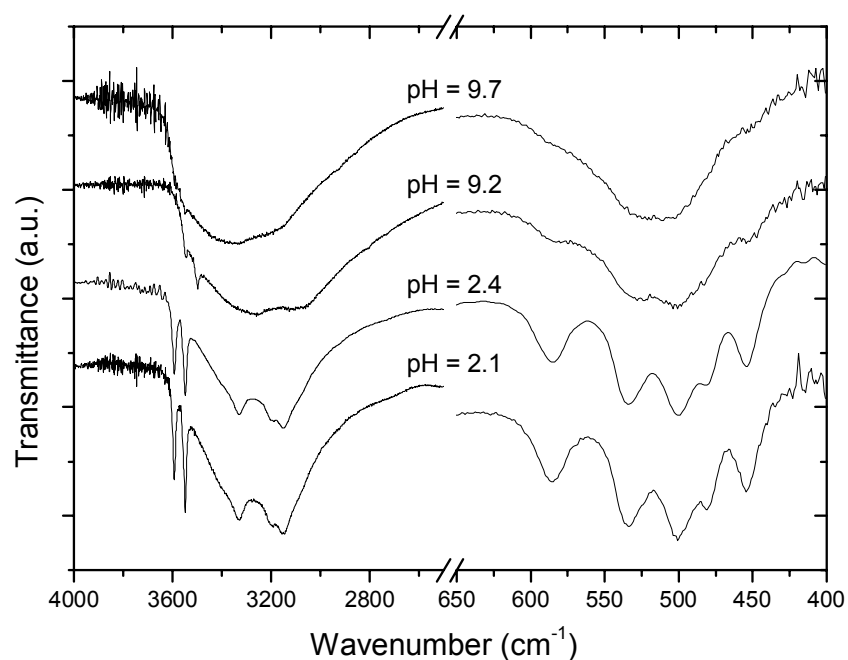


**Fig. 40** IR spectra of the as-prepared powders prepared from tin oxide hydrates which were synthesized at different pH values (KBr pellets). Tin oxide hydrates were dried in a vacuum furnace at 80°C for 2 days.

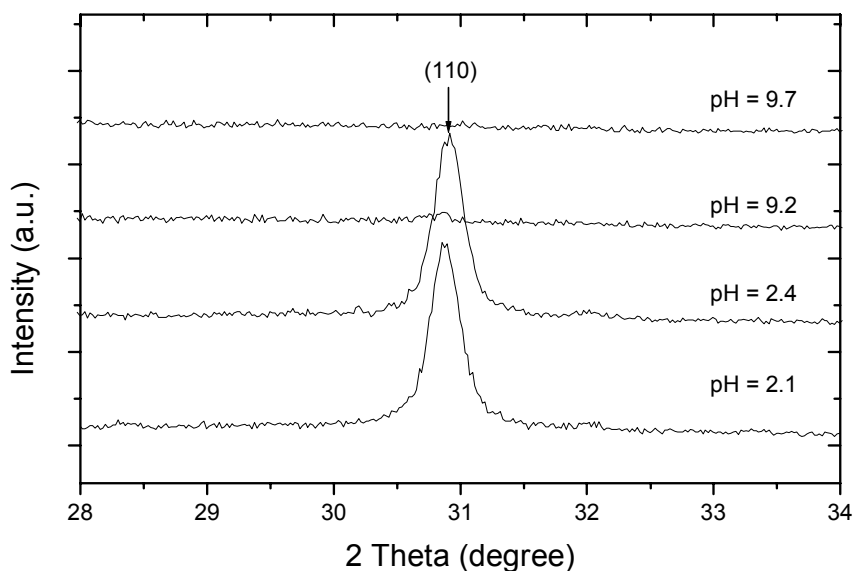


**Fig. 41** XRD patterns of the as-prepared powders calcined at 260°C for 4 hours versus pH, at which the tin oxide hydrate was synthesized.



Fig. 42 shows the SEM micrographs of the powders derived from different tin oxide hydrate. The particles derived from the tin oxide hydrate which was synthesized at pH = 2.1 are rodlike and show smooth surfaces. In contrast, the particles derived from the alkaline precursor (pH = 9.2) are much larger and the surfaces are very coarse.

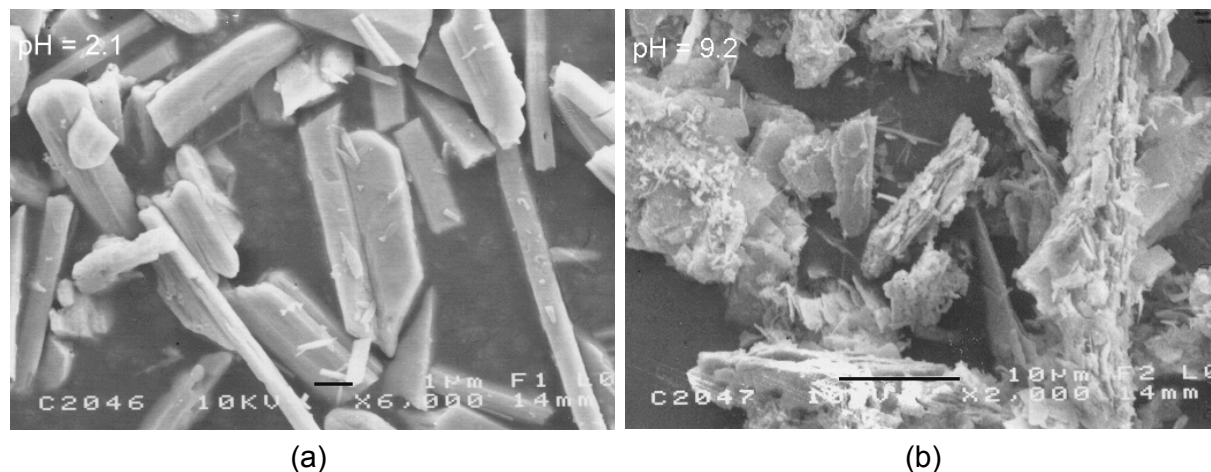
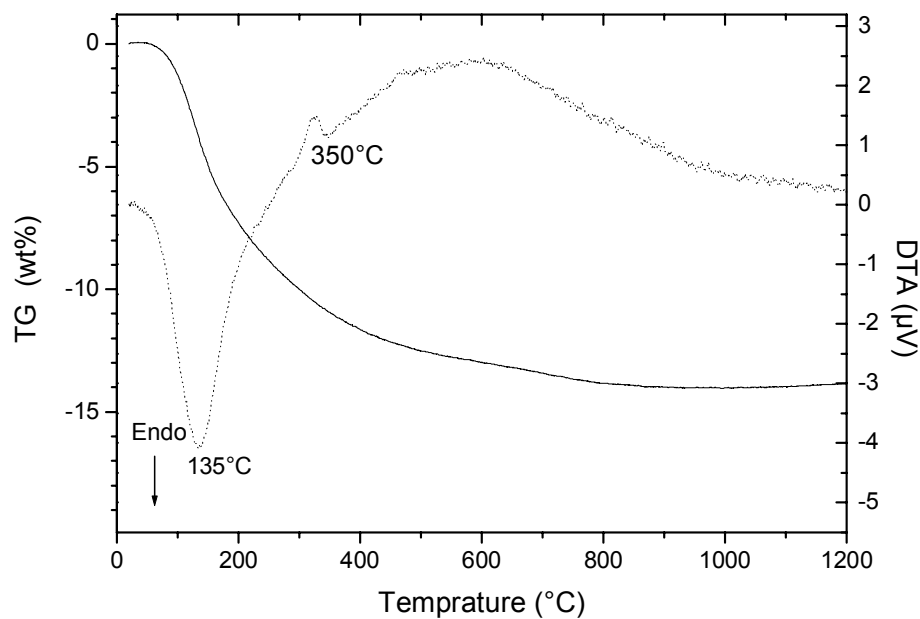


**Fig. 42** SEM micrographs of the powders calcined at 260°C for 4 hours, which were derived from the tin oxide hydrate synthesized at pH: (a) 2.1, (b) 9.2.

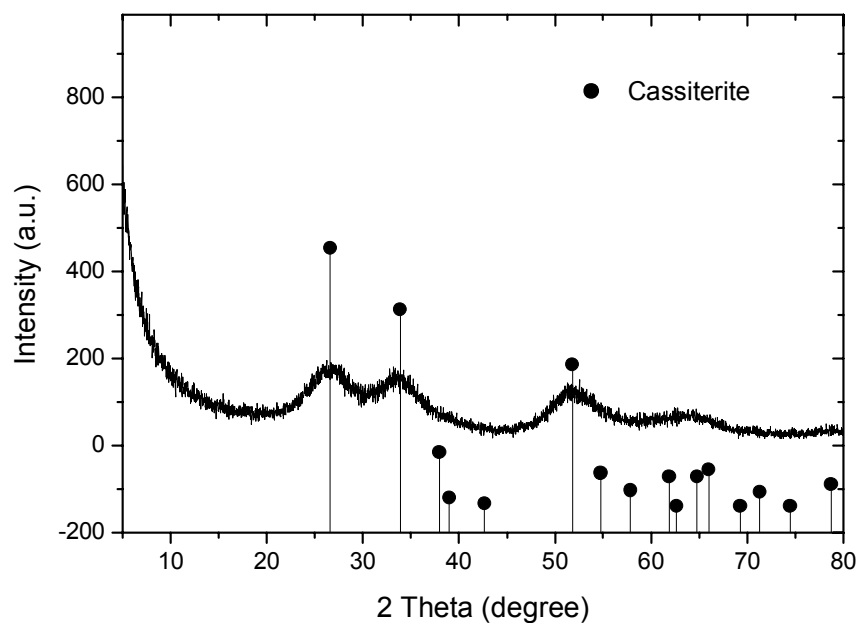
The above results indicate that pH affects the reactivity of tin oxide hydrate with barium hydroxide under hydrothermal conditions. Tin oxide hydrates synthesized in the alkaline region are inactive and cannot be used for preparing BaSnO<sub>3</sub>. In comparison with this, the acidic tin oxide hydrates are active enough to react with Ba(OH)<sub>2</sub> for preparing BaSnO<sub>3</sub>.

#### 5.3.1.4 Properties of tin oxide hydrate gel

The water content  $x$  in the fresh SnO<sub>2</sub>· $x$ H<sub>2</sub>O gel synthesized at pH = 2.1 was calculated from the weight loss by calcining the fresh gel at 800°C for 4 hours. The  $x$  value fluctuated in a range of 36.4 to 46.7. The xerogel was obtained by drying the fresh gel in a vacuum furnace at 60°C for more than two days and its  $x$  value was calculated from the TG-DTA curve (Fig. 43a). The weight loss of 13.7 wt% arising from dewatering of the gel mainly occurs at 135°C and 350°C and corresponds to an  $x$  value of 1.3. It can be found from Fig. 43b that the xerogel consists of the cassiterite phase which has not been crystallized completely. The specific surface area of the xerogel is 190 m<sup>2</sup>/g and its density is 4.60 g/cm<sup>3</sup>.



(a)



(b)

**Fig. 43** (a) TG-DTA curve, (b) XRD pattern of the tin oxide hydrate xerogel.

The electron micrographs of the xerogel are shown in Fig. 44. The scattering absorption contrast picture of the sample (image a) shows no discernible contour of particles but an agglomerated body. The single particle can be identified from the structure contrast image b

and the diameter of the particle lies in the range of 1.5 nm to 4.0 nm which agrees well with the average particle diameter calculated from the specific surface area. Image b also confirms the presence of the cassiterite phase,  $d(110) = 0.338$  nm, characterized by sets of closely spaced parallel lines (marked region).

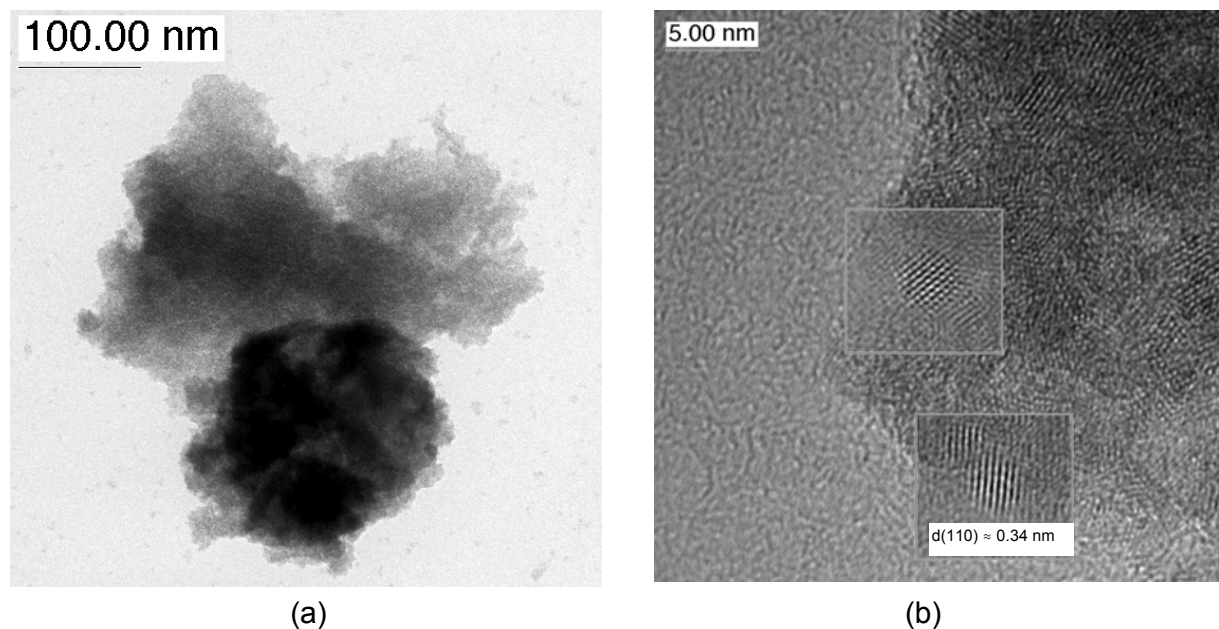


**Fig. 44** HRTEM micrographs of the tin oxide hydrate xerogel: (a) Scattering absorption contrast imaging, (b) structure contrast imaging, selected crystalline regions corresponding to images processed by Fourier transformation and filtering.

### 5.3.2 Hydrothermal reaction between $\text{SnO}_2 \cdot x\text{H}_2\text{O}$ gel and $\text{Ba}(\text{OH})_2$

It is known that the properties of the educt of hydrothermal reaction depend mainly on process parameters. As far as preparation of  $\text{BaSnO}_3$  via this route is concerned, the relationship between the properties of the educt and the process parameters has not been reported in the literature. In this section, the effects of some important parameters on the properties of the obtained powders will be discussed. At the same time, the conversion of the educt to barium stannate through calcination will also be covered.

#### 5.3.2.1 Barium source and concentration

$\text{Ba}(\text{OH})_2 \cdot \text{H}_2\text{O}$ ,  $\text{Ba}(\text{OH})_2 \cdot 8\text{H}_2\text{O}$ , and 0.15 M  $\text{Ba}(\text{OH})_2$  solution as starting materials reacted with the  $\text{SnO}_2 \cdot x\text{H}_2\text{O}$  gel under hydrothermal conditions at 250°C for 4 hours. The XRD patterns of the educts shown in Fig. 45 indicate that the powder derived from  $\text{Ba}(\text{OH})_2$  solution contains a  $\text{BaSn}(\text{OH})_6$  phase (its JCPDS 9-0053 gives no data of above 44°) and

crystallizes better than the others. It was thus determined to use barium hydroxide solution as the barium source for acquiring the best crystallized product.

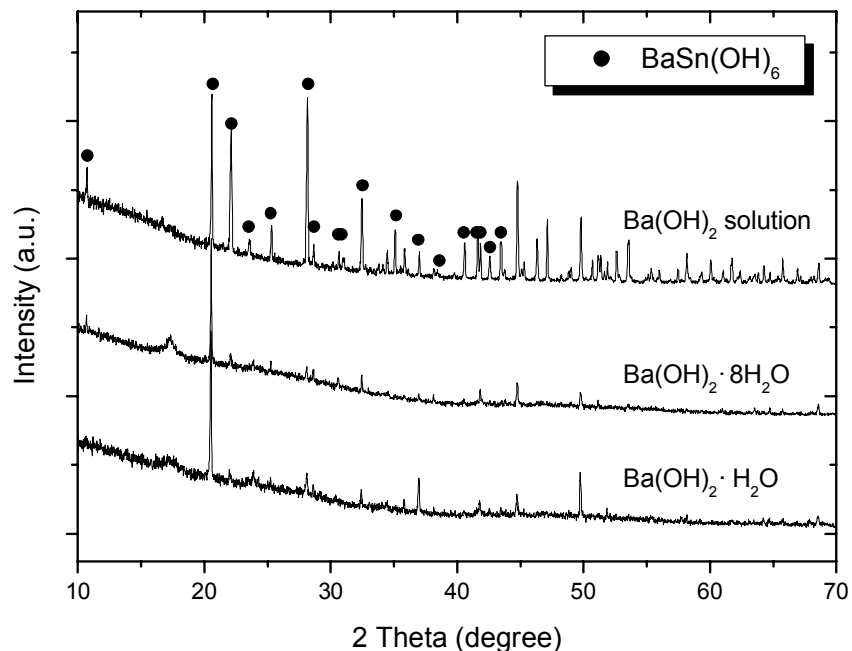
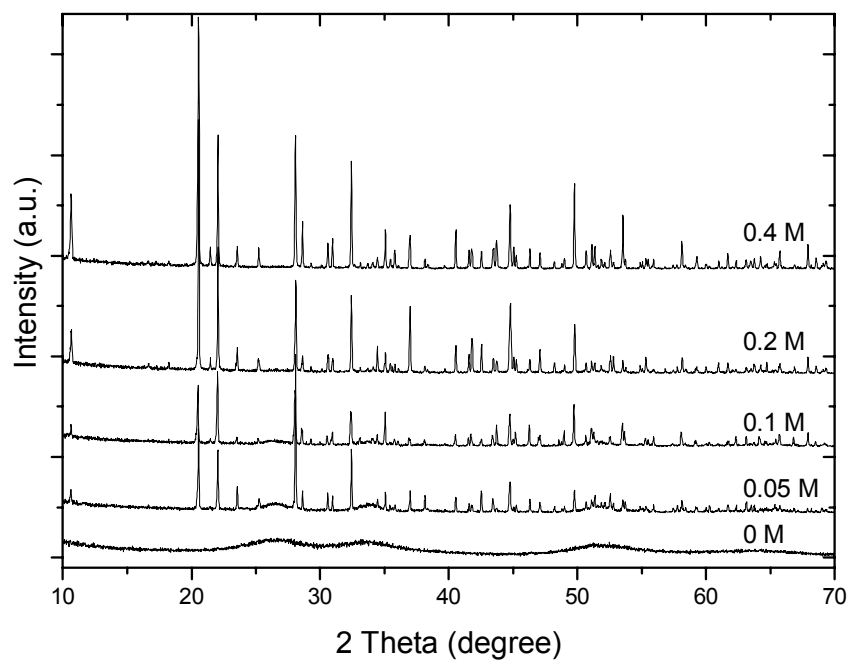
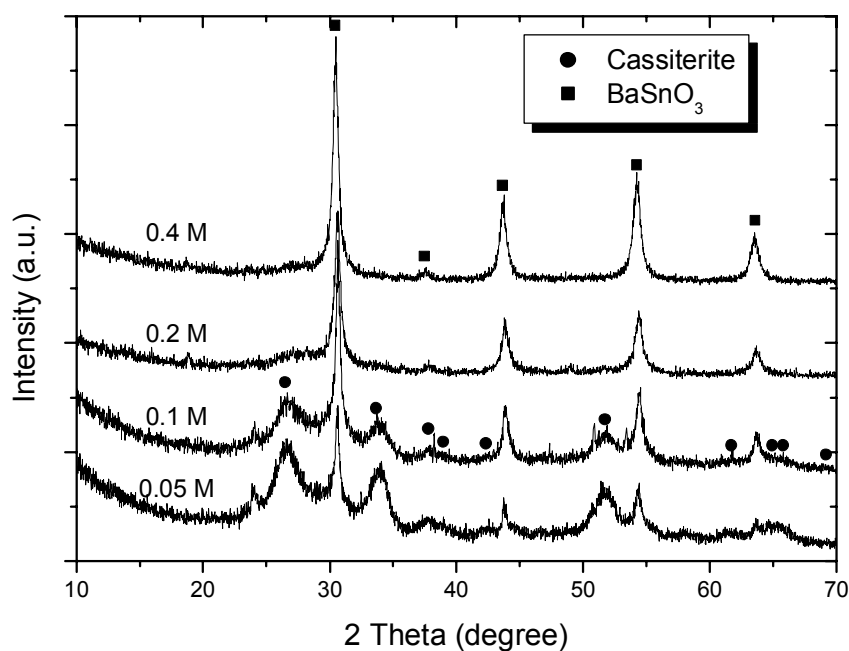


**Fig. 45** XRD patterns of the as-prepared powders derived from different barium sources and hydrothermally treated at 250°C for 4 hours.

The molar concentration of the  $\text{Ba(OH)}_2$  solution was changed from 0.05 M to 0.4 M for studying its influence. The  $\text{Ba(OH)}_2$  solution reacted with the tin oxide hydrate gel under hydrothermal conditions at 250°C for 6 hours. The educt was thereafter calcined at 260°C for 4 hours to obtain  $\text{BaSnO}_3$ . XRD analysis (Fig. 46a) indicates that an increase in the  $\text{Ba(OH)}_2$  concentration promotes the crystallization of the as-prepared powder which consists of  $\text{BaSn(OH)}_6$ . By comparison with tin oxide hydrate ( $\text{Ba(OH)}_2 = 0$  M), we can discover that there are still traces of not reacted tin oxide hydrate existing in the powder in the cases of 0.05 M and 0.1 M while no impure phase in the cases of 0.2 M and 0.4 M. It is shown in Fig. 46b that the end-powders at 0.2 M and 0.4 M are made up of  $\text{BaSnO}_3$  while the end-powders at 0.05 M and 0.1 M contain cassiterite phase besides  $\text{BaSnO}_3$ .



(a)



(b)

**Fig. 46** XRD patterns of (a) as-prepared powders, (b) powders calcined at  $260^\circ\text{C}$  for 4 hours versus the molar concentration of  $\text{Ba}(\text{OH})_2$ . The as-prepared powder was synthesized hydrothermally at  $250^\circ\text{C}$  for 6 hours.

The ratio of Sn to Ba in the calcined powder at 0.05 M and 0.4 M determined by EDS is 5.90 and 1.02 respectively. This agrees well with the XRD analysis and confirms that a very dilute  $\text{Ba}(\text{OH})_2$  solution is not suitable to prepare the  $\text{BaSnO}_3$  powder.

The dependence of the specific surface area and the density of the as-prepared powder on the molar concentration of  $\text{Ba}(\text{OH})_2$  is shown in Fig. 47. It can be found that the specific surface area and the density decrease with an increase in  $\text{Ba}(\text{OH})_2$  concentration up to 0.2 M. As we know, tin oxide hydrate has a larger specific surface area and a higher density, compared to  $\text{BaSn}(\text{OH})_6$  (also see Fig. 39). A part of tin oxide hydrate still exists in the as-prepared powder at the low concentration. Its content in the powder decreases with an increase in  $\text{Ba}(\text{OH})_2$  concentration, which results in a decrease of the specific surface area and the density of the powder. From 0.2 M to 0.4 M there is little change in density and a small decrease in specific surface area. This indicates that a further increase in  $\text{Ba}(\text{OH})_2$  concentration will cause an increase in the average particle size.

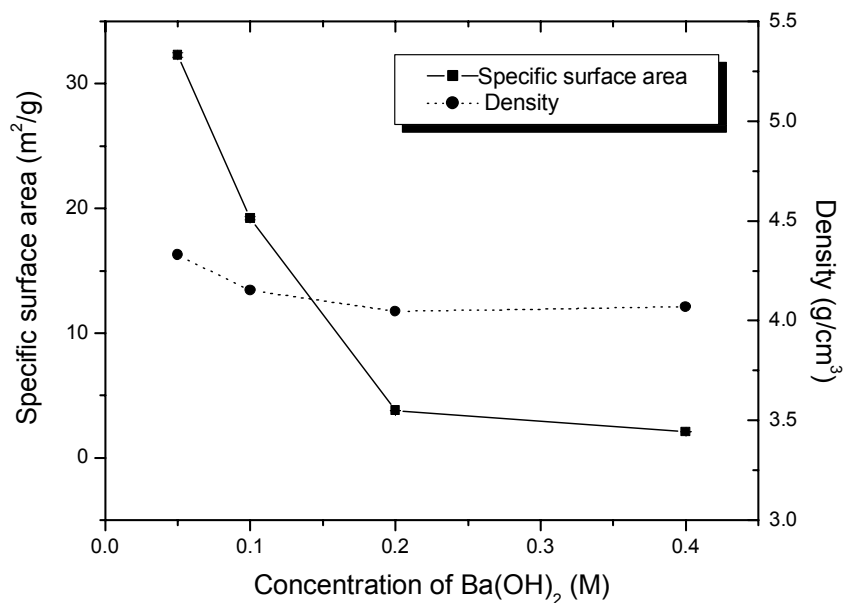


**Fig. 47** Specific surface area and density of the as-prepared powder as a function of the molar concentration of  $\text{Ba}(\text{OH})_2$ .

It can be inferred from above discussions that it is impossible to obtain a  $\text{BaSnO}_3$  powder without impurity if the concentration of  $\text{Ba}(\text{OH})_2$  is less than 0.2 M. A concentration of  $\text{Ba}(\text{OH})_2$  higher than 0.2 M can lead to an increase in particle size. In addition, the saturate solubility of  $\text{Ba}(\text{OH})_2$  at 20°C is 0.20M. Therefore, 0.2 M was determined as the concentration of  $\text{Ba}(\text{OH})_2$  for the further experiments.

### 5.3.2.2 Influence of the ratio of Ba to Sn

The starting material ratio is an important parameter to control the composition of the powder as well as its particle size. As for the synthesis of  $\text{BaSnO}_3$ , it is important to determine in which range a single-phase  $\text{BaSnO}_3$  can be obtained. Here the ratio of Ba to Sn corresponds to the stoichiometrical ratio of  $\text{Ba}(\text{OH})_2$  to  $\text{SnCl}_4$  which was added in the synthesis of the tin oxide hydrate gel (the loss of Sn during processing was neglected).

The ratio of Ba to Sn varied from 0.5 to 2. The educts, after being hydrothermally treated at  $250^\circ\text{C}$  for 6 hours and being separated through centrifugation and washed until its pH is near 7, were calcined at  $260^\circ\text{C}$  for 4 hours to realize the crystallization of  $\text{BaSnO}_3$ . The XRD patterns of the calcined powder are shown in Fig. 48. It indicates that at a low ratio of 0.5 to 0.9, where the content of barium is deficient, cassiterite and  $\text{BaSnO}_3$  exist simultaneously in the powder. Some unknown phases can also be found when the ratio is 0.8 or 0.9. Apparently cassiterite results from the not reacted tin oxide hydrate. In the ratio range of 1 to 1.2, the powder is made up of the single-phase  $\text{BaSnO}_3$ . When the Ba:Sn ratio reaches 1.5, the unknown phases appear again and coexist with  $\text{BaSnO}_3$ . No cassiterite can be discerned. At the ratio of Ba:Sn = 2,  $\text{BaSnO}_3$  coexists with an amorphous phase which can be discerned from the contour of the curve in the powder. It is worth noting that the crystallization degree of the powder is related to the ratio of Ba to Sn. The crystalline peaks of  $\text{BaSnO}_3$  show clearly that the equivalent addition of Ba and Sn promotes the crystallization of  $\text{BaSnO}_3$ .

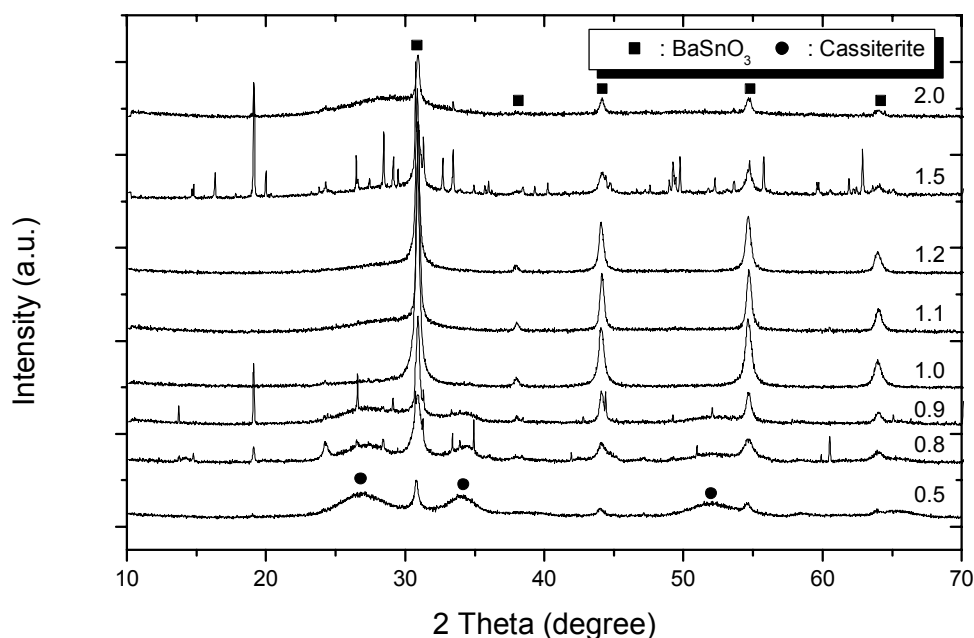


**Fig. 48** XRD patterns of powders hydrothermally synthesized at different Ba:Sn ratios at  $250^\circ\text{C}$  for 6 hours and then calcined at  $260^\circ\text{C}$  for 4 hours.

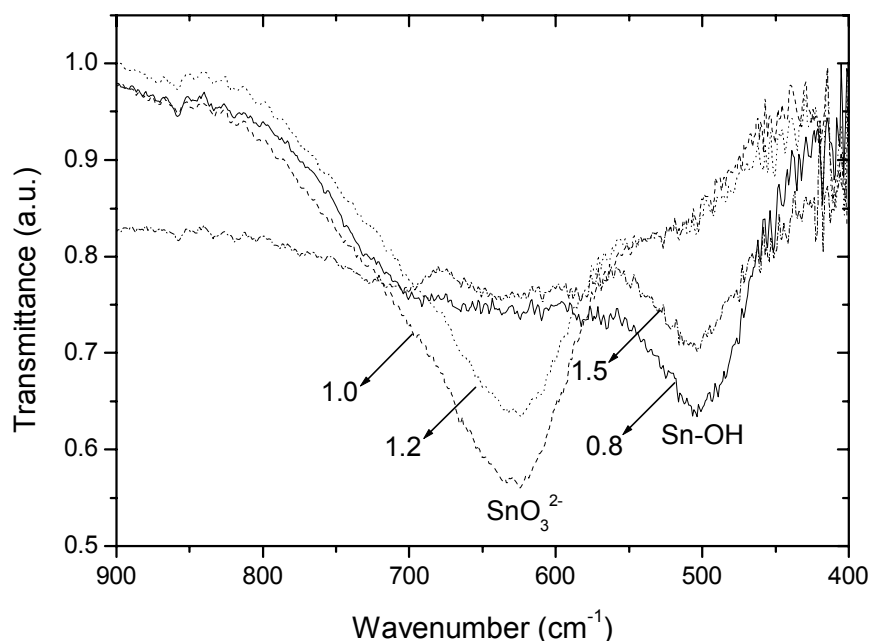


**Fig. 49** IR spectra of the powders calcined at 260°C for 4 hours versus Ba:Sn ratio.

The IR spectra of the calcined powders (Fig. 49) illustrates the structure changes at different ratios. In the case of deficiency or surplus of Barium, the Sn-OH band around 500  $\text{cm}^{-1}$  is obvious. As the ratio of Ba:Sn lies in the range of 1 to 1.2, this band disappears and the band of  $\text{SnO}_3^{2-}$  becomes dominant. Based on this fact, the unknown phases in XRD are most probably tin barium oxyhydrates.

Since the single-phase  $\text{BaSnO}_3$  can only be obtained at a Ba:Sn ratio ranging from 1 to 1.2, it is of interest to study the effects of the Ba:Sn ratio in this range on the properties of the powder. Table 5 shows that an increase in ratio within this range will lead to a decrease in density, specific surface area and an increase in crystallite size of  $\text{BaSnO}_3$ , though the differences are not large. In experiments a Ba:Sn ratio of 1.1 was adopted to guarantee the building of a single-phase  $\text{BaSnO}_3$  despite of the better quality of the powder obtained at the rate of 1.0 (also see Fig. 48 and Fig. 49).

**Table 5** Dependence of the properties of the as-prepared powder on the Ba:Sn ratio

ratio of Ba to Sn	Density ( $\text{g/cm}^3$ )	Specific surface area ( $\text{m}^2/\text{g}$ )	Crystallite size of $\text{BaSnO}_3^*$ (nm)
1.0	4.23	3.42	36
1.1	4.21	2.56	44
1.2	4.13	0.79	46

\* calculated from XRD patterns of the powders calcined at 260°C for 4 hours.



### 5.3.2.3 Hydrothermal temperature and time

The phase transformation as a function of the hydrothermal temperature ranging from 130°C to 350°C was examined. The XRD patterns of the educts obtained at different temperatures are illustrated in Fig. 50. Synthesized at a temperature between 130°C and 250°C, the hydrothermal product consists of  $\text{BaSn}(\text{OH})_6$ . When the temperature is increased to 300°C, though the product consists mainly of  $\text{BaSn}(\text{OH})_6$ , a trace of  $\text{BaSnO}_3$  can be found in it. From 330°C,  $\text{BaSnO}_3$  becomes the dominant phase in the powder. The results indicate for the first time that a  $\text{BaSnO}_3$  powder can be directly synthesized via the hydrothermal reaction when the temperature is high enough. The primary particle of the  $\text{BaSnO}_3$  powder prepared at 330°C has a dimension of 3 - 4  $\mu\text{m}$ . The coexistence of  $\text{BaSnO}_3$  and  $\text{BaSn}(\text{OH})_6$  at 300°C suggests the transformation of  $\text{BaSnO}_3$  directly from  $\text{BaSn}(\text{OH})_6$ . This differs from the phase transformation by calcination, where  $\text{BaSn}(\text{OH})_6$  converts through an amorphous phase into  $\text{BaSnO}_3$ , which will be discussed later. Study of the direct synthesis of  $\text{BaSnO}_3$  via the hydrothermal synthesis route should be a very interesting subject. However, a metal autoclave must be employed as the reaction vessel because of the high reaction temperature. The corrosive reaction of the medium to autoclave will make it difficult to obtain highly pure products. More important is that the high synthesizing temperature leads to the grain growth and limits the possibility to tailoring the properties of the powder such as adding a surfactant. Finally, the specific surface area of the obtained powder is only 0.68  $\text{m}^2/\text{g}$ . Considering the aim at preparing a nanosized powder with a large surface area, the following experiments were focused mainly on the lower temperature range ( $\leq 250^\circ\text{C}$ ), where a teflon autoclave can be used.

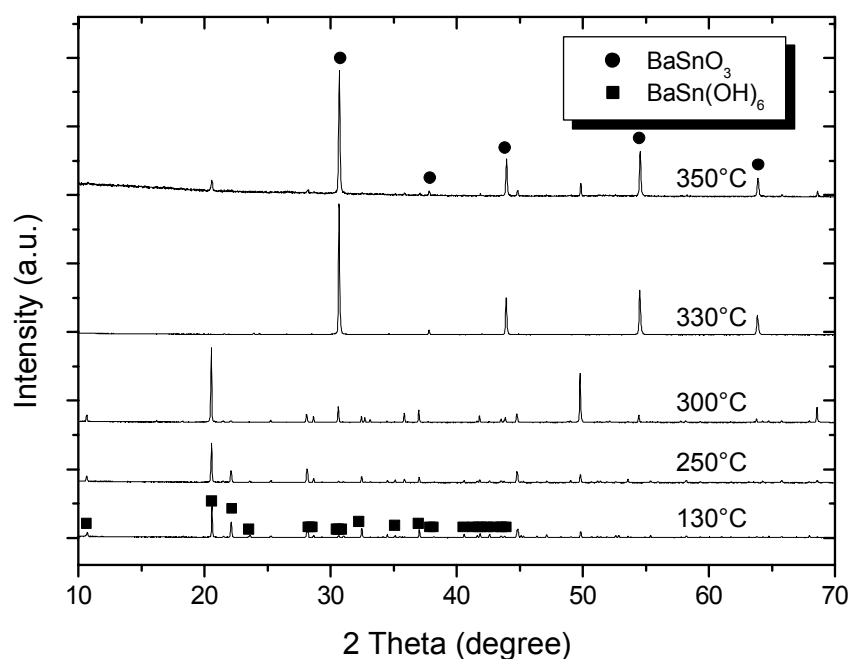
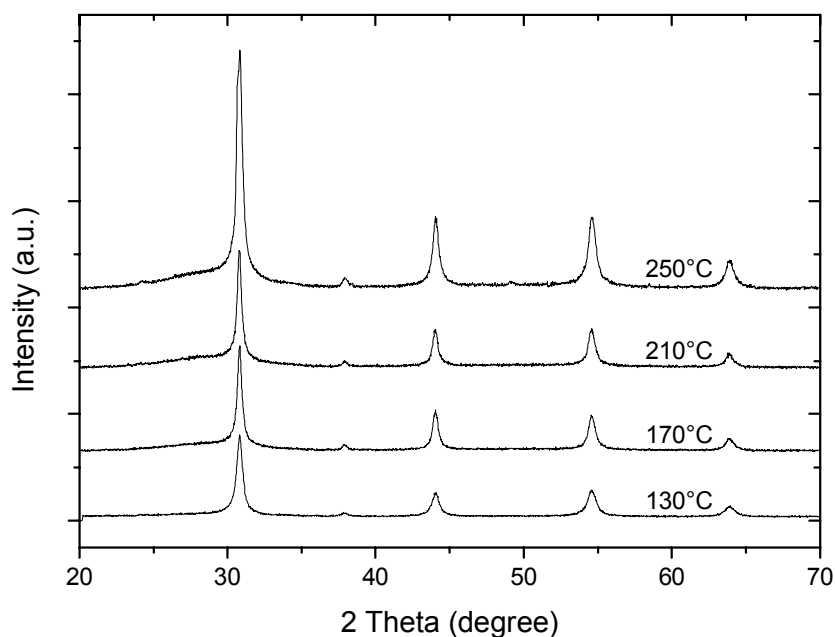


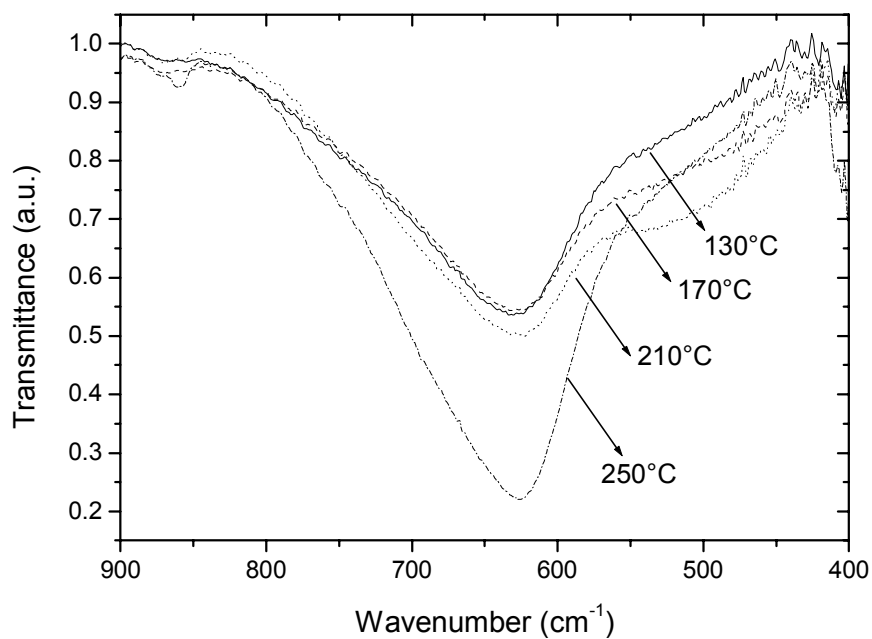
**Fig. 50** XRD pattern of the powder as a function of the hydrothermal temperature.

In the lower temperature range, the as-prepared powder consists of  $\text{BaSn}(\text{OH})_6$  which can convert into  $\text{BaSnO}_3$  by calcination. The XRD patterns and the IR spectra of the powders calcined at  $260^\circ\text{C}$  for 4 hours are shown in Fig. 51. It can be seen from XRD patterns (Fig. 51a) that regardless of the hydrothermal temperature all the calcined powders are made up of  $\text{BaSnO}_3$ . The intensity of crystalline peaks nevertheless increases with an increase in hydrothermal temperature. This suggests that a higher temperature promotes the crystallization of  $\text{BaSnO}_3$ , which can also be reflected from the IR spectra (Fig. 51b). With an increase in hydrothermal temperature the area of the  $\text{SnO}_3^{2-}$  band centered at  $630\text{ cm}^{-1}$  increases.

The effects of the hydrothermal temperature on the specific surface area and the average particle size of the powders are illustrated in Fig. 52. It can be found that the specific surface area of the as-prepared powder increases with an increase in temperature up to  $210^\circ\text{C}$  and then becomes constant. Likewise, the average particle size decreases with increasing temperature up to  $210^\circ\text{C}$  and then becomes constant. As for the calcined powder, the specific surface area increases while the average particle size decreases with an increase in hydrothermal temperature up to  $250^\circ\text{C}$ . The calcined powders show a further change from  $210^\circ\text{C}$  to  $250^\circ\text{C}$  in specific surface area and average particle size, compared to the as-prepared powders. This is considered due to the promotion of the crystallization of  $\text{BaSnO}_3$  at a higher hydrothermal temperature as shown in Fig. 51 (a).



(a)



(b)

**Fig. 51** (a) XRD patterns, (b) IR spectra of the powders calcined at 260°C for 4 hours versus the hydrothermal temperature.

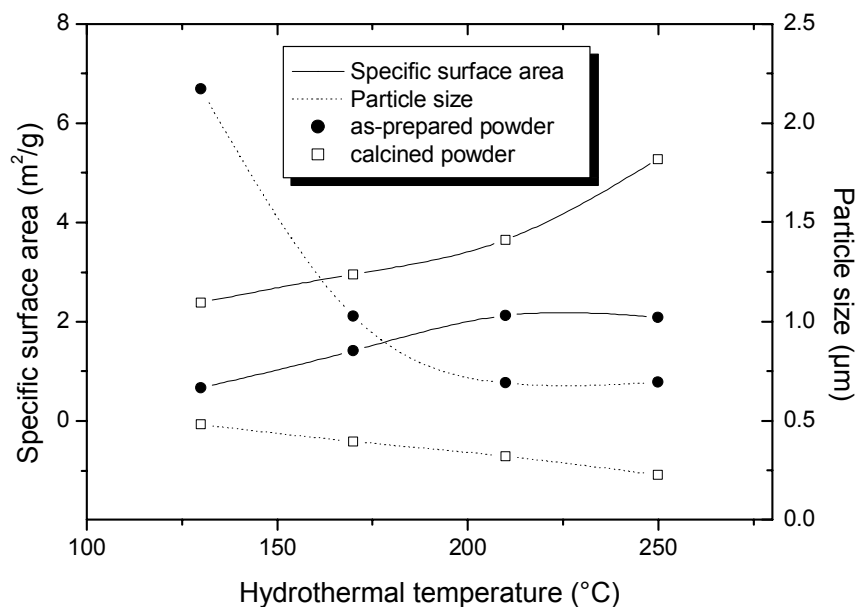


**Fig. 52** Specific surface area and particle size of the as-prepared powder and its at 260°C for 4 hours calcined powder versus hydrothermal temperature.

The above discussions indicate that a higher hydrothermal temperature in the range of 130°C to 250°C can promote the crystallization of BaSnO<sub>3</sub>, increase its specific surface area and decrease the average particle size. Therefore, 250°C was determined to be the hydrothermal temperature in the later experiments.

The duration of the hydrothermal reaction were changed from 0.5 to 10 hours. Its effects on the building of BaSnO<sub>3</sub> can be seen in Fig. 53, where the XRD patterns of the powders calcined at 330°C for 4 hours are shown. It can be found that even when the hydrothermal reaction lasts only 0.5 h, a BaSnO<sub>3</sub> powder can be obtained. The maximal peak intensity appears at 2 h and then the intensity decreases with an increase in reaction time.

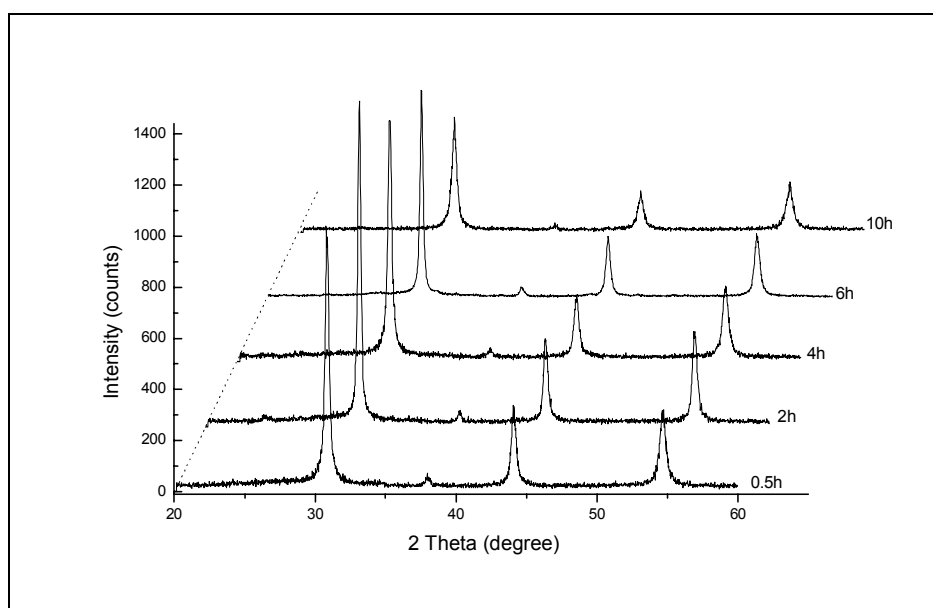


**Fig. 53** XRD patterns of the powder calcined at 330°C for 4 hours as a function of the time of hydrothermal reaction at 250°C.

The crystallite size of the powder is illustrated in Fig. 54. It shows that with the exception of 2 h the crystallite size changes little from 0.5 h to 10 h. It is difficult to explain the appearance of the maximal crystalline intensity and the maximal crystallite size at 2h, but it can be found that the duration of the hydrothermal reaction does not affect the formation and the grain growth of BaSnO<sub>3</sub> so strongly as the temperature.

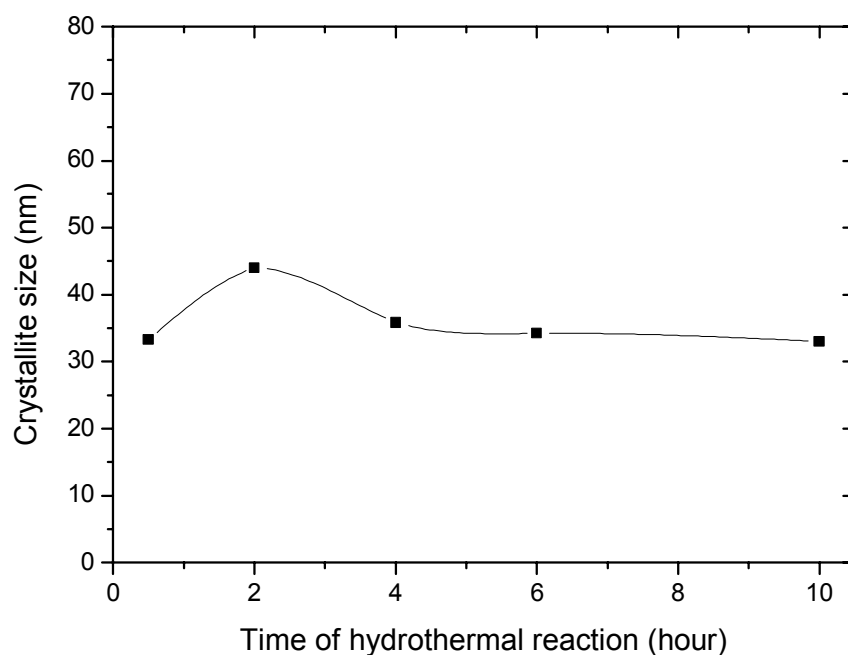


**Fig. 54** Crystallite size of the calcined powder ( $\text{BaSnO}_3$ ) versus the time of hydrothermal reaction at  $250^\circ\text{C}$ . Crystallite size is calculated from the XRD patterns of Fig. 53.

Observed under SEM, the particles of the as-prepared powder ( $\text{BaSn}(\text{OH})_6$ ) change the morphology with the reaction time (Fig. 55). As the time is increased up to 6 hours, the particles change from irregular clumps into small smooth and uniform rods. Thus, 6 hours was determined as the duration of the hydrothermal reaction in the experiment.

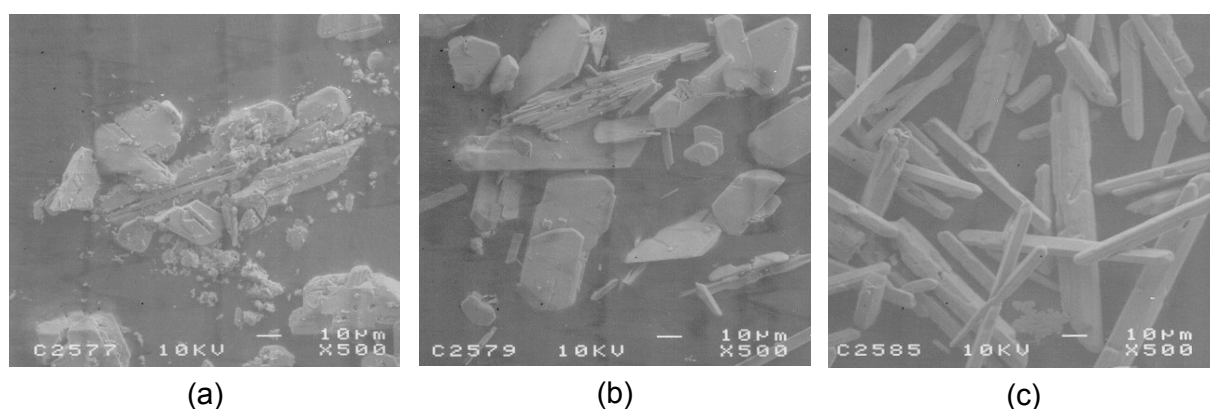
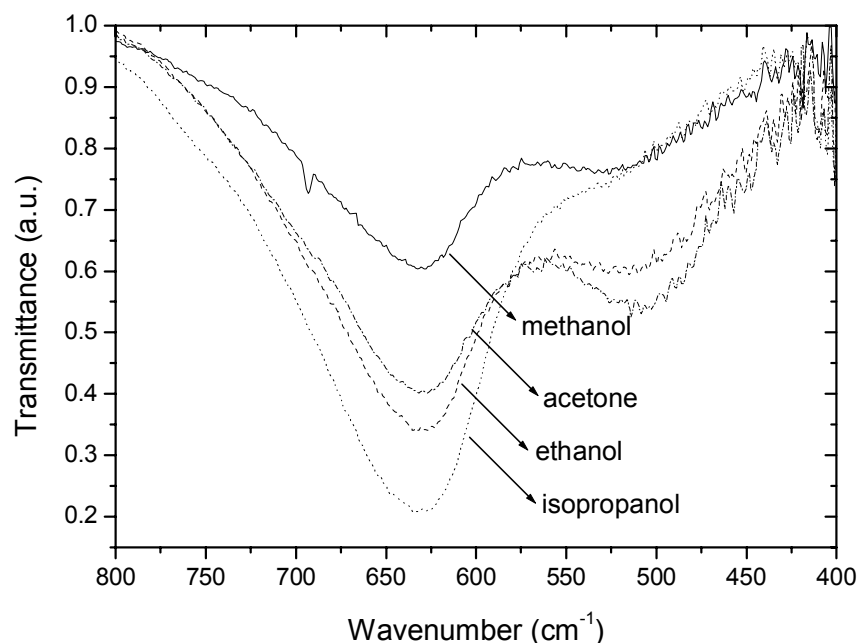


**Fig. 55** SEM micrographs of the as-prepared powder ( $\text{BaSn}(\text{OH})_6$ ) versus the time of hydrothermal reaction at  $250^\circ\text{C}$ : (a) 0.5h, (b) 2h, (c) 6h.

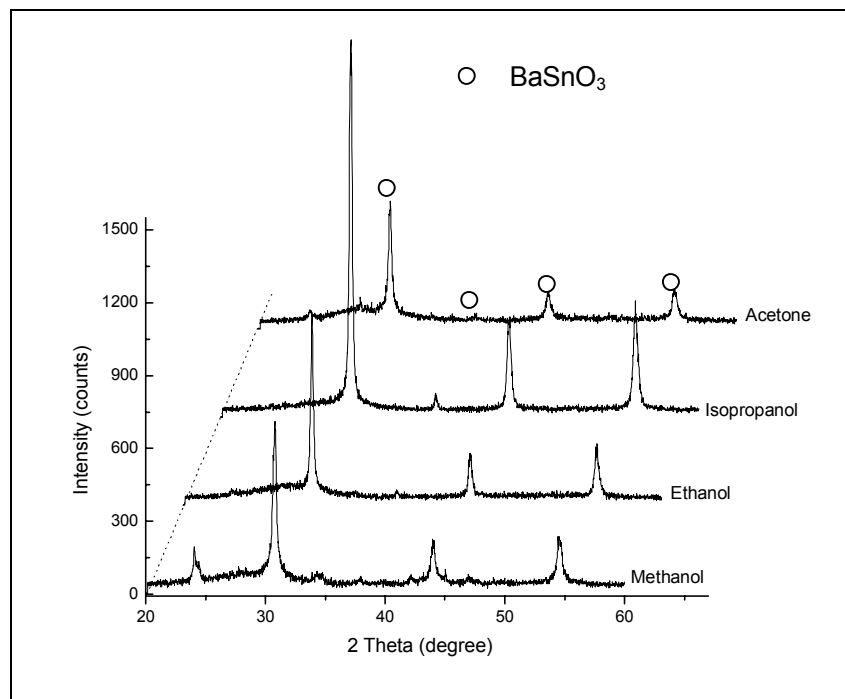
### 5.3.2.4 Effects of the solvent

As described in the literature review, the used medium in hydrothermal reaction affects the properties of the resulting powder. Thus, it has been attempted in the experiments to replace the aqueous medium with methanol, ethanol, isopropanol and acetone, respectively. After hydrothermal reaction products with smaller needle-like particles were obtained. The IR spectra and XRD patterns of the powders calcined at 260°C for 4 hours are shown in Fig. 56. In the alcoholic series the  $\text{SnO}_3^{2-}$  band centered at 630  $\text{cm}^{-1}$  intensifies with an increase in carbon atoms. As for acetone, the  $\text{SnO}_3^{2-}$  band is comparable to that of ethanol. The existence of the band of Sn-OH group around 500  $\text{cm}^{-1}$  in methanol, ethanol and acetone indicates an incomplete conversion of  $\text{BaSn}(\text{OH})_6$  into  $\text{BaSnO}_3$  in the corresponding powders. XRD patterns (Fig. 56b) show that powders synthesized in methanol, ethanol and acetone contain impure phases besides  $\text{BaSnO}_3$  while in isopropanol only  $\text{BaSnO}_3$ . In addition, among these solvents isopropanol can be found to promote the crystallization of  $\text{BaSnO}_3$  according to the crystalline peaks. It can therefore be concluded that isopropanol is more suitable for preparing  $\text{BaSnO}_3$  powder than other three nonaqueous solvents.

The mixture of water and isopropanol with different proportions has also been investigated. The results show that the mixture leads to the building of impure phases. The specific surface area of  $\text{BaSnO}_3$  prepared in isopropanol (1.74  $\text{m}^2/\text{g}$ ) is smaller than that in water (5.27  $\text{m}^2/\text{g}$ ). The crystallite size of  $\text{BaSnO}_3$  prepared in isopropanol is 41.3 nm while in water about 35 nm. This result is contrary to that in the  $\text{SrTiO}_3$  system<sup>173</sup>, where alcoholic medium can lead to a decrease in crystallite size arising from faster nucleation than water. An alcoholic solvent with more carbon atoms seems to be beneficial for preparing  $\text{BaSnO}_3$  powder.



(a)



(b)

**Fig. 56** (a) IR spectra, (b) XRD patterns of the at 260°C for 4h calcined powder derived from different solvents.

### 5.3.3 Improving the properties of the powder by peptization

The results in section 5.3.2 show that a nanoscale BaSnO<sub>3</sub> powder with a primary size of 30 to 40 nm can be prepared via the hydrothermal synthesis route. However, its specific surface area of 2 to 6 m<sup>2</sup>/g, which corresponds to a average particle size of 167 to 500 nm, suggests a strong agglomeration and aggregation in the powder. Since the SnO<sub>2</sub>·xH<sub>2</sub>O gel is suspended in the Ba(OH)<sub>2</sub> solution, the agglomeration in the gel itself will limit the homogeneity of the products and thus leads to the agglomeration in the obtained powder. In view of this fact, the attempts to acquiring a on-the-molecular-level-dispersed SnO<sub>2</sub>·xH<sub>2</sub>O precursor through peptization and the influence of the peptized tin oxide hydrate on preparation of BaSnO<sub>3</sub> will be described in this section.

#### 5.3.3.1 Peptization of the tin oxide hydrate gel

25% ammonia solution was used as the peptizing agent because NH<sub>3</sub> is easily removed and no disturbing ion is imported. Its amount affects the pH value of the SnO<sub>2</sub>·xH<sub>2</sub>O gel suspended in water. The peptizing effect of ammonia to the tin oxide hydrate gel depends

on pH, the reason is that  $\text{OH}^-$  ions provided by ammonia are absorbed on the surface of the particles, the resulted repulsive potential between the particles leads to the deaggregation. Fig. 57 shows that the suspensions at pH = 6.8 and 7.2 are milky white. From pH 8.3 the suspensions become transparent after aging for one day. The peptized solution with pH 8.3 and pH 8.7 changed into transparent gels later while the peptized solution at a pH above 9.0 is still stable after being placed at room temperature for one year.

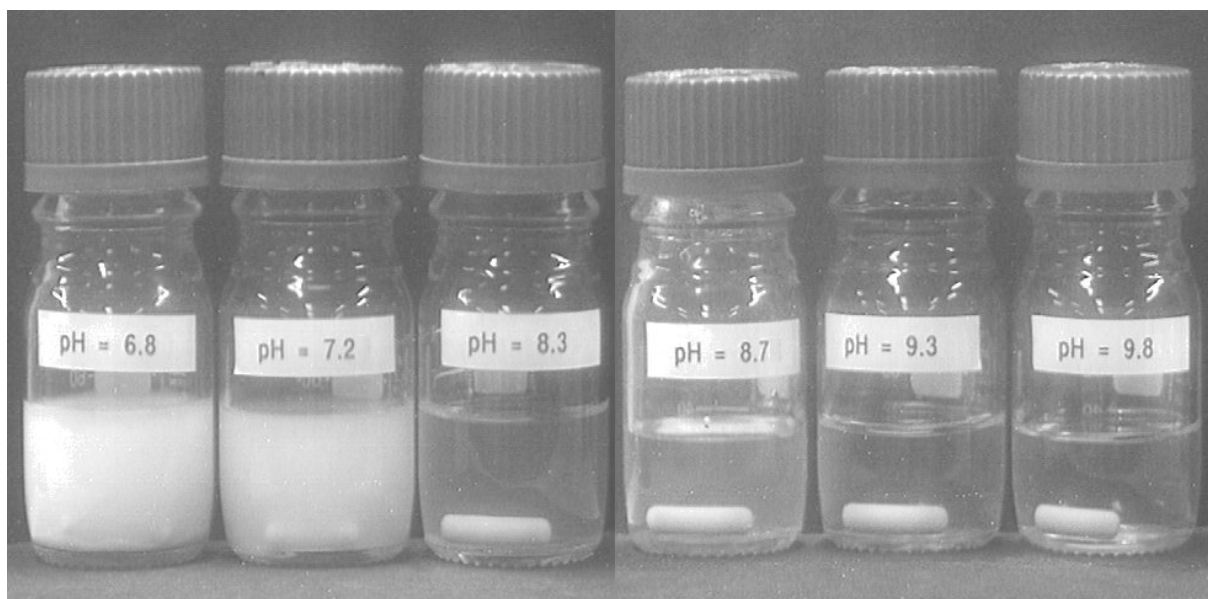
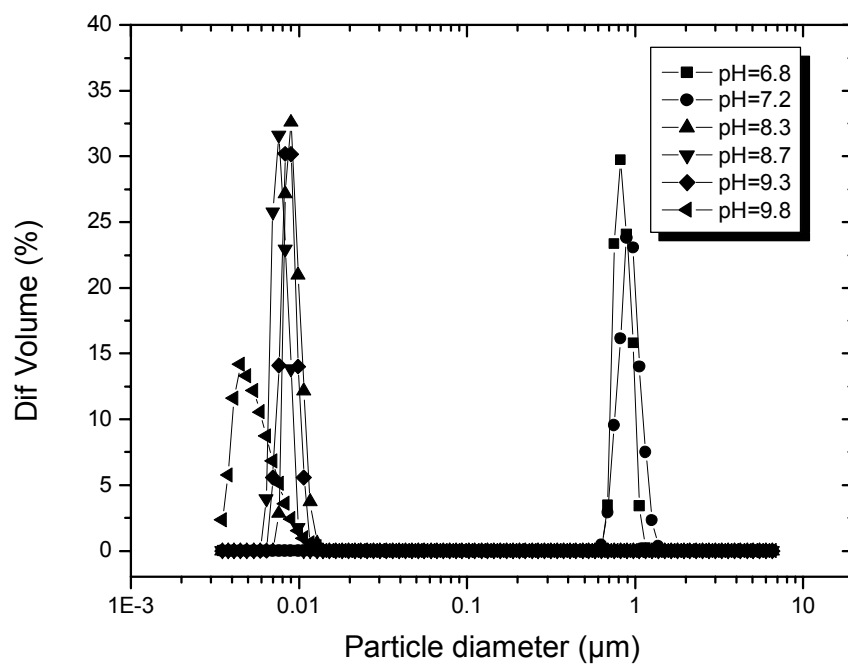


**Fig. 57** Tin oxide hydrate peptized at different pH (25°C) for 1 day.

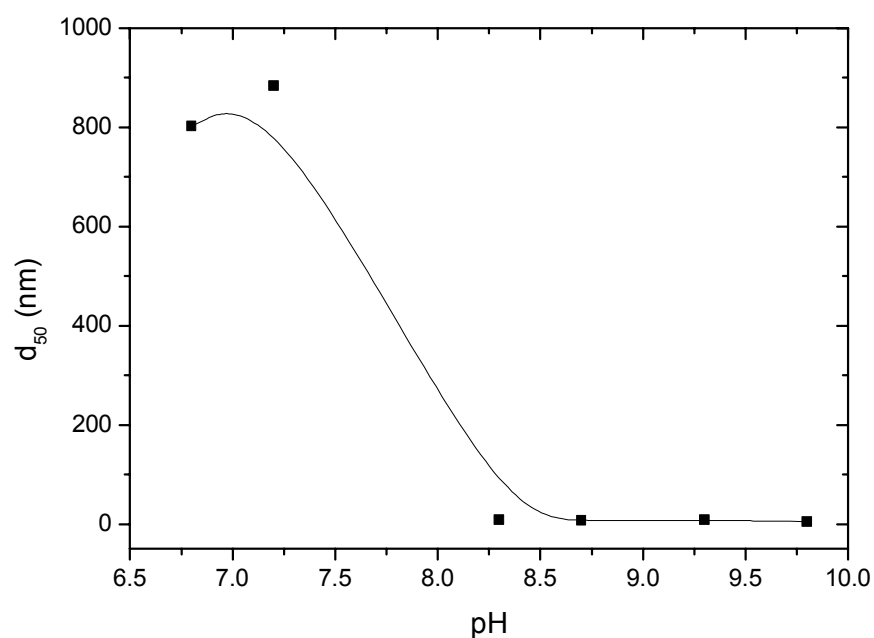
The particle diameter distribution of the samples peptized at 25°C for 24 hours at different pH values was measured by UPA and is showed in Fig. 58. It can be seen from Fig. 58(a) that the particle size contribution is unimodal. The particle diameter of samples at pH 6.8 and pH 7.2 distributes in a range of 0.5 to 1.5  $\mu\text{m}$  while at pH 8.3 to pH 9.8 in a range less than 20 nm. The “jump” of the particle diameter can be attributed to the radical change at the equivalent point of the reaction between the weak base  $\text{NH}_3 \cdot \text{H}_2\text{O}$  ( $\text{pK}_b = 4.75$ ) and the  $\text{SnO}_2 \cdot x\text{H}_2\text{O}$  as a weak acid (its  $\text{pK}_a$  is not clear). At that point,  $\text{pH} = (14 + \text{pK}_a - \text{pK}_b)/2$  when the balance is reached<sup>58</sup>. In the case of tin oxide hydrate, we can nevertheless estimate its  $\text{pK}_a$  value according to this formula. The pH value at equivalent point is about 7.75 (see Fig. 58b). Thus,  $\text{pK}_a$  of  $\text{SnO}_2 \cdot x\text{H}_2\text{O}$  is 6.25, and its acidity is near that of  $\text{H}_2\text{CO}_3$  ( $\text{pK}_{a1} = 6.35$ ). Fig. 58(b) shows the dependence of the mean particle diameter  $d_{50}$  of the samples on the pH value. With an increase in pH,  $d_{50}$  decreases from ca. 800 nm to ca. 8 nm. Therefore it can be concluded that peptization takes place when the pH value of the tin oxide hydrate suspension exceeds 8.3. The particle size of the tin oxide hydrate is effectively decreased through peptization by a factor of 100. The unimodal distribution suggests that the peptized solution is free of agglomeration. In order to obtain a stable peptized solution, the pH value in experiments was controlled to a value of pH = 9.3 by adding the ammonia solution.



Peptization of the gel could not be realized when water was replaced by ethanol, isopropanol or the mixture of water and an alcohol.



(a)



(b)

**Fig. 58** (a) Particle diameter contribution, (b) mean particle diameter  $d_{50}$  of the tin oxide hydrate peptized at different pH at 25°C for 1 day.

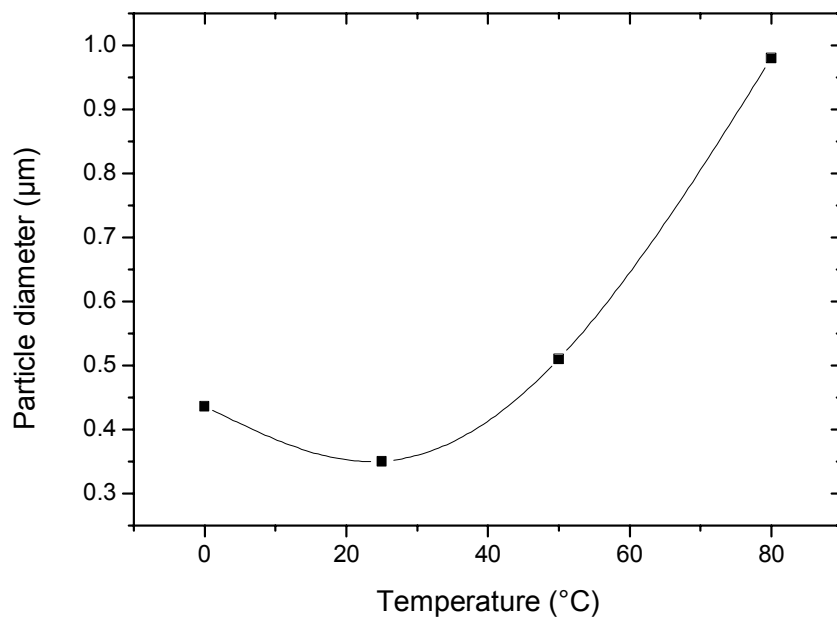


**Fig. 59** Particle diameter of tin oxide hydrate measured by PCS at different peptizing temperatures for 6 hours.

The effect of the temperature on peptization was investigated by using PCS to measure the particle diameter, after the sample being peptized for 6 hours. Fig. 59 indicates that higher temperatures than the room temperature lead to an increase in particle diameter and therefore is not helpful for peptization. Likewise, a decrease in temperature shows a negative effect on peptization. Thus, peptization of the tin oxide hydrate gel was carried out at room temperature.

It should be pointed out the gels used for peptization were freshly synthesized. A gel aging for more than 40 hours was not found to be able to be peptized.

### 5.3.3.2 Influence of the peptization

The peptized tin oxide hydrate solution kept stable up to pH = 14 by adding KOH or an ammonia solution while flocculated immediately by importing a NaOH solution or alcoholic solvents in it. By lowering its pH with acetic acid the peptized solution flocculated at a pH between 4 and 6. A further decrease in pH by adding the HCl acid led to the redissolution of the floccule.

Fig. 60 shows that the tin oxide hydrate peptized at pH = 9.3 is amorphous according to the electron diffraction pattern. It consists of particles with a size of about 10 nm, which is in accordance with the results of the particle diameter contribution.

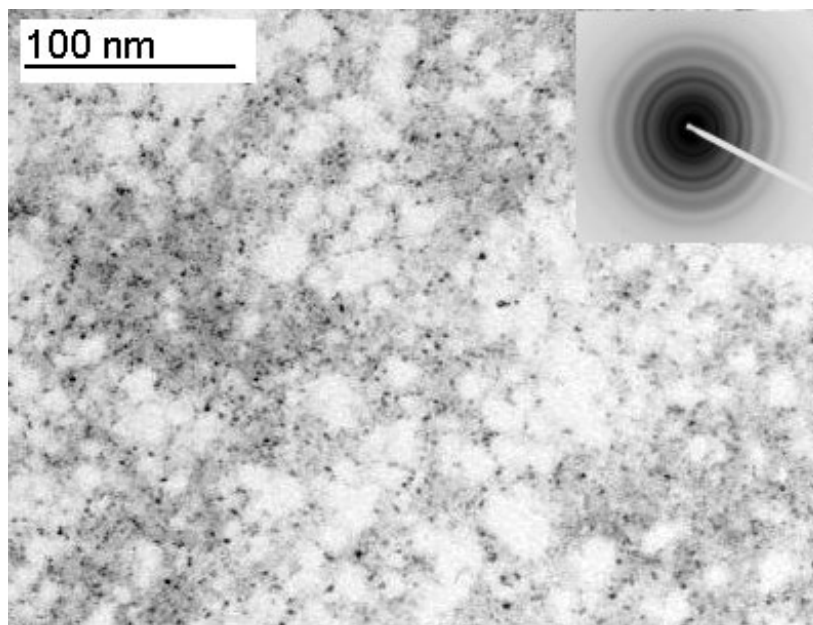


**Fig. 60** TEM micrograph of the peptized tin oxide hydrate gel at pH = 9.3. Inserted diagram is the electron diffraction pattern.

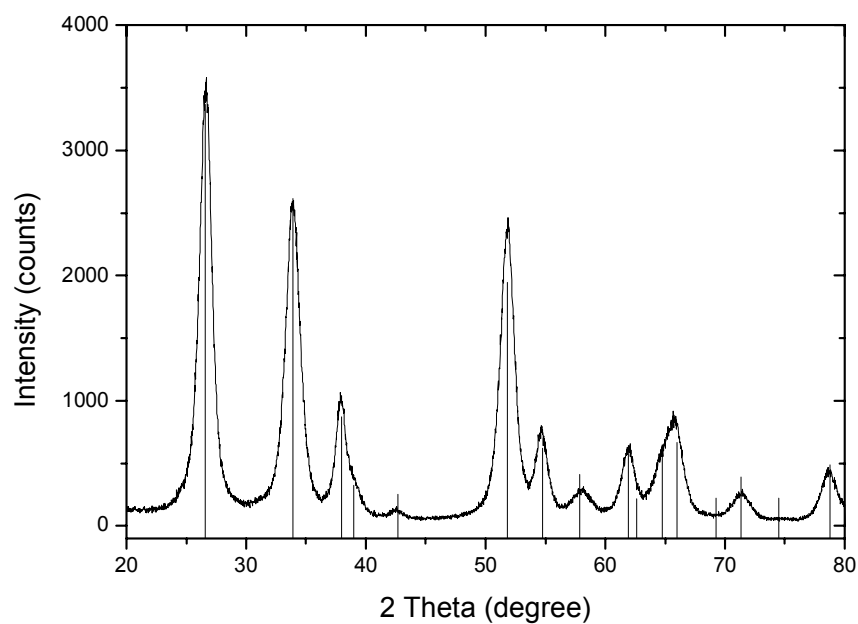
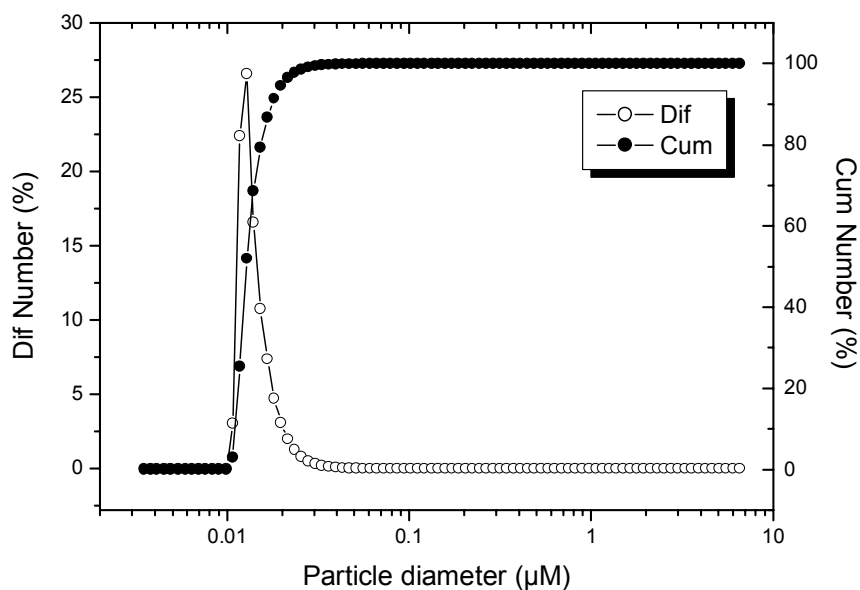
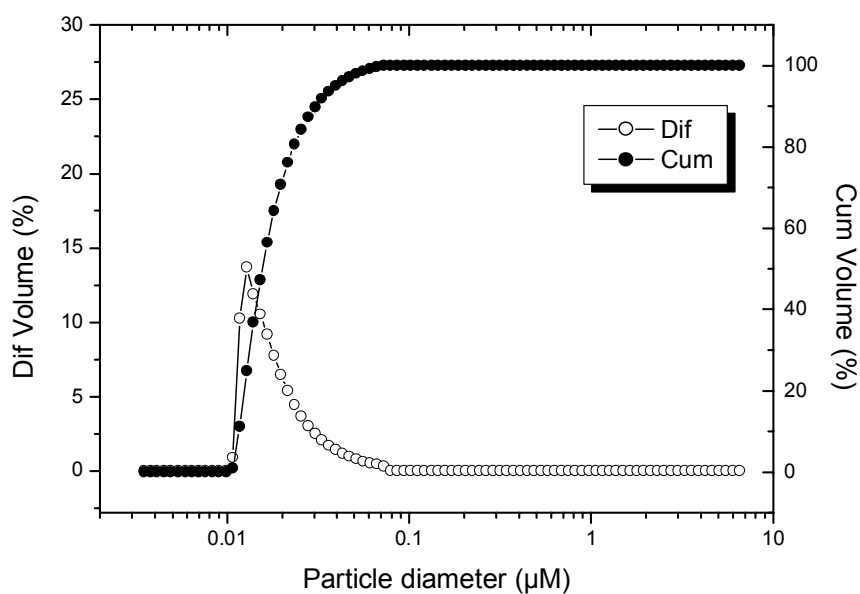


**Fig. 61** XRD pattern of the powder hydrothermally synthesized from the peptized tin oxide hydrate at 250°C for 6 hours. The inserted lines correspond to the JCPDS data of tin dioxide (77-0477).



(a)



(b)

**Fig. 62** Particle size distribution of the tin oxide powder hydrothermally synthesized from the peptized tin oxide hydrate at 250°C for 6 hours: (a) Number distribution, (b) volume distribution.

The peptized solution was treated hydrothermally at 250°C for 6 hours. The obtained product consists of  $\text{SnO}_2$  particles with a cassiterite phase and a crystallite size of 7.8 nm (see Fig. 61). Its particle size distribution measured by UPA is shown in Fig. 62. Fig. 62a shows the number contribution of the particles, where the particles distribute in a range of

10 to 30 nm and the mean particle diameter  $d_{50}^n$  is 12.6 nm. Fig. 62b shows the volume contribution of the particles. 90% of the particles distributes in the range of 10 to 30 nm and the mean particle diameter  $d_{50}^v$  is 15.3 nm, other 10% particles distributes in the range of 30 to 70 nm.

Observed under HRTEM, the primary particle shows a size of 5 to 20 nm (Fig. 63a). The structure image Fig. 63b indicates the agglomeration tendency of the particles along the crystal orientation. This nanosize tin oxide possesses a specific surface area of 128 m<sup>2</sup>/g and a density of 6.21 g/cm<sup>3</sup> (91% of the theoretical density), corresponding to an average particle size of 7.5 nm.

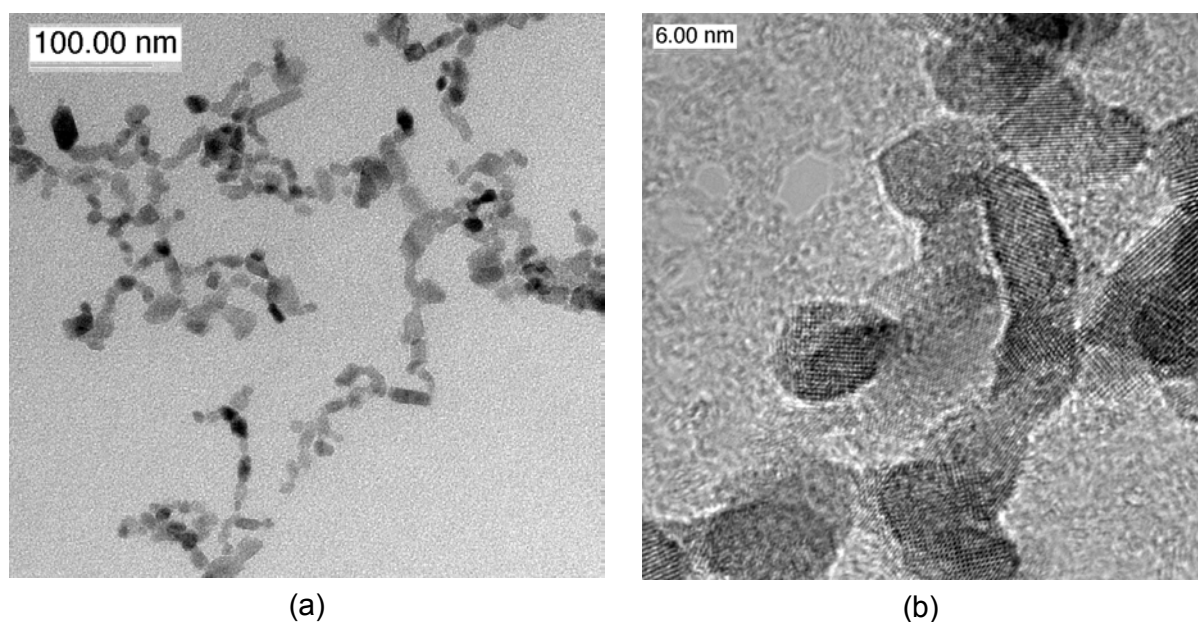


**Fig. 63** HRTEM micrographs of the tin oxide powder synthesized hydrothermally from the peptized tin oxide hydrate at 250°C for 6 hours: (a) Particle habit, (b) structure image.

It can be concluded from above description that the peptized solution is narrowly dispersed on the nanometer scale, and that it can transform into a nanosize tin oxide with a low agglomeration degree under hydrothermal conditions. As far as preparation of BaSnO<sub>3</sub> is concerned, it is still important to determine whether the peptized solution keeps the reactivity with Ba(OH)<sub>2</sub> solution to form BaSn(OH)<sub>6</sub>, and whether the properties of the powders derived from it can be improved.

The results of experiments indicated that the fresh peptized SnO<sub>2</sub>·xH<sub>2</sub>O, similarly to the fresh SnO<sub>2</sub>·xH<sub>2</sub>O gel, could react with Ba(OH)<sub>2</sub> to form BaSn(OH)<sub>6</sub> under hydrothermal conditions at 250°C for 6 hours. The reactivity of the peptized solution nevertheless decreases with increasing aging time. The reason for this lies in the transformation of SnO<sub>2</sub>·xH<sub>2</sub>O from the active  $\alpha$  form to the inactive  $\beta$  form<sup>58</sup>.

Fig. 64a shows the morphology of the as-prepared powder of BaSn(OH)<sub>6</sub> which was synthesized hydrothermally from a SnO<sub>2</sub>·xH<sub>2</sub>O gel at 250°C with 0.2 M Ba(OH)<sub>2</sub> and dried at

60°C in a vacuum furnace after being washed with distilled water. It indicates that the particles are so strongly agglomerated that the primary particle is not recognizable. Structure image b shows that the aggregate is made up of many overlapped crystallites with a diameter of 10 nm to 50 nm.

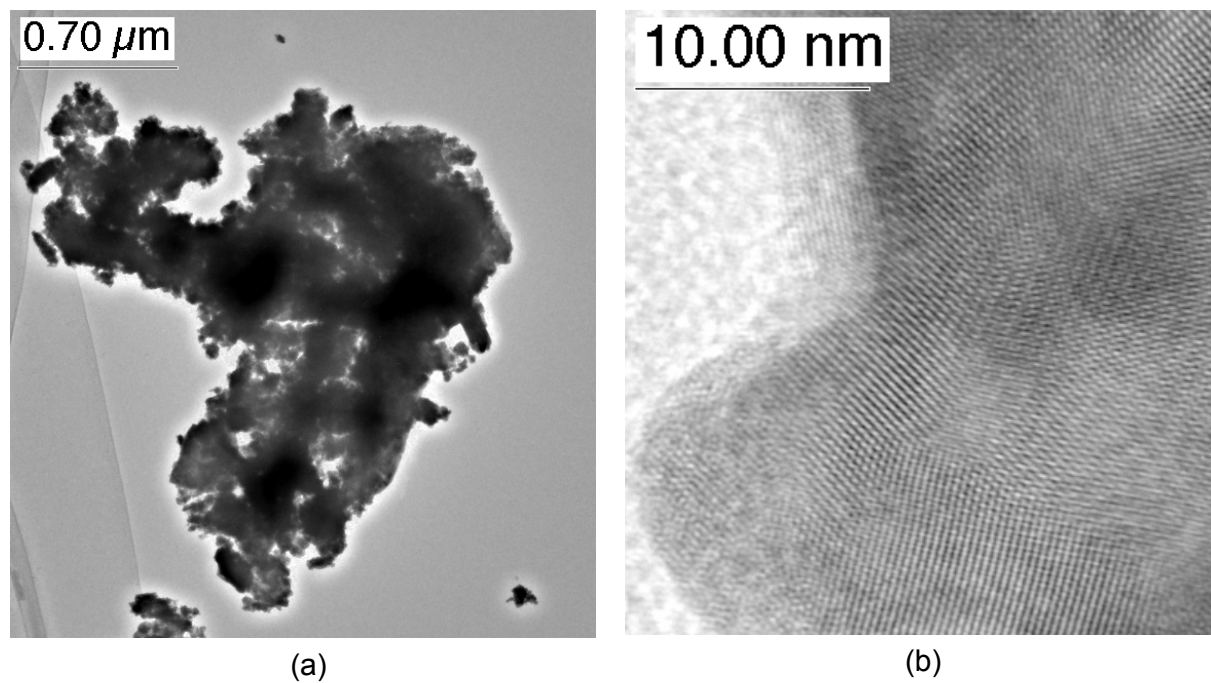


**Fig. 64** HRTEM micrographs of as-prepared powder of  $\text{BaSn}(\text{OH})_6$  derived from  $\text{SnO}_2 \cdot x\text{H}_2\text{O}$  gel: (a) Diffraction and contrast imaging, (b) structure imaging.

In contrast to this,  $\text{BaSn}(\text{OH})_6$  derived from the peptized  $\text{SnO}_2 \cdot x\text{H}_2\text{O}$  solution at the same hydrothermal conditions is constituted of much smaller clusters ranging from 20 to 200 nm. The clusters connect with each other loosely (Fig. 65a). It is shown from the high resolution image (Fig. 65b) that the crystalline nanoparticles have a diameter of about 3 nm. It can be concluded that peptization is helpful for limiting agglomeration of the particles and can lower the particle size of the powder to some degree.

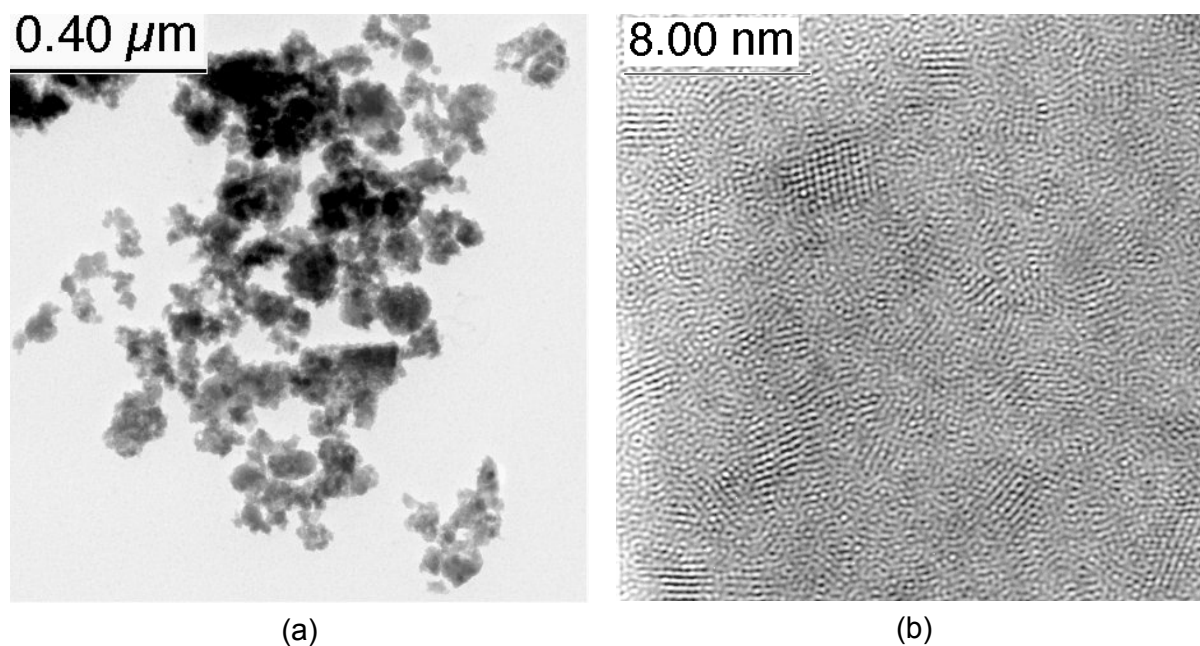


**Fig. 65** HRTEM micrographs of the as-prepared powder of  $\text{BaSn(OH)}_6$  derived from the peptized  $\text{SnO}_2 \cdot x\text{H}_2\text{O}$ : (a) Diffraction and contrast imaging, (b) structure imaging.

### 5.3.4 Improving the properties of the powder by surface modification

Because agglomeration still existed in the powder derived from the peptized  $\text{SnO}_2 \cdot x\text{H}_2\text{O}$ , it was attempted to limit the agglomeration and lower the particle size of the powder by modifying the particle surface with a surfactant. The surfactant, which would stay on the surface of the synthesized powder, was expected to decrease the surface free energy. It is known<sup>171</sup> that the surface free energy determines the particle growth rate. Therefore, it was hoped by controlling the particle growth to lower the particle size and increase the surface area. In this section, the  $\text{SnO}_2 \cdot x\text{H}_2\text{O}$  gel modified with a surfactant during its synthesis was used as the precursor.

#### 5.3.4.1 Preliminary choice of surfactants

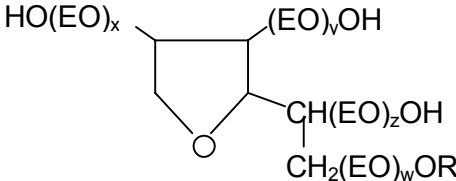
The choice of a cost-effective surfactant, although essential, is not easy due to the bewildering number of commercially available surfactants. Surfactants are generally described as anionic, cationic, amphoteric or non-ionic. However, the type of the surfactant can only give information about some very general properties which help little to choose a surfactant. To reduce the number of the unsuitable surfactants, the selection of modifiers adheres to the following criteria:

1. Solubility. The surfactant should be soluble in the aqueous solution, which means the HLB value of the surfactant should not be less than 10.

2. Good surface active properties such as a low critical micelle concentration (CMC) and a low surface tension in water.
3. Chemical stability. The selected surfactant must be stable in the alkali medium and should not hydrolyze or decompose under hydrothermal conditions.
4. Separability from the powder. The surfactant should be either thermal decomposable or simple separated from powders by washing.
5. No disturbing ions or impurities will be import from the surfactant.
6. The costs, the biodegradation, the toxicity of the surfactant as well as possible byproducts are also supplemental criteria for choosing a surfactant.

Based on above considerations, 10 candidates for the surfactant were chosen (see Table 6). Among these, Arkonal N-080, Genapol X-080, Genapol UD-079 and Tween 80 possess a high surface activity (the surface tension of their aqueous solution with a concentration of 0.5 wt% amounts to 27 - 32 mN/m). PVA with a molecular weight of 160,000 was assumed to be better than another two kinds of PVA because of its lower surface tension in water. Because of their good dispersing ability to ceramic powders DOHS, TMAH, caprolactam, glycerin and TODS were selected in spite of their relative high surface tension in water.

**Table 6** Chemical formula of the used surfactants

Surfactant	Formular	
Arkonal N-080	Nonyl phenol polyglycol ether with 8 EO: $C_9H_{19}C_6H_5O(C_2H_4O)_8OH$	
Genapol UD-079	Polyglycol ether based on $C_{11}$ with 7 EO: $C_{11}H_{23}O(C_2H_4O)_7OH$	
Genapol X-080	Isotridecyl alcohol polyglycol ether with 8 EO: $(CH_3)_2C_{11}H_{21}O(C_2H_4O)_8OH$	
Tween 80	Polyoxyethylen-(20)-Sobitan monoleate: $x+y+z+w = 20,$ $R = (C_{17}H_{33})COO$ EO: Ethoxyl - $CH_2CH_2O$	
PVA	Polyvinyl alcohol: $(CH_2CH(OH))_n$ , molecular weight = 31,000, 130,000 or 160,000	
DOHS	Dioxaheptan acid: $CH_3OC_2H_4OCH_2COOH$	
TODS	3-6-9-Trioxadecan acid: $CH_3(OC_2H_4)_2OCH_2COOH$	
TMAH	Tetramethylammonium hydroxide: $(CH_3)_4NOH$	
Caprolactam	$C_6H_{11}NO$	
Glycerin	$CH_2OHCHOHCH_2OH$	



In experiment, a surfactant (0.5 wt%) was added in  $\text{SnCl}_4$  and ammonia solution to synthesized  $\text{SnO}_2 \cdot x\text{H}_2\text{O}$ . The resulted  $\text{SnO}_2 \cdot x\text{H}_2\text{O}$  then reacted hydrothermally with  $\text{Ba}(\text{OH})_2$  solution in a 250 ml autoclave at  $250^\circ\text{C}$ . This as-prepared powders were thereafter calcined at  $260^\circ\text{C}$  for four hours. Both of the as-prepared powders and the calcined powders were characterized with IR and XRD.

Fig. 66 shows the representative IR spectra of the as-prepared powders modified with different surfactants. The modified powder shows a very similar structure as that of the unmodified one. No characteristic bands arising from surfactants such as glycerin (C-H: around  $2900\text{ cm}^{-1}$ , secondary C-OH:  $1100\text{ cm}^{-1}$ , primary C-OH:  $1040\text{ cm}^{-1}$ ), DOHS (C-H: around  $2900\text{ cm}^{-1}$ , C=O:  $1700\text{ cm}^{-1}$ , C-O-C:  $1100\text{ cm}^{-1}$ ), PVA (C-H: around  $2900\text{ cm}^{-1}$ , C-OH:  $1100\text{ cm}^{-1}$ ), Tween 80 (C-H: around  $2900\text{ cm}^{-1}$ , C=O:  $1700\text{ cm}^{-1}$ , C-O-C:  $1100\text{ cm}^{-1}$ ) and Genapol X-080 (C-H: around  $2900\text{ cm}^{-1}$ , C-O-C:  $1100\text{ cm}^{-1}$ ) have been observed, which means that the added surfactants are separable from the powders. On the other hand, the change of the five-set bands around  $500\text{ cm}^{-1}$  due to Sn-OH stretching vibrations and the change of the free OH bands around  $3600\text{ cm}^{-1}$  indicate the effect of surfactants on the powder structure. Among them the influence of Tween 80 and Genapol X-080 are more obvious.

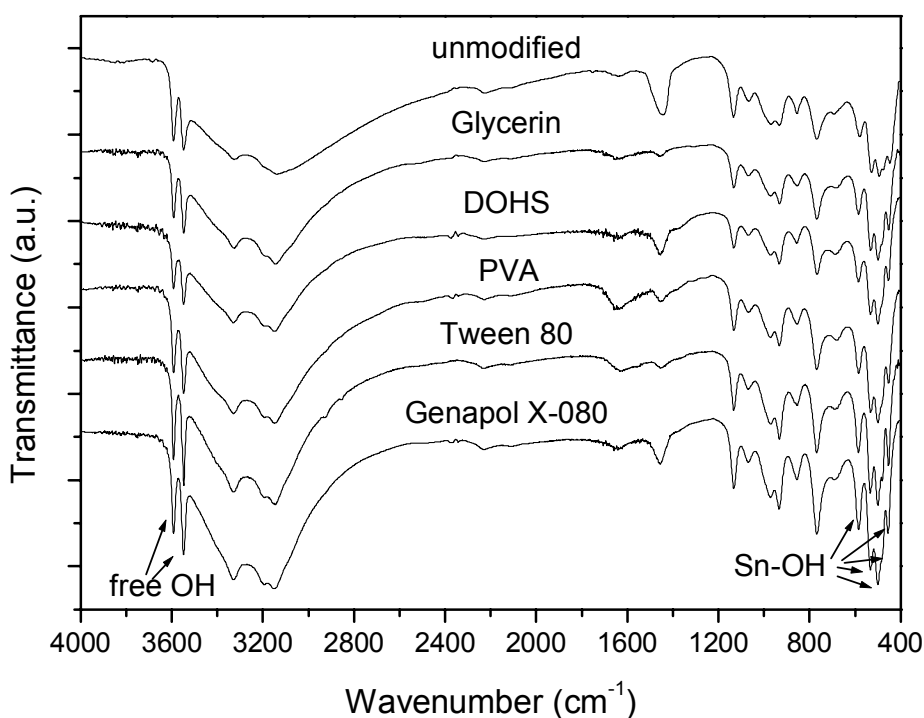


**Fig. 66** IR spectra of the as-prepared powders modified with 0.5wt% different surfactants (KBr pellets) and followed by hydrothermal treatment at  $250^\circ\text{C}$  for 6 h.

The as-prepared powders modified with different surfactants consist mainly of  $\text{BaSn}(\text{OH})_6$ , which can be seen from Fig. 67. All the peaks in the modified powder can be found in the unmodified one. However, the enlarged part on the  $2\theta$  axis between  $20^\circ$  and  $21^\circ$  shows

clearly a shift of the crystalline peaks of  $\text{BaSn}(\text{OH})_6$  (about  $0.25^\circ$ ) in the cases of modification. This suggests that surface modification can affect the crystallinity of the powder.

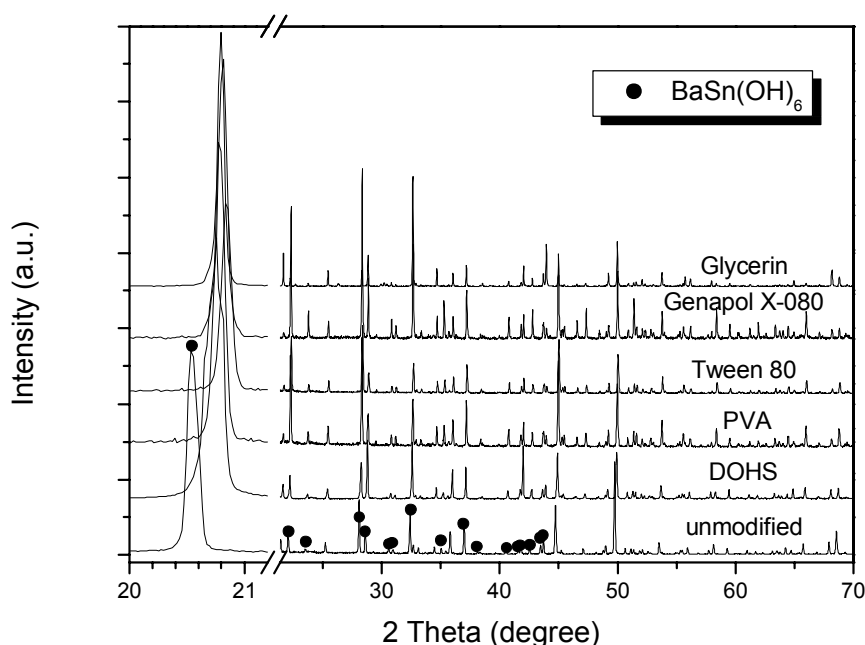


**Fig. 67** XRD patterns of the as-prepared powders modified with 0.5 wt% different surfactants. The powders were hydrothermally synthesized at  $250^\circ\text{C}$  for 6 h. The enlarged part between  $20^\circ$  and  $21^\circ$  shows the shift of the crystalline peak.

As the as-prepared powder was not  $\text{BaSnO}_3$ , it was then calcined at  $260^\circ\text{C}$  for 4h. The IR spectra of the calcined powders is shown in Fig. 68. The OH band around  $3400\text{ cm}^{-1}$  and the peak at  $1640\text{ cm}^{-1}$  indicate the existence of absorbed water that can be absorbed either by KBr pellets or by  $\text{BaSnO}_3$  from the atmosphere. In the region of  $400\text{ cm}^{-1}$  to  $800\text{ cm}^{-1}$  we can see that only the peak at  $630\text{ cm}^{-1}$  corresponding to  $\text{SnO}_3^{2-}$  appears in the powder modified by Genapol UD-079, Genapol X-080, caprolactam, Tween 80, Arkonal N-080 and PVA as well as in the unmodified one. The Sn-OH band localizing at  $500\text{ cm}^{-1}$  can nevertheless be found in the powder modified by glycerin, DOHS, TODS or TMAH, which suggests that the impurity of barium tin hydroxide exists in these powders.

The XRD patterns of these calcined powders are shown in Fig. 69. Although  $\text{BaSnO}_3$  is the main phase in all powders, the trace of an impure phase which is marked with arrows can be recognized in the powders modified by glycerin, TODS, DOHS and TMAH. As for the powder modified by PVA, it contains an amorphous phase besides  $\text{BaSnO}_3$  and another unknown crystalline phase.

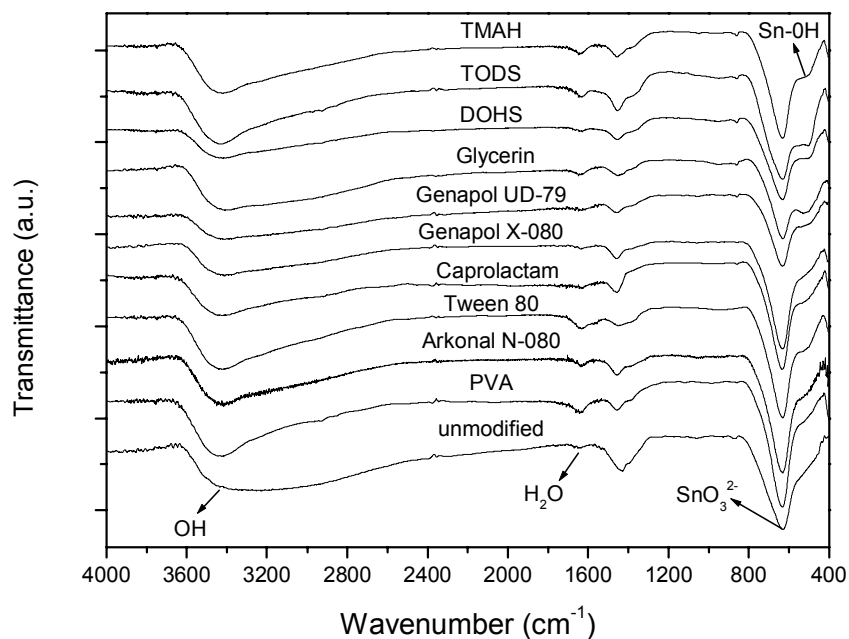


**Fig. 68** IR spectra of powders modified with 0.5 wt% surfactant, hydrothermally synthesized at 250°C for 6h and thereafter calcined at 260°C for 4 hours (KBr pellets).

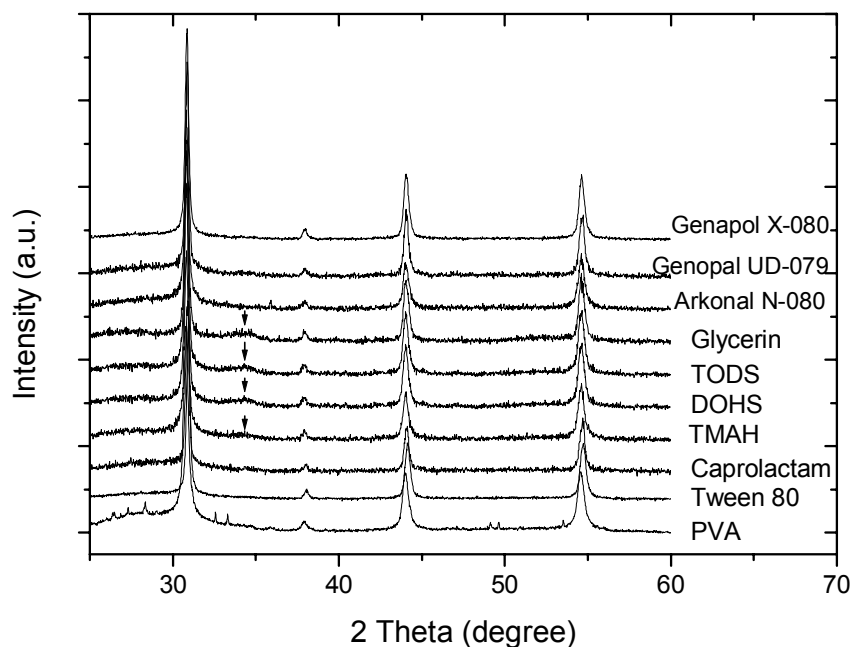


**Fig. 69** XRD patterns of the modified powders (0.5 wt% surfactant) calcined at 260°C for 4 hours, arrows indicate the trace of the impure phase.

Considering the above results, Genapol X-080, Tween 80 and caprolactam were chosen as suitable surfactants for further investigation. Arkonal N-080 was excluded because its molecular structure is very similar to that of Genapol X-080 and the conversion of Sn-OH to  $[\text{SnO}_6]$  in the later is more complete (Fig. 68). Since PVA has ever been used as a surfactant for preparing the  $\text{BaSnO}_3$  powder in the literature<sup>56</sup>, it was chosen as a modifier for a further comparison in spite of its already mentioned negative effects.

#### 5.3.4.2 Determination of surfactants

The powder derived from the tin oxide hydrate gel modified with 5 wt% PVA, caprolactam, Genapol X-080 or Tween 80 was synthesized hydrothermally in an 1l autoclave at 250°C for 6 hours. According to the XRD analysis, the as-prepared powder consists of  $\text{BaSn}(\text{OH})_6$ . In order to obtain  $\text{BaSnO}_3$ , the powder was calcined at 330°C for 4 hours. The effects of the surfactants on the specific surface area, the crystallite size and the average particle size of the end-powder are illustrated in Fig. 70. It can be seen that the addition of a modifier leads to an increase in specific area. In case of caprolactam, Genapol X-080 and Tween 80, the specific surface area is increased by a factor more than 10. On the other hand, these modifiers decrease the crystallite size and the average particle size of the end-powder. With the help of the surfactant the crystallite size is decreased from 35 nm to about 20 nm and the average particle size is lowered by a factor over 10. For the modified powders, the crystallite size matches well with the average particle size. The surfactants influence the properties of the end-powder in the following order: Tween 80 > Genapol X-080 > caprolactam > PVA. It should be pointed out that the differences in affecting efficiency among caprolactam, Tween 80 and Genapol X-080 are not large.

Fig. 71 shows the XRD patterns of the end-powders modified by these surfactants. In the cases of Genapol X-080 and caprolactam the end-powders consist of a single-phase  $\text{BaSnO}_3$  while in the powders modified with PVA and Tween 80 traces of impure phases (marked with arrows) can be found. The results show again, as mentioned in section 5.3.4.1, that addition of PVA as a modifier impedes the transformation of  $\text{BaSn}(\text{OH})_6$  to  $\text{BaSnO}_3$  and causes the appearance of impure phases in the end-powder. The impure phases in the powder modified with Tween 80 can be considered due to the increase in concentration of Tween 80 (5 wt%), because the powder modified with 0.5 wt % Tween 80 consists of a single-phase  $\text{BaSnO}_3$  (Fig. 69). This means, the concentration of the surfactant plays an important role in the surface modification.

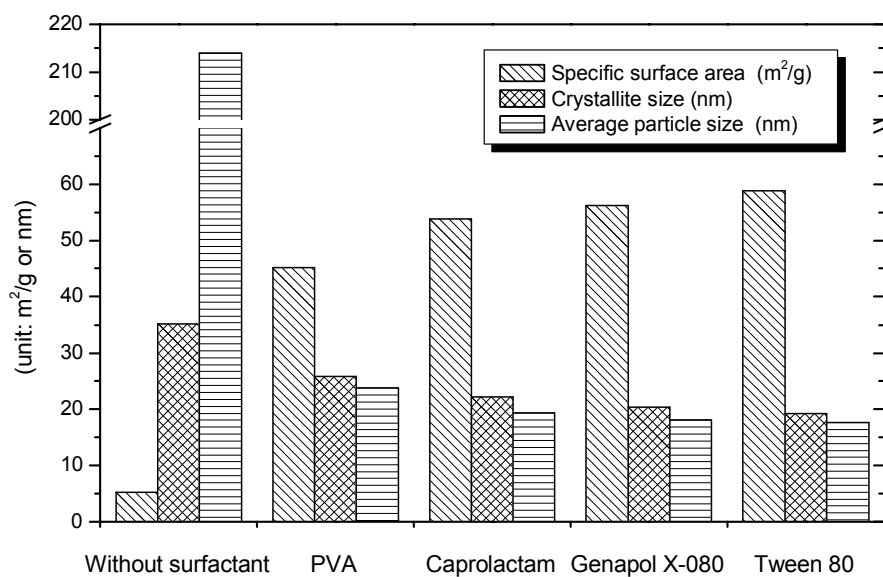


**Fig. 70** Influence of surfactants (5 wt%) on the properties of the powder calcined at 330°C for 4 hours. The powders derived from modified tin oxide hydrate gel were hydrothermally synthesized at 250°C for 6h. Specific surface area in m<sup>2</sup>/g is measured by BET, primary crystallite size in nm is measured by XRD, the average particle size in nm is calculated from density and specific surface area.

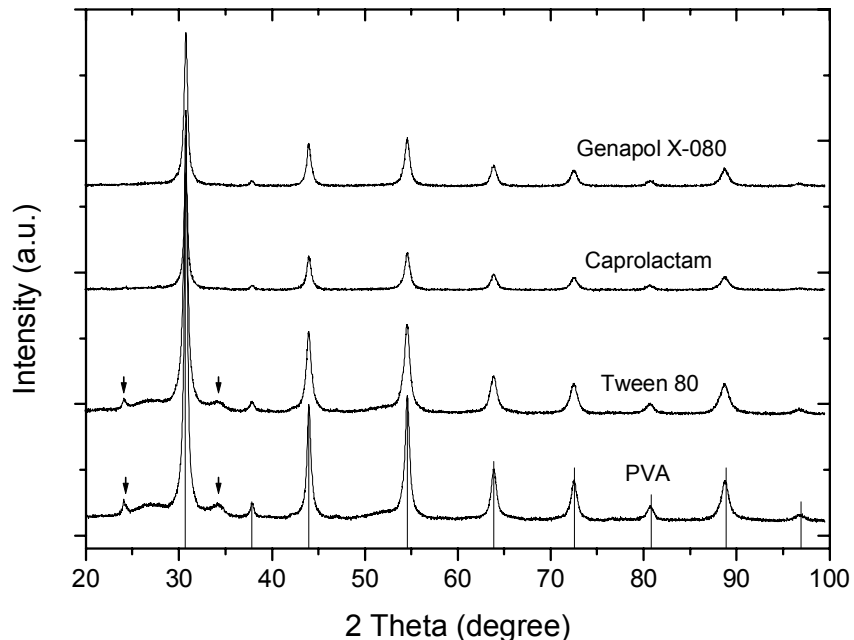


**Fig. 71** XRD patterns of the powders modified with 5 wt% surfactants and calcined at 330°C for 4 hours. The powders derived from modified tin oxide hydrate gel were hydrothermally synthesized at 250°C for 6h. The inserted lines correspond to the JCPDS data of BaSnO<sub>3</sub> (15-0780), the arrows show the existence of impurities.

Considering the effects of the surfactants on the properties of the powder, it can be concluded that Genapol X-080 as a modifier is more suitable for preparing the nanosize  $\text{BaSnO}_3$  powder than other three surfactants. Thus Genapol X-080 was determined as the modifier and was investigated in the later experiments.

#### 5.3.4.3 Influence of surfactant concentration and calcining temperature

The concentration of Tween 80 is relevant to the phase constitution of the end-powder. As to Genapol X-080, it is of importance to determine how its concentration influences the surface area. Fig. 72 shows the dependence of the specific surface area of the powder calcined at  $330^\circ\text{C}$  for 4 hours on the concentration of Genapol X-080. The specific surface area is increased from  $5.3 \text{ m}^2/\text{g}$  to  $56.2 \text{ m}^2/\text{g}$  as the concentration of Genapol X-080 is increased up to 5 wt%. It decreases slightly with a further increase in concentration of the surfactant.

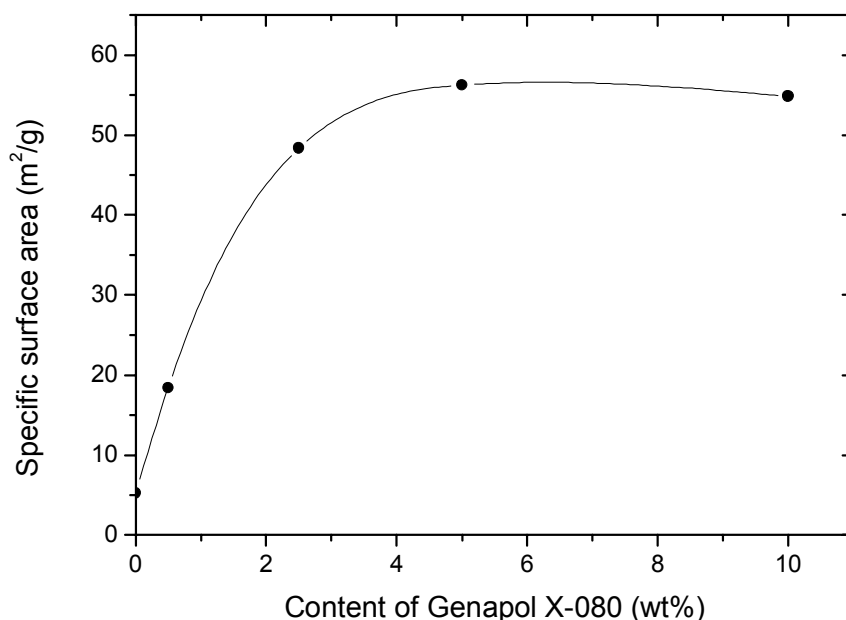


**Fig. 72** Specific surface area of the modified powder calcined at  $330^\circ\text{C}$  for 4 hours as a function of the concentration of Genapol X-080.

It is well known that a surfactant can decrease the surface energy of a solution until its concentration reaches the critical micelle concentration (CMC). The CMC is the highest attainable concentration of a surfactant in a liquid and forces maximum adsorption of the surfactant onto the surface of the liquid. For Genapol X-080, its CMC is  $0.066 \text{ g/l}$ , which corresponds to a concentration of Genapol X-080 less than  $0.1 \text{ wt}\%$ . Above the CMC, most of the added surfactant goes to form micelles instead of into solution. Once the reaction between  $\text{SnO}_2 \cdot x\text{H}_2\text{O}$  and  $\text{Ba}(\text{OH})_2$  takes place, the new formed particles give rise to a new liquid/solid interface in the solution, which destabilizes the balance of the micelles. The attraction force of the  $\text{OH}^-$  groups on the particle surface to the surfactant molecules causes

the release of these molecules from the micelles and then the adsorption on the surface of the particle. The cover of the surfactant on the surface of the particles can limit agglomeration and thus increase the surface area. Before all particles are covered with a monolayer of surfactant, the surface area of the powder can be increased with increasing the surfactant concentration. The concentration of the surfactant at the point of a monolayer cover apparently depends on the size of the primary particle and the area coverage of its molecule on the surface of the particle. If the added amount is over that needed by a monolayer cover, the excess molecules can either exist in the form of micelles or form a second adsorption layer which cannot contribute more to the elevation of the surface face. In addition, with increasing surfactant content a second adsorption layer is likely to be oriented in the opposite sense from the first and thus reduce the compatibility of the particle with the liquid. As a result, reagglomeration takes place, leading to a decrease in surface area.

It can be deduced that 5 wt% Genapol X-080 nearly corresponds to the amount of the surfactant needed for a monolayer cover of the particles. The modifier molecules up to that amount serve to decrease the surface energy of the liquid/liquid and the liquid/solid interface energy, and therefore limits the agglomeration and promotes the elevation of the surface area. A larger amount is wasted and even causes a decrease in surface area.

It is also found that the concentration of Genapol X-080 affects on the crystallization of the as-prepared powder. The calcining temperature of 260°C for the powder modified with 0.5 wt% Genapol X-080 does not prove to be enough for the crystallization of the powder modified with 5 wt%. A calcining temperature as high as 330°C is necessary for the later.

The effects of the calcining temperature on the specific surface area and the average particle size are shown in Fig. 73. It is clear that increasing the calcining temperature results in a decrease in specific surface area and an increase in average particle size. Above 600°C the average particle size increases faster. The reason for this is that the grain growth rate is dependent on the thermodynamic driving force. Normally, the higher the crystallization temperature is, the larger the thermodynamic driving force is. This means, the grain grows faster at a higher temperature. As the particle size increases, the surface area decreases.

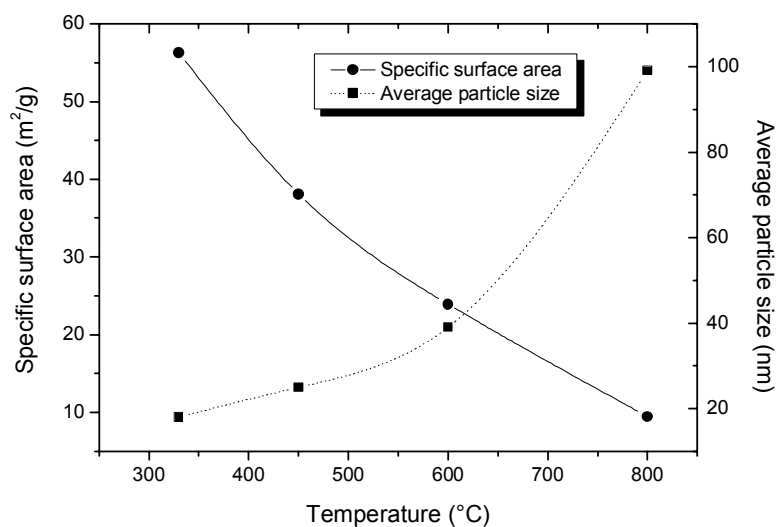


**Fig. 73** Specific surface area of the modified powder (5 wt% Genapol X-080) calcined at different temperatures for 4 hours.



### 5.3.5 Characterization of the powder

It has been noted that the  $\text{BaSnO}_3$  powder can be prepared from the  $\text{SnO}_2 \cdot x\text{H}_2\text{O}$  gel (see 5.3.2), from the  $\text{SnO}_2 \cdot x\text{H}_2\text{O}$  solution peptized by ammonia (see 5.3.3) and from the  $\text{SnO}_2 \cdot x\text{H}_2\text{O}$  gel modified with Genapol X-080 (see 5.3.4). In view of the positive effects of peptization and surface modification on the properties of the powder,  $\text{BaSnO}_3$  powders has also been prepared by combining peptization and surface modification, namely the precursor  $\text{SnO}_2 \cdot x\text{H}_2\text{O}$  was obtained by reacting  $\text{SnCl}_4$  with ammonia solution in the presence of Genapol X-080 and thereafter peptization.

The as-prepared powders to be characterized, were hydrothermally synthesized at  $250^\circ\text{C}$  for 6 hours in an 1l autoclave. To distinguish the powders derived from different precursors, the obtained powders are divided in four systems according to their precursors: The system including the  $\text{SnO}_2 \cdot x\text{H}_2\text{O}$  gel without pretreatment is noted as **G-system**. The system with the peptized  $\text{SnO}_2 \cdot x\text{H}_2\text{O}$  gel is noted as **P-system**. The system with the surface-modified  $\text{SnO}_2 \cdot x\text{H}_2\text{O}$  gel is noted as **M-system**, and the system with the modified and peptized  $\text{SnO}_2 \cdot x\text{H}_2\text{O}$  is noted as **MP-system**. The samples to be characterized are listed in Table 7. The parameters were selected according to the results discussed in section 5.3.2.

Although the negative effect of the isopropanol on the properties of the powders in G-system has been discussed in section 5.3.2.4, it is still of interest to investigate its effect in other systems. However,  $\text{SnO}_2 \cdot x\text{H}_2\text{O}$  cannot be peptized with isopropanol as a solvent, so the effect of isopropanol was only investigated in the M-system. In following discussion, if no special specification, the solvent used in hydrothermal synthesis is water.

**Table 7** Powder samples prepared from different processes

Sample	System	Pretreatment of precursor $\text{SnO}_2 \cdot x\text{H}_2\text{O}$ gel	parameter			hydrothermal conditions (in 1l autoclave)
			$\text{Ba}(\text{OH})_2$	Ba:Sn	solvent	
g1	G	no pretreatment	0.2 M	1.1	water	$250^\circ\text{C}/6\text{h}$
p1	P	peptized at pH 9.3	0.2 M	1.1	water	$250^\circ\text{C}/6\text{h}$
m1	M	modified with 5 wt% Genapol X-080	0.2 M	1.1	water	$250^\circ\text{C}/6\text{h}$
m2	M	modified with 5 wt% Genapol X-080	0.2 M	1.1	isopropanol	$250^\circ\text{C}/6\text{h}$
mp1	MP	modified with 5 wt% Genapol X-080 and peptized at pH 9.3	0.2 M	1.1	water	$250^\circ\text{C}/6\text{h}$

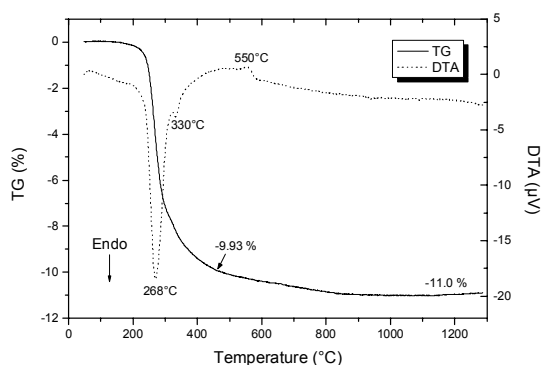
### 5.3.5.1 Thermoanalysis

The as-prepared powders in four systems were analyzed with TG-DTA (see Fig. 74). To detect the released constituents of the powder in M-system during the thermal treatment, TG-DTA coupled with MS was employed. The influence of isopropanol instead of water as the medium in the M-system was also investigated.

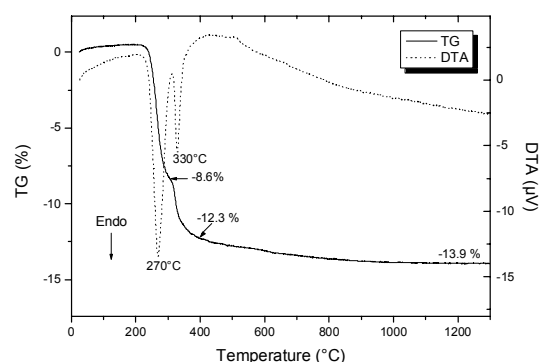
In all DTA curves of the powders synthesized in water, two endothermic peaks located at about 270°C and 330°C can be found, but the intensity of the second peak relative to the first peak in different samples is different. As we see, the second peak in g1 (Fig. 74a) is so small that it is almost integrated into the first one. The second peak in sample p1 (Fig. 74b) is obvious and is separated from the first one. A further increase in the intensity of the second peak in sample m1 (Fig. 74c) and in sample mp1 (Fig. 74d) can be observed. These endothermic peaks resulting from the dehydration of the as-prepared powder can be confirmed from the MS curve in Fig. 74c, where two water-releasing peaks appear at 266°C and 326°C. No other gas inclusive CO<sub>2</sub> is detected during the heating process in sample m1.

As water was replaced by isopropanol in the M-system (sample m2), the second peak is completely integrated with the first one which is centered at 260°C (Fig. 74e). In the corresponding MS curve, a water peak at 265°C and a weak CO<sub>2</sub> peak at 780°C which can be attributed to the decomposition of carbonate<sup>54</sup> are found. This indicates the dehydration at 260°C and suggests the formation of carbonates during heat treatment.

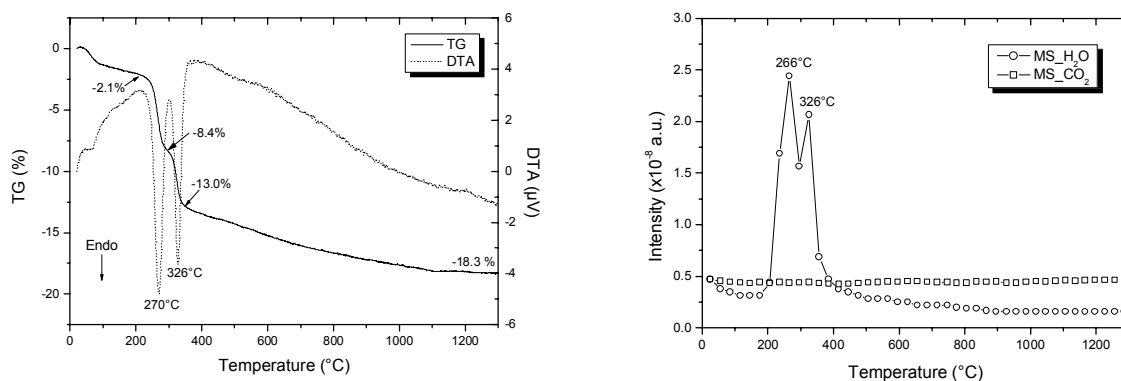
It is also observed that an exothermic peak appears at 550°C and 520°C in Fig. 74a and Fig. 74e respectively. This peak can be attributed to recrystallization of BaSnO<sub>3</sub><sup>55</sup>.



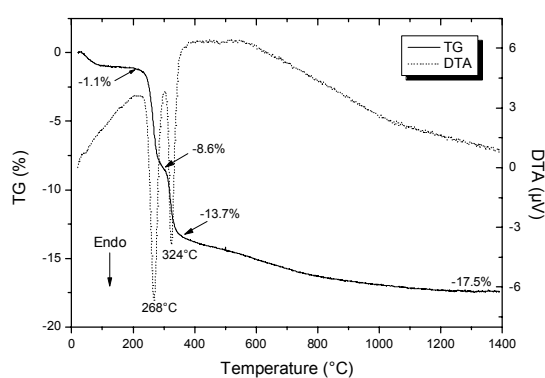
(a)



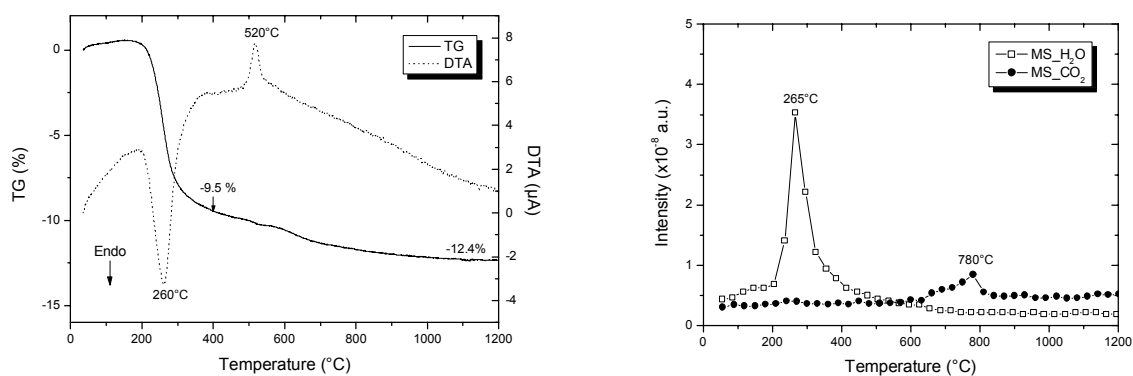
(b)



(c)



(d)



(e)

**Fig. 74** TG-DTA(-MS) curves of sample: (a) g1, precursor:  $\text{SnO}_2 \cdot x\text{H}_2\text{O}$  gel; (b) p1, precursor:  $\text{SnO}_2 \cdot x\text{H}_2\text{O}$  peptized at pH = 9.3; (c) m1, precursor:  $\text{SnO}_2 \cdot x\text{H}_2\text{O}$  modified with 5 wt% Genapol X-080; (d) mp1, precursor:  $\text{SnO}_2 \cdot x\text{H}_2\text{O}$  modified with 5 wt% Genapol X-080 and peptized at pH = 9.3; (e) m2, precursor:  $\text{SnO}_2 \cdot x\text{H}_2\text{O}$  modified with 5 wt% Genapol X-080, isopropanol was used as the solvent in hydrothermal reaction. Powders were hydrothermally synthesized at 250°C for 6h.

The DTA results indicate the effects of peptization, surface modification and the solvent on the dehydration of the as-prepared powder. Peptization and surface modification make the dehydration more difficult because part of the dehydration is shifted to a higher temperature. This means, peptization and surface modification lead to an increase in calcining temperature, at which  $\text{BaSn}(\text{OH})_6$  converts into  $\text{BaSnO}_3$ . In M-system, the substitution of isopropanol (Fig. 74e) for water (Fig. 74c) makes the dehydration easier because of a decrease in the dehydration temperature and the disappearance of the second peak. But the appearance of carbonates will complicate the transformation of  $\text{BaSn}(\text{OH})_6$  into  $\text{BaSnO}_3$ , a negative effect of  $\text{BaCO}_3$  on the formation of  $\text{BaSnO}_3$  has been found in section 5.2.3.1. In sample m1 (M-system) no  $\text{CO}_2$  peak appears in the MS curve. This suggests that most of the surfactant Genapol X-080 has been removed from the powder by washing.

The weight loss in different samples, according to the TG curves, is different. In sample g1, the weight loss mainly lies in the temperature range of 200°C to 460°C, accounting for 90.2% of the total weight loss. In sample p1, m1 and mp1, the weight loss can be divided into three phases, namely the 1<sup>st</sup> phase (corresponding to the 1<sup>st</sup> endothermic peak) from 200°C to 300°C, the 2<sup>nd</sup> phase (corresponding the 2<sup>nd</sup> endothermic peak) from 300°C to about 400°C and the 3<sup>rd</sup> phase from about 400°C to above 1200°C. Since the weight loss before 200°C results from the desorption of the physically absorbed water from atmosphere, it is deducted as the total weight loss is considered. Thus, the total weight loss in g1 (Fig. 74a), p1 (Fig. 74b), m1 (Fig. 74c) and mp1 (Fig. 74d) is 11.0%, 13.9%, 16.1% and 16.4% respectively, which deviates from the theoretic weight loss value of 15.1% corresponding to the transformation of  $\text{BaSn}(\text{OH})_6$  to  $\text{BaSnO}_3$ . This indicates that barium tin hydrates obtained in four systems are not the same.

As suggested in the literature<sup>56</sup>, the as-prepared powder can be considered as a barium tin oxyhydrate  $\text{BaSnO}_y(\text{OH})_{6-2y}$ . Regardless of their structure, both  $\text{BaSn}(\text{OH})_6$  and barium tin oxyhydrate can be simply noted as  $\text{BaSnO}_3 \cdot x\text{H}_2\text{O}$  ( $x = 3-y$ ). Based on this formula, the x value and the amount of water removed at different weight loss phases and its percentage in the total weight loss are calculated from TG curves and given in Table 8.

**Table 8** X value in powders formulated as  $\text{BaSnO}_3 \cdot x\text{H}_2\text{O}$  and the amount and percentage of water removed at different weight loss phases. The results are calculated from TG-curves of Fig. 74 and the physically absorbed water is not considered. In g1 and m2 the first two phases is considered as one because of their integration.

as-prepared powder	x in sample $\text{BaSnO}_3 \cdot x\text{H}_2\text{O}$	water removed in the 1 <sup>st</sup> phase	water removed in the 2 <sup>nd</sup> phase	water removed in the 3 <sup>rd</sup> phase
g1 (G-system)	2.09	1.80H <sub>2</sub> O: 86.1%		0.29H <sub>2</sub> O: 13.9%
p1 (P-system)	2.73	1.69H <sub>2</sub> O: 61.9%	0.73H <sub>2</sub> O: 26.7%	0.31H <sub>2</sub> O: 11.4%
m1 (M-system)	3.26	1.27H <sub>2</sub> O: 39.0%	0.93H <sub>2</sub> O: 28.5%	1.06H <sub>2</sub> O: 32.5%
mp1 (MP-system)	3.31	1.52H <sub>2</sub> O: 45.9%	1.03H <sub>2</sub> O: 31.1%	0.76H <sub>2</sub> O: 23.0%
m2 (M-system)	2.39	1.83H <sub>2</sub> O: 76.6%		0.56H <sub>2</sub> O: 23.4%

The data in the table show that the water content in the as-prepared powder increases obviously by peptization (p1) and modification (m1). A further increase in water content is obtained by combining peptization and surface modification (mp1). In addition, with increasing water content the amount of the removed water decreases in the first stage while increases in the second stage. In this sense, peptization and surface modification makes the dehydration, namely the transformation of barium tin hydroxide to barium stannate more difficult, which agrees with what we see from the DTA curves.

The difference of the water content in the powder of different systems can be traced back to the tin oxide hydrate precursor. Lowering the particle size of tin hydroxide by peptization means increase in surface area of the particles, on which more OH<sup>-</sup> groups can be bonded. This contributes to the increase in water content in the tin oxide hydrate. As we know, the tin oxide hydrate, when rich of water, shows a higher activity<sup>58</sup>. In the case of surface modification, the surface-bonded surfactant molecules can serve to limit the loss of water in the precursor with aging. After hydrothermal reaction, the hydrated water is retained in the resultant, which explains the increase in water content in the as-prepared powder. In this sense, peptization and surface modification can enhance the activity of the precursor.

By comparison of m1 and m2, isopropanol substituting water in the M-system contributes to the decrease in water content in the powder. In addition, the removal of the water in m2 in the first stage is not so complete as that in g1. This suggests the negative influence of the isopropanol on the powder.

### 5.3.5.2 Structure evolution

The structure evolution of the powders prepared via hydrothermal synthesis route by calcining at different temperatures for different time was investigated with the help of IR spectra. The influence of peptization, surface modification and their combination on the structure evolution will be described in this section. In the M-system, the effect of isopropanol instead of water will also be covered.

The IR spectra of the powder derived from the tin oxide hydrate gel (Fig. 75a) show that the five-set peaks around 500 cm<sup>-1</sup> (i.e., Sn-OH groups<sup>79</sup>) round off at 260°C after one hour of calcination and disappear after 4h of calcination. The peak centered at 630 cm<sup>-1</sup> corresponding to [SnO<sub>6</sub>]<sup>220</sup> becomes prominent at 260°C after 4h of calcination.

In contrast to this, in p1 (Fig. 75b) the broad Sn-OH peak around 500 cm<sup>-1</sup> is still dominant at 260°C after 4h of calcination, although a small [SnO<sub>6</sub>] peak at 630 cm<sup>-1</sup> can be discerned. At 330°C after 4h of calcination the Sn-OH peak disappears and the intensity of the [SnO<sub>6</sub>] peak increases.

The structure of the powder m1 modified with Genapol X-080 undergoes the similar evolution as that of the peptized powder p1 by calcinations (Fig. 75c). A difference is that in the former the [SnO<sub>6</sub>] peak at 260°C after 4h of calcination is more obvious.

In the case of combination of peptization and surface modification (Fig. 75d), the IR spectra also illustrate a combining effect. The intensity of the two peaks around 500 and 630 cm<sup>-1</sup> at 260°C/4h, for example, is between that in Fig. 75b and that in Fig. 75c.

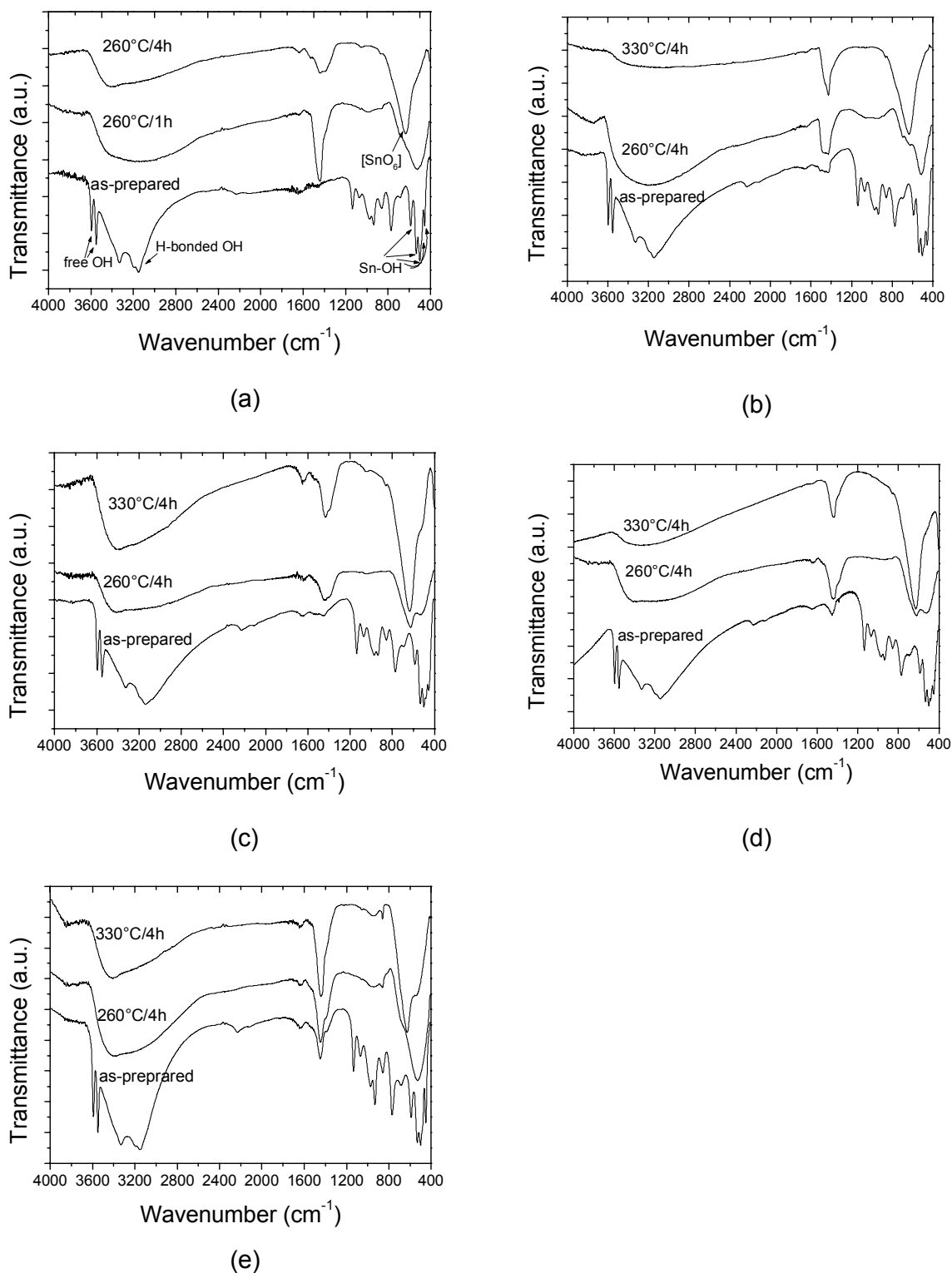


**Fig. 75** IR spectra of powders versus calcining temperature and time (KBr pellets): (a) g1, precursor: SnO<sub>2</sub>·xH<sub>2</sub>O gel; (b) p1, precursor: SnO<sub>2</sub>·xH<sub>2</sub>O peptized at pH = 9.3; (c) m1, precursor: SnO<sub>2</sub>·xH<sub>2</sub>O modified with 5 wt% Genapol X-080; (d) mp1, precursor: SnO<sub>2</sub>·xH<sub>2</sub>O modified with 5 wt% Genapol X-080 and peptized at pH = 9.3; (e) m2, precursor: SnO<sub>2</sub>·xH<sub>2</sub>O modified with 5 wt% Genapol X-080, isopropanol was used as the solvent in hydrothermal reaction. Powders were hydrothermally synthesized at 250°C for 6h.

By comparing the as-prepared powders in the four systems (Fig. 75a, b, c, d), we can find a subtle difference in the Sn-OH multiple peaks. The second peak is more obvious in the M-system (m1) and MP-system (mp1) than the others.

The rounding-off of the Sn-OH band can be attributed to the dehydration and dehydroxylation of the as-prepared powder by calcination. In the G-system (Fig. 75a), this process takes place at 260°C after 1h of calcination and continues with the extension of the calcination. The dehydrate and dehydroxylation is accompanied by the rearrangement of the structure. As a result, the corner-sharing octahedral  $[\text{SnO}_6]$  forms. After being calcined for 4 hours, almost all  $\text{OH}^-$  groups are removed and the formation of  $[\text{SnO}_6]$  finishes.

As the precursor was peptized (Fig. 75b), the dehydrate and dehydroxylation of the as-prepared powder at 260°C become difficult. A calcining temperature as high as 330°C is necessary for accomplishing the evolution of  $[\text{SnO}_6]$  from Sn-OH.

Likewise, the surface modification (Fig. 75c) also leads to the incomplete dehydroxylation at 260°C and therefore a higher calcining temperature for the structure rearrangement is needed.

Since both peptization and modification have the similar effects on the structure evolution, a combining effect observed in the MP-system (Fig. 75d) is easy to understand.

The accomplishment of the structure evolution from Sn-OH to  $[\text{SnO}_6]$  in the M-, P- and MP-system at a higher temperature can be attributed to the more water content in the as-prepared powder resulting from peptization and surface modification (see 5.3.5.1). However, the proportional relation between them is not obvious. For example, the formation of  $[\text{SnO}_6]$  in the M-system is easier than in the P-system although the former contains more water than the later. A possible reason is that the bonding wise of  $\text{OH}^-$  groups within the powder may be different, a proof for this is the subtle difference in the second peak of the Sn-OH band.

The effects of isopropanol replacing water on the structure in the M-system can be seen in Fig. 75e. At first, the second peak of the Sn-OH band almost disappears in the as-prepared powder. Secondly, no  $[\text{SnO}_6]$  peak can be found at 260°C/4h. Furthermore, the Sn-OH band is still obvious after being calcined at 330°C for 4 hours, although the endothermic peak at 330°C disappears in the corresponding TG-DTA curve (Fig. 74e). These reveal that isopropanol replacing water makes the structure rearrangement more difficult despite it lowers the temperature of dehydrate and dehydroxylation.

### 5.3.5.3 Crystallization behavior

The crystallization behaviors of the powders derived from different pretreated  $\text{SnO}_2 \cdot x\text{H}_2\text{O}$  were investigated by calcining the as-prepared powder at a temperature ranging from 260°C to 330°C for different time. The shift of the crystalline peaks in the x-ray patterns of the as-prepared powders and the end-powders ( $\text{BaSnO}_3$ ) were studied. In this section, the influence of isopropanol on the phase transformation in M-system will also be discussed.

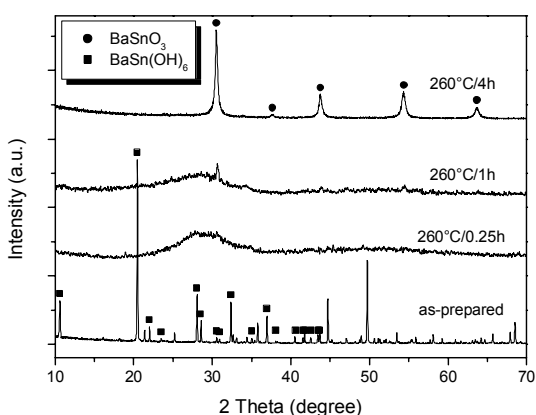
In sample g1 (Fig. 76a), the as-prepared powder from  $\text{SnO}_2 \cdot x\text{H}_2\text{O}$  gel is composed of  $\text{BaSn}(\text{OH})_6$ . It transforms into amorphous after calcining at 260°C for 0.25h. By extending

the time to 1h, a  $\text{BaSnO}_3$  phase appears. The conversion of  $\text{BaSnO}_3$  from the amorphous phase accomplishes after 4h of calcination at  $260^\circ\text{C}$ . The crystallite size of  $\text{BaSnO}_3$  is 35.2 nm.

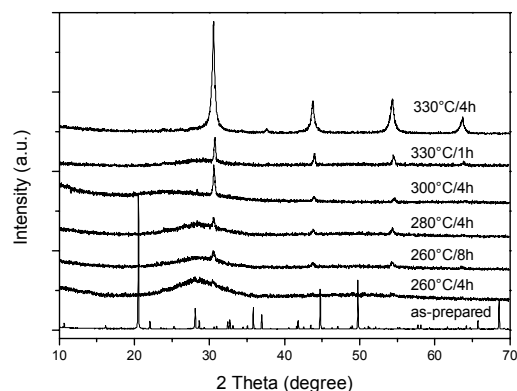
The results reveal that  $\text{BaSn}(\text{OH})_6$  is a meta-stable phase which does not transform directly into  $\text{BaSnO}_3$  but into an amorphous phase. The  $\text{BaSnO}_3$  nuclei form in the amorphous phase and then grow. A simple explanation for this is that the long-ranging order in  $\text{BaSn}(\text{OH})_6$  is destroyed as dehydroxylation takes place. The degree of disorder increases with the dehydroxylation proceeding. As a consequence, the crystalline particles become amorphous. Based on the near-ranging order of the amorphous state, the  $\text{BaSnO}_3$  nuclei forms by overcoming the energy barriers such as the free energy of crystal nucleus formation. Crystal nucleates and grows at the expense of the amorphous phase. It is known<sup>222</sup> that nucleation at interfaces (i.e., heterogeneous nucleation) dominates other nucleation processes. The boundaries of the amorphous solid particles offer such interfaces, and therefore it is reasonable to assume that the nucleation of  $\text{BaSnO}_3$  is a heterogeneous nucleation process.

A similar crystallization behavior of the powder derived from the peptized tin oxide hydrate has also been observed (Fig. 76b). The  $\text{BaSn}(\text{OH})_6$  phase of the as-prepared powder converts into amorphous at  $260^\circ\text{C}$  after 4h of calcination.  $\text{BaSnO}_3$  nucleates from the amorphous phase and grows with increasing time and temperature. The powder of a single-phase  $\text{BaSnO}_3$  was obtained after the as-prepared was calcined at  $330^\circ\text{C}$  for 4h. Its crystallite size is 27.6 nm.

Comparing Fig. 76a and Fig. 76b, it can be found that the nucleation and growth of  $\text{BaSnO}_3$  in the P-system is more difficult than in the G-system. It is known from thermoanalysis that more water is incorporated in p1 by peptization and that a portion of water can only be removed at higher temperatures. These make the conversion of the amorphous phase from  $\text{BaSn}(\text{OH})_6$  in p1 more difficult, which delays the formation of the nuclei of  $\text{BaSnO}_3$ . On the other hand, more remaining water in the powder at above  $260^\circ\text{C}$  can impede the material transfer for the grain growth of  $\text{BaSnO}_3$ .



(a)



(b)



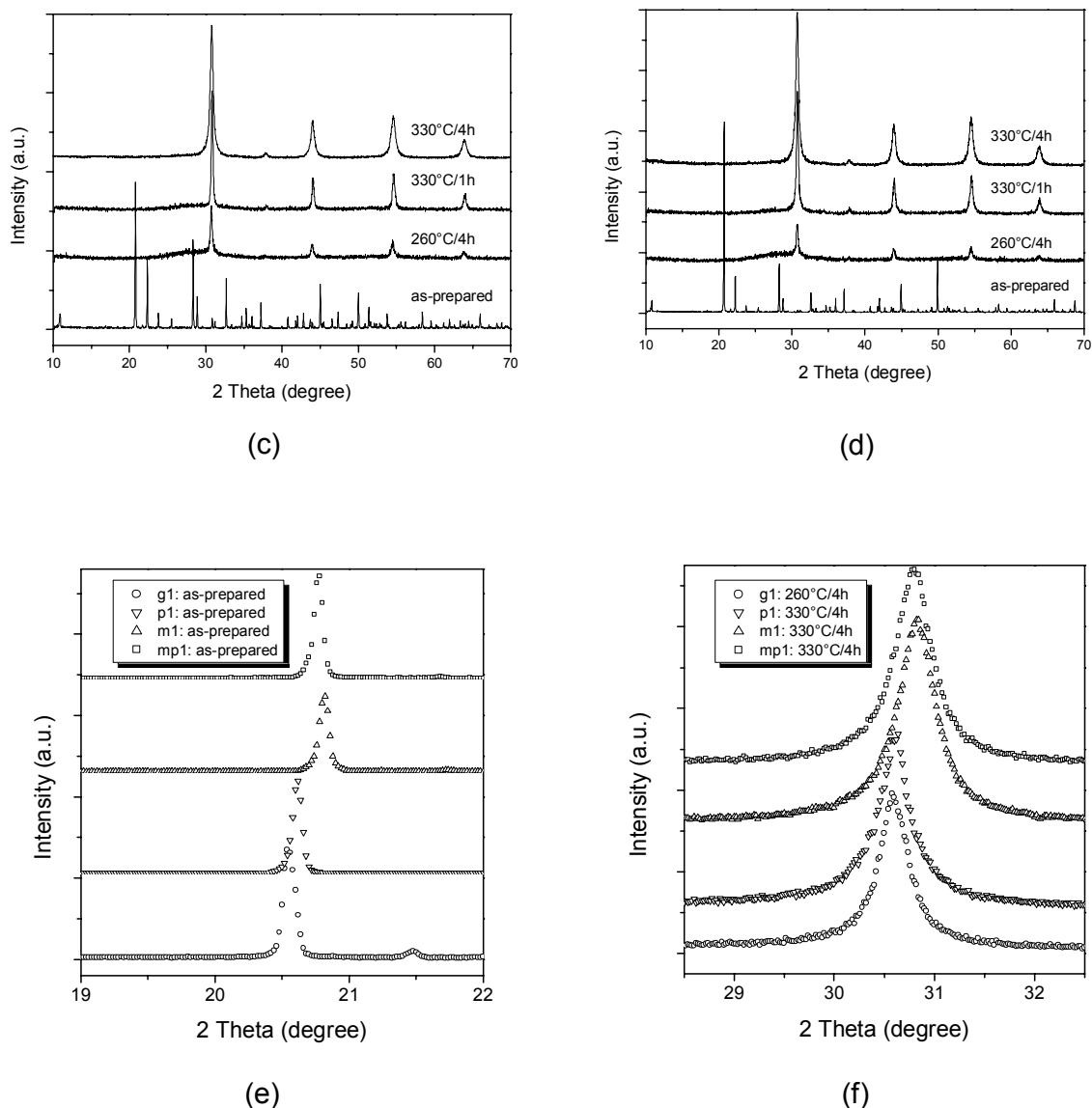


**Fig. 76** Phase transformation of the powders (hydrothermally synthesized at 250°C for 6h) by calcination and shift of the crystalline peaks in different systems: (a) g1, precursor:  $\text{SnO}_2 \cdot x\text{H}_2\text{O}$  gel; (b) p1, precursor:  $\text{SnO}_2 \cdot x\text{H}_2\text{O}$  peptized at pH = 9.3; (c) m1, precursor:  $\text{SnO}_2 \cdot x\text{H}_2\text{O}$  modified with 5 wt% Genapol X-080; (d) mp1, precursor:  $\text{SnO}_2 \cdot x\text{H}_2\text{O}$  modified with 5 wt% Genapol X-080 and peptized at pH = 9.3; (e) shift of the strongest peak of  $\text{BaSn}(\text{OH})_6$ ; (f) shift of the (110) peak of  $\text{BaSnO}_3$ .

Fig. 76c and Fig. 76d show that surface modification and the combination of modification and peptization do not change the crystallization mechanism compared to the G-system. However, they affect the nucleation and growth rate of  $\text{BaSnO}_3$ . A single-phase  $\text{BaSnO}_3$  can only be obtained by calcining the powder at 330°C instead of 260°C. The reason for this should be the same as in the case of peptization. The crystallite size of  $\text{BaSnO}_3$  in m1 and mp1 is 20.4 nm and 23.2 nm respectively.

It is also noted that the nucleation and growth of  $\text{BaSnO}_3$  is easier in the case of surface modification than in the case of peptization. The possible reason is that the modifier of Genapol X-080 decreases the surface free energy of the M-system<sup>171</sup>.

Although the as-prepared powders in the four samples consist of the same phase  $\text{BaSn}(\text{OH})_6$ , a small shift of its crystalline peaks can be observed. Fig. 76e illustrates the shift of the strongest peak in the crystalline phase of the as-prepared powders. The largest shift is found in m1. Similarly, a shift of the crystalline peaks in the obtained single-phase  $\text{BaSnO}_3$  derived from different precursors has also been found. Fig. 76f shows the shift of the  $\text{BaSnO}_3$  phase at (110) peak. A obvious shift can be found in the m1 and mp1.

As the position of the crystal peak is relevant to the lattice constant, above results show that peptization and surface modification affect the lattice structure, and that the influence of the latter is stronger than that of the former.

The influence of isopropanol replacing water in the M-system on the phase transformation of the as-prepared powder by calcination is shown in Fig. 77. The as-prepared powder is comprised of  $\text{BaSn}(\text{OH})_6$ , but the intensity of its peak at  $2\theta = 22^\circ$  relative to that at  $2\theta = 20^\circ$  increases obviously compared to Fig. 76c. No crystalline phase can be found in the powder calcined at  $260^\circ\text{C}$  for 4h. The powder after 4h of calcination at  $330^\circ\text{C}$  nevertheless consists of a  $\text{BaSnO}_3$  phase, an amorphous phase and a  $\text{BaCO}_3$  phase. The amorphous phase disappears after 4h of calcination at  $520^\circ\text{C}$  whereas the trace of  $\text{BaCO}_3$  can still be discerned.

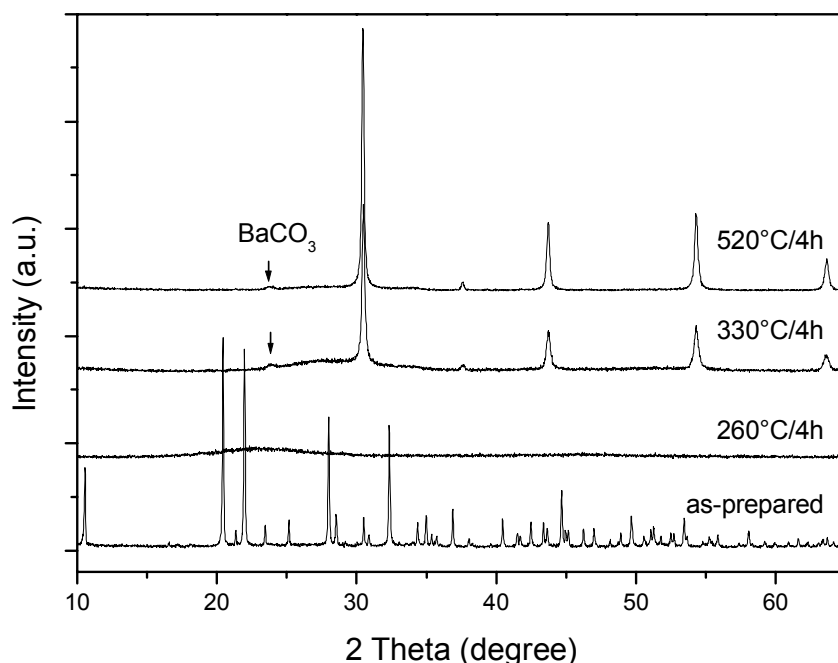


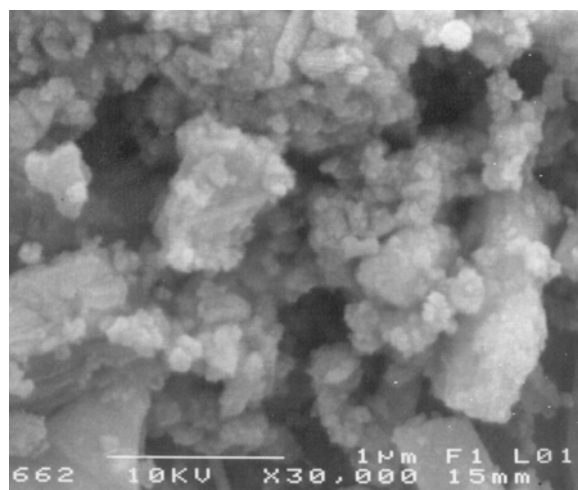
**Fig. 77** Phase transformation of powder m2 in M-system by calcinations. Precursor:  $\text{SnO}_2 \cdot x\text{H}_2\text{O}$  modified with 5 wt% Genapol X-080, isopropanol was used as a solvent in hydrothermal reaction. m2 was hydrothermally synthesized at  $250^\circ\text{C}$  for 6h.

The results show clearly that the crystallization of  $\text{BaSnO}_3$  in the case of isopropanol is slower than that in the case of water (Fig. 76c).  $\text{BaCO}_3$  formed in the powder can also be the reason that impedes structure rearrangement and material transfer, and thereafter limits the nucleation and growth of  $\text{BaSnO}_3$ .

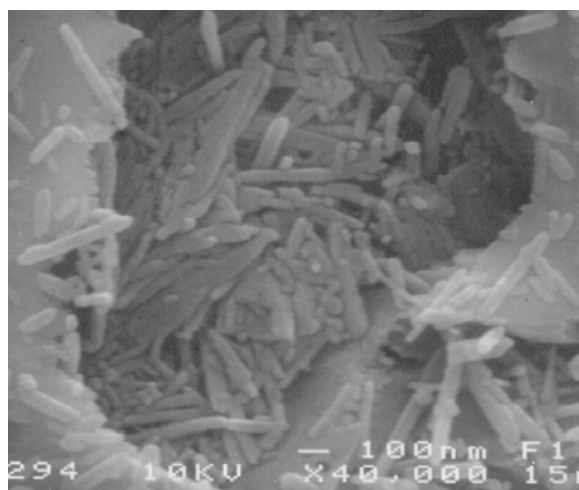
#### 5.3.5.4 Microstructure of the powders

The obtained  $\text{BaSnO}_3$  powders in different systems were observed under SEM. The particles of g1 (Fig. 78a) are aggregated so strongly that it is not easy to discern a single particle. The size of the particle is about 30 to 200 nm. Fig. 78b shows morphology of the particles in p1. The needle-shaped particles with a width of 20-80 nm are well-crystallized and separated from each other. However, a 'wall' of the surface, possibly not well crystallized, can also be found. In m1 (Fig. 78c), the particle size is estimated in a range of 20 to 40 nm. From the contour of the particles it can be deduced that small aggregates, which are composed of several particles, are formed firstly and then incorporate into a large one. In sample mp1 (Fig. 78d), the morphology of the aggregated particles is similar to that in m1. Nevertheless, the small aggregates with a size of 20 nm to 100 nm connect with each other more loosely and the particle size is about 10 to 30 nm.

These results indicate that peptization and surface modification can change the form and the size of the  $\text{BaSnO}_3$  particle. The aggregation degree of the particles can be decreased by combining modification and surface modification.



(a)



(b)

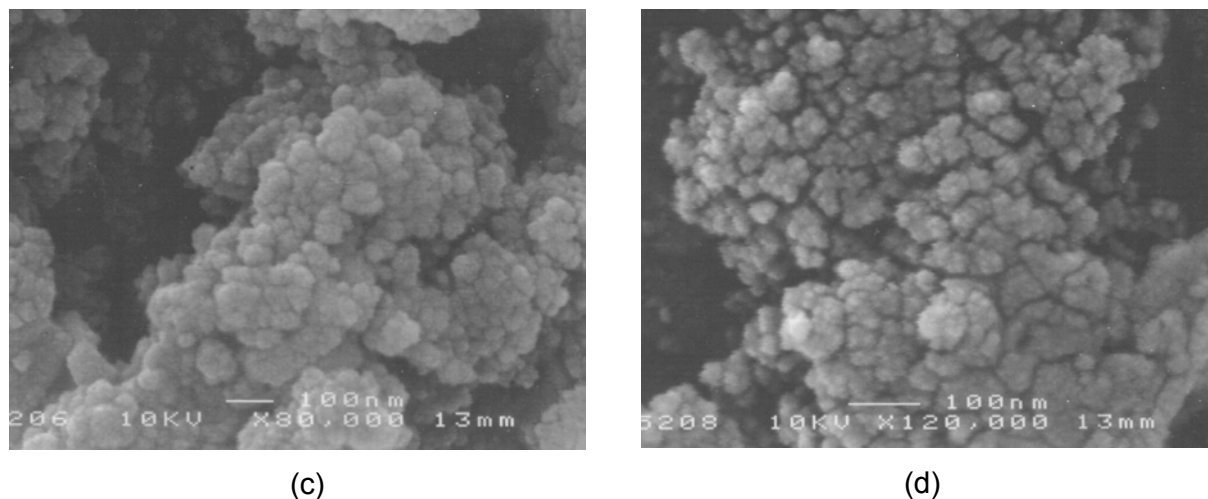


**Fig. 78** SEM images of the  $\text{BaSnO}_3$  powders obtained by calcining: (a) g1 at  $260^\circ\text{C}$  for 4h, precursor:  $\text{SnO}_2 \cdot x\text{H}_2\text{O}$  gel; (b) p1 at  $330^\circ\text{C}$  for 4h, precursor:  $\text{SnO}_2 \cdot x\text{H}_2\text{O}$  peptized at  $\text{pH} = 9.3$ ; (c) m1 at  $330^\circ\text{C}$  for 4h, precursor:  $\text{SnO}_2 \cdot x\text{H}_2\text{O}$  modified with 5 wt% Genapol X-080; (d) mp1 at  $330^\circ\text{C}$  for 4h, precursor:  $\text{SnO}_2 \cdot x\text{H}_2\text{O}$  modified with 5 wt% Genapol X-080 and peptized at  $\text{pH} = 9.3$ .

As mentioned in 5.3.2.3,  $\text{BaSnO}_3$  powders can be prepared without calcination via hydrothermal synthesis route at a high temperature. Fig. 79 shows the SEM micrographs of such  $\text{BaSnO}_3$  samples listed in Table 9. Sample g2 prepared at  $330^\circ\text{C}$  for 6 h from  $\text{SnO}_2 \cdot x\text{H}_2\text{O}$  gel shows the uniform cubic particles with a size of 3 to 4  $\mu\text{m}$  (Fig. 79a). Fig. 79b shows a  $\text{BaSnO}_3$  powder p2 has been synthesized at  $280^\circ\text{C}$  for 4h from peptized tin oxide hydrate. However, its particles with a size of 100 nm to 1  $\mu\text{m}$  are aggregated and not uniform. A  $\text{BaSnO}_3$  powder m3 with the particle size of 1 to 2  $\mu\text{m}$  is prepared from modified  $\text{SnO}_2 \cdot x\text{H}_2\text{O}$  at  $330^\circ\text{C}$  for 0.5 h. In view of the large particle size and the small specific surface area of these powders, a systematic and deep investigation on this region has not been done.

**Table 9**  $\text{BaSnO}_3$  powders obtained directly through hydrothermal synthesis

Samples	Pretreatment of precursor $\text{SnO}_2 \cdot x\text{H}_2\text{O}$	Hydrothermal conditions	Crystalline phase	BET specific surface area ( $\text{m}^2/\text{g}$ )
g2	no pretreatment	$330^\circ\text{C}/6\text{h}$	$\text{BaSnO}_3$	0.68
p2	peptized at $\text{pH} = 9.3$	$280^\circ\text{C}/4\text{h}$	$\text{BaSnO}_3$	2.93
m3	modified with 0.5 wt% Genapol X-080	$330^\circ\text{C}/0.5\text{h}$	$\text{BaSnO}_3$	1.22

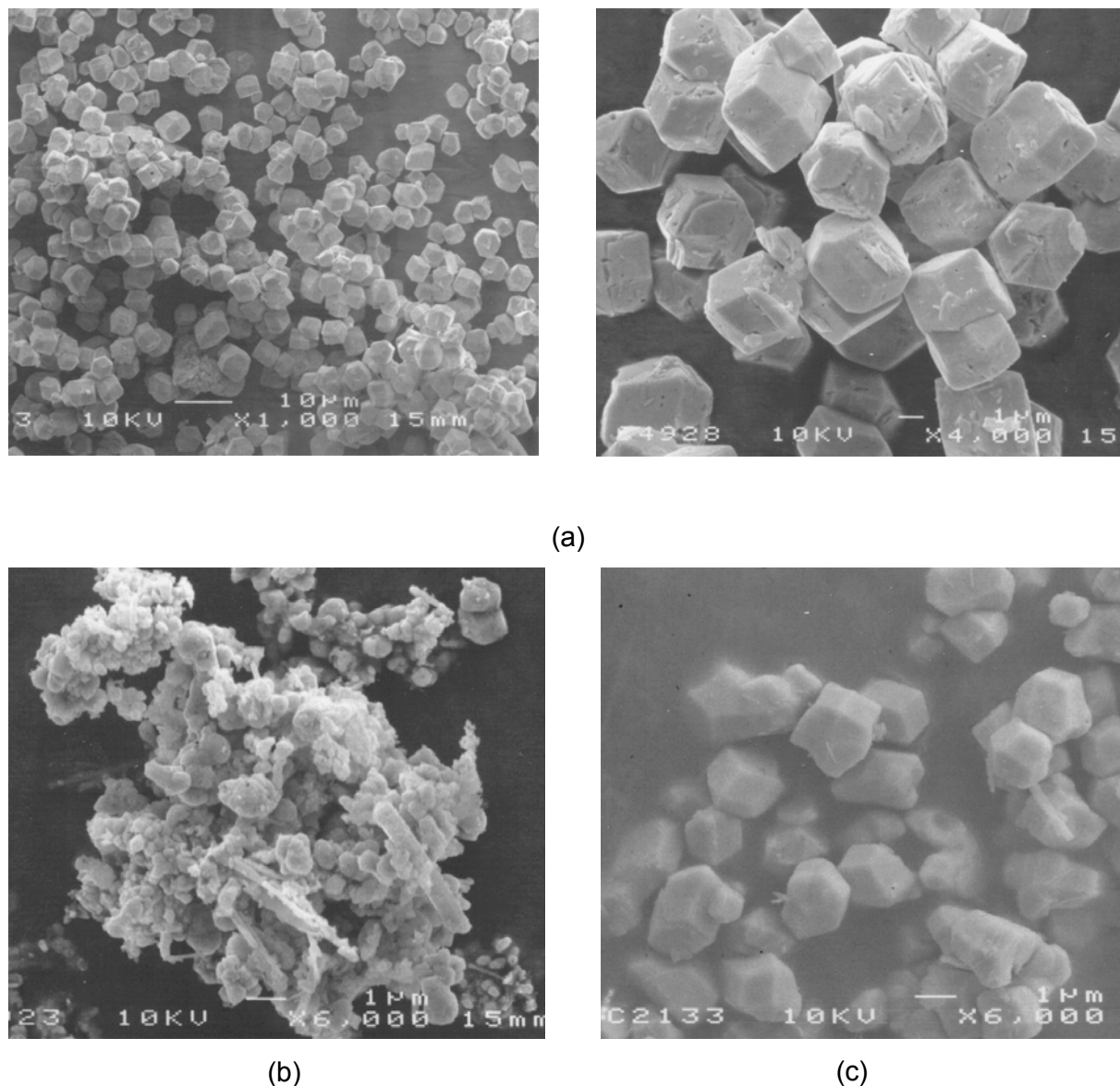


**Fig. 79** SEM images of the  $\text{BaSnO}_3$  powders synthesized hydrothermally at high temperatures without calcinations: (a) g2, (b) p2, (c) m3.

The  $\text{BaSnO}_3$  powders obtained through calcination were investigated by the means of the high resolution TEM. In sample p1 calcined at  $260^\circ\text{C}$  for 4h, the particles with a needle-shaped crystalline habitus are observed (Fig. 80a). The width varies from 20 to 90 nm and the length from 100 to 200 nm. The structure image of the needle-shaped particle nevertheless reveals its multi-crystallite structure. Fig. 80b shows two crystallites with a width of ca. 5 nm and a length of 10 to 15 nm in such a needle-shaped particle. They have different crystalline orientation.

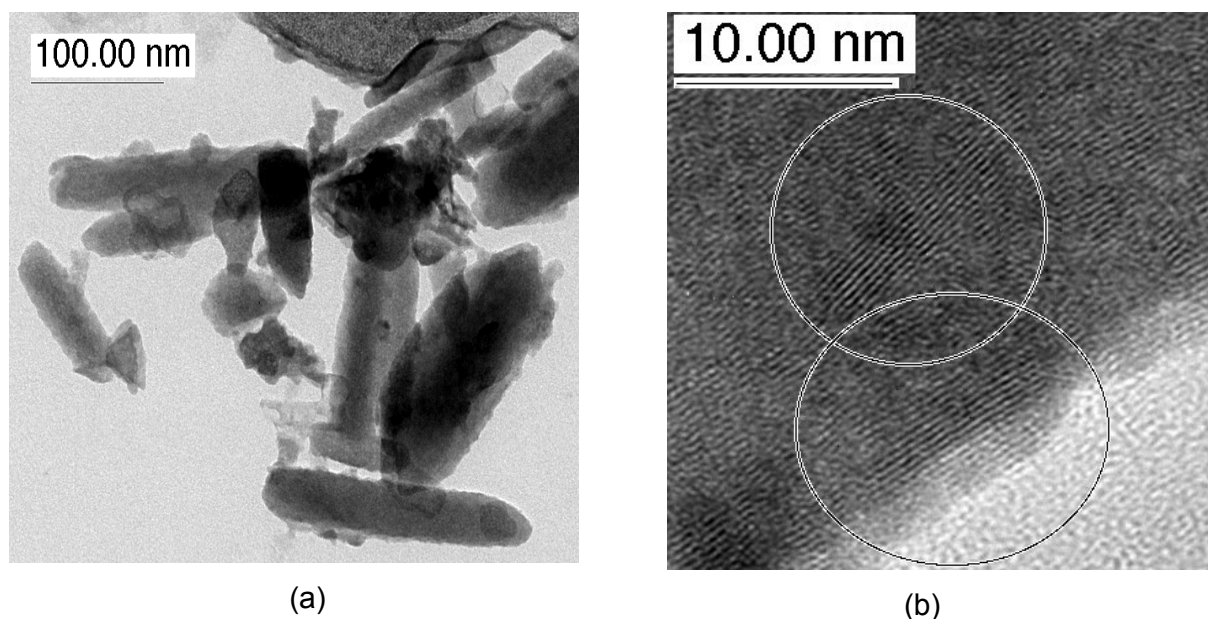


**Fig. 80** HRTEM micrographs of the powder p1 calcined at 260°C for 4h. The precursor  $\text{SnO}_2 \cdot x\text{H}_2\text{O}$  was peptized at pH = 9,3 and p1 was synthesized at a hydrothermal temperature of 250°C for 6h: (a) Diffraction and contrast imaging, (b) structure imaging.

In the case of the surface-modified m1 calcined at 330°C for 4h, the aggregates of particles changing the size from 10 nm to some micrometers in the  $\text{BaSnO}_3$  powder have been observed under HRTEM. Fig. 81a shows a big aggregate. Fig. 81b shows a small aggregate consisting of 4 'particles' which are found to be surrounded with a covering layer. The thickness of the layer varies from 3 to 5.5 nm. The structure image Fig. 81c shows the 'particle', as the same as other aggregates, is composed of many crystallites. These crystallites show a dimension of 2 to 6 nm and usually have an aspect ratio of 2:1. They can be clearly seen from the structure images Fig. 81 c to Fig. 81e.

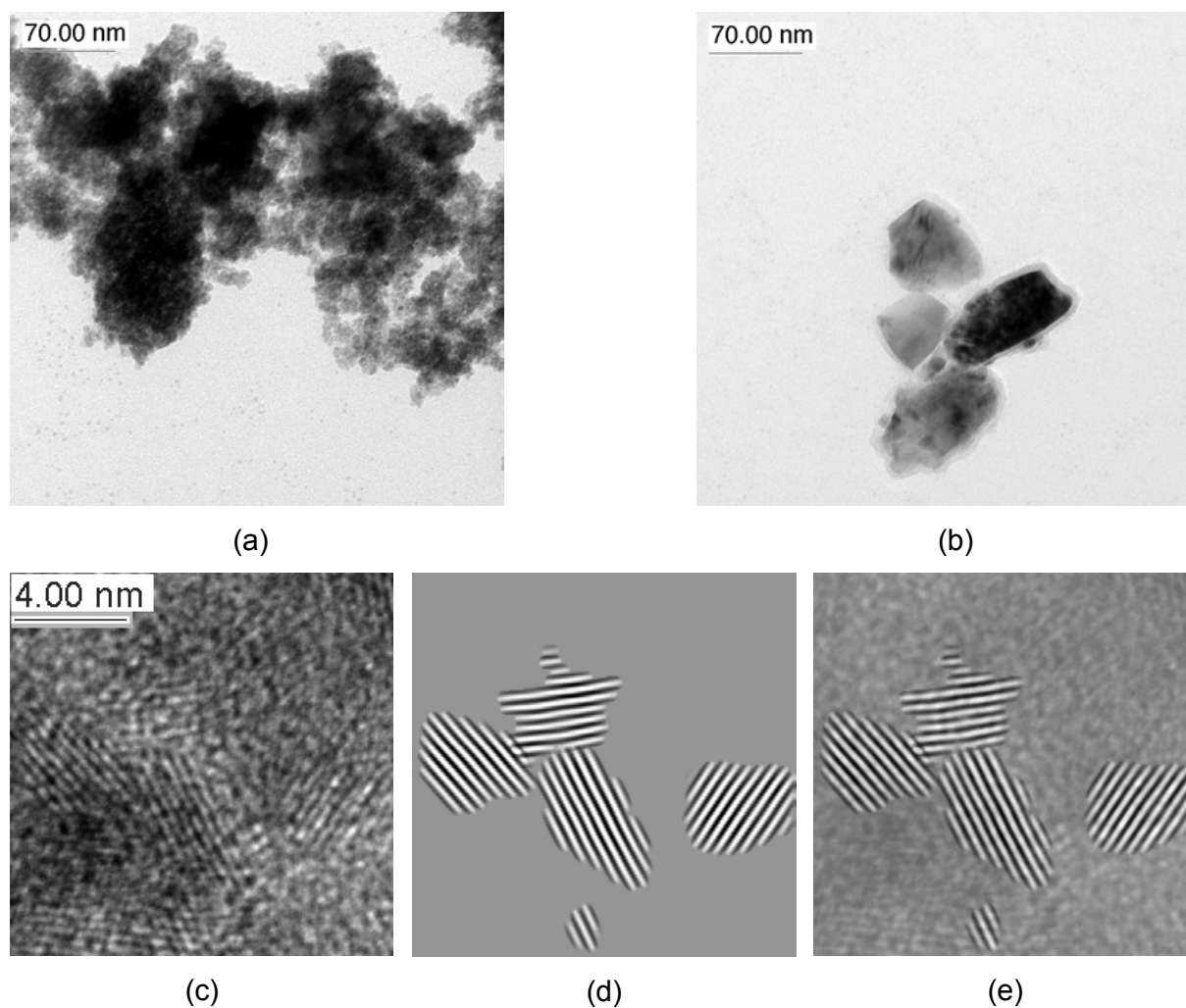


**Fig. 81** HRTEM micrographs of the sample m1 calcined at 330°C for 4h. The precursor  $\text{SnO}_2 \cdot x\text{H}_2\text{O}$  was modified with 5 wt% Genapol X-080 and m1 was synthesized at a hydrothermal temperature of 250°C for 6h: (a)(b) Diffraction and contrast imaging, (c) structure imaging, (d) image c processed by Fourier transformation and filtering, (e) the sum of c and d.

The aggregate in sample mp1 calcined at 330°C for 4h in Fig. 82 shows the similar crystalline structure as in the M-system. An aggregate built up of crystallites and a crystallite with the dimension of 5 x 2.5 nm can be clearly seen.

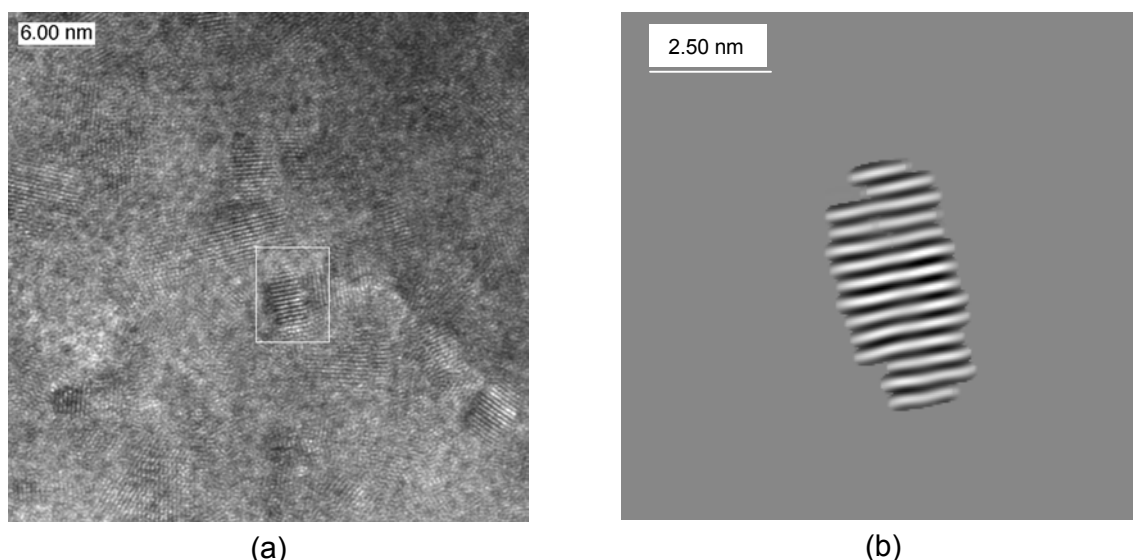


**Fig. 82** HRTEM micrographs of the sample mp1 calcined at 330°C for 4h. The precursor  $\text{SnO}_2 \cdot x\text{H}_2\text{O}$  was modified with 5 wt% Genapol X-080 and peptized at pH = 9.3, and mp1 was synthesized at a hydrothermal temperature of 250°C for 6h: (a) structure imaging, (b) the marked region processed by Fourier transformation and filtering and enlarged.

In sum, the size of the primary particle, either in the case of modification or in the case of peptization, is lowered to a very small value. However, the aggregation degree, although being lowered by peptization and surface modification to some extent, is still severe in the obtained powder of  $\text{BaSnO}_3$ . The particles with a covering layer in the M-system gives a direct proof that the surfactant molecules can modify the surface of  $\text{BaSnO}_3$ . The multocrystallite structure of the particle under the covering layer, on the other hand, suggests that the modified particles can agglomerate again either during the hydrothermal reaction or during the calcination process.

#### 5.3.5.5 Solid state $^{119}\text{Sn}$ NMR

To further compare the prepared  $\text{BaSnO}_3$  powders, Solid state  $^{119}\text{Sn}$  NMR technique has been used to examine the crystallinity of  $\text{BaSnO}_3$ . As a reference, a commercial  $\text{BaSnO}_3$  powder (ABCR) has been analyzed with the Solid state  $^{119}\text{Sn}$  NMR.

It is illustrated in Fig. 83 that the signal in the commercial sample is symmetric and narrow (the half value width = 243 Hz). These show that the sample is crystallized well and Sn is present in high symmetric surroundings. The chemical shift  $\delta$  is -678.7 ppm corresponding to the octahedral  $[\text{SnO}_6]$ . By comparing with the commercial sample, the samples prepared via hydrothermal synthesis route have a chemical shift localizing almost at the same position, which reveals that Sn in these samples exists in the form of  $[\text{SnO}_6]$ . The small shift of  $\delta$  (about -2 ppm) nevertheless reflects the deviation of Sn arrangement in lattice between the commercial and prepared samples (see the dashed line). A signal broadening (the half



value width increases to 806 - 915 Hz) is also observed in the prepared samples. This signal broadening is normally related to a lower crystallization degree.

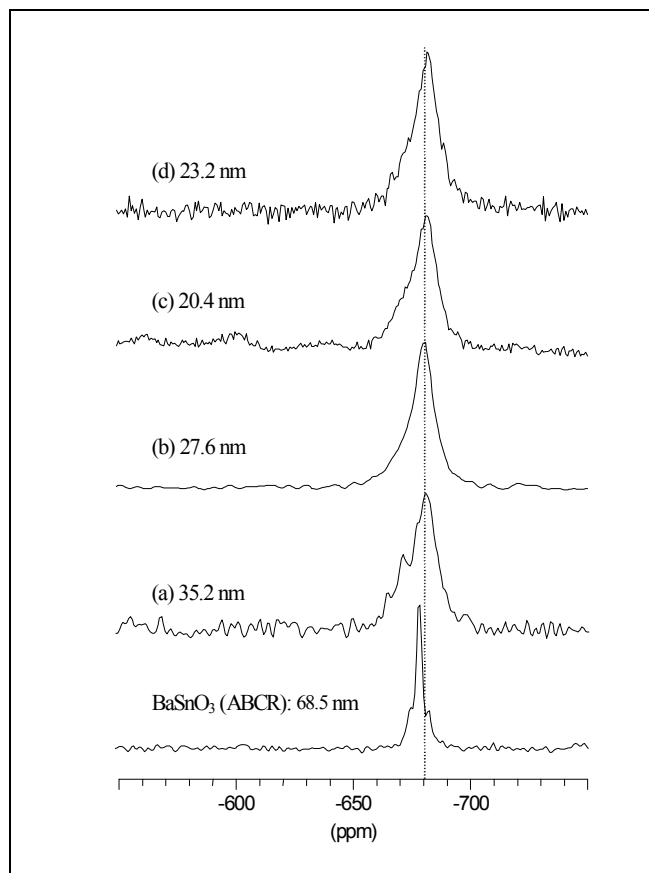


**Fig. 83** Solid state  $^{119}\text{Sn}$  NMR spectra of the  $\text{BaSnO}_3$  powders obtained by calcining: (a) g1 at  $260^\circ\text{C}$  for 4h, (b) p1 at  $330^\circ\text{C}$  for 4h, (c) m1 at  $330^\circ\text{C}$  for 4h, (d) mp1 at  $330^\circ\text{C}$  for 4h - in comparison with that of the commercial  $\text{BaSnO}_3$  powder (ABCR). The size of the primary particle is given out in the diagram.

The spectrum of  $\text{BaSnO}_3$  in the G-system (Fig. 83a) shows an asymmetric signal consisted at least two overlapped resonance ( $-671$  ppm and  $-680$  ppm). This suggests that more than one kind of Sn coordination exists in the sample and that the crystal is low symmetric.

As for the sample in the P-system (Fig. 83b), the signal with a width of the half value of 806 Hz becomes symmetric. Thus, the symmetry of the  $\text{BaSnO}_3$  crystal is improved by peptization.

A maximal width of the half value of the signal (915 Hz) is found in the sample of the M-system (Fig. 83c). The signal is not very symmetric. It can be inferred that Sn arrangement is distorted and  $\text{BaSnO}_3$  is not crystallized well.

In contrast to this, a better symmetry is found in the sample of the MP-system (Fig. 83d). Its width of the half value is 870 Hz. In addition, a double-shoulder structure, as shown in the commercial sample, is observed. It can be assumed that the structure distortion in this sample is small.

The above results indicate that the symmetry of  $\text{BaSnO}_3$  in the prepared powders is lower than in the commercial powder. The crystallization degree in the former is also lower. These can be explained by the much lower calcining temperature employed in the hydrothermal synthesis route, where the grain grows slowly and cannot develop to a perfect crystal. By comparing the four prepared samples, it can be found that peptization and surface modification is helpful to improve the crystallinity of  $\text{BaSnO}_3$ . Through combination of peptization and surface modification, the structure distortion of  $\text{BaSnO}_3$  can be to some extent limited.

### 5.3.5.6 Surface area and density

The specific surface area and the density of  $\text{BaSnO}_3$  obtained from different precursors through calcination are shown in Fig. 84. It can be seen that the specific surface area of the powder can be effectively increased by peptization (P-system) and surface modification (M-system). The specific surface area is increased by a factor of about 5 in P-system and ca. 10 in the M-system. By combining surface modification and peptization (MP-system) it increases only a little compared to the M-system. The density of the powder of  $\text{BaSnO}_3$  among these systems is altered somewhat differently. As the precursor was peptized, the powder shows the lowest density. In the case of modification and combination of modification and peptization, however, the density can be increased to some extent.

The above results show that peptization increases the specific surface area at the cost of a decrease in the density, whereas surface modification can improve both of them. By combining the two measures, the specific surface area and the density of the powder can be further increased.

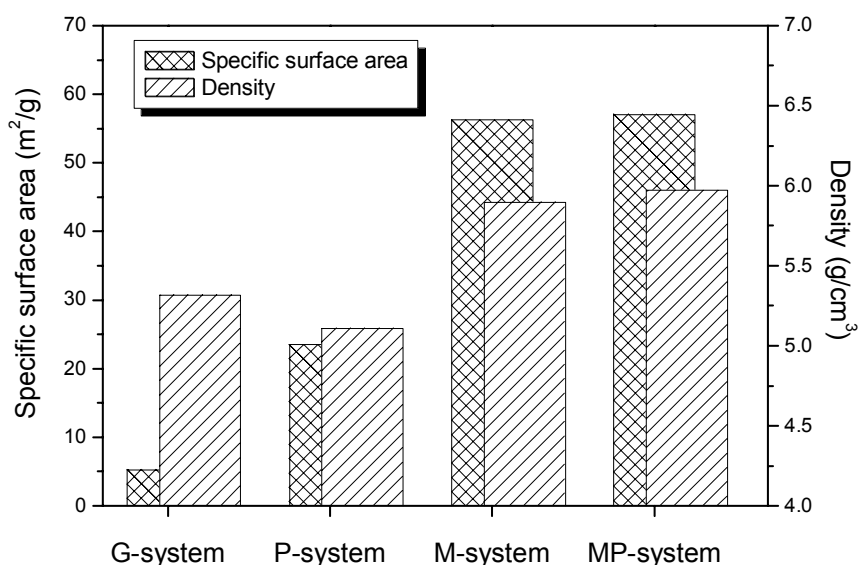


**Fig. 84** BET specific surface area and density of  $\text{BaSnO}_3$  prepared in: (a) G-system: g1 calcined at 260°C for 4h, (b) P-system: p1 calcined at 330°C for 4h, (c) M-system: m1 calcined at 330°C for 4h, (d) MP-system: mp1 calcined at 330°C for 4h.

### 5.3.5.6 Sintering behavior

The shrinkage behavior of the prepared  $\text{BaSnO}_3$  powders (G-system: g1 calcined at  $260^\circ\text{C}$  for 4h; P-system: p1 calcined at  $330^\circ\text{C}$  for 4h; P-system: p1 calcined at  $330^\circ\text{C}$  for 4h; MP-system: mp1 calcined at  $330^\circ\text{C}$  for 4h) was investigated by means of dilatometry. The commercial  $\text{BaSnO}_3$  was used as a reference. The linear shrinkage curves of the samples are presented in Fig. 85. The cylinder samples were formed at 800 MPa by uniaxial pressing. The green density of these samples is also indicated in the diagram. It can be seen that the green density of the prepared samples is lower than that of the commercial one (ABCR). For the commercial sample, its sintering begins at  $1530^\circ\text{C}$  and a shrinkage of only 1.4% is reached at  $1650^\circ\text{C}$ . As to the sample of the G-system, the beginning temperature of its sintering is lowered to  $1450^\circ\text{C}$  and the shrinkage reaches 10% at  $1650^\circ\text{C}$ . The contour of the curve shows clearly that the sintering does not end. In the P-system, the sintering of the sample begins at  $1200^\circ\text{C}$  and ends at  $1650^\circ\text{C}$  with a shrinkage of 17.9%. As far as the sample of the M-system is concerned, the sintering consists of two phases. The sintering proceeds in the first phase ( $950 - 1500^\circ\text{C}$ ) slowly and becomes rapid in the second phase ( $1500 - 1650^\circ\text{C}$ ). The linear shrinkage at  $1650^\circ\text{C}$  is 15.2%. For the sample of the MP-system, its shrinkage behavior in the low temperature region is similar to that in the M-system and in the high temperature region similar to that in the P-system. This reflects the combining effects of surface modification and peptization in the MP-system.

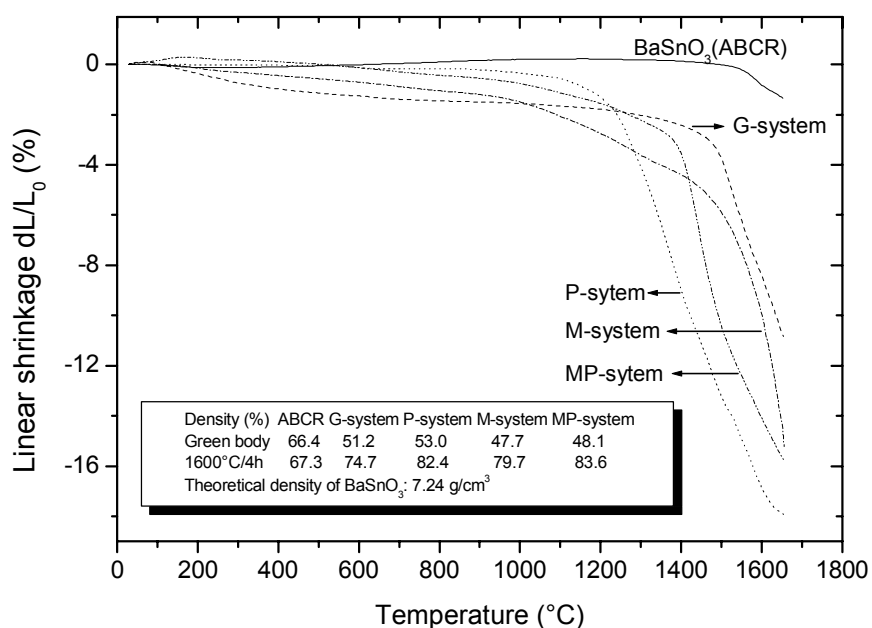


**Fig. 85** Dilatometry curves of the commercial  $\text{BaSnO}_3$  powder and  $\text{BaSnO}_3$  powders prepared in different systems via hydrothermal synthesis route. G-system: g1 calcined at  $260^\circ\text{C}$  for 4h; P-system: p1 calcined at  $330^\circ\text{C}$  for 4h; M-system: m1 calcined at  $330^\circ\text{C}$  for 4h; MP-system: mp1 calcined at  $330^\circ\text{C}$  for 4h. The density of the green bodies and the samples sintered at  $1600^\circ\text{C}$  for 4h are shown.

The bulk density and the porosity of  $\text{BaSnO}_3$  samples sintered at  $1600^\circ\text{C}$  for 4h are illustrated in Fig. 86(a) and (b) (the relative density can be found in Fig. 85). The porosity is calculated according to the theoretical density of  $\text{BaSnO}_3$ . All the prepared samples show a higher bulk density than the commercial one. In addition, the bulk density is improved through peptization and modification by  $0.55$  and  $0.38$   $\text{g}/\text{cm}^3$  respectively. The maximal bulk density of  $6.05$   $\text{g}/\text{cm}^3$  is obtained by combining peptization and surface modification. The porosity of samples nevertheless shows that all samples at this sintering temperature are not completely densified. In the case of the commercial powder, the porosity is as high as 32.7%. By combining peptization and surface modification, the porosity can be lowered to the half (16.4%). This reveals that the densification of  $\text{BaSnO}_3$  can still be largely improved in spite of the nature of its sintering inactivity, as pointed out in section 2.1.

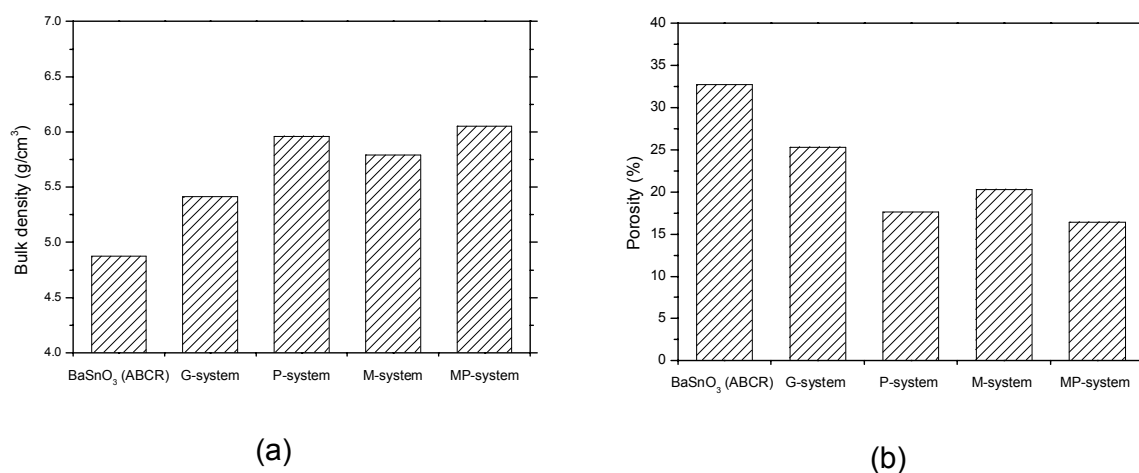


**Fig. 86** (a) Bulk density, (b) Porosity of  $\text{BaSnO}_3$  samples sintered at  $1600^\circ\text{C}$  for 4h. G-system: g1 calcined at  $260^\circ\text{C}$  for 4h; P-system: p1 calcined at  $330^\circ\text{C}$  for 4h; M-system: m1 calcined at  $330^\circ\text{C}$  for 4h; MP-system: mp1 calcined at  $330^\circ\text{C}$  for 4h.

The microstructure of the commercial sample and the sample mp1 of the MP-system sintered at  $1600^\circ\text{C}$  for 4h is shown in Fig. 87. Compared to the commercial one, the sample of the MP-system shows uniform grains and much smaller pores. The microstructure of the latter also shows that several grains make up of a domain, within which a high densification is reached. But the domains fuse with each other loosely so that the interdomain pores are formed. This domain structure can be attributed to the aggregation of the particles.

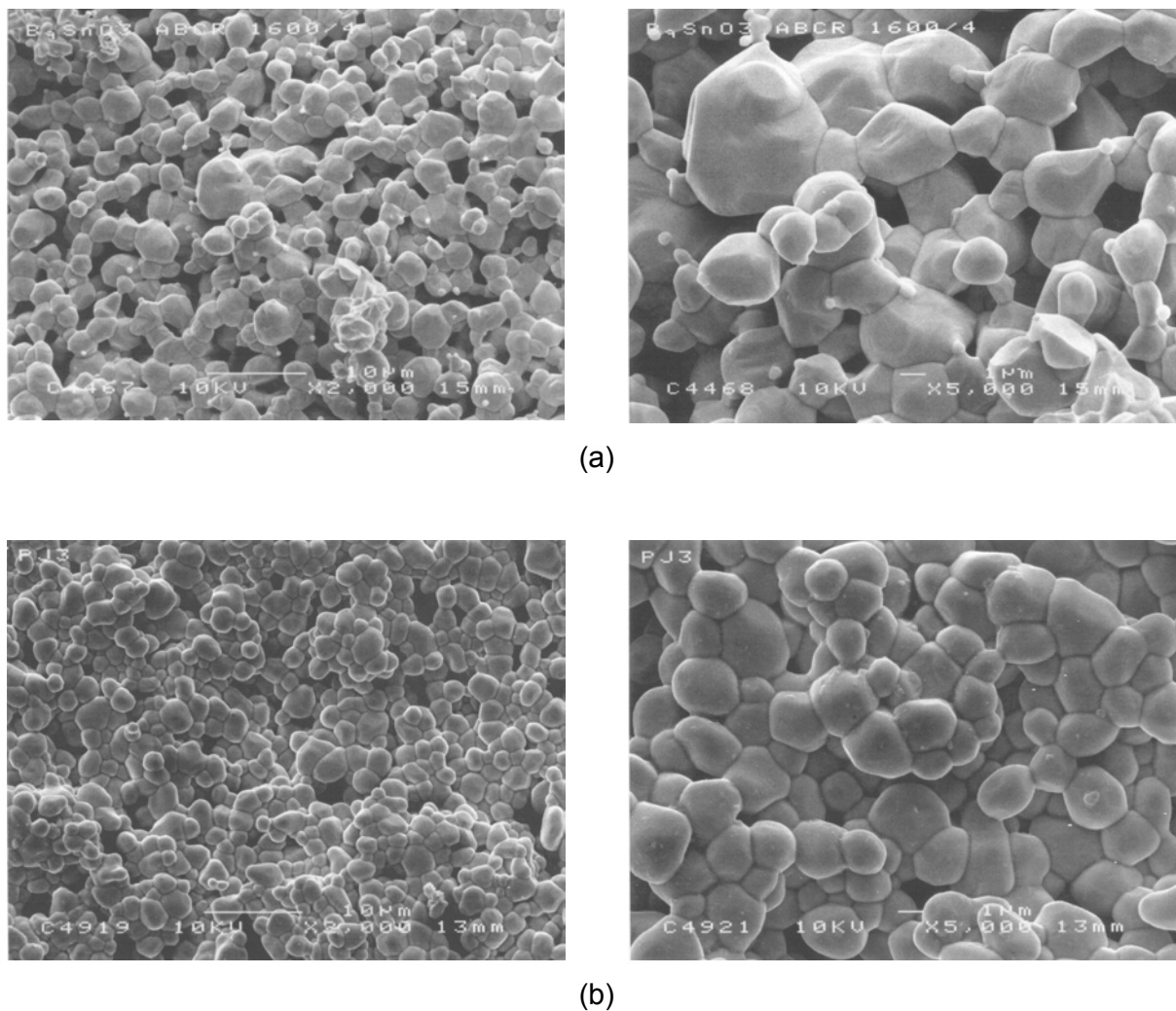


**Fig. 87** SEM micrographs of BaSnO<sub>3</sub> samples sintered at 1600°C for 4h: (a) Commercial (ABCR), (b) MP-system: mp1 calcined at 330°C for 4h.

The above discussions show that the prepared powders are much more sintering-active than the commercial powder. The sintering properties of the prepared powders are improved by peptization and surface modification, which can be attributed to the improved surface area and the decreased particle size. By combining peptization and surface modification a maximal densification of 83.6 % T.D. is reached. Its microstructure shows the formation of interdomain pores.

In this section, we have found that the BaSnO<sub>3</sub> powder of MP-system (mp1 calcined at 330°C for 4h) shows better quality in microstructure, specific surface area, density, sintering properties and crystallinity than those of the other system. It was thus selected as the powder for further study on fabrication of BaSnO<sub>3</sub> tape and its techniques was adapted to prepare doped BaSnO<sub>3</sub> powder.

### 5.3.6 Fabrication of BaSnO<sub>3</sub> tape

When being applied as capacitors or as gas sensor elements, BaSnO<sub>3</sub> powder is normally required to be redispersed in a solvent. According to the modern technology the obtained suspension will be either cast into thin sheets by shape forming or printed on the substrate by the screen printing technique. Because tape casting has been developed to fabricate these thin sheets in large quantity and at low cost, in experiments this technique is employed to fabricate BaSnO<sub>3</sub> thin tape and will be described in this section. The BaSnO<sub>3</sub> powder of the MP-system obtained by calcining mp1 at 330°C for 4 hours was used for the tape casting because of its better quality than others, as discussed in the last section. It was first redispersed in water and then cast on the plastic film to form a green tape.

#### 5.3.6.1 Redisperison of the powder

In order to obtain a uniform green tape through tape casting, BaSnO<sub>3</sub> powder must be well redispersed. This includes disintergration of the large agglomerates into the size of primary particles and stabilization of the powder against reagglomeration. The former is usually carried out by using milling and ultrasonic desintergating. For avoiding the reagglomeration of the particles, a dispersing agent is added to the suspension to form either an electrostatic stabilization or a steric stabilization between the particles.

The powder particles are charged with the ions adsorbed on their surface, which causes an electrostatic interaction between these particles including the attractive and repulsive forces. The attractive forces, mainly Van de Waals force, are the sources of reagglomeration and cannot be easily manipulated. Repulsive forces depend principally on the interactions of the layers of adsorbed surface ions surrounding the particles. The thickness of the layer and hence the effective range of the interaction potential depends on surface charge density and ionic strength. Zeta-potential is usually used to characterized this interaction potential.

Fig. 88 indicates that the zeta-potential of the BaSnO<sub>3</sub> particles depends on pH. The isoelectric point (IEP) of this powder locates at pH = 3.82. The particles are positively charged before the IEP and negatively charged after the IEP. The rapid change and the low absolute value of the zeta-potential in the pH range of 3 to 6 indicate the instability of the suspension. The stabilization of the suspension can nonetheless realized at the pH range of 6 to 10 because the zeta-potential is larger and relatively stable. It is therefore helpful to disperse and stabilize the suspension through adjusting the pH value. In the experiments the pH value of the suspension was adjusted to 10 with ammonia solution.

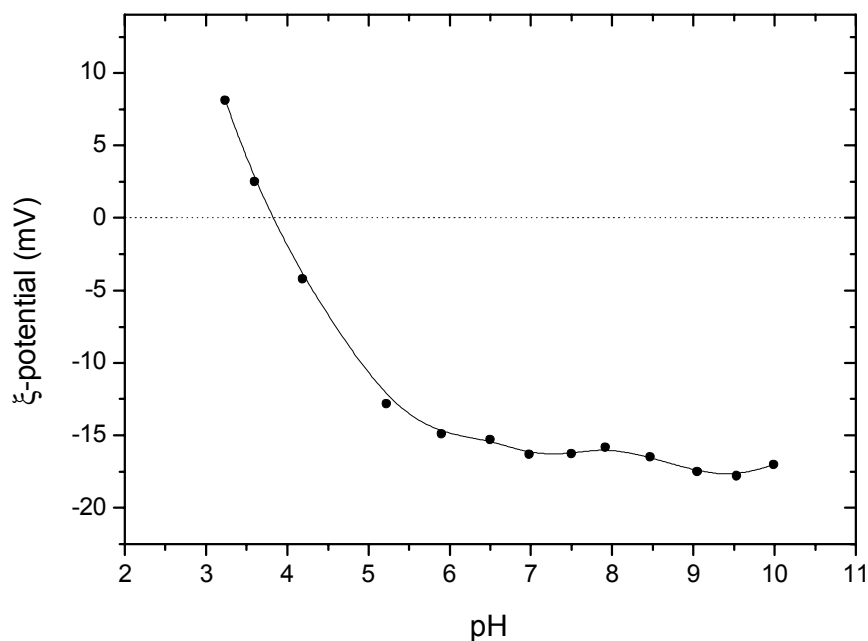


**Fig. 88** Zeta-potential of the BaSnO<sub>3</sub> powder (mp1 calcined at 330°C for 4h) as a function of pH.

To determine the dispersing agent and its concentration, four surfactants were chosen. There are TMAH ((CH<sub>3</sub>)<sub>4</sub>NOH)), TEA (triethyl amine: N(C<sub>2</sub>H<sub>5</sub>)<sub>3</sub>), PEI-SC (polyethyl imine with short chains: (-NHC<sub>2</sub>H<sub>4</sub>-)<sub>x</sub>[-N(C<sub>2</sub>H<sub>4</sub>NH<sub>2</sub>)C<sub>2</sub>H<sub>4</sub>-]<sub>y</sub>C<sub>2</sub>H<sub>4</sub>, MW: 1200) and PEI-LC (polyethyl imine with long chains, MW: 50,000 – 100,000). The effects of these surfactants on the surface charge of the particles were analyzed with the particle charge detector (PCD). The results are presented in Fig. 89. It is shown that increasing the concentration of TMAH, PEI-LC as well as PEI-HC will lead to an increase in PCD-potential (negative) of the particles. This means a decrease in repulsive force between particles. In contrast, the addition of TEA to the suspension can further lower the negative potential. The potential becomes constant as the added TEA reaches 2 wt%. The results indicate that TEA is suitable to disperse and stabilize the suspension of BaSnO<sub>3</sub>. 2.5 wt% TEA was used in the experiment to disperse and stabilize the suspension.

As the BaSnO<sub>3</sub> powder is strongly aggregated, it was milled in a mortar mill. The milled powder was redispersed with 2.5 wt% TEA and thereafter ultrasonically disintegrated for 30 minutes. The particle distribution of the suspension before and after redispersion was measured with UPA and presented in Fig. 90. It can be seen that the particles mainly distribute in the range of 0.8 to 5 μm before redispersion and in the range of 0.25 to 1 μm after redispersion. Through redispersion the mean particle diameter  $d_{50}^n$  is lowered from 1.60 μm to 0.54 μm and  $d_{50}^v$  from 2.08 μm to 0.53 μm.

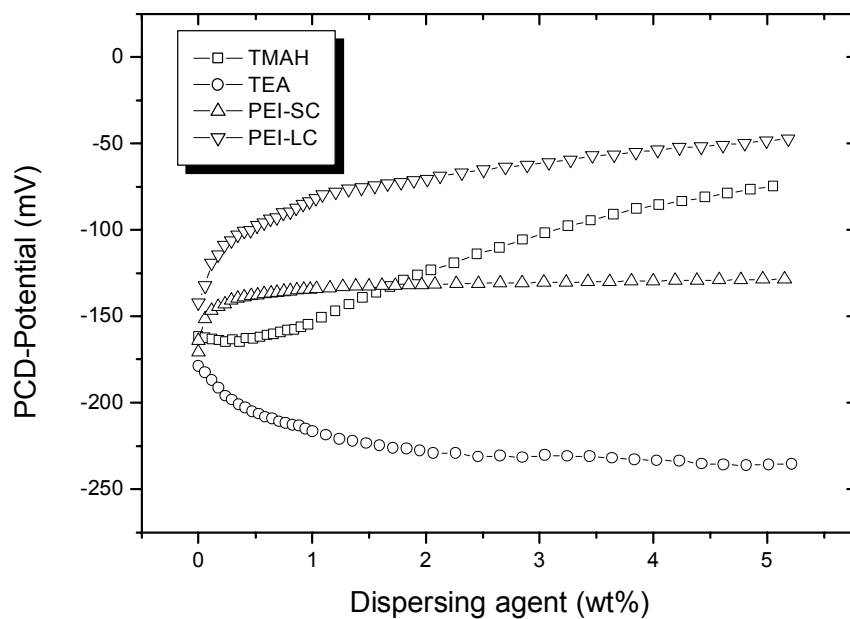


**Fig. 89** Particle charge of the  $\text{BaSnO}_3$  suspension (concentration: 5 wt%) tritreated with different dispersing agents (concentration: 1 wt%).  $\text{BaSnO}_3$  was obtained by calcining mp1 at  $330^\circ\text{C}$  for 4h.

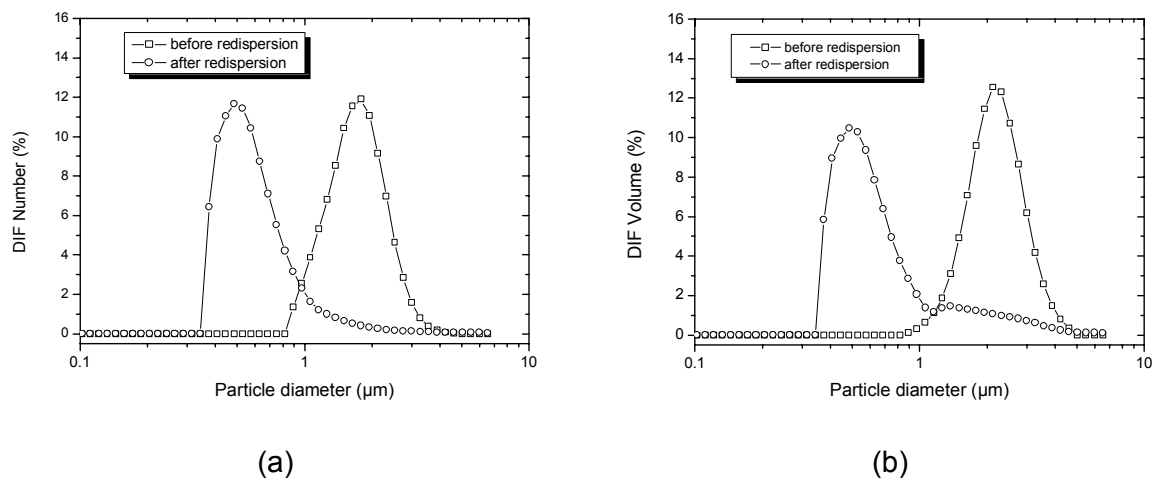


**Fig. 90** Particle diameter distribution of the  $\text{BaSnO}_3$  powder (mp1 calcined at  $330^\circ\text{C}/4\text{h}$ ) redispersed by TEA: (a) Number distribution, (b) volume distribution.



### 5.3.6.2 Tape casting

To obtain the slurry for tape casting, PVA and glycerin were added to the well-dispersed suspension. PVA was used as a binder which gives the green tape the flexibility and strength to enable handling. Glycerin was serviced as a plasticizer to soften the binder thus improving the flexibility of the type. The thickness of the wet tape can be changed from 40 to 200  $\mu\text{m}$ . After being dried in a furnace at 80°C for several minutes, the tape can be easily separated from the plastic film. Fig. 91 shows the prepared green tapes with a thickness of 11, 32 and 51  $\mu\text{m}$  which corresponds to a wet thickness of 40, 100 and 200  $\mu\text{m}$  respectively.

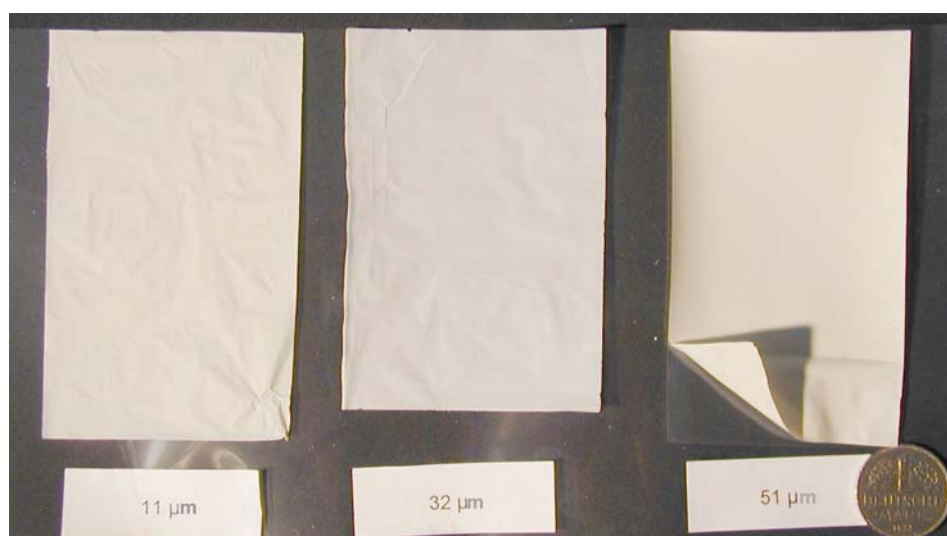


**Fig. 91** Green tapes of  $\text{BaSnO}_3$  (mp1 calcined at 330°C for 4h) with different thickness formed by tape casting. The right one is partly separated from the plastic film.

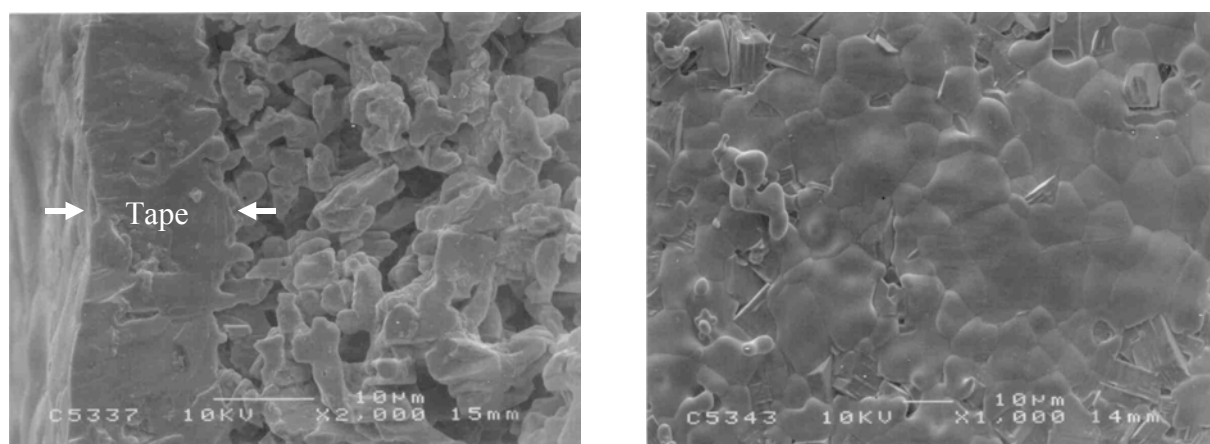


**Fig. 92** SEM micrographs of the green tape (51  $\mu\text{m}$ ) sintered at 1500°C on the  $\text{Al}_2\text{O}_3$  substrate: (a) Cross-section, (b) surface.

These green tapes have been sintered on the  $\text{Al}_2\text{O}_3$  substrate at  $1500^\circ\text{C}$ . Fig. 92 shows the cross section and the surface of a sintered tape, whose green body is  $51\ \mu\text{m}$  thick. It can be seen from the cross section that the sintered tape is very densified and its thickness varies from  $12$  to  $14\ \mu\text{m}$ . The porous part is the  $\text{Al}_2\text{O}_3$  substrate. The surface of the tape indicates the fusion of the particles. The sintered tapes of the green body with a thickness of  $11\ \mu\text{m}$  and  $32\ \mu\text{m}$  are about  $2\ \mu\text{m}$  and  $\mu\text{m}$  thick respectively.

### 5.3.7 Antimony doped barium stannate

$\text{Sb}^{3+}$ , when replacing  $\text{Sn}^{4+}$  in  $\text{BaSnO}_3$ , becomes an acceptor which will have an effective negative charge.  $\text{Sb}^{5+}$  with a higher positive charge than  $\text{Sn}^{4+}$  as a substituent ion is a donor which owns an effective positive charge. As a result of the doping, the charge density in  $\text{BaSnO}_3$  will increase and its conductivity will be improved. Thus, it is of interest to prepare the doped  $\text{BaSnO}_3$  powder and to investigate its properties.

A doped  $\text{SnO}_2 \cdot x\text{H}_2\text{O}$  precursor was obtained by reacting the mixture of  $\text{SbCl}_3$  (or  $\text{SbCl}_5$ ) and  $\text{SnCl}_4$  which was modified by Genapol X-080 (5 wt%) and thereafter peptizing at pH 9.3. The  $\text{Sb}^{3+}$  doped  $\text{SnO}_2 \cdot x\text{H}_2\text{O}$  is transparent and shows a violet red color, whereas the  $\text{Sb}^{5+}$  doped  $\text{SnO}_2 \cdot x\text{H}_2\text{O}$  is transparent and yellow. The as-prepared powder was synthesized through hydrothermal reaction at  $250^\circ\text{C}$  for 6 hours, which was then calcined at  $330^\circ\text{C}$  for 4 hours to realize the crystallization of  $\text{BaSnO}_3$ . The whole procedure for preparing the doped powder is the same as that for preparing mp1.

#### 5.3.7.1 $\text{Sb}^{3+}$ doped $\text{BaSnO}_3$

The as-prepared powder, hydrothermally synthesized at  $250^\circ\text{C}$  from the modified (5 wt% Genapol X-080) and peptized (pH = 9.3)  $\text{SnO}_2 \cdot x\text{H}_2\text{O}$  which doped with 10 at.%  $\text{Sb}^{3+}$ , consists of  $\text{BaSn}(\text{OH})_6$  phase. Its TG-DTA curve is shown in Fig. 93. Two endothermic peaks appear at  $260^\circ\text{C}$  and  $325^\circ\text{C}$  respectively, which correspond to the dehydration of the powder. This thermal behavior is similar to that of the undoped powder mp1 (see Fig. 74d). The border of its 1<sup>st</sup> ( $200^\circ\text{C}$  to  $300^\circ\text{C}$ ) and 2<sup>nd</sup> ( $300^\circ\text{C}$  to  $400^\circ\text{C}$ ) weight loss phases is not obvious. The sum of the weight loss in these two phase is only 9.9 wt% and is less than that in the undoped case (13.7 wt%, see Fig. 74d). From  $400^\circ\text{C}$  the weight loses slowly and this trend keeps up to  $1400^\circ\text{C}$  in air atmosphere. This is different from that in the undoped sample mp1, in which the weight becomes constant at about  $800^\circ\text{C}$ . These results indicate that water is difficult to remove from the  $\text{Sb}^{3+}$  doped as-prepared powder, which will give rise to a negative effect on the transformation of  $\text{BaSnO}_3$  from  $\text{BaSn}(\text{OH})_6$ .

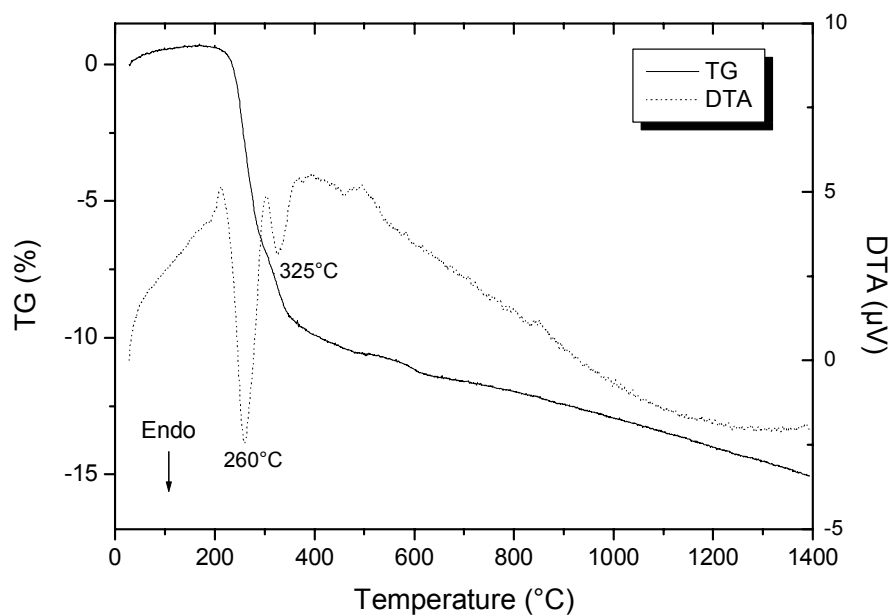


**Fig. 93** TG-DTA curve of the as-prepared powder synthesized hydrothermally at 250°C for 6h from the modified (5 wt% Genapol X-080) and peptized (pH = 9.3)  $\text{SnO}_2 \cdot x\text{H}_2\text{O}$  which was doped with 10 at.%  $\text{Sb}^{3+}$ .

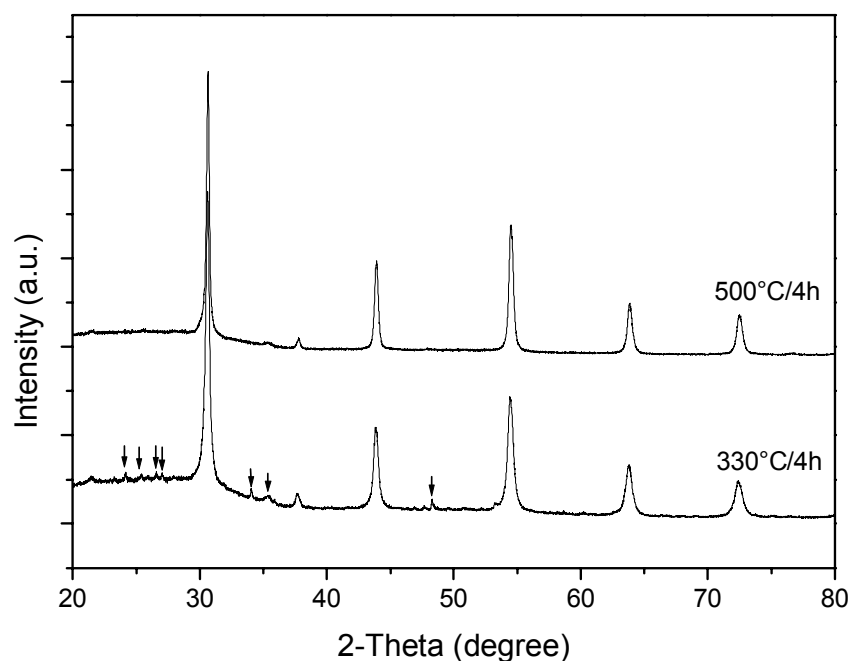


**Fig. 94** XRD patterns of the  $\text{Sb}^{3+}$ -doped powder calcined at 330°C and 500°C for 4h. The powder was hydrothermally synthesized at 250°C for 6h from the modified (5 wt% Genapol X-080) and peptized (pH = 9.3)  $\text{SnO}_2 \cdot x\text{H}_2\text{O}$  which was doped with 10 at.%  $\text{Sb}^{3+}$ . The arrows show the existence of the impure phase.

The content of the doping  $\text{Sn}^{3+}$  ion in the as-prepared powder calcined at  $330^\circ\text{C}$  for 4h determined by ICP is 9.82 at.%, which is very near the stoichiometric value (10 at.%). The effect of the  $\text{Sb}^{3+}$  doping ion on the crystallization of  $\text{BaSnO}_3$  was investigated by x-ray analysis. Fig. 94 presents the XRD patterns of the powder calcined at  $330^\circ\text{C}$  and  $500^\circ\text{C}$ . It can be found that although the main phase at  $330^\circ\text{C}$  is  $\text{BaSnO}_3$ , there still exists an impure barium tin hydrate phase (marked with arrows). The impure phase disappears at  $500^\circ\text{C}$ . This means that improving the calcining temperature is unavoidable for preparing  $\text{Sb}^{3+}$  doped  $\text{BaSnO}_3$ . Because a high calcining temperature will lead to the grain growth and a smaller surface area, the following work will focus on the  $\text{Sb}^{5+}$  doped  $\text{BaSnO}_3$ .

### 5.3.7.2 $\text{Sb}^{5+}$ doped $\text{BaSnO}_3$

As the powder synthesized hydrothermally at  $250^\circ\text{C}$  for 6h from the modified (5 wt% Genapol X-080) and peptized (pH = 9.3)  $\text{SnO}_2 \cdot x\text{H}_2\text{O}$  which was doped with 10 at.%  $\text{Sb}^{5+}$ , it consists of a pure  $\text{BaSnO}_3$  powder after calcination at  $330^\circ\text{C}$  for 4h. To investigate the solid solution region of  $\text{BaSb}_x\text{Sn}_{1-x}\text{O}_3$ , the doping content  $x$  of  $\text{Sb}^{5+}$  was changed from 0.04 to 0.20 (corresponding to 4 at.% to 20 at.%).

The XRD patterns of the doped powders which were calcined at  $330^\circ\text{C}$  (Fig. 95) show that these powders consist of  $\text{BaSnO}_3$ . However, from  $x = 0.12$  the 'left shoulder' of the (110) crystalline peak becomes broader with increasing  $x$ . The shoulder is marked with arrows in the diagram and indicates the formation of a second phase. It can be determined that the solid solution region of  $\text{BaSb}_x\text{Sn}_{1-x}\text{O}_3$  exists for  $0 \leq x < 0.12$ .

The dependence of the cubic-lattice parameter and the crystallite size of  $\text{BaSnO}_3$  on the doping content is illustrated in Fig. 96. As  $\text{Sb}^{5+}$  is added up to  $x = 0.12$ , the crystallite size shows only a little change. The further addition of the dopant leads to the obvious increase in crystallite size. A linear increase in the lattice parameter up to  $x = 0.12$  is observed. At larger  $x$  values there is no further increase in lattice parameter. The change of the lattice parameter with doping content is contrary to what is expected. It is surprising that the lattice parameter increases by replacing  $\text{Sn}^{4+}$  with  $\text{Sb}^{5+}$ , because the ion radius of the latter (0.062 nm) is less than that of the former (0.071 nm). A possible reason is that Sb exists in the lattice in the form of  $\text{Sb}^{3+}$  (its ion radius is 0.076 nm) or in the mixing form of  $\text{Sb}^{3+}$  and  $\text{Sb}^{5+}$ . Although the antimony is imported from  $\text{SbCl}_5$ , its valence can possibly be changed by hydrothermal reaction or calcination. When  $x$  is larger than 0.12, the doping ion cannot enter the  $\text{Sn}^{4+}$  site any more. Thus the lattice parameter becomes constant. The excess doping ions then form a second phase, as indicated in Fig. 95.

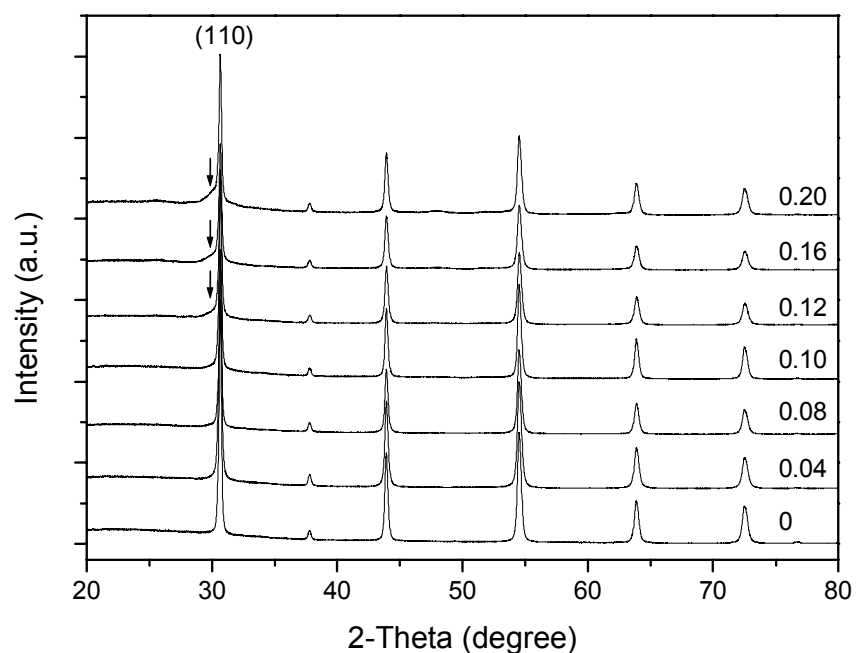


**Fig. 95** XRD patterns of the  $\text{Sb}^{5+}$ -doped powder calcined at  $330^\circ\text{C}$  for 4h with different  $x$  ( $\text{BaSb}_x\text{Sn}_{1-x}\text{O}_3$ ). The powder was hydrothermally synthesized at  $250^\circ\text{C}$  for 6h from the modified (5 wt% Genapol X-080) and peptized (pH = 9.3)  $\text{SnO}_2 \cdot x\text{H}_2\text{O}$  which was doped with  $\text{Sb}^{5+}$ .

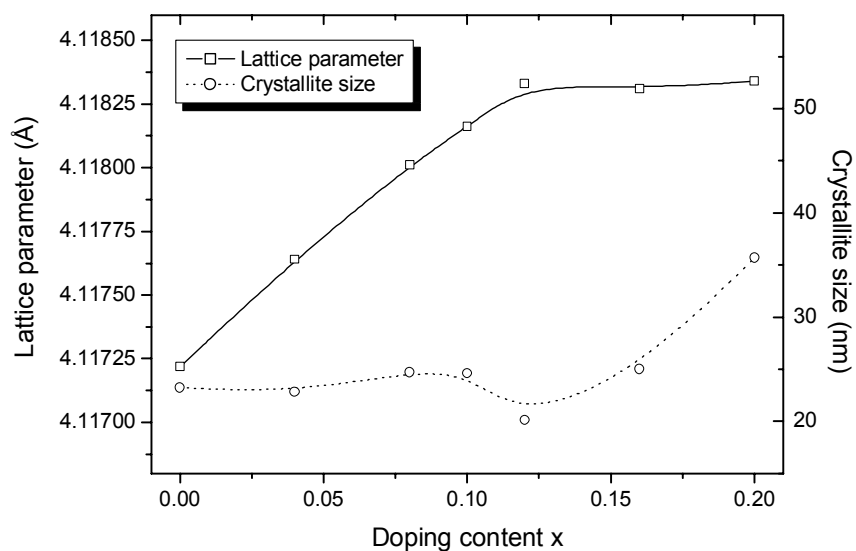


**Fig. 96** Lattice parameter and crystallite size of  $\text{BaSb}_x\text{Sn}_{1-x}\text{O}_3$  (calcined at  $330^\circ\text{C}$  for 4h) as a function of the doping content  $x$ . The as-prepared powder was hydrothermally synthesized at  $250^\circ\text{C}$  for 6h from the modified (5 wt% Genapol X-080) and peptized (pH = 9.3)  $\text{SnO}_2 \cdot x\text{H}_2\text{O}$  which was doped with  $\text{Sb}^{5+}$ .

Although the dopant was added according to the stoichiometric formula  $\text{BaSb}_x\text{Sn}_{1-x}\text{O}_3$ . The loss of Sn and Sb during the processing is possible. Therefore the atom rate of the doping ion Sb to Sn in the end-powder was measured with ICP. The results are summarized in Table 10. The deviation of the measured value from the expected value in the range of  $x = 0.08$  to  $0.12$  is relatively smaller.

**Table 10** Expected and measured doping content of  $\text{Sb}^{5+}$  in  $\text{BaSb}_x\text{Sn}_{1-x}\text{O}_3$ . The experimental values were determined by ICP

Composition	x value of $\text{BaSb}_x\text{Sn}_{1-x}\text{O}_3$					
stoichiometric	0.04	0.08	0.10	0.12	0.16	0.20
measured	0.031	0.074	0.103	0.114	0.143	0.234

As above discussed,  $\text{Sb}^{5+}$  can form a solid solution with  $\text{BaSnO}_3$  when  $x$  is smaller than  $0.12$ . The further investigation on the doping effect of  $\text{Sb}^{5+}$  is thus concentrated on the sample with  $x = 0.10$ .

The thermal behavior of the as-prepared powder doped with 10 at.%  $\text{Sb}^{5+}$  is shown in Fig. 97. Its TG-DTA curve is very similar to that of the undoped sample mp1 (see Fig. 74d). Two endothermic peaks appear at  $265^\circ\text{C}$  and  $330^\circ\text{C}$  respectively, which correspond to the dehydration of the powder. The weight loss in the 1<sup>st</sup> phase ( $200^\circ\text{C}$  to  $300^\circ\text{C}$ ) and in the 2<sup>nd</sup> phase ( $300^\circ\text{C}$  to  $400^\circ\text{C}$ ) is 6.4 wt% and 5.2 wt% respectively. From  $400^\circ\text{C}$  the weight loses slowly and shows little change after  $800^\circ\text{C}$ . The sum of weight loss up to  $1400^\circ\text{C}$  is 16.1 wt%, which is comparable to 16.4 wt% in the case of the undoped sample.

As described above, 10 at.% doping  $\text{Sb}^{5+}$  can enter lattice and substitute for  $\text{Sn}^{4+}$  sites. It means this substitution should lead to no change in Sn coordination compared with the undoped  $\text{BaSnO}_3$  (mp1 calcined at  $330^\circ\text{C}$ ). To check it the solid state  $^{119}\text{Sn}$  NMR spectrum of the  $\text{Sb}^{5+}$ -doped  $\text{BaSnO}_3$  is analyzed and shown in Fig. 98. Its chemical shift of -680 ppm and the half value width of its signal of 870 Hz are almost equal to these of the undoped  $\text{BaSnO}_3$ . Furthermore, the contour of the signals of the doped sample and the undoped one is very similar. The results confirm that doping Sb ions enter the lattice and substitute for the Sn site. The substitution of  $\text{Sb}^{5+}$  with an amount of 10 at.% for  $\text{Sn}^{4+}$  causes no change in the coordination and no obvious structural distortion.

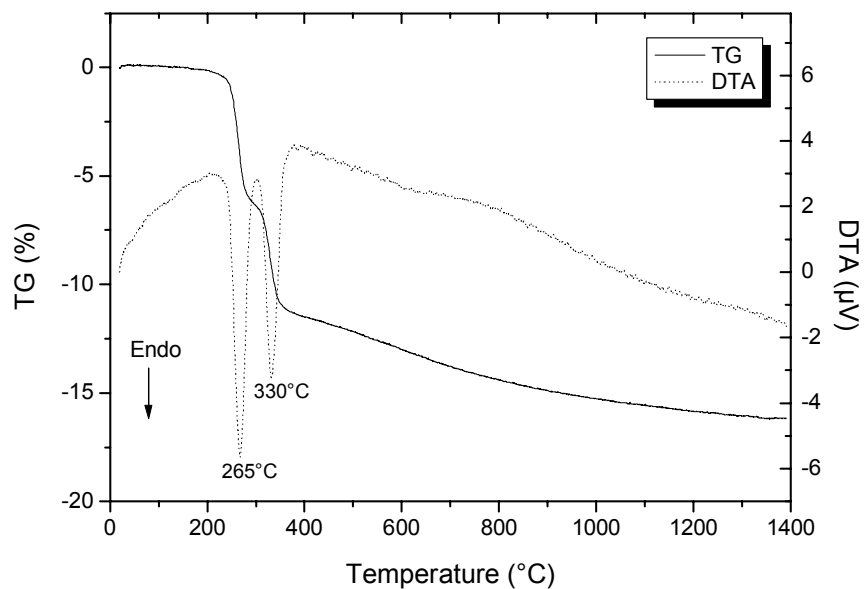


**Fig. 97** TG-DTA curve of the  $\text{Sb}^{5+}$ -doped as-prepared powder ( $x = 0.10$ ). The as-prepared powder was hydrothermally synthesized at  $250^\circ\text{C}$  for 6h from the modified (5 wt% Genapol X-080) and peptized (pH = 9.3)  $\text{SnO}_2 \cdot x\text{H}_2\text{O}$  which was doped with  $\text{Sb}^{5+}$ .

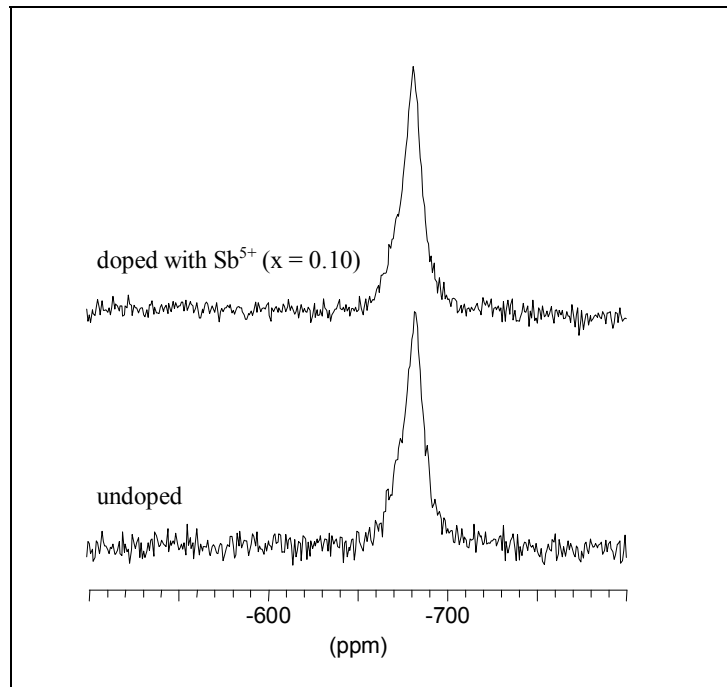


**Fig. 98** Solid state  $^{119}\text{Sn}$  NMR spectra of the  $\text{Sb}^{5+}$ -doped ( $x = 0.10$ , calcined at  $330^\circ\text{C}$  for 4h) and the undoped  $\text{BaSnO}_3$  (mp1 calcined at  $330^\circ\text{C}$  for 4h).

The doping effects of  $\text{Sb}^{5+}$  on the electric resistance of the powder is shown in Fig. 99. The pellets (see 4.4.11) were pressed from the powders calcined from  $330^\circ\text{C}$  to  $700^\circ\text{C}$  for 4 h, in this range the crystallite size of the powder is less than 100 nm. With increasing the calcining temperature, the resistance of  $\text{BaSnO}_3$  decreases. As 10 at.% of  $\text{Sn}^{4+}$  is replaced by  $\text{Sb}^{5+}$ , the resistance of the pellet is lowered from  $0.637\text{ M}\Omega$  to  $0.460\text{ M}\Omega$  at  $330^\circ\text{C}$ . No matter how high the calcining temperature is, the resistance of the doped sample is always lower than that of the undoped one. It can be concluded that the conductivity of  $\text{BaSnO}_3$  is improved by doping  $\text{Sb}^{5+}$  ions.

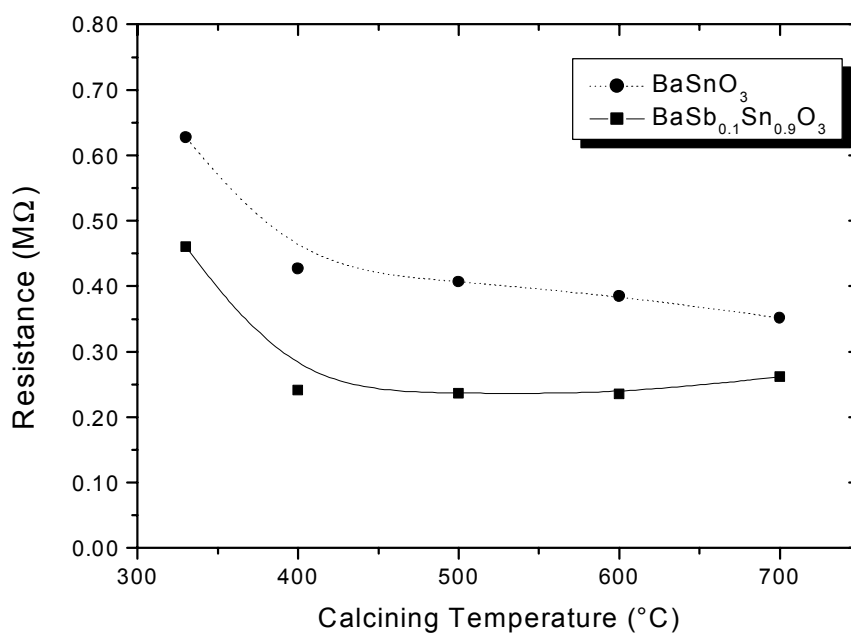


**Fig. 99** Resistance of the  $\text{Sb}^{5+}$ -doped ( $x = 0.10$ ) and the undoped (mp1)  $\text{BaSnO}_3$  pellet as a function of the calcining temperature. Pellets ( $\Phi 10\text{mm} \times 1\text{mm}$ ) was sputtered with a Pt film ( $\Phi 8.5\text{ mm}$ ) on both side.



## 6 Summary and conclusions

In the first part of this work the LTAS route was employed to synthesize the  $\text{BaSnO}_3$  powder. However, no  $\text{BaSnO}_3$  but a  $\text{SnO}_2$  phase was found in the prepared powder, even if the pH value of the solution was increased by substituting NaOH for  $\text{NH}_3\cdot\text{H}_2\text{O}$  and the solution was treated under hydrothermal conditions. A powder of  $\text{SnO}_2$  with the size of 5 nm has been obtained. Preparation of  $\text{BaSnO}_3$  via LTAS route, although being reported in the literature, maybe requires restricted synthesis conditions.

A metal alkoxide route as an alternative method has been developed to synthesize the nanocrystalline  $\text{BaSnO}_3$ . In this route a double metal alkoxide was first synthesized. As a starting material, metal barium is superior to barium alkoxide. The former can react with tin alkoxide to form a homogenous precursor. Its corresponding precursor can hydrolyze more completely, which is beneficial to lowering the calcining temperature.

The obtained barium tin alkoxides from metal barium were characterized with IR, XRD, TG-DTA, SEM and ICP.  $\text{BaSn}(\text{OEt})_6$  and  $\text{BaSn}(\text{OPr}^i)_6$  are amorphous and susceptible to water. The former hydrolyzes faster than the latter. As for the thermal behavior,  $\text{BaSn}(\text{OPr}^j)_6$  is more thermally stable than  $\text{BaSn}(\text{OEt})_6$ . These two precursors show different morphology under microscope. The measured molar rate of Ba to Sn in both bimetal alkoxides is near 1. These bimetal alkoxides, however, show a low solubility in alcohol. To stabilize their alcoholic solutions, DEA was chosen as the stabilizer because it shows the best stabilizing effect on the precursor among EGME, EGME and DEA. Its stabilizing efficiency is correlated with the concentration of the starting solutions. The precursor can be stabilized with DEA only when their concentrations are not more than 0.2 M. The stabilizing effect of DEA can be attributed to the coupling interaction of hydroxyl groups among precursor, DEA and alcohol.

The addition of DEA and the molar ratio of water to precursor as well as the temperature affect the properties of the hydrolysis products. In the case of using DEA as the stabilizer, employing excess water ( $R_w \geq 60$ ) and a higher temperature is beneficial to a complete hydrolysis.

The hydrolysis product of  $\text{BaSn}(\text{OH})_{6-x}(\text{OR})_x$  is amorphous. As it being calcined in a furnace, dehydroxylation and the decomposition of the remaining OR groups take place between 200°C to 350°C. As a result,  $\text{BaSnO}_3$  is formed. Accompanied these processes, the molecular structure of the powder rearranges and an impure  $\text{BaCO}_3$  phase forms. The dehydroxylation proceeds after 350°C.  $\text{BaCO}_3$  disappears in the temperature range of 500 - 600°C. At the same temperature range the dehydroxylation accomplishes. As a consequence, the phase transformation of the powder finishes. The single-phase  $\text{BaSnO}_3$  derived from ethoxide and isopropoxide appears at 550°C and 600°C respectively. The further increase in temperature only contributes to the grain growth of  $\text{BaSnO}_3$ .

As an alternative calcination technique, hydrothermal treatment has been attempted to crystallize the hydrolysis products because it is possible to decrease the temperature of the phase transformation significantly through improving the pressure. Although the educt can be crystallized,  $\text{BaSn(OH)}_6$  other than  $\text{BaSnO}_3$  is formed in the powder, whose composition nevertheless depends on  $R_w$ . Therefore a further calcination of the powder is necessary and it was carried out in a furnace. In the case of the low  $R_w$ , the decomposition of the remaining organic species in the powder leads to the formation of a large amount of  $\text{BaCO}_3$  which limits the building of  $\text{BaSnO}_3$ . No single-phase  $\text{BaSnO}_3$  is obtained even if the calcining temperature is elevated to  $720^\circ\text{C}$ . In the case of  $R_w = 500$ , the  $\text{BaSn(OH)}_6$  phase transforms in an amorphous phase at  $260^\circ\text{C}$ , from which  $\text{BaSnO}_3$  nucleates. A powder of  $\text{BaSnO}_3$  with impurities has been obtained at  $350^\circ\text{C}$ . For preparing a single-phase  $\text{BaSnO}_3$ , a higher temperature is necessary. Thus, the hydrothermal calcination is not a suitable alternative to the conventional calcination.

After the as-prepared powder derived from  $\text{BaSn(OEt)}_6$  being calcined at  $760^\circ\text{C}$ , a well-crystallized  $\text{BaSnO}_3$  powder is obtained and is made up of clusters with a dimension of 200 to 900 nm. Its primary particles with a size of 10 to 100 nm and a cubic habitus have been observed under HRTEM. The strong aggregation and even coalescence of these particles contributes to the small surface area of the powder ( $4.2 \text{ m}^2/\text{g}$ ). Its crystallite size calculated from XRD and the average particle size calculated from BET are larger than 100 nm.

In contrast to this, the  $\text{BaSnO}_3$  powder prepared from  $\text{BaSn(OPr)}_6$  shows a better quality such as a larger specific surface area ( $17.0 \text{ m}^2/\text{g}$ ), a smaller crystallite size (60 nm) and a smaller average particle size (50 nm). The microstructure analysis of the formation of  $\text{BaSnO}_3$  by calcination indicates that the hydrolysis product consists of skeleton-structured clusters. The breaking of the bridge bond resulted from dehydroxylation takes place with increasing the temperature. As the result of the structure rearrangement,  $\text{BaSnO}_3$  nuclei form at  $350^\circ\text{C}$ . The well-crystallized  $\text{BaSnO}_3$  particles at  $760^\circ\text{C}$  show a spherical form. These primary particles with a size of 20 to 60 nm are nevertheless strongly aggregated.

Up to now, the metal alkoxide route has been employed successfully to prepare the nanocrystalline  $\text{BaSnO}_3$ . However, as far as the application of this powder as a sensor material is concerned, its drawbacks such as the high calcining temperature, the low yield rate and the low surface area are obvious. Therefore, a third synthesis route - hydrothermal synthesis, was employed to synthesize the nanosized  $\text{BaSnO}_3$ .

The first and also a key step to prepare  $\text{BaSnO}_3$  via hydrothermal route is to synthesize a reactive tin oxide hydrate ( $\text{SnO}_2 \cdot x\text{H}_2\text{O}$ ). The properties of the obtained tin oxide is found to be determined by pH, which is dependent on the ratio of  $\text{SnCl}_4$  to  $\text{NH}_3 \cdot \text{H}_2\text{O}$ , the temperature, the reaction time and the mixing wise. According to experimental results the pH value was controllable by slow addition of  $\text{NH}_3 \cdot \text{H}_2\text{O}$  to  $\text{SnCl}_4$  at  $0^\circ\text{C}$  with stirring for 1 hour.

The  $\text{SnO}_2 \cdot x\text{H}_2\text{O}$  gel and the  $\text{SnO}_2 \cdot x\text{H}_2\text{O}$  precipitate can be reproducibly synthesized in the pH range of 1 - 4 and 8 -10 respectively. The former exhibits a larger surface area and a lower average particle size than the latter. A nanocrystalline  $\text{BaSnO}_3$  cannot be prepared from the  $\text{SnO}_2 \cdot x\text{H}_2\text{O}$  precipitate but from the  $\text{SnO}_2 \cdot x\text{H}_2\text{O}$  gel. Therefore the  $\text{SnO}_2 \cdot x\text{H}_2\text{O}$  gel was

selected as the precursor to prepare BaSnO<sub>3</sub>. An optimal pH for synthesizing a SnO<sub>2</sub>·xH<sub>2</sub>O gel is pH = 2.0. By washing 4 - 6 times the SnO<sub>2</sub>·xH<sub>2</sub>O gel is free of Cl<sup>-</sup>.

The xerogel of SnO<sub>2</sub>·xH<sub>2</sub>O was characterized with TG-DTA, BET, XRD and HRTEM. It consists of the cassiterite phase which does not crystallize well and its BET specific surface area is 197 m<sup>2</sup>/g. The xerogel observed under HRTEM is an agglomerated body with no definite form. The x value varies from 36.4 to 46.7 in the wet gel and is 1.3 in the xerogel.

The SnO<sub>2</sub>·xH<sub>2</sub>O gel reacted with barium hydroxide under hydrothermal conditions. The important parameters during this process which affect the properties of the product have been investigated. The barium hydroxide solution as a starting materials is better than any solid source of Ba(OH)<sub>2</sub>. Its concentration affects the composition and the particle size of the obtained powder. The optimal concentration lies in 0.2 M.

The Ba:Sn rate mainly influences the composition of the resulting powder. A single-phase BaSnO<sub>3</sub> can only be prepared at a Ba:Sn ratio ranging from 1 to 1.2. A ratio of 1.1 is selected for guaranteeing the building of BaSnO<sub>3</sub>.

The hydrothermal temperature shows its influence on the phase formation and the particle size of the powder. A BaSnO<sub>3</sub> powder can be directly synthesized at a temperature no lower than 330°C. Although the particles with a size of 3 to 4 μm are uniform and not aggregated, they are far from nanosized. In contrast to this, the educt synthesized at a temperature in the range of 130°C to 250°C is made up of the BaSn(OH)<sub>6</sub> phase. BaSn(OH)<sub>6</sub> converts into nanocrystalline BaSnO<sub>3</sub> after being calcined at 260°C. Just in the above referred temperature range, a higher temperature can promote the crystallization of BaSnO<sub>3</sub>, increase its specific surface area and decrease the average particle size. Based on these facts, 250°C was determined as the optimal hydrothermal temperature.

The duration of the hydrothermal reaction influence on the morphology of the particles rather than the composition of the resulting powder. The reaction under the hydrothermal condition lasting for at least 6 hours is necessary for obtaining uniform and smaller particles. As the hydrothermal reaction is carried out in a nonaqueous solvent, isopropanol is superior to the other three chosen solvents for preparing BaSnO<sub>3</sub>. In contrast to water, isopropanol nevertheless leads to the decrease in surface area and the increase in crystallite size of the BaSnO<sub>3</sub> powder. Therefore water is selected as the medium for preparing BaSnO<sub>3</sub> via hydrothermal route.

The BaSnO<sub>3</sub> powder prepared by optimizing the above parameters, however, show a small surface area (5.27 m<sup>2</sup>/g), which results from the agglomeration and aggregation of the particles. To minimize the agglomeration and aggregation and thereafter to increase the surface area of the powder, a taken measure was to peptize the SnO<sub>2</sub>·xH<sub>2</sub>O gel on the molecular level.

The SnO<sub>2</sub>·xH<sub>2</sub>O gel can be peptized by using ammonia as a peptizing agent and controlling the pH value of the suspension over 8.30. Nevertheless, a stable peptized SnO<sub>2</sub>·xH<sub>2</sub>O solution can only be obtained at pH > 9.0. The peptized solution at pH = 9.3 is narrowly distributed on the nanometer scale (d<sub>50</sub> = 8 nm) and can transform into a nanosize tin oxide with a low agglomeration degree under hydrothermal conditions. The as-prepared powder of BaSn(OH)<sub>6</sub> derived from the peptized SnO<sub>2</sub>·xH<sub>2</sub>O shows a lower degree of agglomeration and a smaller particle size compared with that derived from the SnO<sub>2</sub>·xH<sub>2</sub>O gel. The specific

surface area of the  $\text{BaSnO}_3$  powder was improved to  $23.5 \text{ m}^2/\text{g}$  through peptization. However, the particles of the powder are still strongly aggregated, when being observed under HRTEM. Therefore, it was attempted to limit the agglomeration and aggregation by surface modification.

The reason for employing surface modification is that a suitable surfactant can decrease the surface free energy, which determines the particle growth rate. It was hoped to lower the particle size by controlling the particle growth and thereafter to increase the surface area of the prepared powder. Thus, an important task was to choose the surfactant.

Four modifiers (Genapol X-080, Tween 80, caprolactam and PVA) were chosen from 10 surfactants by means of IR and XRD. The study of their effects on the properties of the obtained powder indicated that among them Genapol X-080 has the most positive effects on the powder. By adding 5 wt% Genapol X-080, a phase-pure  $\text{BaSnO}_3$  powder has been obtained, its specific surface area was increased to  $56.2 \text{ m}^2/\text{g}$ , and its crystallite size and its average particle size was lowered to 20 nm and 18 nm respectively.

The surface area of the  $\text{BaSnO}_3$  powder is dependent on the concentration of Genapol X-080. It increases with increasing the concentration of the modifier up to 5 wt% and then becomes constant. This phenomenon can be explained by the monolayer cover of the surfactant molecules on the particle surface.

The surface area of the powder is also affected by the calcining temperature. It decreases with increasing the temperature because of the grain growth. When the calcining temperature is over  $800^\circ\text{C}$ , the average particle size of  $\text{BaSnO}_3$  is no more in the nanometer range.

In view of the positive effects of peptization and surface modification on the properties of the powder, it was attempted to prepared  $\text{BaSnO}_3$  powder by combining the two techniques. The powders prepared from different systems were characterized.

The thermal behaviors of the as-prepared powders show that peptization and surface modification make the dehydration more difficult. On the other hand, the obvious increase in water content in the as-prepared powders by peptization and modification reveal that they can enhance the activity of the precursor. Although the substitution of isopropanol for water makes the dehydration easier, the appearance of carbonates gives rise to a negative effect on the formation of  $\text{BaSnO}_3$ .

The structure evolution of the powders with increasing temperature and treating time is analyzed by means of IR. In the G-system, the building of the corner sharing octahedral  $[\text{SnO}_6]$  in the powder accomplishes at  $260^\circ\text{C}$ . It is shifted to  $330^\circ\text{C}$  in the M- and P-system. In the case of isopropanol instead of water, this structure rearrangement becomes more difficult. The delay of the structure evolution can be attributed to the increase in water content of the powders and to the difference in the bonding wise of  $\text{OH}^-$  in the powder.

The  $\text{BaSnO}_3$  powder prepared via hydrothermal route can be explained by a heterogeneous nucleation mechanism. The as-prepared powder of  $\text{BaSn}(\text{OH})_6$  transforms into an amorphous phase, from which  $\text{BaSnO}_3$  nucleates and grows. Although peptization and modification lead to the increase in transformation temperature of  $\text{BaSnO}_3$  to  $330^\circ\text{C}$ , they lower the crystallite size obviously and also effect the lattice structure of  $\text{BaSnO}_3$ .

Isopropanol replacing water causes the formation of  $\text{BaCO}_3$  which impedes the building of  $\text{BaSnO}_3$ .

A combining effect of the combining peptization and surface modification is reflected from the thermal behavior, the structure evolution and the crystalline behavior of the powder in the MP-system.

The microstructure of the  $\text{BaSnO}_3$  powders are observed under SEM and HRTEM. The needle particles in the P-system show a width of 20 to 80 nm and consist of crystallites with a dimension of 10 to 15 nm x ca. 5 nm. The particle size in the M-system is 20 to 40 nm and the particle is made up of crystallites with a dimension of 2 to 6 nm and an aspect ratio of 2:1. The surface of some particles is found to be modified with a thin layer of the modifier with a thickness of 3 to 5.5 nm. Among the  $\text{BaSnO}_3$  powders, the lowest degree of agglomeration and aggregation appears in the powder obtained by combination of peptization and modification. The particles with a size of 10 to 30 nm also consists of polycrystallites.

The  $\text{BaSnO}_3$  powders prepared via hydrothermal route show a lower symmetry and structure distortion than the commercial one. The crystallinity of  $\text{BaSnO}_3$  can nevertheless be improved through combination of peptization and surface modification, which can also improve the density and the surface area obviously. The  $\text{BaSnO}_3$  powder in the MP-system (mp1) has a specific surface area of  $57.0 \text{ m}^2/\text{g}$  and a density of  $5.97 \text{ g}/\text{cm}^3$ .

The prepared  $\text{BaSnO}_3$  are much more sintering-active than the commercial powder. The sintering properties of the prepared  $\text{BaSnO}_3$  are improved by peptization and surface modification. By combining peptization and surface modification a maximal densification of 83.6 % T.D has been reached after the sample was sintered at  $1600^\circ\text{C}$ .

In sum, a nanoscaled  $\text{BaSnO}_3$  powder has been prepared via hydrothermal synthesis route by combining peptization and surface modification. The prepared powder exhibit a high quality such as large surface area and sintering-active.

To redisperse this  $\text{BaSnO}_3$  powder TEA was chosen as the dispersing agent. Its concentration was determined to be 2.5 wt%. The dispersed suspension has been cast by tape casting into green tapes with a thickness of 11 to 51  $\mu\text{m}$ . A densified ceramic tape has been obtained by calcining the green tape at  $1500^\circ\text{C}$ .

In order to improve the charge density of  $\text{BaSnO}_3$ , it was doped with  $\text{Sb}^{3+}$  and  $\text{Sb}^{5+}$  respectively. It is found that a  $\text{BaSnO}_3$  powder doped with  $\text{Sb}^{3+}$  is difficult to prepare at a low calcining temperature. As for  $\text{Sb}^{5+}$  doped  $\text{BaSnO}_3$ , the crystallization can be accomplished at  $330^\circ\text{C}$ . The solid solution region of  $\text{BaSb}_x\text{Sn}_{1-x}\text{O}_3$  exists for  $0 \leq x < 0.12$ . An x value over 0.12 leads to an increase in crystallite size and the formation of impure phases. The doped  $\text{BaSnO}_3$  ( $x = 0.10$ ) shows a similar thermal behavior and crystallinity as those of the undoped one. The conductivity of  $\text{BaSnO}_3$  has been improved by doping 10 at.%  $\text{Sb}^{5+}$ .

## 7. Appendix

### 7.1 Chemicals used

**Table 1** Sources of barium and tin used

Starting material	Molecular Formula	Supplier
Metal barium (99.97%)	Ba	Chempur
Barium chloride dihydrate	BaCl <sub>2</sub> ·2H <sub>2</sub> O	Merck
Barium hydroxide octahydrate	Ba(OH) <sub>2</sub> ·8H <sub>2</sub> O	Fluka
Barium hydroxide solution (0.3N)	Ba(OH) <sub>2</sub>	Fluka
Barium(II) isopropoxide	Ba(OC <sub>3</sub> H <sub>7</sub> ) <sub>2</sub>	Chempur
Tin tetrachloride	SnCl <sub>4</sub>	Aldrich
Tin(IV) ethoxide	Sn(OC <sub>2</sub> H <sub>5</sub> ) <sub>4</sub>	ABCR
Tin isopropoxide-isopropanol adduct	Sn(OC <sub>3</sub> H <sub>7</sub> ) <sub>4</sub> ·C <sub>3</sub> H <sub>7</sub> OH	ABCR

**Table 2** Surfactants in the experiment

Surfactants	Chemical name and important parameters	Supplier
Arkonal N-080	Nonyl phenol polyglycol ether with about 8 mol EO, HLB=12	Hoechst
Caprolactam	6-Caprolactam, purum, ≥ 98%, C <sub>6</sub> H <sub>11</sub> NO	Fluka
DOHS	Dioxaheptan acid	Clariant
Genapol UD-079	Polyglycol ether based on C <sub>11</sub> with about 7 mol EO, HLB=12	Hoechst
Genapol X-080	Fatty alcohol polyglycol ether based on isotridecyl alcohol with about 8 mol EO, HLB= 13	Clariant
Glycerin	Glycerol, C <sub>3</sub> H <sub>8</sub> O <sub>3</sub>	Merck
Moviol 04-28 (PVA)	Polyvinyl alcohol, MW(molecular weight)=31,000	Hoechst
Moviol 18-88 (PVA)	Polyvinyl alcohol, MW(molecular weight)=130,000	Hoechst
Moviol 26-88 (PVA)	Polyvinyl alcohol, MW(molecular weight)=160,000	Hoechst
TMAH	Tetramethylammonium hydroxide solution, 25% in water.	Fluka
TODS	3-6-9-Trioxadecan acid (purum)	Clariant
Tween 80	Polyoxyethylen-(20)-Sobitan monooleat, HLB=15	ICI

**Table 3** Other chemicals used in the experiment

Chemicals	Molecular Formula	Supplier
Ammonia solution (25%)	$\text{NH}_3 \cdot \text{H}_2\text{O}$	SDS
Antimony (III) chloride	$\text{SbCl}_3$	Aldrich
Antimony (V) chloride	$\text{SbCl}_5$	Aldrich
Barium stannate	$\text{BaSnO}_3$	ABCR
Diethanol amine (DEA)	$\text{NH}(\text{C}_2\text{H}_4\text{OH})_2$	Aldrich
Diethylen glycol-monobutyl ether	$\text{CH}_3(\text{CH}_2)_3\text{OC}_2\text{H}_4\text{OC}_2\text{H}_4\text{OH}$	Aldrich
Ethylen glycol (EG)	$\text{HOCH}_2\text{CH}_2\text{OH}$	Aldrich
Ethylen glycol-monobutyl ether (EGMBE)	$\text{CH}_3(\text{CH}_2)_3\text{OC}_2\text{H}_4\text{OH}$	Aldrich
Ethylen glycol-monoethyl ether (EGMEE)	$\text{C}_2\text{H}_5\text{OC}_2\text{H}_4\text{OH}$	Aldrich
Polyethylen imine (PEI, MW: 1200)	$(-\text{NHC}_2\text{H}_4-)_x[-\text{N}(\text{C}_2\text{H}_4\text{NH}_2)\text{C}_2\text{H}_4-]_y\text{C}_2\text{H}_4$	Aldrich
Polyethylen imine (PEI, MW: 5000-10000)	$(-\text{NHC}_2\text{H}_4-)_x[-\text{N}(\text{C}_2\text{H}_4\text{NH}_2)\text{C}_2\text{H}_4-]_y\text{C}_2\text{H}_4$	Aldrich
Potassium stannate trihydrate	$\text{K}_2\text{SnO}_3 \cdot 3\text{H}_2\text{O}$	ABCR
Potassium hydroxide	$\text{KOH}$	Aldrich
Sodium hydroxide	$\text{NaOH}$	Aldrich
Triethyl amine (TEA).	$\text{N}(\text{C}_2\text{H}_5)_3$	Aldrich

## 7.2 List of instruments and equipment used

Ammeter: Keithley 485 auto-ranging picoammeter  
Atom absorption spectrometer (AAS): ICP - JY24, Jobin Yvon  
Autoclave: Steel 250ml, Medimex  
Autoclave: Teflon 1l, stepmotor, Berghof  
Autoclave: Teflon 250ml, DAH 904, Berghof  
BET gas adsorption analysis: ASAP2400, Micrometrics  
C/H analyzer: RC-412, Leco  
Centrifugal ball mill: pulverisette 6, Fritsch  
Centrifuge Megafuge: 2.0R, Heraeus  
Conductivity: Microprocessor conductivity meter LF2000, WTW  
Cold isostatic press: Paul-Otto Weber  
Differential dilatometer: Linseis  
DTA-TG differential thermal and thermogravimetric analysis: STA 501, Bähr  
DTA-TG-MS: TG-DTA (STA409) - mass spectrometer (QMS420), Netzsch  
FTIR spectrometer: IFS 25v and IFS 66v, Bruker  
Gas pycnometer: Micrometrics  
High resolution scattering electron microscope (SEM): JSM 6400F, Jeol  
High resolution transmission electron microscope (HRTEM): CM 200 FEG, Philips  
Karl Fischer titrator: MKS-210, Kyoto electronics  
Impedance spectrometer: SI1260, Solatron  
Particle charge detector: PCD02, Müttek  
Mortar mill: Retsch  
pH meter: pH535, WTW; pH320, WTW  
Photon correlation spectrometer (PCS): ALV5000 DLS and SLS, ALV-Laser  
Tensiometer: K12, Krüss  
Solid state  $^{119}\text{Sn}$ -NMR: MSL200, Bruker  
Sputter equipment: SCD 030, Balzers  
Three roller grinding mill: Exact  
Transmission electron microscope (TEM): JEM -200CX, Jeol  
Ultrafine particle analyzer (UPA): UPA 400, Grimm  
Ultrasonic disintegrator: Branson-Sonifier  
Uniaxial press: Paul-Otto Weber  
Vacuum drying furnace: VTR 5036, Heraeus  
X-ray diffractometer: D500, Siemens  
X-ray diffractometer: X'Pert MRD, Philips  
Zeta-potential meter: Zetasizer, Malvern



## 8. References

---

- 1 Will, K., Einführung in die Kristallographie, Belin: Verlag Technik, (1990) p161
- 2 Swanson, H.E., Morris, M.C., Evans, E.H. and Ulmer, L., Natl. Bur. Std.[US] Monograph Nr.25, TI. **3** (1864) 1 - 64
- 3 Wagner, G. and Binder, H., Z. Anorg. Allgem. Chem., **297** (1958) 328 - 346
- 4 Dietzel, A., Poch, W., Radex Rumdschau. (1960) 52-61
- 5 Piercy, B., Trans. Faraday Soc., **55** (1959) 39 - 51
- 6 Coffin, W.W., J. Am. Ceram. Soc. **36** (1953) 207-14
- 7 Upadhyay, S., Sahu, A. K., Kumar and D., Parkash, O., J. Appl. Phys., **84**(2) (1998) 827 - 832
- 8 Subbarao, E. C., Ceramic dielectrics for capacitors. Ferroelectrics, **35** (1981) 143-148
- 9 Vivekanandan, R. and Kutty, T. R. N., Ceram. Int., **14** (1988) 207-216
- 10 Wernicke R., Influence of microstructure on the electrical properties of intergranular capacitors. *Ber. Dtsch. Keram. Ges.*, **55** (1978) 356-358
- 11 Brauer H., Z. Angew. Phys., **29** (1970) 282-287
- 12 Williams, D. E., Tofield, B. C., McGeehin, P., Patent GB2149121
- 13 Ostrick, B., J. Am. Ceram. Soc., **80**(8) (1997) 2153-56
- 14 McGeehin, P., Moseley, P. T., Williams, D. E., Adewoyin, A., Gleeson, P. A., Patent WO9728441
- 15 Ishihara, T., Kometani, K., Mizuhara, Y., Takita, Y., Chem. Lett. **10** (1991), 1711-14
- 16 Ishihara, T., Kometani, K., Mizuhara, Y., Takita, Y., J. Electrochem. Soc. **139**(10) (1992) 2881-5
- 17 Ishihara, T., Kometani, K., Mizuhara, Y., Takita, Y., Sens. Actuators, B **13**(1-3) (1993) 470-2
- 18 Jayaraman, V., Mangamma, G., Gnanasekaran, T., Periaswami, G., Solid State Ionics, **86-88** (Pt. 2) (1996) 1111-1114
- 19 Lampe, U., Gerblinger, J., Meixner, H., Sens. Actuators, B, **B25**(1-3) (1995), 657-60
- 20 Moseley, P. T., Williams, D. E., McAleer, J. F., Maignan, A., Patent GB2186090
- 21 Lampe, U., Gerblinger, J., Meixner, H., Sens. Actuators, B, **B26**(1-3) (1995) 97-8
- 22 McGeehin, P., Williams, D. E., Patent WO9308467
- 23 Kurosawa, H., Hasei, S., Yamazoe, N., Miura, N., Patent JP08062174, US5897759A
- 24 Sasaki, K., Patent EP157328, JP60205342, US4701739
- 25 Sasaki, K., Patent JP61155746
- 26 Matsubara, T., Kuroki, Y., Okinaga, K., Patent JP05232058
- 27 Komatsu, K., Kuroki, Y., Hanada, M., Patent JP05232060
- 28 Okano, M., Kuroki, Y., Okinaga, K., Patent JP05232067
- 29 Komatsu, K., Kuroki, Y., Hanada, M., Patent JP05232065
- 30 Satake, K., Hanada, M., Okino, K., Komatsu, K., Patent US4911914
- 31 Shimabukuro, M., Onaga, K., Kajiyama, Y., Matsuura, S., Komatsu, K., Takami, A., Proc. - Electrochem. Soc.(1993), 93-7(Proceedings of the Symposium on Chemical Sensors II, 1993), 428-34
- 32 Komatsu, K., Kuroki, Y., Hanada, M., Shimabukuro, M., Patent JP05232064
- 33 Yoshida, Y., Onaga, K., Hanada, M., Komatsu, K., Patent DE3922989, JP02193053, US5006828
- 34 Takagi, K., Kuroki, Y., Okinaga, K., Patent JP05232057
- 35 Okano, M., Kuroki, Y., Hanada, M., Yoshida, Y., Patent JP05232056
- 36 Kakumoto, H., Kuroki, Y., Hanada, M., Shimabukuro, M., Patent JP05232063
- 37 Sasaki, K., Patent JP61147150
- 38 Sasaki, K., Patent JP61155947, JP05003899
- 39 Sasaki, K., Patent DE3545372, JP61147146, JP04043233, US4658632

- 
- 40 Shimizu, Y., Shimabukuro, M., Arai, H., Seiyama, Chem. Lett., **7** (1985) 917-20
- 41 Zhou, Z., Zhao, G., Ferroelectrics **101** (1990), 43-54
- 42 Zhou, Z., Zhao, G., Wei, M., Zhang, Z., Sens. Actuators **19**(1) (1989) 71-81
- 43 Sano, H. and Herber, R. H., J.Inorg. Nucl. Chem., **30** (1968) 409-13
- 44 Hien, P. Z., Shpinel, V. S., and Viskov, A. S., Zh. Eksperim. i Teor. Fiz., **44** (1963) 1889-995
- 45 Wagner, G. and Binder, H., Z. Anorg. Allegem. Chem., **297** (1958) 328-46
- 46 Upadhyay, S., Parkash, O., and Kumar, D., J. Mater. Sci. Lett., **16** (1997) 1330-2
- 47 Azad, A. M., Hon, N. C., J. Alloys Comp., **270** (1998) 95-106
- 48 Paff, C., J. Eur. Ceram. Soc. **12** (1993) 159-164
- 49 Savos'kina, A. I., Goroshchenko, Ya. G. and Selivanova, L. Ya., Izu, Akad. Nauk. SSSR, Neorg. Mater., **20**(3) (1984) 472-475
- 50 Leoni, M., Viviani, M., Nanni, P. and Buscaglia, V., J. Mater. Sci. Lett., **15** (1996)1302-4
- 51 Bao, M., Li, W., Zhu, P., J. Mater. Sci., **28** (1993) 6617-21
- 52 Hass, P. A., Chem. Eng. Prog., **85** (1989) 44-50
- 53 Pechini, M. P., Patent US3330697
- 54 Licheron, M., Jouan, G. and Husson, E., J. Eur. Ceram. Soc., **17** (1997) 1453-7
- 55 Udawatte C.P., Kakihana, M. and Yoshimura, M., Solid State Ionics, **108** (1998) 23-30
- 56 Kuttu, R.N. and Vivekanaden, R., Mat. Res. Bull., **22**(11) (1987) 1457-65
- 57 Wakkad, S. E. S., Shams, A. M., Kotb, H., J. Electrochem. Soc., **105** (1958) 47-51
- 58 Hollman K., Arnold F., Lehrbuch der Anorganischen Chemie, Berlin: Walter de Gruyter, 1985
- 59 Kleinschmidt, A., Monatsch. Chem. **39** (1918) 149-78
- 60 Havestadt, L., Fricke, R., Z. Anorg. Allgem. Chem. **188** (1930) 357-95
- 61 Williams, R. L., Pace, R. J., J. Chem. Soc. (1957) 4143-44
- 62 Goodman, J. F., Gregg, S. J., J. Chem. Soc., (1960) 1162 -1167
- 63 Duan, X., Huang, W., J. Cent. South Univ. Technol., **30** (2) (1999) 176-178
- 64 Ocana, M., Serna, C. J., Matijevic, E., Mater. Letters , **12** (1991) 32-36
- 65 Brito, G. E. S., Pulcinelli, S. H., Santilli, C. V., J. Sol-Gel Sci. Technol., **2** (1994) 575-79
- 66 Ribeiro, S. J. L., Hiratsuka, R. S., Massabni, A. M. G., Davolos, M. R., Santilli, C. V., Pulcinelli, S. H., J. Non-Crystal. Solids, **147&148** (1992) 162-66
- 67 Harrison, P. G., Perry, C. C., Creaser, D. A., Li, X., Blake, D. J., in Henchm L., West J. (edited), Chemical Processing of Advanced Materials, USA: John Wiley and Sons, Inc., (1992) 187-96
- 68 Kulshrestha, N. K., Dey, A. K., Ghosk, S., Kolloid Z., **132** (1953) 143-145
- 69 Giesekke, E. K., Gutowsky, H. S., Kirkov, P., Laitinen, H. A., Inorg. Chem. **6** (1967) 1294-97
- 70 Dumanski, A., Kniga, A., Kolloid Z., **44** (1928) 273-277
- 71 Ghosh, S., Dhar, R., J. Phys. Chem. **31** (1927) 187-206
- 72 Aditya, S, J. Indian Chem. Soc., **29** (4) (1952) 296-300
- 73 Segal, D., Chemical synthesis of advanced ceramic materials, Cambridge: Cambridge Univ. Press, 1989
- 74 Jones, P. W., Fundamental principles of sol-gel technology, Lodon: Institute of Metals, 1989
- 75 Brinker, C. J., Sherer, G. W., Sol-gel science: the physics and chemistry of sol-gel processing, California: academic press, 1990
- 76 Sanchez, C., Livage, Henre, M., Babonneau, F., J. Non-Cryst. Solids **100** (1988) 65-72
- 77 Lamehr, V. K., Dinegar, R. H., J. Am. Chem. Soc., **72** (1950) 4847-55
- 78 Brown, W. B., Ball, R. C., J. Phys., **A18** (1985) L517-30
- 79 Bradley, D. C., Mehrotra, R. C., Gauer, D.P., Metall Alkoxides, London: Academic Press, 1983
- 80 Mehrotra, R. C., J. Non. Crystal. Sci., **100** (1998) 1-15

- 
- 81 Meerwein, H., Bersin, T., Ann., **476** (1929) 113 - 117
  - 82 Agrawal, M. M., Ph. D. Thesis, Univ. of Rajasthan, Jaipur, India, 1968
  - 83 Mazdiyasi, K. S., Dolloff, R.T., Smith II, J. S., J. Amer. Ceram. Soc., **52**(10) (1969 ) 523-26
  - 84 Jain, N. C., Rai, A. K., Mehrotra, R. C., J. Inorg. Nucl. Chem., **40** (1978) 349-56
  - 85 Suyama, Y., Nagasawa, M., J. Am. Ceram. Soc., **72** (1994) 603-605
  - 86 Hirano, S., Yogo, T., Kituta, K., Yamagiwa, K., J. Am Ceram. Soc., **75** (1992) 2590-92
  - 87 Yogo, T., Sakamoto, W., Isaji, T., Kikuta, K., Hirano, S., J. Am. Ceram. Soc., **80** (1997)1767-72
  - 88 Sakamoto, W., Yogo T., Kikuta, K., Ogiso, K., Kawase, A., Hirano, S., J. Am.Ceram. Soc., **79** (1996) 2283-88
  - 89 Katayama, S., Sekine, M., , J. Mater. Chem., **2** (1992) 888-890
  - 90 Naka, S., Nakakita, F., Suwa, Y., Inagaki, M., Bull. Chem. Soc. Jpn. 41 (1974) 1168-72
  - 91 Ravindranathen, P., Komarneni, S., Bahlla, A., Roy, R., Cross, L. E., J. Mater. Res., 3 (1998) 810-812
  - 92 Fukui, T., Sakurai, C., Okuyama, M., J. Mater. Sci., **32** (1997) 189-196
  - 93 Gulliver, E. A., Garvey, J. W., J. Am. Ceram. Soc., **74** (1991) 1091-1094
  - 94 Hirano, S., Hayashi, T., Hatton, A., J. Am. Ceram. Soc., **74** (1991) 1320-1324
  - 95 Haberkro, K., Pyda, W.,in Clausen, N., Rühle, M., Heuer, A. H. (Eds.): Adv. Ceram. 12. OH, USA: Am. Ceram. Soc. Columbus, 1984, p774
  - 96 Morey, G.W., J. Am. Ceram. Soc., **36**(9) (1953) 279-85
  - 97 Laudise, R. A., Crockett, J. H., Ballman, A. A., J. Am. Cerm. Soc., **45**(2) (1962) 51-53
  - 98 Franck, E. U. in Somiya, S. (Eds.), Proc. 1st Internat. Symp. on Hydrothermal Reactions, Tokyo: Assoc. Sci. Doc. Inform., 1983 p1
  - 99 Somiya, S., Mat. Res. Soc. Symp. Proc., **24** (1984)256-71
  - 100 Somiya, S., Adv. Ceram. 3 (Meet.), 3rd (1990), Meeting date 1988, 207-243
  - 101 Somiya, S., Hydrothermal reactions for materials science and engineering: an overview of research in Japan, London and New York: Elsevier Science Publishers Ltd., 1989
  - 102 Kriechbaum, G. W., Kleinschmit, P., Angew. Chem., **101** (1989) 10, 1446-53
  - 103 Dawson, W.J., Ceramic Bulletin, **67** (1998) 10, 1673-78
  - 104 Rabenau, A., Angew. Chem. Int. Ed. Engl., **24** (1985) 1026-40
  - 105 Saito, S., Fine Ceramics, Tokyo: Ohmsha Ltd., 1985
  - 106 Fanelli, A. J., Burle, W.J., J. Am. Ceram. Soc., **69**(8), (1986) C174-75
  - 107 Claussen, N., Rühle, M., Advances in ceramics, Vol. 12: Am. Ceram. Soc., (1984) 806-15
  - 108 Bacsa, R. R., Graetzel, M., J. Am. Ceram. Soc., **79**(8) (1996), 2185-88
  - 109 Chen, H., Ma, J., Zhao, Z., Qi, L.,, Chem. Mter., **7** (1995) 663-68
  - 110 Lin, J., Duh, J., J. Am. Ceram. Soc., **80**(1) (1997) 92-98
  - 111 Boutz, M. M. R., Scholtenhuis, R. J. M. O., Winnubst, A. J. A., Burggraaf, A. J., Mat. Res. Bull., **29** (1994) 31-40
  - 112 Somiya, S., Yoshimura, M., Adv. Ceram. , Vol 21: Ceram. Powder Sci. (1987), Am. Ceram. Soc., Inc, 43-55
  - 113 Cheng, H., Wu, L., Ma, J., Zhao, Z., Qi, L., J. Mater., **15** (1996) 895-97
  - 114 Hirano, M., Kato, E., J. Am. Ceram. Soc., **79**(3) (1996) 777-80
  - 115 Zhou, Y. C., Rahaman, M. N., J. Mater. Res., **8**(7) (1993) 1680-86
  - 116 Hirano, M., Kato, E., J. Mater. Sci. Lett., **15** (1996) 1249-50
  - 117 Hench, L. L., Ulrich, D. R., Ultrastructure processing of ceramics, glasses and composites, New York: John Wiley & Sons, 1984, 334-52

- 
- 118 Abe, K., Matsumoto, S., *Ceram. Tran.*, Vol.22: *Ceram. Powder Sci. IV*, Am. Ceram. Soc. Inc. (1991) 15-25
- 119 Wang, C., Hu, Y., Qian, Y., Zhao, G., *Nanostr. Mat.*, **7** (1996) 421-23
- 120 Kutty, T. R. N., Vivekanandan, R., *Mater. Chem. Phys.*, **19** (1988) 534-46
- 121 Kutty, T.R.N., Vivekanandan, R., *Mater. Lett.*, **5**(3) (1987), 79-83
- 122 Fukai, K., Hidaka, K., Aoki, M., Abe, K., *Ceram. Inter.*, **16** (1990)285-90
- 123 Komarneni, S., Roy, R., Li, Q., *Mat. Res. Bull.*, **27** (1992) 1393-405
- 124 Dutta, P.K., Asiaie, R., Akbar, S. A., Zhu, W., *Chem. Mater.*, **6** (1994) 1542-48
- 125 Chien, A.T., Speck, J. S., Lange, F. F., Daykin, A. C., Levi, C. G., *J. Mater. Res.*, **10**(7) (1995) 1784-89
- 126 Kerchner, J. A., Moon, J., Chodelka, R. E., Morrone, A. A., .Adair J. H, *ACS Symp. Ser.*, **681** (1998) 106-19
- 127 Quon, D. H. H., Wang, S. S. B., Wheat, T. A., *Interceram.*, **41**(4) (1992) 257-59
- 128 Sato, S., Murakata, T., Yanagi, H., Miyasaka, F., *J. Mater. Sci.*, **29** (1994) 5657-63
- 129 Cheng, H., Ma, J., Zhao Z., Qi, L., *J. Mater. Sci. Lett.*, **15** (1996) 1245-46
- 130 Petrovic, I., Lencka, M. M., Anderko, A., Riman, R. E., ISAF'96, *Proc. IEEE Int. Symp. Appl. Ferroelectr.*, 10th, 735-738
- 131 Beal, K.C., *Adv. Ceram.*, vol 21: *Ceram. Powder Sci.: Am. Ceram. Soc., Inc.*, (1987) 33-41
- 132 Yonezawa, M., Ohno, T., Iwase, K., Takasa, T., Kiyama, M., Akita, T., Patent US3963630
- 133 Vivekanandan, R., Philip, S., Kutty, T. R. N., *Mat. Res. Bull.*, **22** (1986) 99-108
- 134 Rozman, M., Drogenik, M., *J. Am. Ceram. Soc.*, **78** (1995), 2449
- 135 Hirano, S., Messing, G. L., Hausner, ed., *Ceramic Transactions*, vol. 22: *Ame. Ceram. Soc. Inc.*, 1991, 15-25
- 136 Matijevic, E., Simpson, C. M., Amin, N., Arajs, S., *Colloids and Surf.*, **21** (1986) 101-08
- 137 Takamori, T., David, L. D., *Am. Cermic. Soc. Bull.*, **65** (1986) 1282-86
- 138 Komarneni, S., Roy, R., Breval, E., Ollinen, M., Suwa, Y., *Adv. Ceram. Mater.*, **1** (1986) 87-92
- 139 Huang, W., Shuk, P., Greenblatt, M., *Chem. Mater.*, **9** (1997) 2240-45
- 140 Kanai, H., Harada, K., Yamashita, Y., Hasegawa, K., Mukaeda, S., Handa, K., *Japn. J. Appl. Phys.*, **35** (1996) 5122-25
- 141 Hattori, T., Iwadate, Y., Kato, T., *J. Mater. Sci. Lett.*, **8** (1989) 305-06
- 142 Liu, H, Chin, T., Lai, L., Chiu, S., Chung, K., Chang, C., Lui, M., *Ceram. Inter.*, **23** (1997) 19-25
- 143 Futagami, R. S., Ioku, L., Nishizawa, H., Yamasaki, N., *J. Mater. Schi. Lett.*, **13** (1994) 533-34
- 144 Dogan, F., Orouke, S., Oian, M, Sarikaya, M., *Mater. Res. Soc. Symp. Proc.*, 457: *Nanophase and Nanocomposite Materials II*, (1997) 69-74
- 145 Penn, R. L., Banfield, J. F., Voigt, J., *Mater. Res. Soc. Symp. Proc.*, 432: *Aqueous chemistry and geochemistry of oxides, oxyhydroxides, and related materials*, (1997), 175-81
- 146 Stammbaugh, E. P., Miller, J. F., *Proc. 1st Symp. rydrothermal reactions*, (1983) 859
- 147 Goebbert, C., Nonninger, R., Aegerter, M. A., Schmidt, H., *Thin Solid films* **351** (1999) 79 -84
- 148 Goebbert, C., Bischt, H., Al-Dahoudi, N., Nonninger, R., Aegerter, M. A., Schmidt, H., *J. Sol-Gel Sci. and Techn.* **19** (2000) 201-204
- 149 Goebbert, C., Aegerter, M. A., Burgard, D., Nass R., Schmidt, H., *J. Mater. Sci.*, **9** (1999) 253-58
- 150 Schmidt, H. K., *Mol. Crys. and Liq. Cryst.*, **353** (2000) 165-179
- 151 Schmidt, H. K., Naß, R., Burgard, D, Nonninger, R., *Mater. Res. Soc. Symp. Proc.* (1998) 520 (*Nanostructured powders and their industrial applications*), 21-23
- 152 Nonninger, R., Sepeur, S., Mennig, M., Aegerter, M. A., Schmidt, H., in: *Polymer; Symposium 10: Smulation Polymere: Symposium 14*, ed. Jürgen Heinrich u.a – Weinheim: Wiley – VCH, 1999, *Werkstoffwoche 98, Band VIII*, 739-744

- 
- 153 Schmidt, H. K., *Sci. and Techn. Polym. and Adv. Mater.*, ed. by Prasad, P. N. et al. Plenum Press, New York, 1998, 663-674
- 154 Ph.D. thesis Bendzko, N., (1999), University of the Saarland
- 155 Sharma, P. K., Jilavi, M. H., Burgard, D., Nass, R., Schmidt, H., *J. Am. Ceram. Soc.*, **81**(10) (1998), 2732-34
- 156 Frank, E. U., *Int. Corros. Conf. Ser.*, (1973) 463
- 157 Frank, E. U., *Pure Appl. Chem.*, **24** (1970) 13
- 158 Toedheide, K. in F. Franks (Ed.), *Water, a comprehensive treatise*, Vol. 1, New York: Plenum, (1972) 463
- 159 Helgeson, H. C., *Phys. Chem. Earth*, **13/14** (1981) 133
- 160 Rabenau, a., Rau, H., *Philips Tech. Rundsch.*, **30** (1969/70) 53
- 161 Liu, H., Chin, T., L.Lai, Chiu, S., Chung, K., Chang, C.S., Lui, M., *Ceram. Inter.*, **23** (1997) 19-25
- 162 Lu, C., Lo, S., Lin, H., *Mater. Lett.*, **34** (1998) 172-176
- 163 Futagami, R. S., Ioku, K., Nishizawa, H., Yamasaki, N., *J. Mater. Sci. Lett.*, **13** (1994) 533-534
- 164 Kutty, T. R. N., Padmini, P., *J. Mater. Sci. Lett.*, **15** (1996) 1973-75
- 165 Padmini, P., Kutty, T. R. N., *J. Mater. Chem.*, **4**(12) (1994) 1875-81
- 166 Kutty, T. R. N., Padmini, P., *Mat. Res. Bull.*, **27** (1992) 945-52
- 167 Kaiser, A., Berger, A., Sporn, D., Bertagnolli, H., *Ceram. Trans.*, vol 51: *Ceram. Proc. Sci. Tech.*, (1995) 51-55, Am. Ceram. Soc., Inc.
- 168 Laudise, R. A., *Prog. Inorg. Chem.*, **3** (1962) 1
- 169 Hattori, T., Iwadate, Y., Kato, T., *J. Mater. Sci. Lett.*, **8** (1989) 305-306
- 170 Morse, J., Gratzel, M., *J. Amer. Chem. Soc.*, **105** (1983) 6547-51
- 171 Schmidt, H. K., *KONA powder and particle*, **14** (1996) 92-103
- 172 Jacobs, H., Schmidt, D., *curr. Top. Mater. Sci.*, **8** (1982) 381-88
- 173 Avudathai M., Kutty, T. R. N., *Mat. Res. Bull.*, **22** (1987) 641-50
- 174 Chen, D., Xu, R., *J. Mater. Chem.*, **8**(4) (1998) 965-8
- 175 Kaiser, A., Sporn, D., Bertagnolli, H., *J. Euro. Ceram. Soc.*, **14** (1994) 77-83
- 176 Komarneni, S., Menon, V. C., Li, Q. H. in *Ceram. Trans.*, Vol. 62: *Science, technology and commercialization of powder synthesis and shape processing*, (1996) 37-46
- 177 Stambaugh, E. P., Dawson, W. J., Adair J. H., Kim, B. C., *Technology for New/Improved Hydrothermal Processes*, Battelle Handbook, Dec. 1984
- 178 Lencka, M. M., Riman, R. E, *Chem. Mater.*, **5** (1993) 61-70
- 179 Hair, J. H., Denkewicz, R. P., Arriagada, D. L., Osseo-Asare, K., in *Ceram. Trans.*, Vol. 1: *Ceramic powder science II*, B, USA: the American Ceramic Society, Inc., (1988) 135-45
- 180 Matijevic, E, *Accounts of Chem. Res.*, **14** (1981) 22-29
- 181 Kutty, T. R. N., Padmini, P., *Mater. Chem. Phys.*, **39** (1995) 200-208
- 182 Tompa, G. S., Morton, D. C., Khan, B. A., *MRS Symp. Proc.*, Vol. 358: *Mat. Res. Soc.*, (1995) 705
- 183 Guizard, C., Julbe, A., Larbot, A., Lot, C., *Key Eng. Mater.*, **61&62** (1991) 47-56
- 184 Krug, H., Schmidt, H., *Proc. first workshop on hybrid organic-inorganic materials*, Chateau de Bierville, France, November 8 - 10, (1992) 127-41
- 185 Fitz-Gerald, J., Singh, R. K., *MRS Symp. Proc.*, Vol. 501: *Mat. Res. Soc.*, (1998) 351-62
- 186 Strehlow, P., *J. Non-Cryst. Solids*, **107** (1988) 55
- 187 Pfüller, U., *Mizellen - Versikel - Mikroemulsionen: Tensidassoziate u. ihre Anwendung in Analytik u. Biochemie*, Berlin: Springer-Verlag, 1986
- 188 Brezesinski, G., *Grenzflächen und Kolloide: physikalisch - chemische Grundlagen*, Heidelberg: Hans-Jörg Mögel, 1993

- 
- 189 Porter, M. R., Handbook of surfactants, New York: Chapman and Hall, 1991
- 190 Nelson, R. D. in Williams, J. C., Allen, T. (editors), Handbook of powder technology, vol. 7: Dispersing powders in liquids, Netherland: Elsevier Science Publishers B. V., 1988
- 191 Hansner, H., Messing, G. L., Hirano, S., Ceramic Powder Processing Science, Köln: Deutsche Keramische Gesellschaft e.V., 1990
- 192 Paul, B. K., Moulik, S. P., J. Disper. Sci. & Techn., **18**(4) (1997) 301-67
- 193 Shinoda, K., Lindman, B., Langmuir, **3**(2) (1987) 135-49
- 194 Eastoe, J., Warne, B., Cun. Opin. Colloid Interface Sci., **1**(6) (1996) 800-05
- 195 Larramona, G., Gutierrez, C., Pereira, I., Nunes, M. R., Costa, F. M. A., J. Chem. Soc., Faraday Trans. 1, **85**(4) (1989) 907-16
- 196 Williams, D. E., Mosely, P. T., J. Mater. Chem., **1** (1991) 809-14
- 197 McGeehin, P., Moseley, P. T., Williams, D. E., Henshaw, G. S., Gellman, L. J., Patent US6046054
- 198 Zhuang, Y., Li, X., Huazhong Ligong Daxue Xuebao, **22**(Zengkan) (1994) 99-102 (Chinese)
- 199 Roberts, A. J., Flavell, W. R., Hoad, D. R. C., Egdell, R. G., Randall, S., Wincott, P. L., Teehan, D., Surf. Sci., **311**(1-2) (1994) 181-88
- 200 Teslenko, S. P., Motorny, A. V., Raevskii, I. P., Gindin, E. I., Unshchikova, T. I., Vopr. Primeneniya Yader. Izluch. Mosk. Inzh.-fiz. In-t (MIFI), M. (1991) 123-28 (Russian)
- 201 Claessen, R., Smith, M. G., Goodenough, J. B., Allen, J. W., Phys. Rev. B, **47**(4) (1993) 1788-93
- 202 Cava, R. J., Gammel, P., Batloff, B., Krajewski, J. J., Peck, W. F., Rupp, L. W., Felder, R., Dover, R. B., Phys. Rev. B, **42**(7) (1990) 4815-18
- 203 Lu, W., Jiang, S., Zhou, D., Gong, S., Sensors and Actuators, **80** (2000) 35-37
- 204 Herrmann, J.-M., Nunes, M. R., Costa, F. M. A., J. Chem. Soc., Faraday Trans. 1, **78**(6) (1982) 1983-91
- 205 McGeehin, P., Williams, D. E., Dawson, D. H., Gellman, L. J., Patent WO9500836
- 206 Lu, W., Li, B., Fu, M., Hunag, Z., Sensors and Actuators, **80** (2000) 38-41
- 207 Hinatsu, Y., J., Solid State Chem., **122**(2) (1996) 384-89
- 208 Hinatsu, Y., Kidorui, **28** (1996) 268-69
- 209 Hinatsu, Y., Edelstein, Norman, J. Alloys Compd., **250**(1-2) (1997) 400-04
- 210 Hinatsu, Yukio, Tezuk, Keitaro, J. Solid State Chem., **138**(2) (1998) 329-33
- 211 Roh, K. S., Kim, M. G., Ryu, K. S., Yo. C. H, Solid State Commun., **100**(8) (1996) 565-69
- 212 Trari, M., Doumerc, J.-P., Dordor, P., Pouchard, M., Behr, B., Krabbes, G., J. Phys. Chem. Solids **55**(11) (1994) 1239-43
- 213 Bogatina, V. N., Bogatin, A. S., Krist. Svoistva Krist., **1** (1974) 124-7 (Russian)
- 214 Li, Y., Chen, H., Yang, Y., Gaodeng Huaxue Xuebao, **14**(6) (1993) 760-63 (Chinese)
- 215 Reddy, C.V.G., Manorama, S.V., Rao, V. J., Lobo, A., Kulkarni, S. K., Thin Solid Films, **348** (1999) 261-65
- 216 Scherrer, P., Gött. Nachrichten, conference on July 26, 1918, 98-100
- 217 Walter, W., Lehrbuch der Organischen Chemie, S. Hirzel Verlag Stuttgart 1988.
- 218 Oliveira, L., J. Sol-Gel Sci. and Techn., **2**(1994)263-267.
- 219 Li, Q., Zeng, G., Xi, S., Chin. J. Appl. Chem. **12**(1994)2, 67-71 (Chinese)
- 220 Sadtler Research Laboratories, Division of Bio-Rad Laboratories, Inc., The infrared spectra handbook of inorganic compounds, USA: 1984
- 221 Budavari, S., O'Neil, M., Smith, A., Heckelman, P., The merck index (eleventh edition): an encyclopedia of chemicals, drugs and biologicals, Merck & Co., INC, New York, 1989
- 222 Willy-VCH, Ullmann's Encyclopedia of Industrial Chemistry, Sixth Edition (Electronic format), 2002: Crystallization and Precipitation.